

A Regional Climate Modelling Experiment for Southeast Asia

Using PRECIS Regional Climate Model
and selected CMIP₃ Global Climate Models

April 2014

This technical report is a product of the Southeast Asia Climate Analyses & Modeling (SEACAM) Framework which was initiated by the Centre for Climate Research Singapore of the Meteorological Service Singapore (CCRS-MSS) and in collaboration with the Met Office Hadley Centre (MOHC). It assessed the performance of the PRECIS Regional Climate historical simulations and analysed future changes for S.E. Asia up to year 2100. The report was contributed by climate researchers from the region's National Meteorological & Hydrological Services (NMHSs) and Research Institutes (RIs), as well as scientists from the MOHC.



Contributing Authors

Raizan Rahmat⁹ (report coordinator), Boonlert Archevarahuprok¹, Chai Ping Kang², Chung Jing Xiang³, David Hein⁴, Dodo Gunawan⁵, Erasmo Buonomo⁴, Grace Redmond⁴, Haji Sidup Haji Sirabaha⁶, Han Swe⁷, Itesh Dash⁸, Jacqueline Lim See Yee⁹, Jose Rizal⁵, Kornrawee Sitthichivapak¹, Kumarenthiran Subramaniam¹⁰, Lalit Dagar¹¹, Liew Ju Neng³, Ling Leong Kwok¹⁰, Lyhon Ho¹³, Mai Van Khiem¹², Matt Palmer⁴, Monichoth So Im¹³, Muhammad Yunus Ahmad Mazuki¹⁴, Ngai Sheau Tieh³, Ngo Duc Thanh¹⁵, Saiful Azmi bin Haji Husain¹¹, Shamsuddin Shahid², Simon Tucker⁴, Srivatsan V.¹⁶, Suppakorn Chinvanho¹⁷, Thelma Acebes Cinco¹⁸, Thuy Tran Thanh¹², Vo Van Hoa¹⁹, and Wittyi Soe⁷.

¹ Thailand Meteorological Department (TMD)

² Universiti Teknologi Malaysia (UTM)

³ Universiti Kebangsaan Malaysia (UKM)

⁴ Met Office Hadley Centre (MOHC)

⁵ Badan Meteorologi, Klimatologi, dan Geofisika, Indonesia (BMKG)

⁶ Brunei Darussalam Meteorological Department

⁷ Department of Meteorology and Hydrology, Myanmar (DMH)

⁸ Regional Integrated Multi-Hazard Early Warning System (RIMES, Thailand)

⁹ Centre for Climate Research, Singapore (CCRS)

¹⁰ Malaysian Meteorological Department (MMD)

¹¹ University Brunei Darussalam (UBD)

¹² Vietnam Institute of Meteorology, Hydrology and Environment (IMHEN)

¹³ Department of Meteorology, Cambodia

¹⁴ University Malaya (UM)

¹⁵ Hanoi University of Science

¹⁶ Tropical Marine Science Institute (TMSI), National University of Singapore (NUS)

¹⁷ S.E. Asia START Regional Center, Thailand

¹⁸ Philippines Atmospheric, Geophysical and Astronomical Services Administration (PAGASA)

¹⁹ National Center for Hydro-Meteorological Forecasting (NCHMF), Vietnam

Acknowledgement

SEACAM would like to thank all participants involved in this project for their contributions in analysing and documenting the results from the regional climate modelling experiments. These include climate researchers from the region's National Hydrological & Meteorological Services (NMHSs) and Research Institutes (RIs), as well climate modelling and analysis experts from the Met Office Hadley Centre (MOHC) (see list of authors). We would also like to acknowledge the professional training and assistance provided by the experts from the MOHC in running the PRECIS model and processing its output data.

In addition, SEACAM would like to thank the UK Foreign Commonwealth Office (UKFCO) for having partially funded the project.

Table of Contents

1.	Introduction.....	11
1.1.	The geography and climate of Southeast Asia.....	11
1.2.	The impacts of climate change on S.E. Asia	12
1.3.	The SEACAM experiments	12
1.3.1.	Generating future climate change scenarios.....	12
1.3.2.	Analysing regional climate model outputs	13
2.	Literature Review.....	15
2.1.	Need for higher resolution climate projections.....	15
2.2.	Climate change projections on S.E. Asia from AR5.....	16
3.	Assessment of End-users' Needs.....	21
3.1.	Quantitative responses	21
3.2.	Qualitative responses.....	23
4.	Model Configuration, Datasets and Experimental Design	25
4.1.	Regional climate models and the formulation of HadRM3P	25
4.2.	Domain.....	26
4.3.	Driving data and emissions scenario	27
4.3.1.	Choice of emissions scenario	28
4.3.2.	The 'QUMP' 17 Member Perturbed Physics Ensemble (PPE).....	28
4.3.3.	Other types of global data and their availability for downscaling	29
4.3.4.	Driving GCMs for the SEACAM experiments	29
4.4.	Time periods for analyses	30
4.5.	Observational data used for the evaluation.....	30
5.	Assessment of Historical RCM Simulations	32
5.1.	Why assess/evaluate RCM outputs?	32
5.2.	Method of evaluation.....	32
5.3.	Evaluation of temperature and precipitation annual cycle.....	33
5.3.1.	Annual temperature cycle.....	33
5.3.2.	Annual precipitation cycle	36
5.4.	Evaluation of seasonal spatial distribution of temperature	40
5.4.1.	Seasonal mean temperature.....	40
5.4.2.	Seasonal minimum and maximum temperature	43

5.5.	Evaluation of seasonal spatial rainfall distribution	48
5.6.	Evaluation of the Southwest Summer Monsoon	51
5.6.1.	Monsoon circulations.....	51
5.6.2.	Precipitation	52
5.6.3.	Spatial patterns of precipitation extreme.....	53
5.7.	Evaluation of the Northeast Winter Monsoon	55
5.7.1.	Monsoon circulation	55
5.7.2.	Spatial patterns of circulation.....	55
5.7.3.	Precipitation	59
5.7.4.	Spatial patterns of precipitation extreme.....	59
5.8.	Evaluation of extreme rainfall indices.....	61
5.8.1.	Annual maximum one day rainfall (Rx1day)	61
5.8.2.	Annual maximum consecutive five days rainfall (Rx5day).....	63
5.8.3.	Annual maximum of consecutive dry days (CDD)	65
5.8.4.	Trends in extreme rainfall indices	67
5.9.	Evaluation of extreme temperature indices.....	70
5.9.1.	Mean annual minimum average daily temperature, TMn	70
5.9.2.	Mean annual maximum average daily temperature, TMx.....	71
5.9.3.	Maximum day time temperature, TXx and Maximum night time temperature, TNx	73
5.9.4.	Trends in extreme temperature indices of TMx and TMn	74
5.10.	Evaluation of 5-year return level indices (TMx and Rx1day).....	75
5.11.	Evaluation of precipitation tele-connection with ENSO.....	77
6.	Mid- and Long-term Climate Change Projections.....	79
6.1.	Annual temperature cycle projections.....	79
6.2.	Annual precipitation cycle projections	83
6.3.	Seasonal mean temperature	86
6.4.	Seasonal minimum temperature	91
6.5.	Seasonal maximum temperature.....	95
6.6.	Diurnal temperature range.....	100
6.7.	Seasonal mean rainfall	102
6.8.	Southwest Summer Monsoon	108
6.9.	Northeast Winter Monsoon	115
6.10.	Extreme rainfall indices	116

6.11.	Extreme temperature indices	118
6.12.	Five-year return level for maximum daily temperature and precipitation.....	120
7.	Bibliography.....	122
8.	List of Abbreviations	126

Background

- SEACAM's regional climate modelling experiment provides high-resolution (25 km) information on future climate change projections for the S.E. Asia region up to year 2100. This was done by dynamical downscaling of 5 selected members of the Met Office HadCM3Q ensemble and the ECHAM5 model (from the Max Planck Institute for Meteorology) using the Met Office PRECIS model {§4.1}. The selection of members from the HadCM3Q ensemble was done by assessing their ability to simulate the major features of S.E. Asian climate and capturing the broadest range of future projections for temperature, monsoon characteristics and precipitation {§4.3.4}.
- Model simulations were evaluated against appropriate observation datasets available, which includes APHRODITE and CRU {§4.5}. In instances where direct observations were not accessible, the ERA-40 reanalysis was used to compare against the simulations. The ERA-40 reanalysis was also used to drive the PRECIS model and the downscaled reanalysis outputs were also compared against the model simulations to assess the performance of the regional climate model on its own, without (or with minimal) errors coming from the driving global climate model data {§4.3.4}.
- A literature survey was carried out to identify the scientific issues and gaps relevant to the region {§2} and a questionnaire was also conducted to gather the needs of the end-users of climate projections in the region {§3}. These two surveys helped inform the formulation of the regional downscaling experiment in terms of its configurations and analyses.

Evaluation of Model Simulations

- Evaluations were carried out for temperature and precipitation in the annual cycle, their spatial distribution, and selected extreme indices. In addition, monsoon circulations and the associated precipitation patterns were also analysed {§5.2}.
- In the evaluation of the seasonal temperature cycle, downscaled climate model simulations generally performed well by capturing the observed temperature peaks and dips across the year, especially for the Mainland Southeast Asia. Overall biases (warm or cold) range between 1.0 to 2.0°C {§5.3.1}.
- The seasonal precipitation cycle was not simulated as well, as expected due to the more challenging nature in predicting precipitation in this region. Nevertheless, the RCM simulations generally captured the rainfall cycle better for places with pronounced precipitation seasonality, such as in the northern and southern parts of the region. In the near equatorial regions where the seasonality is smaller, simulations tended to be more chaotic, but the (wet) biases were relatively smaller {§5.3.2}.

- When evaluating precipitation simulations against observations, the choice of observations (e.g. between APHRODITE and CRU) can have a significant impact on the outcomes of the analyses. Caution needs to be exercised when making conclusions about biases in simulations as these could be severely influenced by deficiencies in observational datasets (§5.3.2).
- Analyses of mean regional temperature simulations by seasons reveal that these tended to have biases in the range between $\pm 4^{\circ}\text{C}$ with considerable spatial and seasonal variations. The biases were larger than the annual temperature cycle biases as these had not been averaged in space. In general, warm biases were observed in the simulation in the early part (Mar – May) of the calendar year while cool biases were observed in the later part (Sep – Nov). This is broadly consistent with the biases shown in the analyses of the annual cycle (§5.4.1).
- Spatial biases structure of the seasonal *maximum* temperature and seasonal mean temperature were similar with generally warmer temperatures simulated in the continental region of S.E. Asia, and cooler temperatures simulated in the maritime region. For the seasonal *minimum* temperature, generally warm biases were observed everywhere in the region and these were seasonally invariant in the southern half of the domain (§5.4.2).
- Relative to temperature, precipitation patterns by nature are more sporadic and less uniform. As a result, bias patterns of seasonal rainfall simulations showed more location-specific variability. Overall, moderate wet biases of up to 40% were observed except for the western mainland S.E. Asia where dry biases were observed. The wet biases were stronger (up to 80%) in certain seasons (DJF and MAM) and certain locations (Cambodia and Central Borneo). As the annual cycle analyses have shown (§5.3.2), these biases could partially be due to under-representation of rainfall in the observational dataset, APHRODITE (§5.5).
- The RCM simulations generally demonstrated good skill in simulating the spatial patterns of the average circulations (or wind flow) patterns for both the northeast (boreal winter) and southwest (boreal summer) monsoon seasons. Average precipitation patterns during monsoon seasons were also generally well-captured. Extreme precipitation (95% of monsoon seasonal rainfall), however, was generally underestimated and varied depending on locations and seasons (§5.6 and 5.7).
- Extreme indices of precipitation and temperature were also analysed. Large biases of Rx_{1day} (annual maximum 1-day rainfall) were generally found in high-elevation places. Otherwise, spatial structures of Rx_{1day} were generally well-captured by model simulations. Similar characteristics were observed in the simulations of Rx_{5day} (annual maximum consecutive five days rainfall). For CDD (consecutive dry days), the models simulated it well, reasonably capturing both the spatial patterns and the magnitude of the CDD (§5.8). In terms of capturing the historical trends, the RCM was able to

reproduce the sign of the trends (for Rx1day and Rx5day) and the inter-annual variability of the observed rainfall indices (for Rx5day and CDD){§5.8.4}.

- Both the mean annual *minimum* average daily temperature (TMn: coolest day of the year averaged over many years) and the mean annual *maximum* average daily temperature (TMx: warmest day of the year) were well simulated. The simulations were generally warmer of up to only 2°C for TMn, and around 5°C for TMx in isolated locations {§5.9}. Historical trends in the extreme temperature were also captured by the RCM, especially in the TMx {§5.9.4}.

Model Projections

- Model projections are made for the mid-century (also “mid-term”) for the 30-year period between 2031 and 2060 and also for the end-century (also “long-term”) for the 30-year period between 2071 and 2100. For all projections, the changes are reported relative to the baseline period of 1971-2000 {§6}.
- Annual cycle change in temperature for the mid-term projections ranged around 2°C, and for the long-term around 4.0°C. These were statistically significant projections with fairly consistent changes registered across the year. In contrast to temperature projections, the projections for precipitation showed a lot more variations across countries and seasons which lead to difficulties in interpretation of the annual cycle plots. There were, however, instances of statistically significant projections in the annual precipitation cycle change observed over specific locations and seasons {§6.2}.
- Across the region, similar projection ranges (to the annual temperature cycle) were observed for the gridded seasonal mean temperature for the mid-century (2-4 °C warmer) and end-century (3-5°C warmer). Spatial warming patterns in the seasonal minimum and maximum temperatures closely resemble that of the seasonal mean, but towards the end-century the warming rate of the seasonal minimum temperature is slightly lower than the mean. Coupled with the higher warming rate of the seasonal maximum (relative to the seasonal mean) for the same period, the temperature difference between the maximum and minimum is expected to widen, on average, during the end-century {§6.3 - 6.5}. However, projections for diurnal temperature changes (maximum minus minimum) indicate large spatial and seasonal variations {§6.6}.
- Unlike for temperature, changes in rainfall projections show large spatial and seasonal variations. Generally, the projections show drier climate over the sea and wetter climate over land. The land-sea contrast is more obvious towards the end of the century. In all of the HadCM3Q projections, drier climate is projected over most areas during boreal winter except central mainland S.E. Asia. However, wetter climate was projected south of the equator in ECHAM5. Generally, inter-model agreement is high except during winter (DJF) {§6.7}.

- During the boreal summer monsoon (JJAS), generally more rainfall is projected in the northern part of the region (approximately from 20°N northward), whereas drier conditions are projected for the Maritime Continent. Similar signals are expected for both the mid- and end-century projections, but with the end-century showing larger magnitude of changes than the mid-century. These projections are accompanied by end-century strengthening of westerly winds at the 850 hPa level. For the boreal winter monsoon (DJF), the scale of projected precipitation changes (e.g. increases over land) for extremes is not as significant as the summer monsoon. In contrast to HadCM3Q projections, ECHAM5 projections do not provide the same signs of rainfall changes for both mid-century and end-century periods {§6.8 - 6.9}.
- For extreme rainfall indices, Rx1day and Rx5day for the end-century are projected to increase in areas north of the 15°N latitude. On the other hand, all projections show an increase in CDD (i.e. longer dry spells) south of 15°N latitude in both time periods. For these projections, model agreement tends to be good {§6.10}.
- For extreme temperature indices, a 1-3°C change is projected for most land regions of S.E. Asia across all RCM projections for the mid-century and a 3-5°C change for the end of the century. The magnitudes of change for these two time periods are comparable across all four indices (TXx, TNx, TMx, and TMn) considered. The projection ranges are also similar to that of the annual cycle and seasonal temperature projections for the two periods {§6.11}.

1. Introduction

1.1. The geography and climate of Southeast Asia

Southeast Asia (S.E. Asia, henceforth) is an area of major river systems, tropical forests, mountain ranges and over 20,000 islands. In total, the region contains 173,000 kilometres of coastline, with many major cities and associated economic activity located in coastal areas. The region spans 3,300 kilometres from north to south and 5,600 kilometres from east to west. It rests between the waters of the Indian Ocean and the Pacific Ocean, and contains a mainland section to the north (Cambodia, Laos, Thailand, Peninsular Malaysia, and Vietnam – henceforth the mainland S.E. Asia) and a maritime section to the south (Brunei, the Philippines, Singapore, East Malaysia, East Timor, and Indonesia – henceforth the Maritime Continent) (see Figure 1.1).

It is also a region of the world which is expected to experience serious, negative impacts of climate change due to its fast-growing and urbanising population, as well as the reliance of many of its people on climate-sensitive sectors such as agriculture, fisheries and natural resources.

S.E. Asia is annually affected by extreme weather events, particularly tropical cyclones, droughts and floods. Large areas of S.E. Asia are prone to flooding, and much of the region is heavily influenced by monsoon systems which often bring extreme weather. As the climate warms, these types of extreme weather events are projected to increase in frequency and intensity, threatening the lives and livelihoods of millions of people (Yusuf & Francisco, 2009).

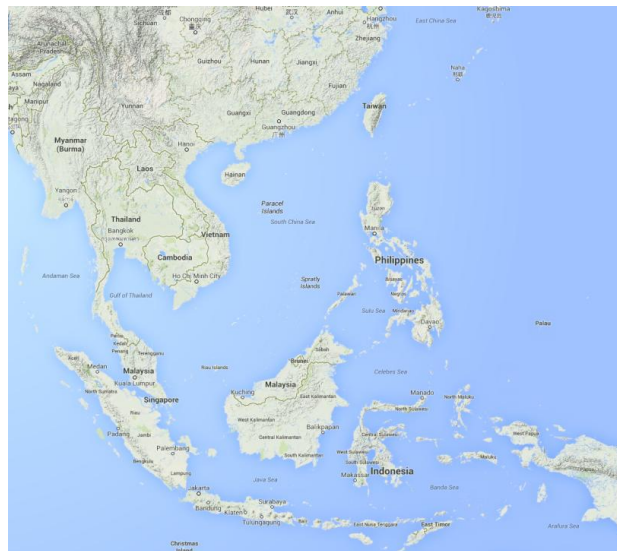


Figure 1.1: Map showing the continental section of S.E. Asia on the top-left and the maritime section to its south and east. (Image credit: Google Map)

1.2. The impacts of climate change on S.E. Asia

The impacts of climate change will not be evenly distributed across the region. Differences in economic level, population density, technological capacity, and urbanisation mean that some regions may experience harsher impacts than others. Given the potential negative impacts, governments and policy-makers in the region need reliable information to inform decisions made and to respond to a changing climate in a way guided by the best science available. However, S.E. Asia has not been sufficiently studied to meet this need, especially in comparison with other major regions of the world, e.g. North America (the NARCCAP project¹) and Europe (the ENSEMBLES project²).

The need for further in-depth research, especially the need for more climate change projections for S.E. Asia, was the main driving force in the creation of the SEACAM (S.E. Asia Climate Analysis and Modelling) framework.

The need for further in-depth research, especially the need for more climate change projections for S.E. Asia, was the main driving force in the creation of the SEACAM (S.E. Asia Climate Analysis and Modelling) framework.

1.3. The SEACAM experiments

1.3.1. Generating future climate change scenarios

SEACAM brought together representatives from 8 of the 10 Association of South East Asian Nations (ASEAN) member countries at a planning workshop in June 2012 in Singapore. At that meeting, the need for a dedicated project for S.E. Asia using a regional climate model (RCM)



Trainers and participants at the June 2012 workshop in Singapore.

driven by several global models was discussed. Those in attendance decided to share the work load required to run these models (as RCM runs are computationally expensive and require large amounts of storage space). Six 150-year PRECIS (Jones, et al., 2004) regional climate model experiments, nicknamed the DURIAN³ experiments, were designed over a common domain which encompassed all ASEAN member countries (see section 4.2 details on domain), and the responsibility

for running one or more of the six experiments was voluntarily chosen by participants. Following the workshop, the common domain was further refined in a series of discussions in

¹ <https://www.narccap.ucar.edu/>

² <http://www.ensembles-eu.org/>

³ DURIAN is short for Downscaling for Useful Regional Impacts Assessment.

which SEACAM participants corrected the land representation, to ensure that the small islands were represented in the regional model as land points, as far as practically possible.

In Phase 2 of SEACAM was initiated, in which current and newly recruited participants of SEACAM would jointly analyse the 900 years (150 years times six experiments) of climate model output data from the DURIAN experiments. Funding for the SEACAM phase 2 was provided by CCRS-MSS, the MOHC and the U.K. Foreign and Commonwealth Office (UKFCO).

1.3.2. Analysing regional climate model outputs

Phase 2 began with a workshop in Phnom Penh, Cambodia in August 2013. Almost all of the participants from the initial SEACAM project were in attendance, with approximately ten additional participants, including two from a further ASEAN member country (Cambodia). During the five days of the workshop, participants voluntarily arranged themselves into four groups, who would carry out the foundational analysis of the DURIAN experiments in areas of greatest relevance to policy-makers as well as to provide a basis for any specific future research using data from the DURIAN experiments. The four areas were annual cycle of temperature and precipitation; mean temperature and precipitation; circulation patterns during the monsoon seasons; and extreme precipitation and temperature.

Participants spent the five days analysing the relevant data in these four areas and the production of plots and text describing the results. Following the workshop, team leaders of the four areas were responsible for coordinating further analyses, including the production of plots and written results during the four month period between this and the subsequent workshop.



Trainers and participants at the August 2013 workshop in Phnom Penh, Cambodia.

The subsequent workshop, in February 2014 at CCRS-MSS in Singapore, brought together almost all participants again to review the work done since the workshop in Phnom Penh and finalise the report. Several experienced climate scientists joined the workshop in order to provide guidance on the analyses, review the work done to-date, and review the final product.

The contents of this SEACAM report come from the efforts of over 30 climate researchers from the region's National Meteorological and Hydrological Services (NMHSs) and research institutes, all but five of which are from ASEAN member countries, and some of whom are either early career scientists or postgraduate researchers. The production of the report has been a learning experience for all involved and has increased their capacity in analysing climate model output data and summarising the results, a skill which is important for all participants and one which is of increasing importance across S.E. Asia, as the issue of a



Trainers and participants at the February 2014 workshop in Singapore.

changing climate in the region becomes more of a priority. SEACAM has furthermore led to closer contacts between climate researchers in the region, especially at the NMHSs. Closer cooperation will enhance future research as more scientists are able and willing to review the work, and it will also provide precedent for future collaborative research projects initiated by other institutes across S.E. Asia, such as the S.E. Asia CORDEX project⁴.

⁴ <http://www.ukm.my/seaclid-cordex/>

2. Literature Review

2.1. Need for higher resolution climate projections

The primary goal of SEACAM Phase 1 (June 2012- June 2013) was the production of climate projections for S.E. Asia. Creation of climate projections requires climate models to be run into the future. Since climate models were first created in the 1960s, a plethora of global climate models (GCMs) have been run, simulating the Earth's atmosphere, ocean and other important processes. The computational expense of simulating the atmosphere and ocean in three dimensions with a climate model means that the resolution is constrained: if the resolution is too high the GCM takes too long to run to be of any use.

As S.E. Asia contains very complex terrain, the region is a logical choice for regional climate model (RCM) simulations. A review of the climate change related scientific literature reveals a lack of regional model downscaling experiments over S.E. Asia.

A way to address the limitations of GCMs is to *downscale* them using higher resolution RCMs. Use of high resolution RCMs to dynamically downscale coarser resolution global climate models has been shown on numerous occasions to add value to and/or improve upon the realism of the global models (Jones, et al., 1995). This is mainly due to the fact that regional climate is most influenced by the local land and surface features (e.g. mountains and coastlines) which the global models cannot explicitly resolve. The coarser the global model resolution, the “smoother” the land-surface representation becomes (as each grid box in the model is by definition an area-average representation of the land in the whole grid box). This process can yield unrealistic local climate information in global models, even if the large scale climate is (on average) well represented.

The characteristics of regional climate for S.E. Asia are determined by local weather systems which bring in heat, moisture and momentum into the S.E. Asian region. The definition of regional climate takes into consideration the mean climate, the variance (how the climate of the region naturally varies), the co-variance (how climates of nearby regions affect climate) and the extremes (impactful weather events which are very high/very low and rare).

As S.E. Asia contains very complex terrain, the region can in principle benefit from the use of RCM simulations to provide climate scenarios. A review of the climate change related scientific literature reveals a lack of regional model downscaling experiments over S.E. Asia. In comparison to other major land areas in the world (Europe, the Americas, Africa, and more), S.E. Asia (as defined by the land areas covered by ASEAN member countries) has not been rigorously studied using an ensemble of dynamically downscaled global models over the S.E. Asian region. Most of the climate change projections for S.E. Asia have been derived from global model runs, including those which informed the Intergovernmental Panel of Climate

Change Fifth Assessment Report, or the IPCC AR5 (IPCC, 2013) or have involved the use of regional models over individual S.E. Asian countries.

2.2. Climate change projections on S.E. Asia from AR5

At the time of its release at the end of 2013, the IPCC AR5 was the most comprehensive assessment of the evidence for climate change that has been produced. AR5's section (14.8.12) on S.E. Asia (Christensen, et al., 2013) notes that temperature has been increasing at a rate of 0.14°C to 0.20°C per decade since the 1960s (Tangang, et al., 2007) and that there have been an increasing number of hot days and warm nights with an overall decline in cooler weather (Manton, et al., 2001; Caesar, et al., 2011). Furthermore, an increase in the frequency of heavy (top 10% by amount) and light (bottom 5%) rain events and a negative trend in moderate (25 to 75%) rain events has been observed (Lau & Wu, 2007). Annual total rainfall has increased by 22 millimetres per decade, while rainfall from extreme rain days has increased by 10 mm per decade (Alexander, et al., 2006; Caesar, et al., 2011), with a component of the increased rainfall down to more intense tropical cyclones making landfall. Meanwhile, AR5 notes reduced precipitation in Indonesia during July to October due to the pattern of Indian Ocean warming. It is important to emphasise that it is currently unclear to what extent the regional changes are a consequence of anthropogenic climate change. There are large natural decadal fluctuations of rainfall in the region and the relative importance of these compared to anthropogenic influences has yet to be established.

For future climate, AR5 indicates a median increase in temperature over land ranging from 0.8°C in RCP2.6 ("low" greenhouse gas concentrations) to 3.2°C in RCP8.5 ("high" greenhouse gas concentrations) by the end of this century (2081–2100). A moderate increase in precipitation is projected for S.E. Asia: 1% in RCP2.6 ("low" greenhouse gas concentrations), increasing to 8% in RCP8.5 ("high" greenhouse gas concentrations) by 2100 (see Figure 2.1 below for results for RCP4.5, "medium" greenhouse gas concentrations). On islands neighbouring the southeast tropical Indian Ocean, rainfall is projected to decrease during July to November, consistent with a slower ocean warming in the east than in the west tropical Indian Ocean. However, owing to the poor ability of climate models to accurately simulate some of the important circulation features in the region, such as the Madden Julian Oscillation, future projections of regional climate extremes in West Asia, S.E. Asia and Australia are of low confidence.

Table 14.1 (continued)

RCP4.5			Temperature (°C)					Precipitation (%)				
REGION	MONTH*	Year	min	25%	50%	75%	max	min	25%	50%	75%	max
Southeast Asia (land)	DJF	2035	0.3	0.5	0.7	0.8	1.1	-2	1	2	4	12
		2065	0.6	1.1	1.3	1.6	2.2	-1	1	3	8	13
		2100	0.8	1.4	1.6	2.2	3.0	-5	2	6	9	19
	JJA	2035	0.3	0.6	0.7	0.8	1.2	-3	0	1	3	7
		2065	0.7	1.1	1.2	1.5	2.2	-2	0	3	7	13
		2100	0.8	1.4	1.5	2.0	2.7	-3	2	4	9	19
	Annual	2035	0.3	0.6	0.7	0.8	1.2	-2	0	1	3	8
		2065	0.7	1.1	1.2	1.6	2.2	-1	1	3	7	13
		2100	0.8	1.4	1.6	2.1	2.7	-2	2	5	10	18
Southeast Asia (sea)	DJF	2035	0.3	0.5	0.6	0.7	1.1	-3	0	2	3	9
		2065	0.6	0.9	1.1	1.3	1.9	-4	0	3	6	10
		2100	0.9	1.2	1.4	1.7	2.5	-5	1	3	6	11
	JJA	2035	0.3	0.5	0.6	0.6	1.0	-4	0	1	2	7
		2065	0.7	0.9	1.1	1.3	1.9	-2	2	3	5	9
		2100	0.9	1.2	1.4	1.7	2.5	-1	2	3	6	16
	Annual	2035	0.3	0.5	0.6	0.7	1.0	-4	0	2	3	8
		2065	0.6	1.0	1.1	1.3	1.9	-2	1	3	5	7
		2100	0.9	1.2	1.4	1.7	2.5	-3	2	4	6	9

Figure 2.1: Percentage changes in temperature and precipitation for S.E. Asia according to model in the CMIP5 ensemble using RCP 4.5 (medium level greenhouse gas concentrations).

The El Niño Southern Oscillation (ENSO) has a significant impact on both temperature and rainfall in many parts of S.E. Asia. In AR5, confidence in projected changes in ENSO and related regional phenomena for the 21st century remains low. However, because of increased moisture availability, the remote rainfall response associated with ENSO could increase in amplitude. Studies since AR5 have indeed demonstrated that this is the case for the western Pacific region (Power, et al., 2013) but the analysis for the S.E. Asian region has yet to be carried out.

AR5 notes improved skill of climate models in reproducing climatological features of the global monsoon. This is noted specifically for the southwest summer Asian monsoon in climate models used in AR5 (the “CMIP5” models) in comparison to models used in the previous assessment report (Sperber, et al., 2012). These climate models show agreement with each other in how the monsoon is predicted to change in the future. In summary, the global monsoon system (considering all global monsoon systems together) is likely to strengthen in the 21st century with increases in its area and intensity, while the monsoon circulation weakens. Monsoon onset dates are likely to become earlier or not to change much and monsoon retreat dates are likely to be delayed, resulting in lengthening of the monsoon season in many regions. These results are generally confirmed by CMIP5 projections (Chaturvedi, et al., 2012; Seth, et al., 2013). Furthermore, AR5 notes that future increases in precipitation extremes related to the monsoon is very likely in S.E. Asia and other regions of the world. There is less agreement among global models regarding monsoon-related interannual precipitation variability, resulting in “medium confidence” that it will increase in the future.

The above results have relevance to the northern regions of S.E. Asia but less so in the western Maritime Continent region. In fact, the analysis in Ar5 did not consider impacts of climate change directly on the monsoon systems in this latter region. The mechanisms by which rainfall changes in the tropical region are quite complex and appear to be a combination of the ‘warm gets wetter’ and ‘wet gets wetter’ mechanisms that have been widely discussed in the literature (see Huang, et al., 2013).

While an increasing frequency of extreme events has been observed in northern areas of S.E. Asia, decreasing trends in such events are reported in other regions (Chang, 2011). In Peninsular Malaysia during the Southwest Monsoon season, total rainfall and the frequency of wet days decreased, but rainfall intensity increased in much of the region (Deni, et al., 2010). During the Northeast Monsoon, total rainfall, the frequency of extreme rainfall events, and rainfall intensity all increased over the peninsula (Suhaila, et al., 2010). However, as already noted, there is little direct evidence that these changes can be attributed to man-made climate change and naturally occurring decadal variability has also probably played some role. An important question for the region is to establish on what timescale is the increases in rainfall extremes expected from global warming, can be expected to ‘emerge’ beyond the range of natural decadal timescale variability.

High-resolution model simulations are necessary to resolve complex terrain such as in S.E. Asia (Nguyen, et al., 2012). In a RCM downscaling simulation using the SRES A1B “medium” emission scenario (Chotamonsak, et al., 2011), regional average rainfall was projected to increase with an increase in summer monsoon, though there is a lack of consensus on future ENSO changes. The spatial pattern of change is similar to that projected in the previous IPCC (fourth) assessment report (IPCC, 2007). The ECHAM5 GCM, one of the GCMs used in the DURIAN experiments, was downscaled over a sub-region of S.E. Asia (among other regions in Asia) using the RegCM4 regional climate model, showing an increase of 3-5 degrees Celsius for temperature and indeterminate change in rainfall, with the **recommendation that ensemble simulations using additional RCMs driven by other GCMs are needed** (Gu, et al., 2012).

Figure 2.2 and Figure 2.3 below, taken from the supplementary material of AR5 chapter 14, show a common feature for projections of temperature and precipitation in the global climate models (the CMIP5 GCM ensemble) that were used to inform AR5. These figures show results over S.E. Asia land only for two different seasons (June to August for temperature and April to September for precipitation). A colour is assigned to each RCP greenhouse gas concentration, and to the right of the plot, the total range is given for each RCP, with the median a horizontal line through the middle box. These figures illustrate that there is greater certainty in the model results as far as changes to average surface air temperature (in which the results for various RCPs are distinguishable from each other, and all increasing in reference to present-day averages) than for precipitation (in which no strong change can be detected in the RCPs). Overall, the confidence in increasing surface air temperature is much higher than confidence in changes to precipitation for the region.

All in all, AR5 reports this for S.E. Asia: **warming is very likely to continue with substantial sub-regional variations. There is medium confidence in a moderate**

increase in rainfall over continental S.E. Asia but to the south there is generally a drying tendency, although this may not be significant relative to the natural decadal variations in this region. Strong regional variations are expected because of terrain. Extreme heavy rainfall events are projected to increase across the whole region.

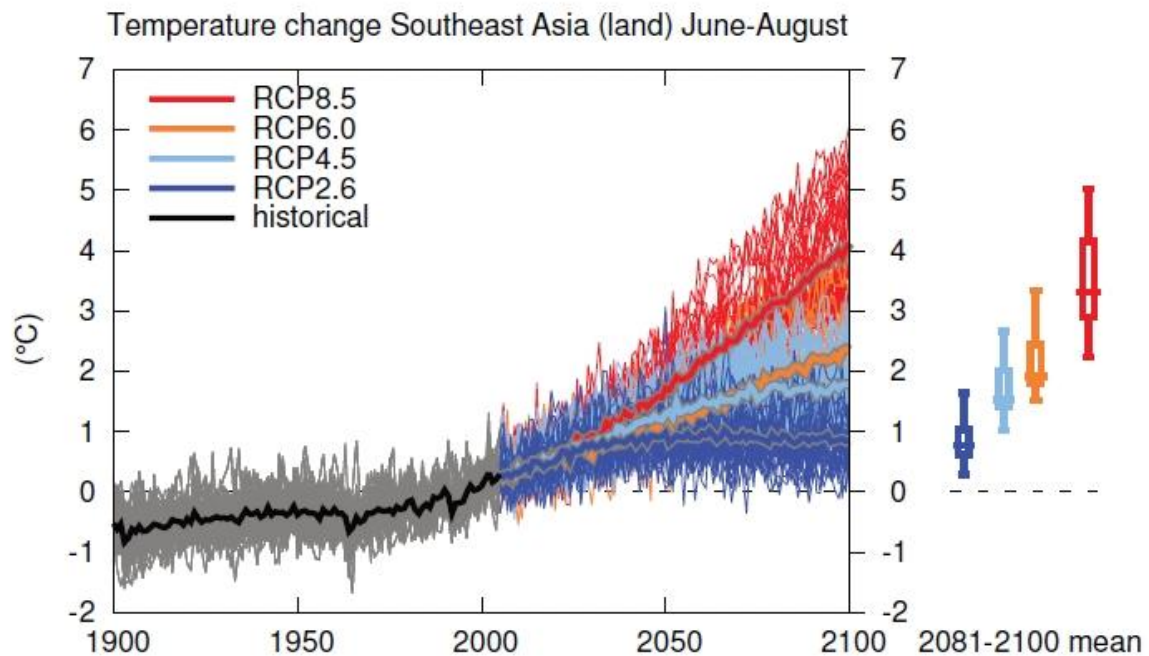


Figure 2.2: Temperature change for S.E. Asia (land areas only) during June-August only in CMIP5 global models for the four RCP greenhouse gas concentration levels. The changes in temperature are clearly identifiable in the various RCPs.

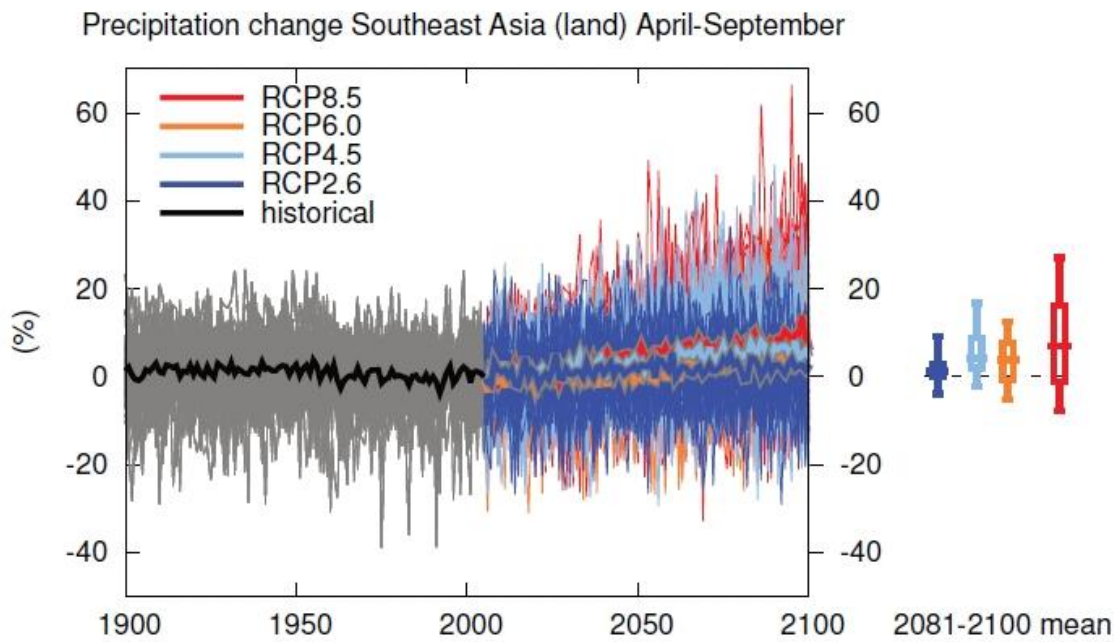


Figure 2.3: Precipitation change for S.E. Asia (land areas only) during April-September only in CMIP5 global models for the four RCP greenhouse gas concentration levels. The results for precipitation are not clearly distinguishable among the RCPs.

3. Assessment of End-users' Needs

A survey was conducted prior to the Phase 1 workshop in Cambodia to gather information on the needs of potential users of regional climate projections. This helped in scoping the project and in directing the type of analyses that were needed to be done. In the survey, example of questions that were asked touched on the type of climate variables the respondents required and the corresponding time frequency, the data format that they would be comfortable with, their focus areas in climate change, as well as how the climate projections data would be used.

3.1. Quantitative responses

All together there were 41 respondents from 25 national agencies and research institutes around the region. Of these, a large proportion of the respondents come from the hydrology (54%), the ocean/marine (41%), and the agricultural sectors (39%) (Figure 3.1).

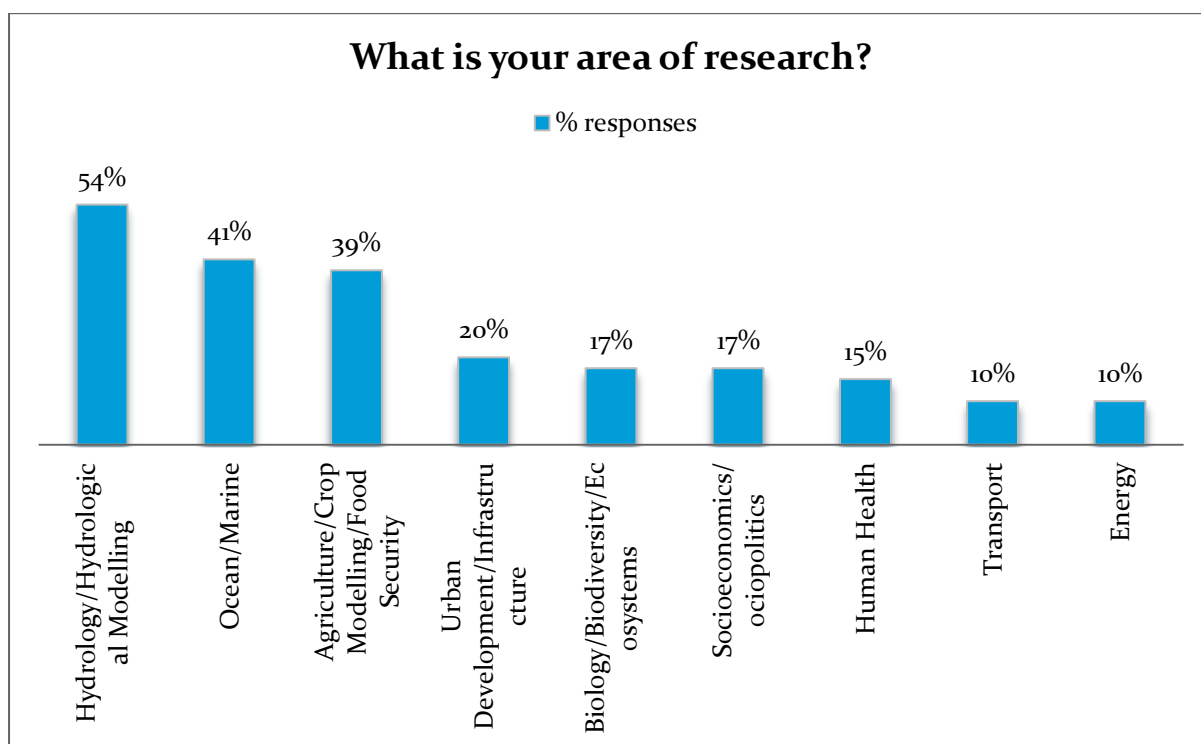


Figure 3.1: Respondents' area of research or work. Note that percentages do not add up to 100% as some respondents were involved in multi-faceted work areas.

Among the climate variables that could be generated by regional climate models, surface air temperature, large scale precipitation, surface winds, and convective precipitation came up as being the more commonly required variables (Figure 3.2). Respondents also indicated interest in all time-resolution for the data, which include annual, seasonal, monthly and daily mean values. Such requirements for the climate variables tie in well with the area of research or focus that most respondents were involved in (Figure 3.1). On the logistical aspects of the climate data, most respondents preferred the NetCDF data format, followed by the text or CSV format (Figure 3.3). The HTTP and FTP modes were preferred for downloading of data for use in further work and analyses (Figure 3.4).

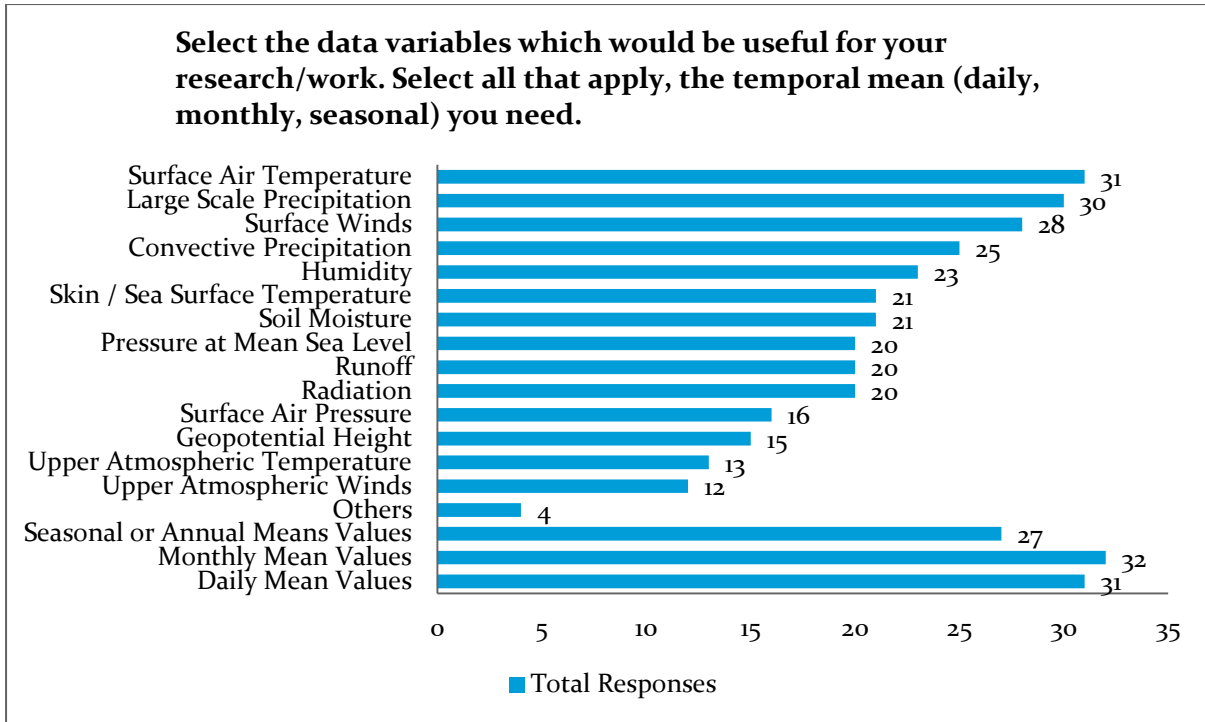


Figure 3.2: Climate variables required by respondents including the time resolution required for the variables.

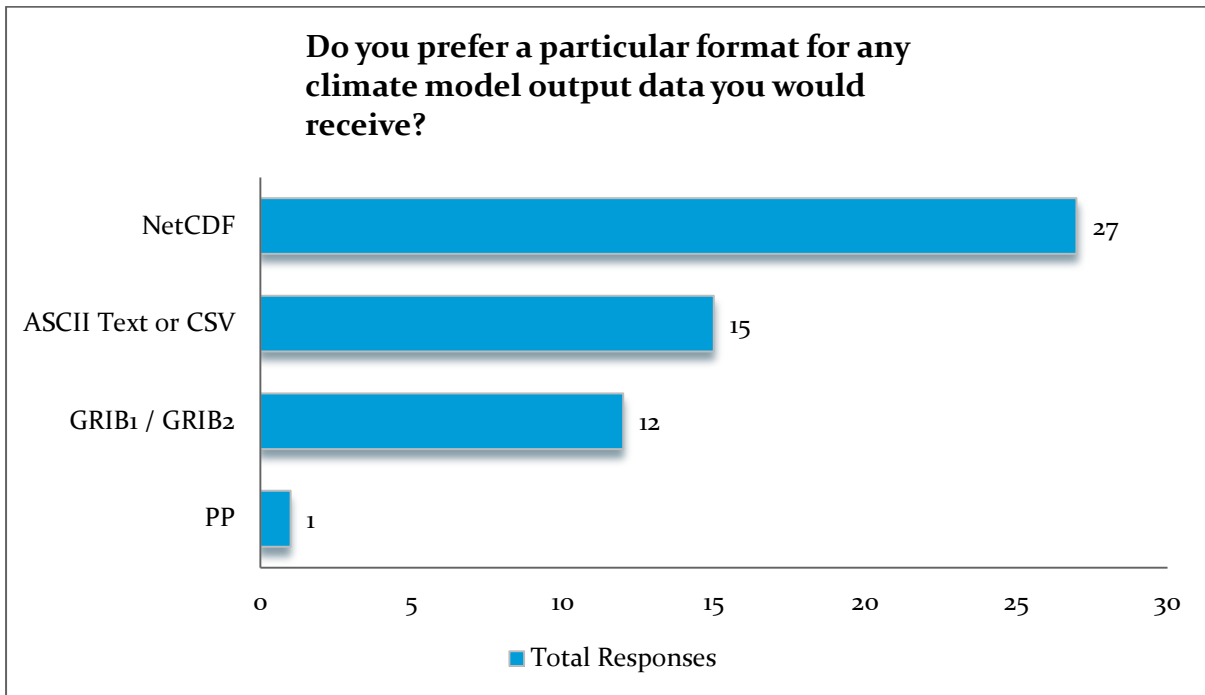


Figure 3.3: Data format for regional climate model output that user would prefer.

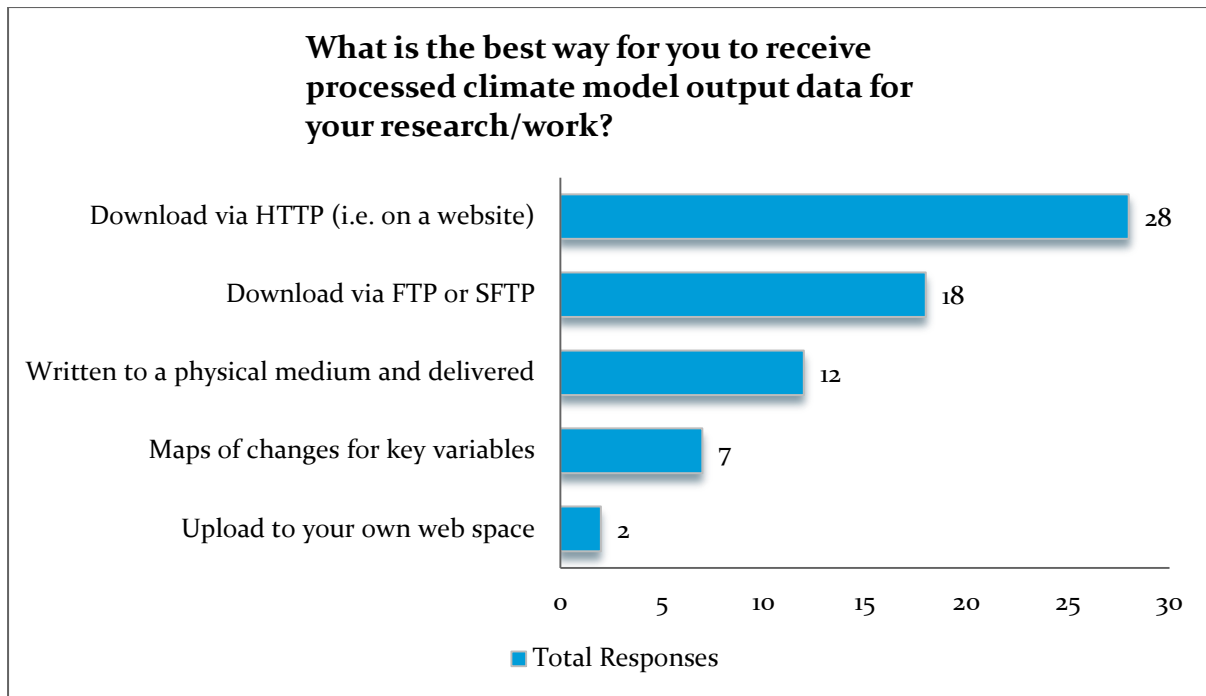


Figure 3.4: Modes of delivery and availability of regional climate model output data.

3.2. Qualitative responses

A number of questions were designed as open-ended to seek free-flowing comments and suggestions from the respondents on regional climate work and data. In terms of the work and research objectives that the respondents undertake and how they could have previously used regional climate projections data, a significant number responded saying much of the work they were doing was to support downstream studies in climate impacts and adaptation, which would require downscaled outputs from regional climate models. The areas where the work they were doing would be applied to include, water resources and drainage management (droughts and floods), and the management of risk from extreme events such as heavy rainfall and extreme temperatures. A number of notable qualitative responses were also compiled to highlight the issues faced and areas of focus by the respondents and the region they represent. These relevant sections of the replies are quoted as follows:

- “... assess the impact of climate change on its **water resources** in order to manage it in sustainable way...”
- “... alarming change in the past decade with respect to climate and its effects on **agriculture, fisheries, drought**. But **proper training** in using/running these models are missing. Appreciate if you can conduct a training in S.E. Asia ...”
- “... **sea level rise, coastal erosion, (flash) flooding, landslides**, groundwater salinisation, increasing temperature and warm nights/days ...”
- “... impact on **rainforest, haze**...”
- “... The land-use change, increasing temperatures and **erratic pattern** of weather ...”

- “... agricultural, fisheries influence of climate change, **food security, renewable energy ...**”
- “... we need **adaptation strategy ...**”
- “... users need to **truly know the meaning** of climate projections so as to avoid making wrong decisions ...”
- “... variables must demonstrate sufficient validity (bias correction, ability to reasonably replicate seasonality, etc.). Merely uploading variables **without sufficient user education** is dangerous...”
- “... The **need for greater access** to various types of climate information products is immense; however, **capacity to interpret and correctly use the information is low**. I greatly worry that information portals without sufficient user education and outreach will actually cause greater harm and ultimately lead to **maladaptation...**”
- “... change in rainfall patterns and inter-annual **variability...**”
- “... change in **tropical cyclone** numbers, ENSO, NE Monsoon...”
- “... cold spells, hot spells ...”

In summary, the responses from the survey provided useful insights into the requirements of potential users of regional climate projections data. They have highlighted a number of vulnerability areas related to climate change, which include water resources, agriculture, fisheries, coastal erosion, and extreme weather impacts on the population. They have also highlighted on the training needs to process, analyse, and most crucially to interpret climate data. These responses had help to formulate the design of the SEACAM experiments (discussed in the next section) and the subsequent provision of climate data to the regional community.

4. Model Configuration, Datasets and Experimental Design

This section of the report briefly describes the configuration of HadRM3P (the regional climate model used in PRECIS), the experimental design of the SEACAM project and the data used for evaluation. It is split into the following subsections:

- Regional climate models and the formulation of HadRM3P
- Domain
- Driving data and emissions scenario
- Time periods for analysis
- Observational data used for the evaluation

4.1. Regional climate models and the formulation of HadRM3P

Climate models divide the atmosphere and/or ocean into three dimensional grids of discrete computational units, which are called grid boxes. On this grid, discrete versions of the equations of motion and energy transfer are formulated and integrated forward in time. In addition to the discretised equations, climate models must also be able to represent atmospheric processes that occur at spatial scales smaller than the area of the model grid box (e.g. clouds). The average effect of these small scale processes over the whole grid box is estimated. This is referred to as *parameterisation*.

Global climate models (GCMs) cover the whole globe and typically contain atmosphere, ocean and land components. In contrast, regional climate models (RCMs) cover only a limited area of the Earth's surface. RCMs are typically run at higher resolution than GCMs in order to add detail to the 'big picture' description given by GCMs, a process also known as downscaling. As RCMs cover a limited area, they require input data to be provided at the edges of their regional domain. This meteorological input data can either come from a GCM or from observations. RCMs typically do not include ocean models and consequently sea surface temperatures need to be provided (again these can either come from a GCM or from observations).

Global climate models (GCMs) cover the whole globe and typically contain atmosphere, ocean and land components. In contrast, regional climate models (RCMs) cover only a limited area of the Earth's surface. RCMs are typically run at higher resolution than GCMs in order to add detail to the 'big picture' description given by GCMs, a process also known as downscaling

In SEACAM, we use a modified version of the HadRM3P regional climate model which is based on the atmospheric and land surface components of the HadCM3 climate model (Gordon, et al., 2000), and described in more detail in Annex 1 of the PRECIS scientific handbook (Jones, et al., 2004).

In HadRM₃P, surface boundary conditions are required over ocean grid boxes, where the model needs a sequence of successive values of sea surface temperatures. Lateral boundary conditions (LBCs) provide dynamical atmospheric information at the latitudinal and longitudinal edges of the regional model domain. LBCs contain surface pressure, horizontal wind components and measures of atmospheric temperature and humidity. Lateral boundary conditions (including sulphur dioxide, sulphate aerosols and associated chemical species) for the representation of the atmospheric sulphur cycle¹ are provided when downscaling a HadCM₃Q model (see below).

HadRM₃P can be run at two resolutions: 0.44° (~50 km) and 0.22° (~25 km). We use 0.22° in this project to allow for the better representation of small islands and coastlines, which are very important in Southeast Asia. The model used in this project differs from HadRM₃P only in the version of the land surface scheme used. This is the sub-model that climate models use to simulate interactions between the land and the atmosphere. Our modified version of HadRM₃P uses the MOSES 2.2 land surface scheme (Essery, et al., 2003).

4.2. Domain

Regional climate models are designed to add local details to the 'big picture' description given by the driving GCM (i.e. the GCM which is providing input to the RCM at the boundaries). Maintaining this consistency with the driving GCM ensures that a similar range of future climate projections in the driving global models are present in the RCM results. The improved representation of smaller spatial scales is the reason for performing downscaling experiments. Careful consideration of both the size and location of the domain is required to ensure that these criteria are met.

The SEACAM domain was originally designed to include all of the ASEAN countries; however the size of the original region caused technical problems with the model runs and would have required too long to simulate. Consequently it became necessary to reduce the eastern extent of the domain to 135°E, causing the West Papua region of Indonesia to be excluded.

The proposed domain was sent to participants of the SEACAM project such that they could ensure that any grid boxes containing islands or cities near the coast in their countries were represented as land points and not as ocean. The final domain is shown in Figure 4.1 and was agreed upon by all participating institutes.

¹ The atmospheric sulphur cycle describes the transportation of sulphur in the atmosphere along with the transformations (caused by chemical reactions) between the different compounds that contain sulphur (see http://www.atmosphere.mpg.de/enid/Nr_6_Feb__2__6_acid_rain/C__The_sulphur_cycle_5j9.html)



Figure 4.1: Domain used in experiments. Blue indicates that the grid box is an ocean grid box. Green indicates that the grid box is land. Political boundaries are marked with red lines. The darker rim between the edge of the picture and the orange line is where the lateral boundary conditions (LBCs) are applied - output in this region is not analysed.

4.3. Driving data and emissions scenario

Exploring the range or spread of future climate projections from different GCMs enables us to gain a better understanding of the uncertainties in climate change scenarios that result from differences in each GCM's specific model formulation. The selection of global climate models to downscale for SEACAM has been strategically chosen to sample this range.

Climate change projections made using different future greenhouse gas emission scenarios and one climate model often follow the same spatial patterns of change and only vary in terms of magnitude. This is not the case for climate change projections produced using different climate models. Consequently in SEACAM, we have decided to focus resources on downscaling a range of different global climate models and use just one emissions scenario.

The remainder of this sub section describes:

- The emission scenario
- Two different types of climate model ensembles that sample different sources of modelling uncertainty
- The selection of global models chosen for SEACAM

4.3.1. Choice of emissions scenario

The special report on emissions scenarios (SRES) was written in 2000 by the (IPCC, 2001). This report presented a set of six emissions scenarios ('the SRES scenarios') that were used in the third and fourth IPCC assessment reports. Emissions scenarios are plausible representations of future levels of substances that influence the total energy/heat in the atmosphere (e.g. green house gases) or which can affect the heat-contributing atmospheric substances (e.g. sulphur dioxide, which forms sulphate aerosols). The scenarios are based on a coherent and internally consistent set of driving forces such as demographic and socio-economic developments.

In SEACAM, the A1B scenario is used for all projections. This scenario is based on the following assumptions:

- Rapid economic growth.
- A global population that reaches 9 billion in 2050 and then gradually declines.
- The quick spread of new and efficient technologies.
- A convergent world - income and way of life converge between regions. Extensive social and cultural interactions worldwide.
- A balanced emphasis on all energy sources (i.e. between fossil and non-fossil).

4.3.2. The 'QUMP' 17 Member Perturbed Physics Ensemble (PPE)

As described in Section 4.1, climate models must be able to represent atmospheric processes that occur at spatial scales smaller than the area of the model grid box (e.g. clouds) through a method called parameterisation. Often parameterisations are based on statistical relationships with large scale variables and hence have various parameters associated with them. The true values of these parameters are often unknown.

An approach pioneered by the Met Office Hadley Centre (Murphy, et al., 2004) and climateprediction.net (Stainforth, et al., 2005) has been the use of climate model ensembles (sets of model simulations) that systematically explore the implication of known uncertainties in model parameters. Parameters are identified that are known to be uncertain and important for the model response to changing greenhouse gas concentration levels. A large number of model simulations are run that sample model parameter values across credible ranges that are determined by experts. This is called a Perturbed Physics Ensemble (PPE).

Boundary conditions that can be used to drive HadRM3P were output from a 17-member PPE that used the HadCM3Q climate model (Murphy, et al., 2007; Collins, et al., 2011). HadCM3Q is based on HadCM3 but differs in that it:

- Uses "flux adjustments" to correct systematic errors in sea surface temperature and ocean salinity. This helped produce a more realistic representation of the present day climate than in standard HadCM3.
- Includes the same representation of the atmospheric sulphur cycle that is used in HadRM3P.

The particular parameter combinations that make up the 17-member HadCM3Q ensemble were selected from a much larger ensemble of model configurations. These 17 models are often

referred to as the 'QUMP' ensemble, the name of the project under which they were developed (Quantifying Uncertainty in Model Predictions). The individual ensemble members are referred to as Q₀–Q₁₆, where Q₀ has the same parameter values used in the standard HadCM₃ coupled model.

4.3.3. Other types of global data and their availability for downscaling

In contrast to the perturbed physics ensemble approach, a multi-model ensemble contains many different climate models (rather than simply varying the parameters used in one model) and hence account for a wider range of structural choices in model formulation. Two examples of such ensembles include the Coupled Model Intercomparison Project, phase 3 (CMIP₃) (Meehl, 2007) and phase 5 (CMIP₅) (Taylor, et al., 2012).

Note that the GCM data required as input for driving regional climate models was not provided by all GCMs in the CMIP₃ ensemble, limiting the choice of input data to what GCMs had provided this data. **At the beginning of the SEACAM project, models from the CMIP₅ ensemble, the most up to date ensemble of GCMs, were not yet available.** Therefore data availability needed to be considered when selecting non Hadley Centre GCMs for the SEACAM experiments.

4.3.4. Driving GCMs for the SEACAM experiments

The QUMP members used for SEACAM are taken from the recommendations of McSweeney, et al. (2012). In this study the authors first assess whether individual ensemble members should be eliminated due to particularly poor performance in simulating the major features of S.E. Asian climate (specifically, the Asian summer monsoon). They then select members that capture a broad range of responses in temperature, monsoon characteristics and precipitation. **Their recommendations are the following members: Q₀, Q₃, Q₁₀, Q₁₁ and Q₁₃.**

The Max Planck Institute ECHAM₅ (Roeckner, et al., 2003) was also selected as a non Hadley Centre global model in order to provide some element of a Multi-Model Ensemble (MME). The choice of ECHAM₅ rather than another non Hadley Centre model was made largely by data availability, however McSweeney, et al. (2012) applied the same evaluation criteria used in determining the selection of appropriate QUMP models to all of the CMIP₃ models (including ECHAM₅), and they found no reason to eliminate ECHAM₅ due to poor performance.

In addition to climate models, we also downscale the ERA-40 reanalysis (Uppala, et al., 2006). Numerical weather prediction (i.e. forecasting) systems use observations to analyse the current state of the weather. Reanalysis data is produced by applying the same systems to past weather observations in order to build up a record of the past weather (i.e. of the three dimensional state of the atmosphere). **Driving regional models with reanalysis data allows us to assess the performance of the regional climate model on its own, without (or with minimal) errors coming from the driving data.**

4.4. Time periods for analyses

The global models in the SEACAM experiments were downscaled by HadRM3P from 1950-2100, however in this report we study three thirty-year sections. Thirty year sections have been chosen to adequately represent how the climate can vary naturally on scales of decades (for example, different phases of the ENSO)

To evaluate the ability of the models to reproduce the present day climate, we study the period 1971-2000. This period overlaps with the dates of the ERA-40 reanalysis (1957-2001). Two time periods have been chosen to analyse future climate projections. **The period 2071-2100 has been chosen in order to give a strong detectable signal for any possible climate changes, whilst 2031-2060 has been chosen as it is more policy relevant for near future adaptation activities.**

4.5. Observational data used for the evaluation

To evaluate surface air temperature and precipitation, we use two different gridded datasets. Gridded datasets represent an area average value over a grid box making them directly comparable to climate model output (which also contains averages of values over the whole grid box). The reliability of such datasets is known to be dependent on the number of observational stations (at fixed points) that are used in forming the gridded data, which is dependent on both the date and location. It is also known that there is more confidence in monthly averages of the gridded datasets in comparison to daily average data (see for example Haylock, et al., 2008). When evaluating the E-OBS dataset¹, a dataset of daily gridded temperature and precipitation, Haylock, et al. (2008) also find a systematic underestimation of extreme values. Differences in the interpolation methods used in the construction of gridded observational datasets also cause differences in their estimated values. **By using two datasets we explore some of these uncertainties associated with observations (although it should be remembered that the underestimation of extremes is typical in most gridded observational datasets).**

The datasets we use are APHRODITE (Yatagai, et al., 2012; Yasutomi, et al., 2011) and CRU-TS₃ (Harris, et al., 2013). The CRU-TS₃ data contains a time series of monthly mean data at a spatial resolution of a 0.5° square grid. APHRODITE contains daily mean precipitation and temperature on a 0.25° and 0.5° square grids. We use the 0.25° version as this is a similar resolution to our RCM output. The inclusion of daily mean data allows for the evaluation of extreme weather events, whilst noting the caveats in the above paragraph. Figure 4.2 shows the number of underlying stations used in the construction of the two datasets (for precipitation). In general, APHRODITE has a denser network of stations than CRU, although this is not the case everywhere. In addition, there are some areas (e.g. Borneo) where the station coverage is poor in both datasets.

¹ www.ecad.eu/E-OBS/

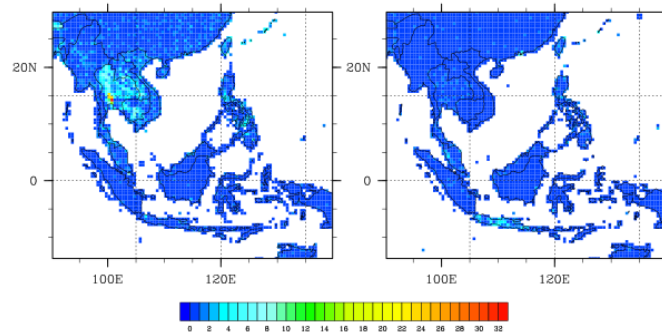


Figure 4.2: Left. The percentage of 0.05° sub grid boxes of each 0.5° grid box that contain actual precipitation observations used in APHRODITE for the year 2000. Right. The number of actual precipitation observations per grid box used in the CRU-TS₃ dataset for the year 2000.

In addition to the gridded datasets, a limited set of station data from Brunei and Singapore was used to evaluate the precipitation annual cycle, as the 2 gridded datasets used, CRU and APHRODITE showed some discrepancy. ERA-40 reanalysis data has been used to evaluate the 850 hPa and 200 hPa winds (the winds in the upper atmosphere). These levels have been chosen as they are important for evaluating monsoon circulation.

5. Assessment of Historical RCM Simulations

5.1. Why assess/evaluate RCM outputs?

An integral part of carrying out regional climate simulations of future climate change is to also generate historical simulations that can be compared with observations. With the availability of historical simulations, it enables assessing (or evaluating) the extent to which regional climate model (RCM) is able to realistically simulate the atmospheric processes and conditions in the statistical or climatological sense. Evaluating the RCM provides information on the extent to which the higher-resolution RCM is able to provide added-value over the coarse-resolution global climate model (GCM). Such information is important to users of future climate change projections, because it reveals aspects of the simulations which need to be treated with caution; for example, if there are systematic biases (or errors) arising from the model's limitations in simulating certain aspects of the long-term climate. On the other hand, evaluation of RCM outputs can also determine particular aspects of the long-term climate that are simulated well, and hence provide a degree of confidence in the use of the corresponding future climate change scenarios.

5.2. Method of evaluation

Six simulations were carried out for a period of 150 years from 1949-2099 by the MOHC PRECIS RCM at a horizontal resolution of 25 km. The RCM was driven by 6 different boundary conditions obtained from the GCM ensemble runs of HadCM3Q0, HadCM3Q3, HadCM3Q10, HadCM3Q11, HadCM3Q13 (Murphy, et al., 2007) and ECHAM5 (Roeckner, et al., 2003) and including ERA-40 reanalysis driven runs (Uppala, et al., 2006) (see sections 4.3.2 and 4.3.3 for details). Historical simulations from these, which run from 1949-2000, were evaluated against various datasets appropriate for the respective applications and also for subsets of the period that match available data. The evaluations were done in four broad categories (also termed “work packages”) as follow:

1. Annual cycle of temperature and precipitation
2. Mean temperature and precipitation
3. Circulation patterns during the Northeast and Southwest Monsoons, and
4. Extreme precipitation and temperature.

It is important to note that while comparisons of model outputs against observations provide some degree of information of model's ability to simulate the current climate, the datasets used in the assessment may have their own limitations (e.g. limited coverage in time and space, coarser grid-resolution than the model). Thus, where models are not able to simulate certain processes, and perhaps over certain regions (such as places of high elevation), these may not entirely be due to the model's own shortcomings, but could be contributed in part by errors in the observational dataset itself.

5.3. Evaluation of temperature and precipitation annual cycle

The annual cycles of temperature and precipitation (rainfall) represent the seasonal changes of temperature and precipitation averaged over an area. In general, model simulations of the annual cycle would be considered good if they are able capture the magnitude of maximum and minimum locations of the temperature and precipitation at the right times of the year.

5.3.1. Annual temperature cycle

Figure 5.1 and Figure 5.2 show the annual cycle plots of temperature averaged over the baseline period for individual S.E. Asia countries derived from the 6 RCM simulations, ERA-40 simulations, APHRODITE temperature dataset (Yatagai, et al., 2012) and CRU temperature dataset (Harris, et al., 2013). In all of the plots in Figure 5.1 and Figure 5.2, the spatial average of the monthly values for individual countries had been derived by averaging over their respective masks. Although spatial averaging by country can be considered less than ideal for countries that span a wide range of longitudes and latitudes and therefore multiple climatologies (e.g. Indonesia), such information is nevertheless useful for end-users of climate projections as they need to know the overall performance of the RCM simulations over the areas within their national boundaries.

The hottest months for most of the countries in the region typically occur between March to June and the variations across different countries depend on the relative position in the latitudes. The cooler months, usually follow either the arrival of the Southwest Monsoon season where the large-scale precipitation cools down land surfaces (for regions in the higher latitudes – i.e. mainland S.E. Asia, and the Philippines), or the arrival of the cooler winter air from the north during the Northeast Monsoon season (for the entire region in general) and

Terminology for model outputs

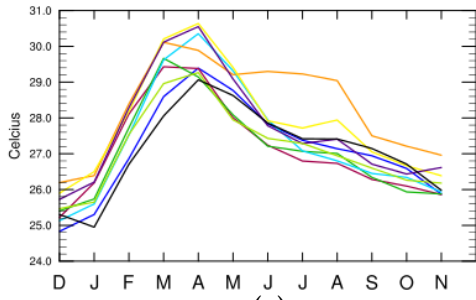
For better readability, we will be referring to the RCM-driven output of the HadCM3Q ensemble simply as 'HadCM3Q simulations', the RCM-driven output of ECHAM5 simply as 'ECHAM5 simulations', and the RCM-driven outputs of the ERA-40 reanalysis dataset simply as 'ERA-40 simulations'. All the 6 HadCM3Q and ECHAM5 simulations will be collectively referred to as the 'RCM simulations'. In drawing the distinction between the 'ERA-40 simulations' and the actual ERA-40 reanalysis dataset (not the output of from the RCM that is driven by ERA-40 itself), we will refer to the latter simply as 'ERA-40 reanalysis'. The projections from respective models will be called 'projections' itself.

the associated monsoon rain (for regions in the lower latitudes). Details of the temperature cycle that are unique to each country or sub-region are therefore influenced by the interaction between factors on various spatial and temporal scales, such as the seasons, the atmospheric circulation patterns, the monsoon systems, and the terrain (Chang, et al., 2005).

In general, all the downscaled climate model **simulations are able to simulate the temperature cycle well by capturing the observed peaks and dips across the year.** This is especially true for countries in the mainland S.E. Asia region which includes Cambodia, Laos, Myanmar, Thailand, and Vietnam, as well as the Philippines (Figure 5.2). A general feature of the RCM simulations over these regions, with the exception of the Philippines, is the over-prediction (warm bias) of the warm months and the under-prediction (cool bias) of the cooler months. These biases are consistent with respect to both APHRODITE and CRU as the observational datasets are in good agreement. On average, the warmer biases are stronger than the cool biases. As these characteristics are also observed in the ERA-40 simulations, it can be said that the annual temperature cycle for these countries has been artificially enhanced to some degree by the RCM. Slightly early onsets (by about a month) for some of the simulations are also observed in these parts of S.E. Asia.

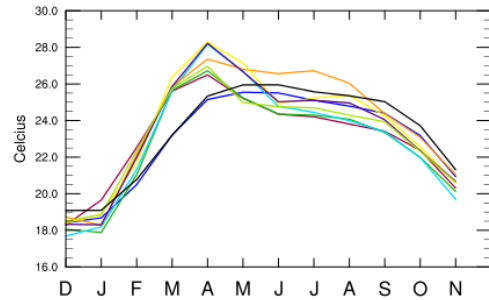
As for countries closer to the equator such as Brunei, Indonesia, Malaysia, Singapore and Timor Leste (Figure 5.2), the 6 RCM simulations show larger variability in comparison. These simulations under-predict for Brunei (with respect to APHRODITE; but not in relation to CRU) and over-predict for Singapore throughout the year (with respect to both APHRODITE and CRU). As for Malaysia and Indonesia, the biases are GCM-dependent; with the HadCM3Q0, HadCM3Q3, ECHAM5 simulations having cool biases, while the rest (HadCM3Q10, HadCM3Q11 and HadCM3Q13) have warm biases. In this instance the preceding analyses hold true for APHRODITE for both countries, but for Indonesia using CRU, all simulations have cool biases. For the Philippines, simulations generally have cool biases in the temperature cycle. **Overall, simulations generate biases that range from 1.0 to 2.0°C.**

Mean annual surface air temperature cycle for Cambodia



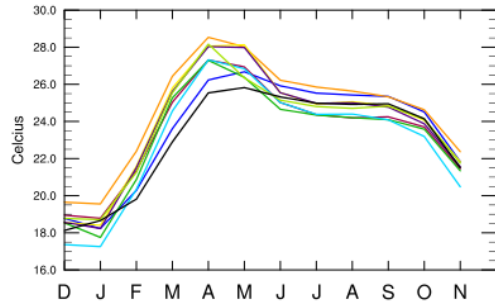
(a)

Mean annual surface air temperature cycle for Laos



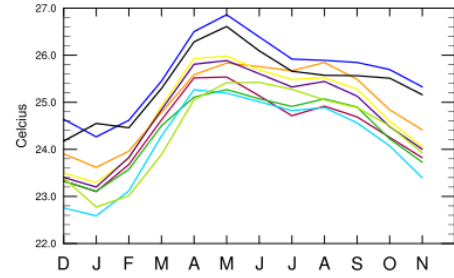
(b)

Mean annual surface air temperature cycle for Myanmar



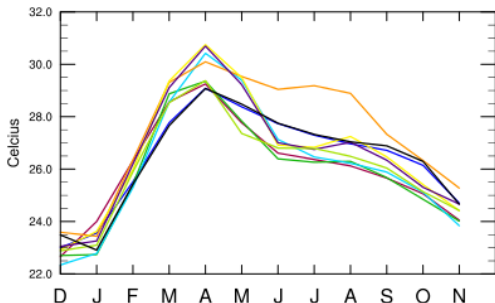
(c)

Mean annual surface air temperature cycle for Philippines



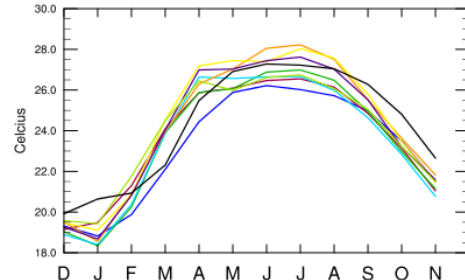
(d)

Mean annual surface air temperature cycle for Thailand



(e)

Mean annual surface air temperature cycle for Vietnam



(f)

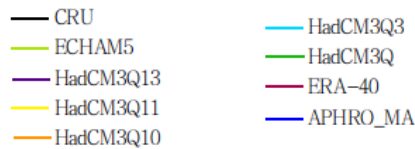


Figure 5.1: Annual cycle of observed (APHRODITE in dark blue; CRU in black), ERA-40 simulations (in maroon) and simulated surface temperature (HadCM₃Q₀: green, Q₃: light blue, Q₁₀: orange, Q₁₁: yellow, and Q₁₃: purple) for countries in the northern half of the region, i.e., (a) Cambodia, (b) Laos, (c) Myanmar, (d) Philippines, (e) Thailand, and (f) Vietnam for the baseline period (1971-2000) in degrees Celsius (°C).

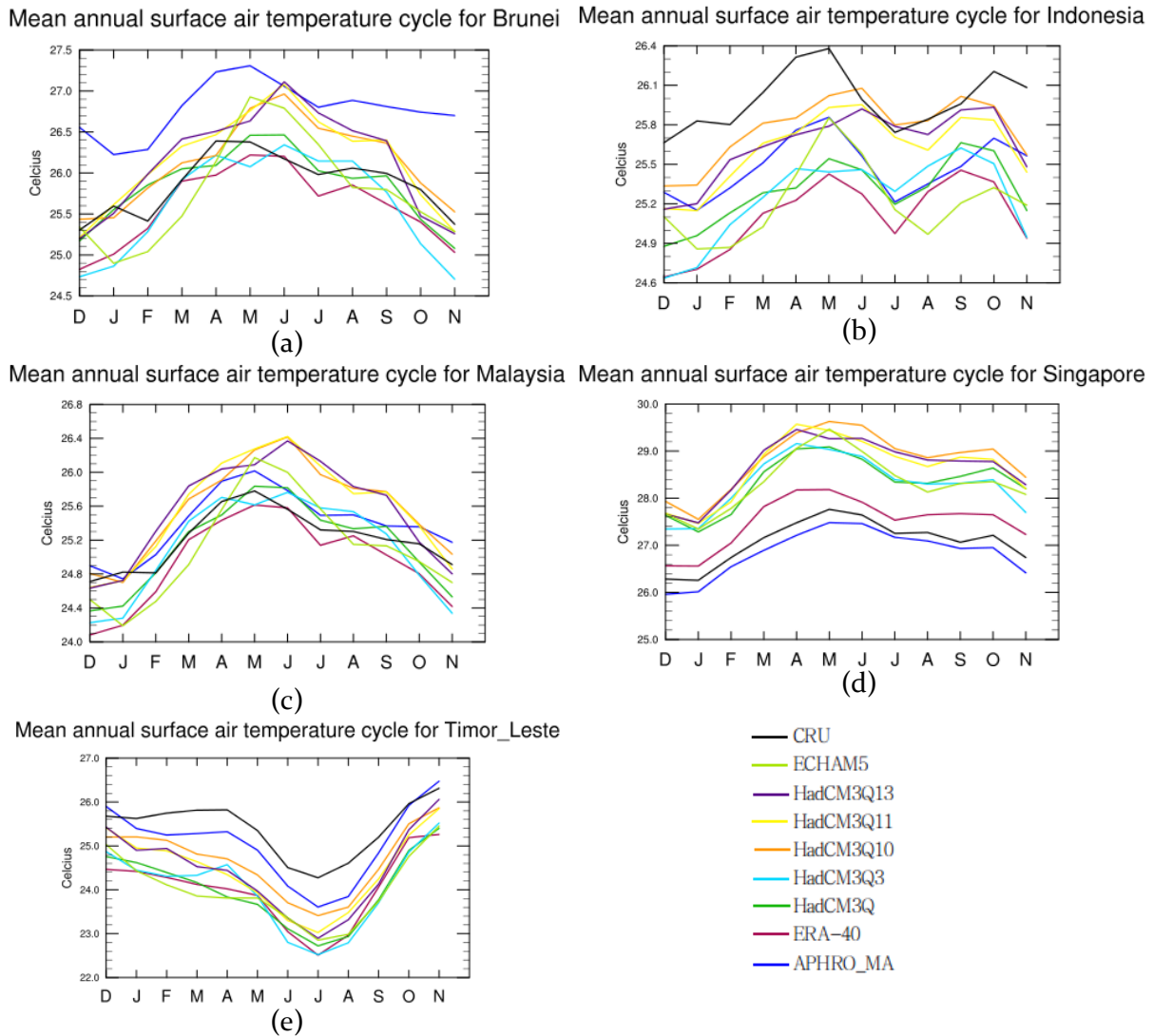


Figure 5.2: Annual cycle of observed (APHRODITE in dark blue; CRU in black), ERA-40 simulations (in maroon) and simulated surface temperature (HadCM₃Q_o: green, Q₃: light blue, Q₁₀: orange, Q₁₁: yellow, and Q₁₃: purple) for countries in the southern half of the region, i.e. (a) Brunei, (b) Indonesia, (c) Malaysia, (d) Singapore, and (e) Timor Leste for the baseline period (1971-2000) in degrees Celsius (°C).

5.3.2. Annual precipitation cycle

In Figure 5.4 and Figure 5.5, the annual rainfall cycles of the simulations are evaluated in a similar manner to the temperature cycle against APHRODITE and CRU for precipitation. For precipitation cycle, S.E. Asia can generally be divided into 3 sub-regions; in the north where the Southwest Monsoon is dominant during the middle part of the year (i.e. Cambodia, Laos, Myanmar, Philippines, Thailand, and Vietnam - Figure 5.4); in the middle, near the equator (i.e. Brunei, Malaysia and Singapore - Figure 5.5 (a), (c) and (d)) where rainfall is fairly uniform throughout the year, and is usually dominated by local, convective thunderstorms and consequently a *relatively* more subdued seasonality in precipitation; and in the south (i.e. Indonesia and Timor Leste - Figure 5.5 (b) and (e)) where the wet and dry seasons are mirror images of the counterparts in the north.

When the relative performance of the RCM simulations in these 3 regions was compared, the simulations' ability in capturing seasonal (monsoonal) rainfall of large-scale nature in the higher latitudes of the region stands out, compared to the ability in capturing local,

thunderstorm development in the lower latitudes. **The results for regions in the north and south are thus encouraging with the RCM simulations able to pick out the seasonal rainfall maxima during the June-September season (JJAS) for Cambodia, Laos, Myanmar, Philippines, Thailand and Vietnam and during the November-April season (NDJFMA) for Indonesia and Timor Leste. In contrast, the precipitation cycles, or lack thereof, for Brunei, Malaysia and Singapore are poorly captured in the RCM.** This could be due to the complexity of the processes that contribute to the rainfall in these regions, or their interactions with the terrain that have either not been captured well by the dynamics of the RCM or the resolution at which the RCM was run.

Although the model is able to simulate seasonal rainfall in the northern parts well in general (Figure 5.4), there are issues with regards to double-peaks, early onsets, and largely wet biases (especially in relation to APHRODITE with biases of up to 4.0-5.0 mm/day) in the simulations. In the southern locations, the simulations for Indonesia and Timor Leste seem to suggest early onsets of the dry season by about 2 months and late onset of the wet season by about 1-2 months. For the equatorial regions, no particular simulation stands out in being able to simulate the precipitation cycle reasonably. Despite this, wet biases in this region are relatively smaller in the range of 3.0-4.0 mm/day (Figure 5.5). It is worth bearing in mind that the biases may not necessarily indicate an over-estimation of mean rainfall, but could be contributed in part by under-estimations of precipitation by the gridded-observation dataset. As can be seen when comparing between APHRODITE and CRU, APHRODITE seem to suggest that the simulations have serious wet biases, but these are not evident in the CRU dataset. Thus, simulations compare better against CRU, with the exception of the artificially looking peaks in January rainfall (see Figure 5.5a – d), which can be considered artefacts in CRU upon comparison with local station datasets for Brunei and Singapore (Figure 5.3).

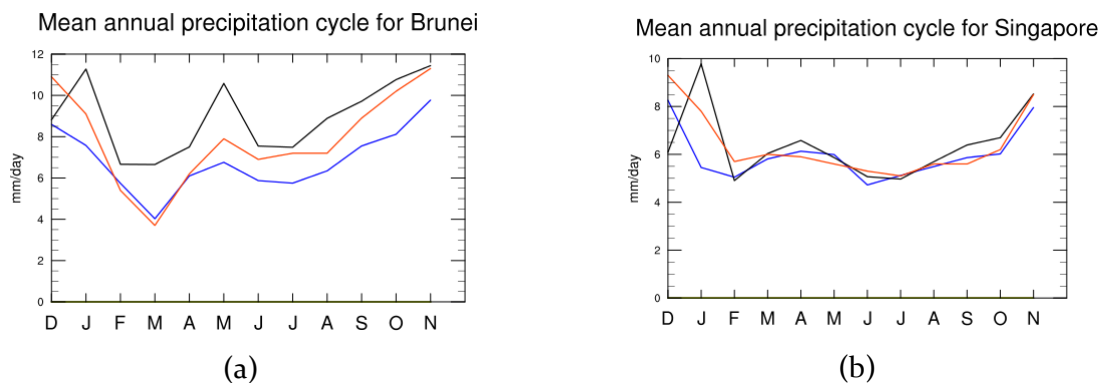
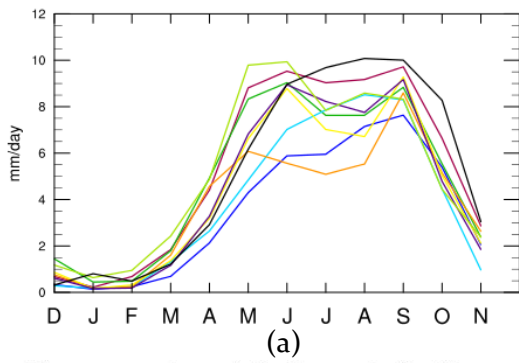
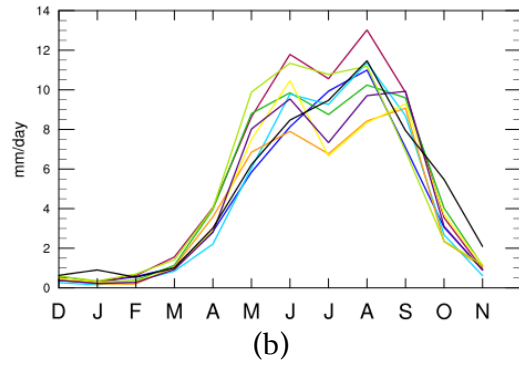


Figure 5.3: Comparisons of datasets between CRU (black), APHRODITE (blue), and station dataset (red) for (a) Brunei and (b) Singapore. This limited comparison suggests that the kink in CRU dataset for January is an artefact.

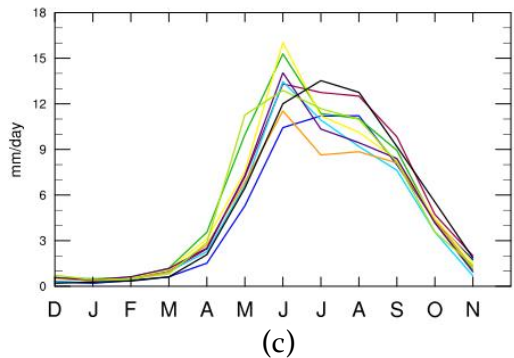
Mean annual precipitation cycle for Cambodia



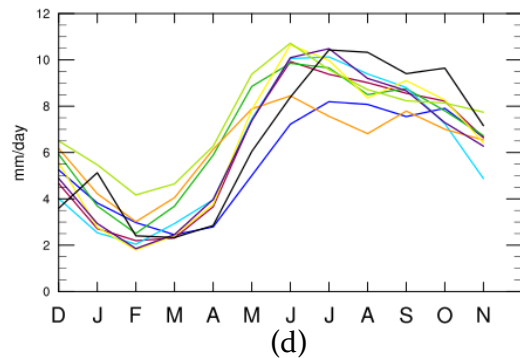
Mean annual precipitation cycle for Laos



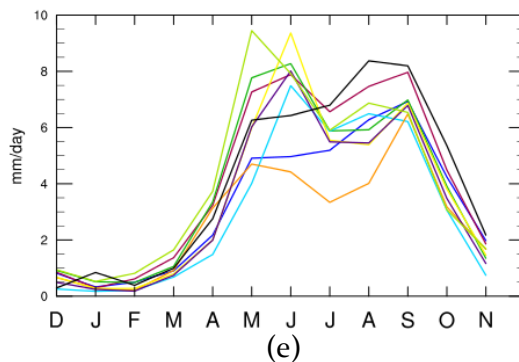
Mean annual precipitation cycle for Myanmar



Mean annual precipitation cycle for Philippines



Mean annual precipitation cycle for Thailand



Mean annual precipitation cycle for Vietnam

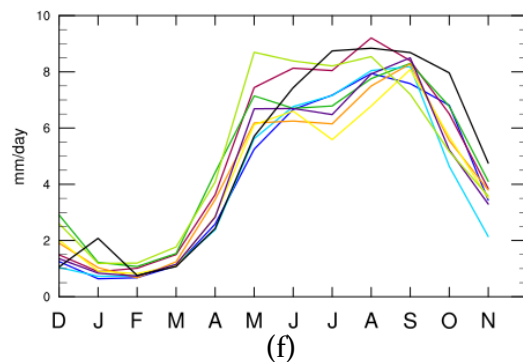


Figure 5.4: Annual cycle of observed (APHRODITE in dark blue; CRU in black), ERA-40 simulations (in maroon) and simulated precipitation (HadCM₃Q₀: green, Q₃: light blue, Q₁₀: orange, Q₁₁: yellow, and Q₁₃: purple) for countries in the northern half of the region, i.e., (a) Cambodia, (b) Laos, (c) Myanmar, (d) Philippines, (e) Thailand, and (f) Vietnam for the baseline period (1971-2000) in mm/day.

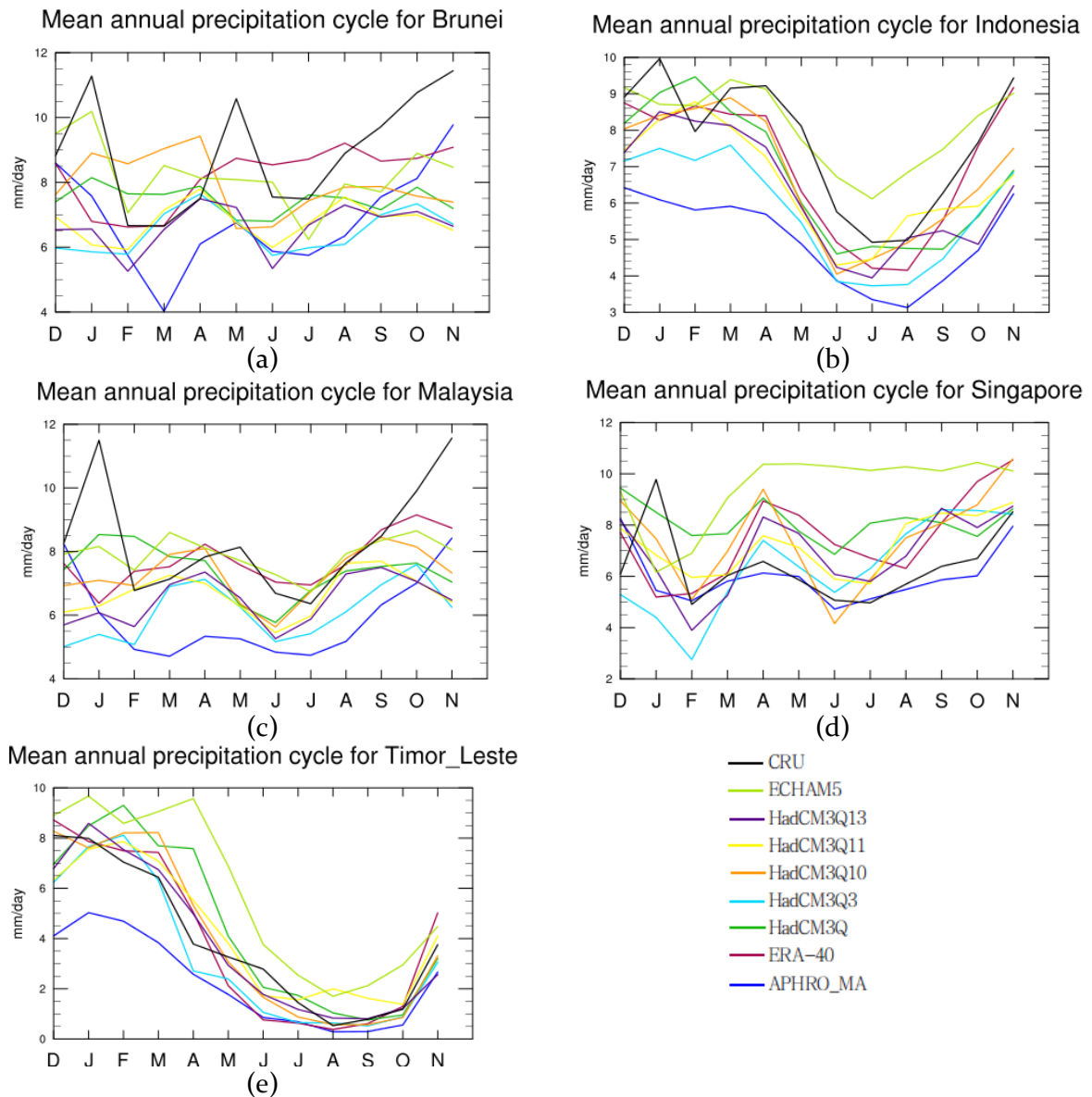


Figure 5.5: Annual cycle of observed (APHRODITE in dark blue; CRU in black), ERA-40 simulations (in maroon) and simulated precipitation (HadCM3Q0: green, Q3: light blue, Q10: orange, Q11: yellow, and Q13: purple) for countries in the southern half of the region, i.e. (a) Brunei, (b) Indonesia, (c) Malaysia, (d) Singapore, and (e) Timor Leste for the baseline period (1971-2000) in mm/day.

5.4. Evaluation of seasonal spatial distribution of temperature

Evaluation of seasonal *spatial distribution* of temperature (and also rainfall) across the domain provides additional information over the evaluation for annual cycle, which has been spatially averaged. For example, it can provide details of the location of biases unlike the annual cycle. Analysing model simulations in tandem with information on terrain can provide clues to the reasons behind reasonable or poor performance in the simulations. The downside of this type of analysis, however, is that the distribution of temperature or rainfall in time (as shown by the annual cycle plots) is not immediately obvious. The analyses from both types of assessment should thus complement, and provide a degree of consistency-check between them.

The surface temperature from the downscaling simulations was compared to the CRU gridded dataset used as observation. Before comparing, the PRECIS data was bi-linearly interpolated to the CRU's $0.5^{\circ} \times 0.5^{\circ}$ grids (Harris, et al., 2013). The biases were then calculated as the differences between the simulations and observations at each of the grid points (see Figure 5.6 - Figure 5.9 below).

5.4.1. Seasonal mean temperature

Generally, **the mean seasonal temperature biases range between $\pm 4^{\circ}\text{C}$ with considerable spatial and seasonal variations.** The biases are largely positive (warm biases) during the March - May (MAM) season especially over the mainland S.E. Asia region (Figure 5.6), while during September - November (SON) season, the biases are generally negative - i.e. cool biases (Figure 5.9). This is broadly consistent with findings from the evaluation of the annual cycle in temperature in Section 5.3.1. Consistent cold biases throughout the year are noted over the western coast of the Sumatra Island and larger parts of Indonesian Archipelago, eastern coast of Vietnam and northern Philippines. Over western Sumatra, Peninsular Malaysia and western Borneo, the biases are consistently positive (warm). Note that the model consistently produced cooler climate over the north-western edge of the simulation domain where the relief is considerably steep and complex. Also, the magnitude of the biases is generally larger over the northern region of the domain. This may indicate influence of noise propagating from the lateral boundaries from the northern side of the simulation domain.

Simulations vs Observation - DJF (1970-2000)

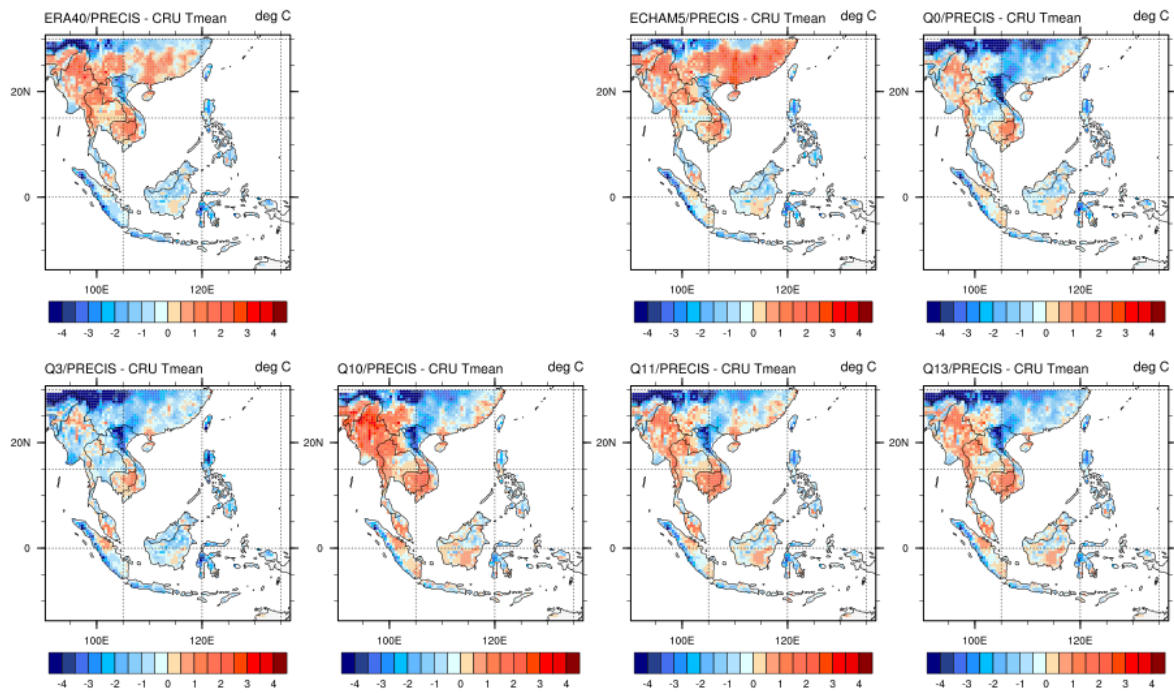


Figure 5.6: Difference between the spatial distribution of simulated (ERA-40, ECHAM5 and HadCM3Q0, 3, 10, 11, 13 simulations) and observed (CRU) DJF seasonal mean temperature in degrees Celsius (°C). Red shades show warm biases of simulations, while blue shades show cool biases of simulations.

Simulations vs Observation - MAM (1970-2000)

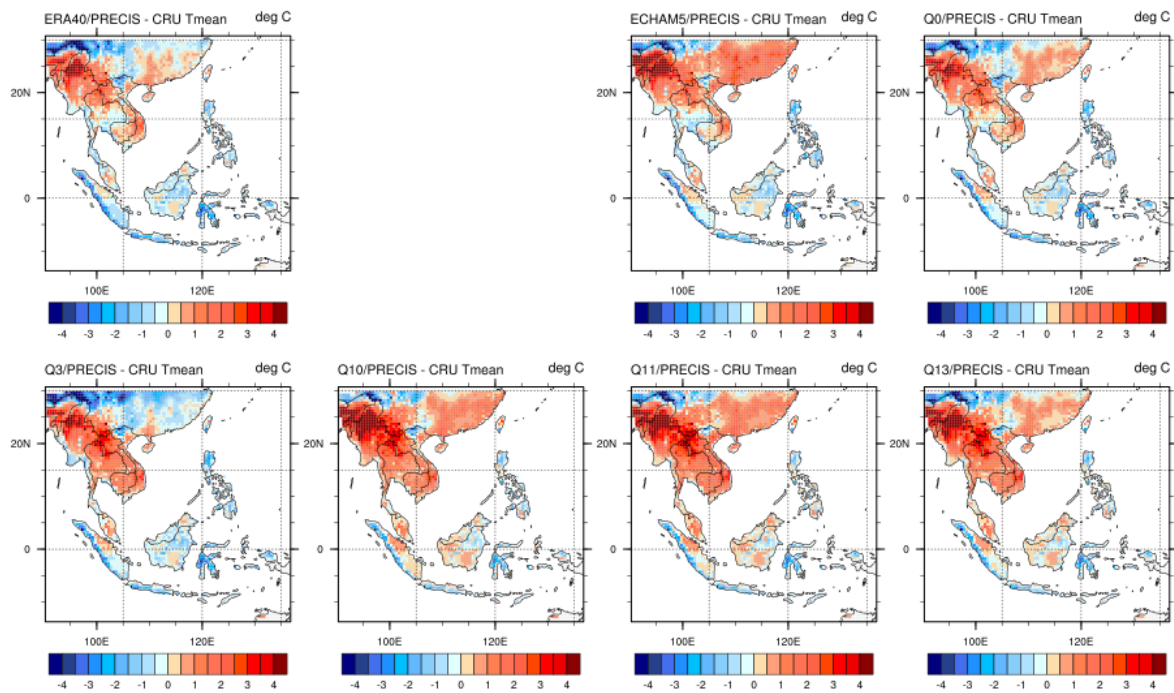


Figure 5.7: Difference between the spatial distribution of simulated (ERA-40, ECHAM5 and HadCM3Q0, 3, 10, 11, 13 simulations) and observed (CRU) MAM seasonal mean temperature in degrees Celsius (°C). Red shades show warm biases of simulations, while blue shades show cool biases of simulations.

Simulations vs Observation - JJA (1970-2000)

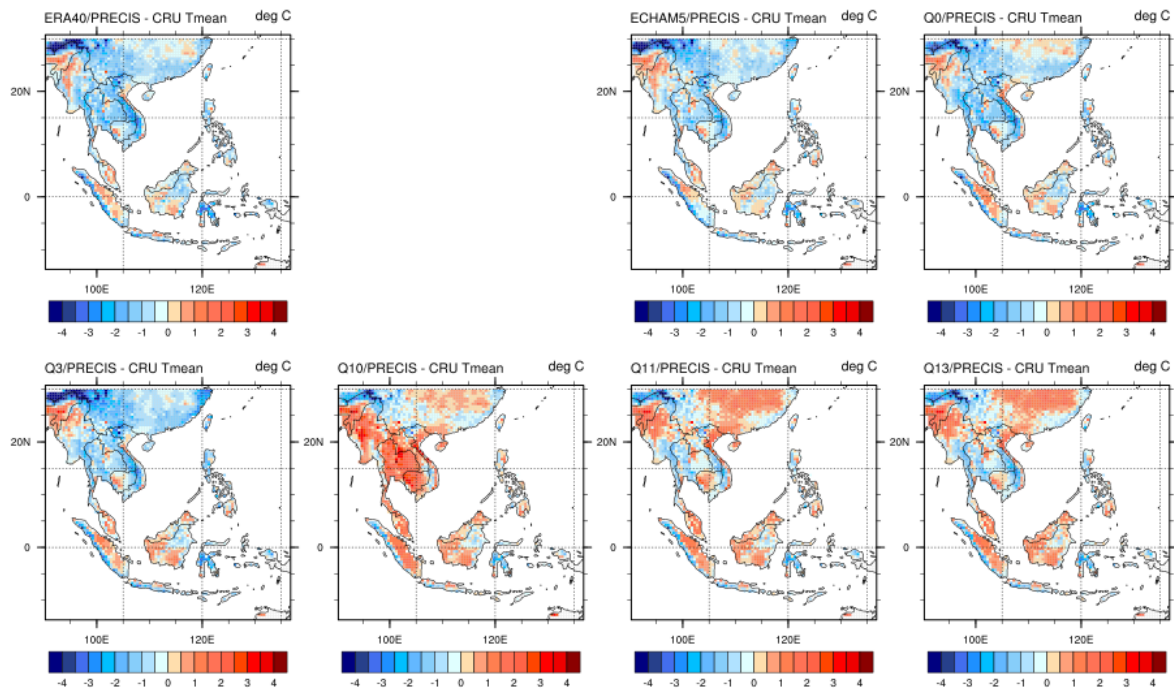


Figure 5.8: Difference between the spatial distribution of simulated (ERA-40, ECHAM5 and HadCM3Q0, 3, 10, 11, 13 simulations) and observed (CRU) JJA seasonal mean temperature in degrees Celsius (°C). Red shades show warm biases of simulations, while blue shades show cool biases of simulations.

Simulations vs Observation - SON (1970-2000)

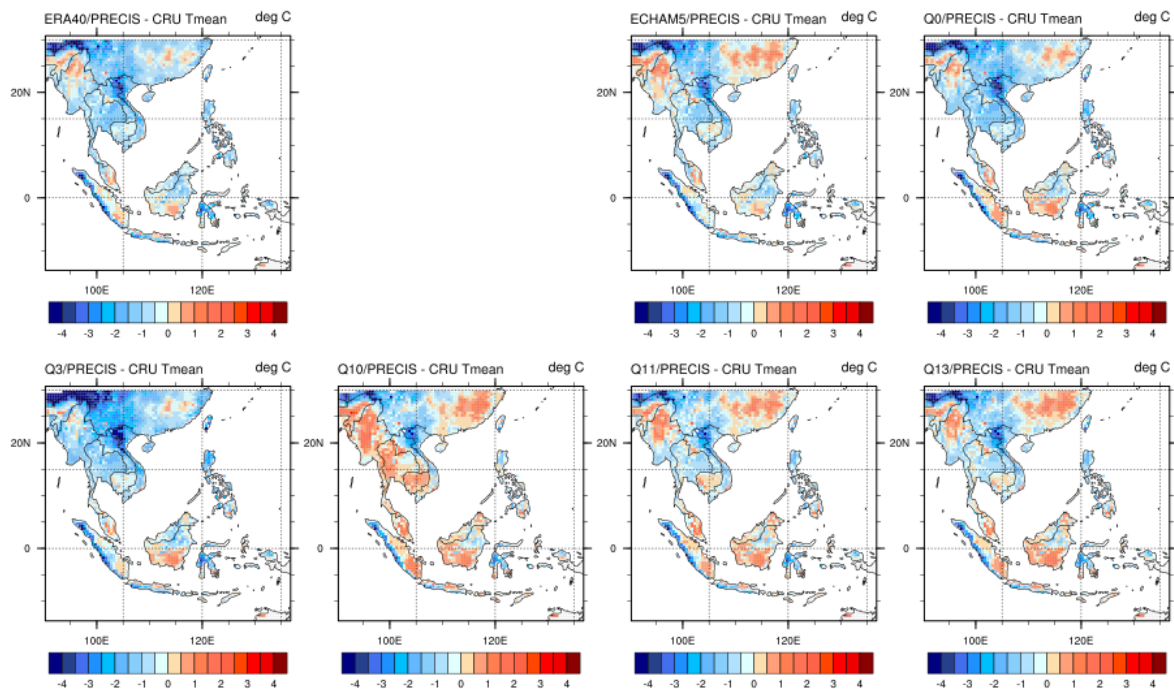


Figure 5.9: Difference between the spatial distribution of simulated (ERA-40, ECHAM5 and HadCM3Q0, 3, 10, 11, 13 simulations) and observed (CRU) SON seasonal mean temperature in degrees Celsius (°C). Red shades show warm biases of simulations, while blue shades show cool biases of simulations.

Generally, **spatial patterns of the biases in the RCM simulations closely resemble those in the ERA-40 simulations.** This indicates that the biases are largely sourced from the regional climate model that may not represent the regional land surface processes properly. In addition, the 0.22° (~25 km) grid resolution may still be too coarse to resolve the steep topography where the temperature gradient can be large, particularly over western Sumatra and eastern regions of mainland S.E. Asia near Vietnam. The ECHAM5 simulations generally show similar results to ERA-40 simulations. Among the HadCM3Q simulations, the HadCM3Q10 shows larger discrepancy especially during the June – August (JJA) season (Figure 5.9) and the SON (Figure 5.8) season. During these seasons, comparatively large warm biases extend from central to southern mainland S.E. Asia in the HadCM3Q10 simulation. It is expected that these large biases were inherited from the HadCM3Q10. During the December – February (DJF) season (Figure 5.6), the HadCM3Q3 simulations shows generally cooler climate over the mainland S.E. Asia region compared to other QUMP models.

5.4.2. Seasonal minimum and maximum temperature

The seasonal averaged maximum (Figure 5.10 - Figure 5.13) and minimum (Figure 5.14 - Figure 5.17) temperature were also examined and compared to CRU. Performance in reproducing correctly these two variables indicates how well the RCM simulations simulated the day time and the night time temperature processes. Generally, **the spatial biases structure of the seasonal maximum temperature is similar to the seasonal mean temperature.** The simulations of maximum temperature are generally colder near the equatorial region with consistently largest bias ($\sim 4^\circ\text{C}$) over the west-coast of Sumatra. Over the mainland S.E. Asia region, the simulations are warmer than the observations, except at the centre of the region near $\sim 20^\circ\text{N}$. Consistent with the mean temperature biases, large warm biases are noted over the mainland S.E. Asia region especially during MAM (Figure 5.11). Considerable variations of biases among the simulation members can be observed over the northern part of the domains. All the HadCM3Q simulations produce biases patterns which resemble that of the ERA-40 simulations, except MAM, suggesting that the biases are largely sourced from the process-representations of the regional climate model itself. During MAM (Figure 5.11), while the ECHAM5 simulations show consistent biases pattern similar to that of the ERA-40 simulations, most of the HadCM3Q simulations produced large warm biases over the entire region of the mainland S.E. Asia. Out of the five simulations, the HadCM3Q10 simulations show largest difference over western mainland S.E. Asia extending down south to the Peninsular Malaysia. These differences are particularly large during the JJA (Figure 5.12) and SON (Figure 5.13).

Simulations vs Observation - DJF (1970-2000)

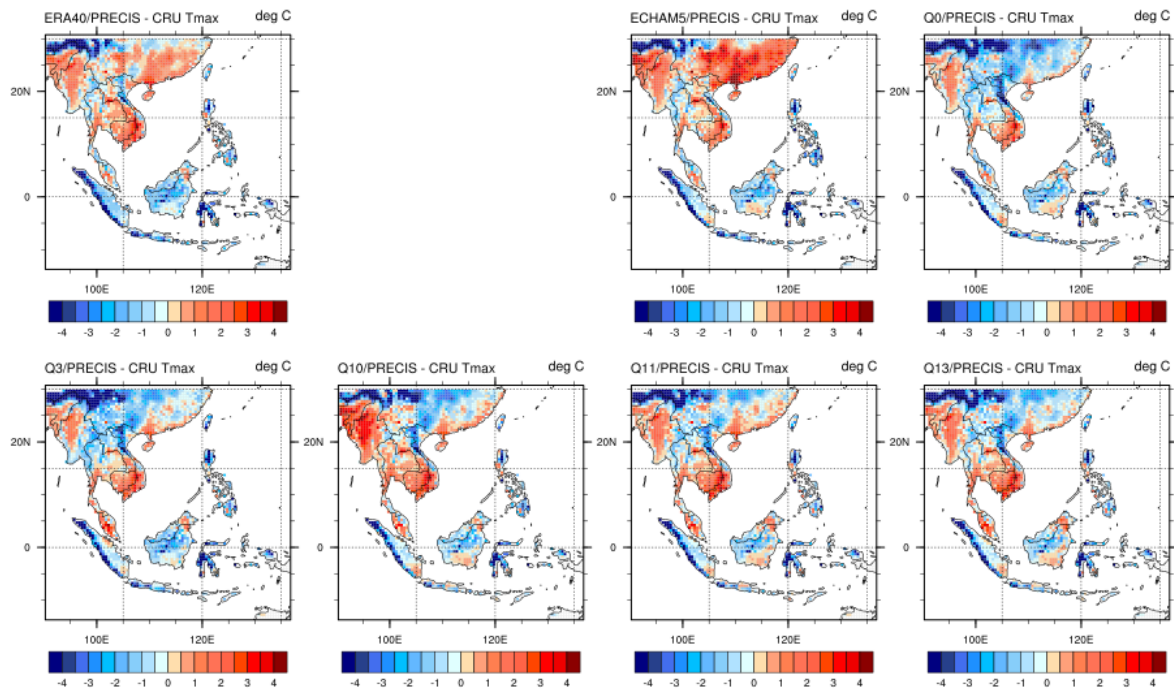


Figure 5.10: Difference between the spatial distribution of simulated (ERA-40, ECHAM5 and HadCM3Q0, 3, 10, 11, 13 simulations) and observed (CRU) DJF seasonal maximum temperature in degrees Celsius ($^{\circ}\text{C}$). Red shades show warm biases of simulations, while blue shades show cool biases of simulations.

Simulations vs Observation - MAM (1970-2000)

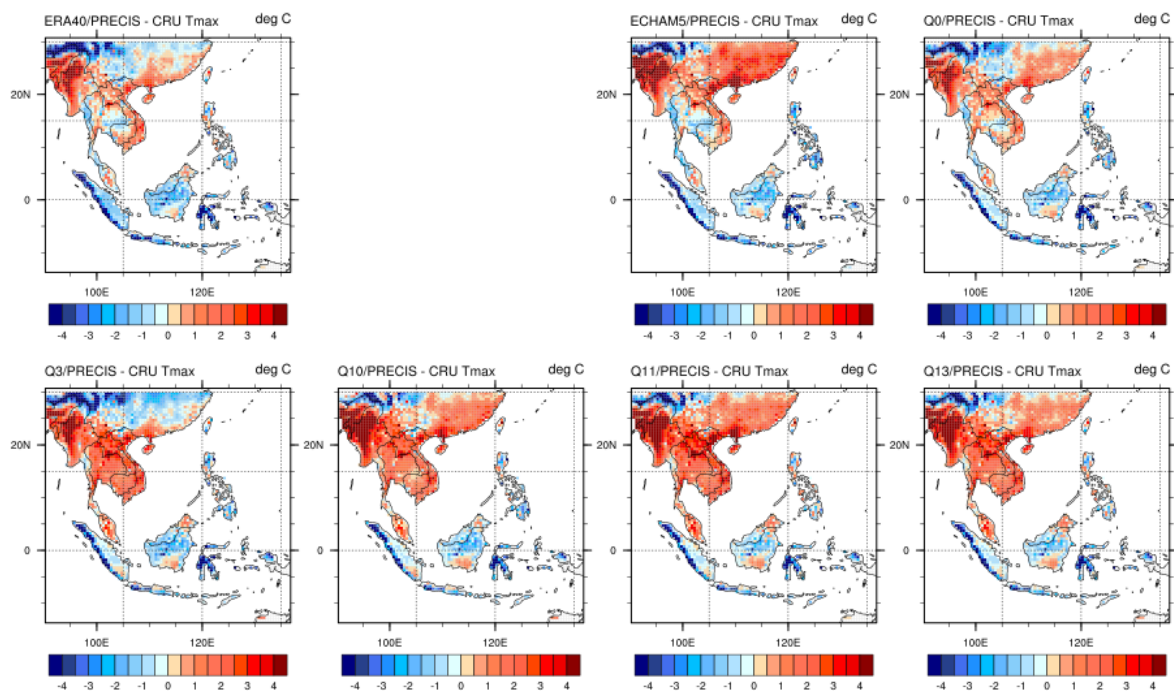


Figure 5.11: Difference between the spatial distribution of simulated (ERA-40, ECHAM5 and HadCM3Q0, 3, 10, 11, 13 simulations) and observed (CRU) MAM seasonal maximum temperature in degrees Celsius ($^{\circ}\text{C}$). Red shades show warm biases of simulations, while blue shades show cool biases of simulations.

Simulations vs Observation - JJA (1970-2000)

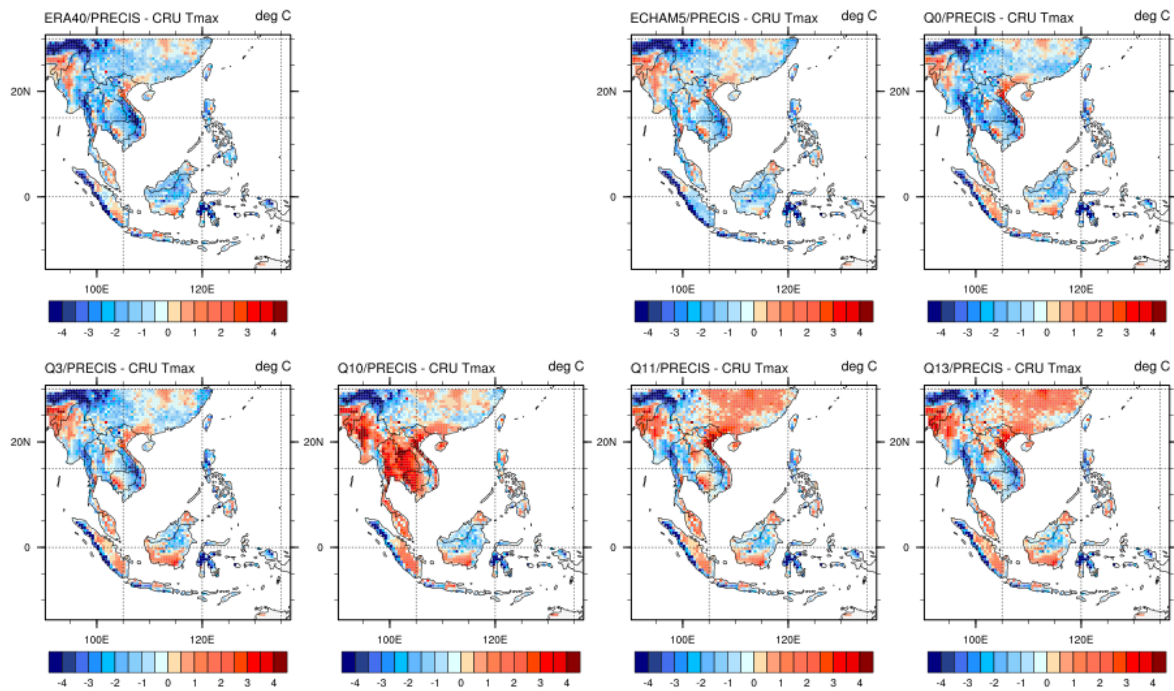


Figure 5.12: Difference between the spatial distribution of simulated (ERA-40, ECHAM5 and HadCM3Q0, 3, 10, 11, 13 simulations) and observed (CRU) JJA seasonal maximum temperature in degrees Celsius (°C). Red shades show warm biases of simulations, while blue shades show cool biases of simulations.

Simulations vs Observation - SON (1970-2000)

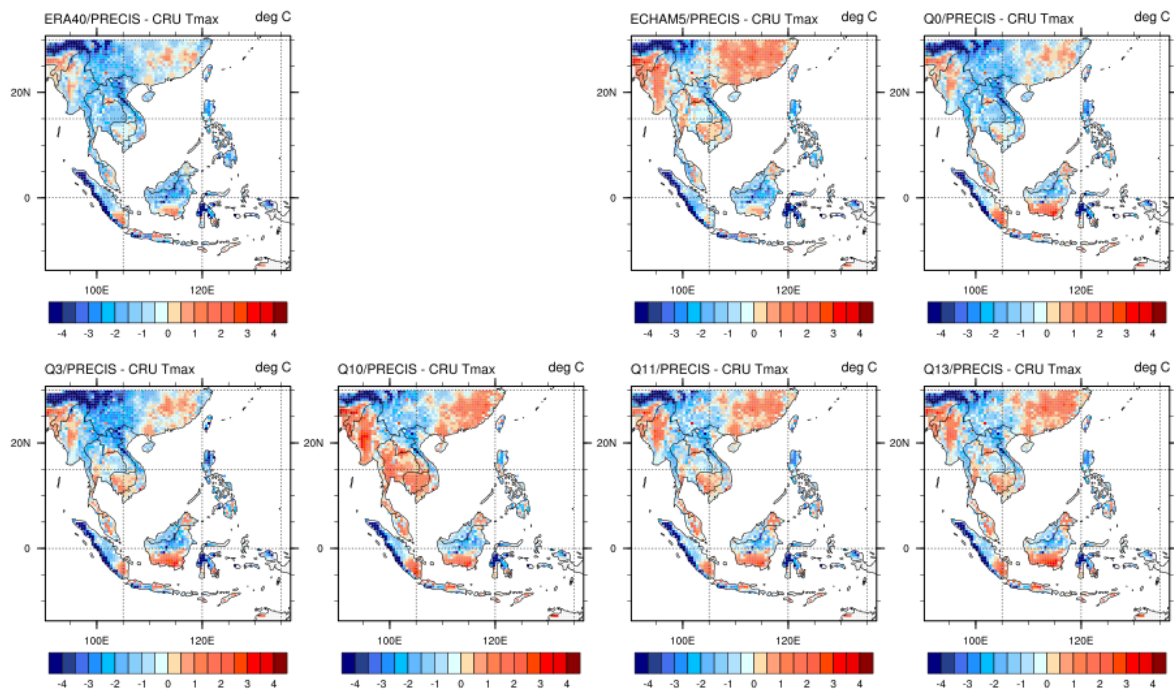


Figure 5.13: Difference between the spatial distribution of simulated (ERA-40, ECHAM5 and HadCM3Q0, 3, 10, 11, 13 simulations) and observed (CRU) SON seasonal maximum temperature in degrees Celsius (°C). Red shades show warm biases of simulations, while blue shades show cool biases of simulations.

The simulated seasonal mean *minimum* temperature shows generally warm biases with larger magnitude (3-4°C) over western-central mainland S.E. Asia (Figure 5.14 - Figure 5.17). The biases magnitudes are generally larger during DJF (Figure 5.14) and MAM (Figure 5.15). Although generally lower at magnitudes 1-2°C, the warm biases remain seasonally invariant over the southern half of the simulation domain. **The pattern is opposite to that of the seasonal mean maximum temperature where biases are largely negative in these areas. This indicates that the simulations produce much warmer nights, hence smaller diurnal temperature range compared to the observation.** Over the mainland S.E. Asia, a small region at the northern part of Vietnam shows consistently cold biases. All the 6 RCM simulations show very similar bias patterns to that of the ERA-40 simulations, suggesting that the biases may largely be sourced from the regional climate model itself rather than inherited from the GCMs.

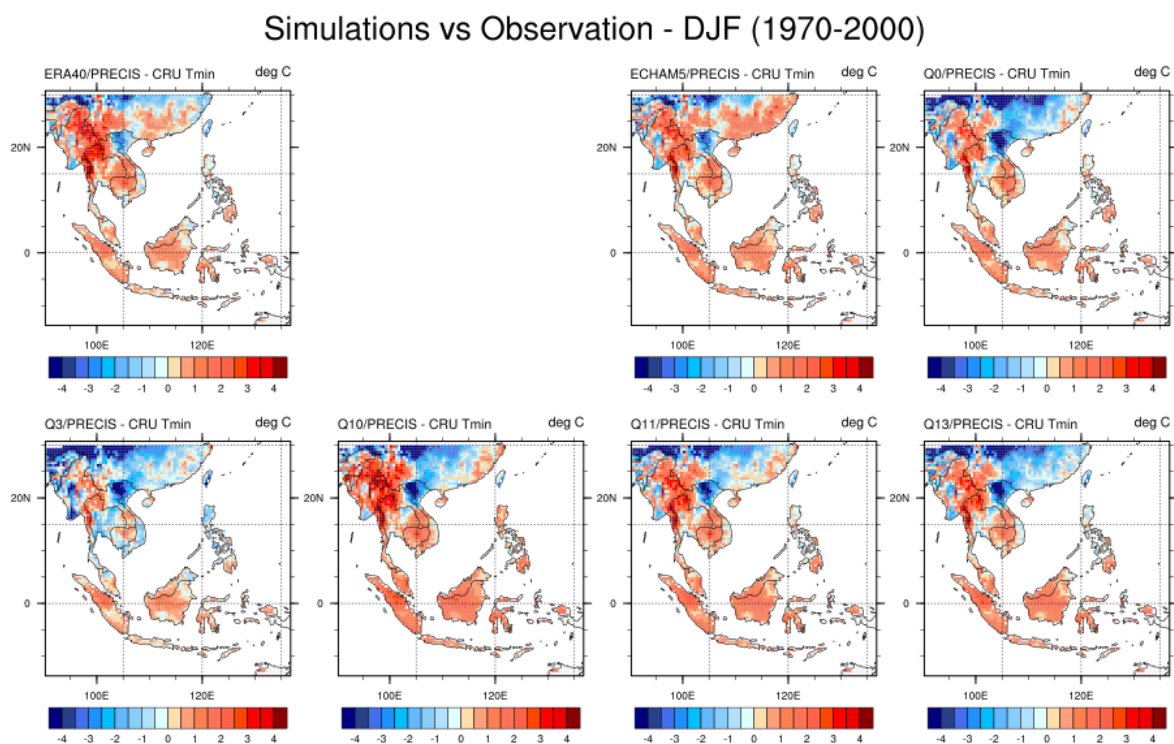


Figure 5.14: Difference between the spatial distribution of simulated (ERA-40, ECHAM5 and HadCM3Q0, 3, 10, 11, 13 simulations) and observed (CRU) DJF seasonal minimum temperature in degrees Celsius (°C). Red shades show warm biases of simulations, while blue shades show cool biases of simulations.

Simulations vs Observation - MAM (1970-2000)

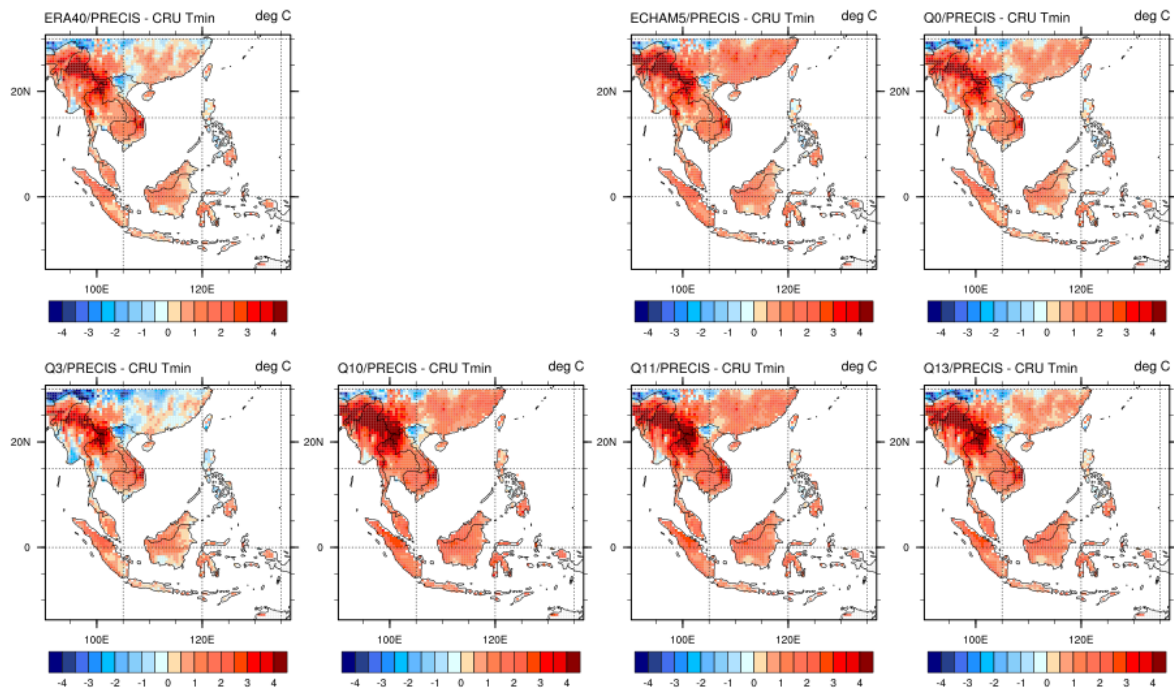


Figure 5.15: Difference between the spatial distribution of simulated (ERA-40, ECHAM5 and HadCM3Q0, 3, 10, 11, 13 simulations) and observed (CRU) MAM seasonal minimum temperature in degrees Celsius (°C). Red shades show warm biases of simulations, while blue shades show cool biases of simulations.

Simulations vs Observation - JJA (1970-2000)

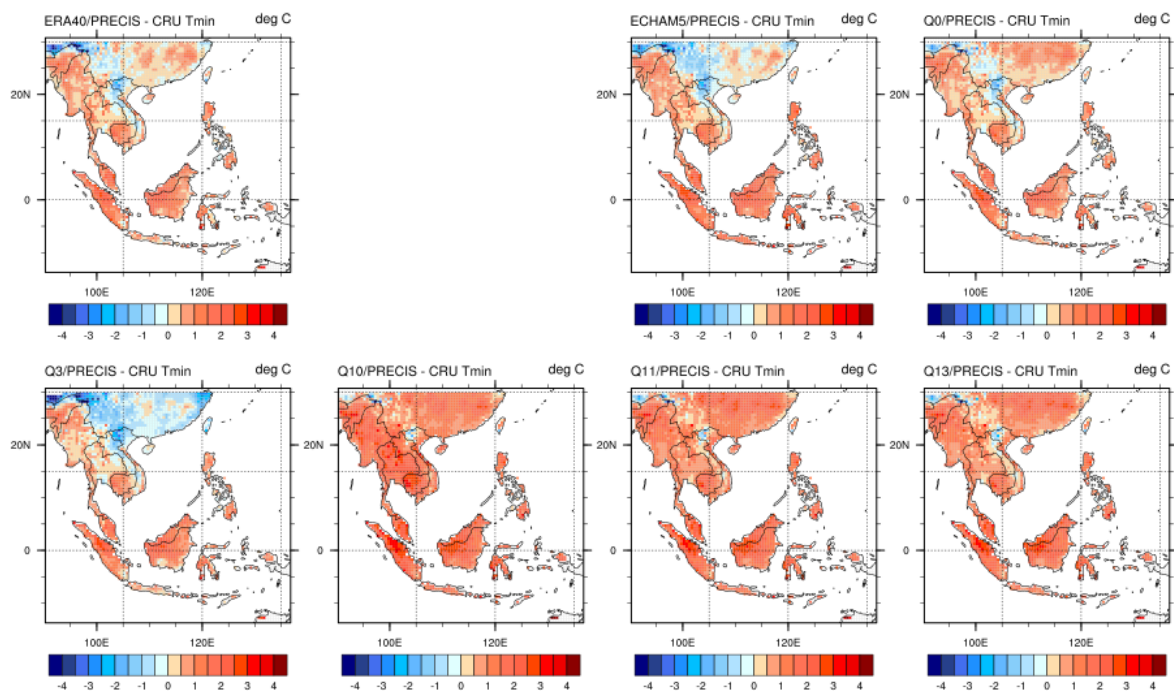


Figure 5.16: Difference between the spatial distribution of simulated (ERA-40, ECHAM5 and HadCM3Q0, 3, 10, 11, 13 simulations) and observed (CRU) JJA seasonal minimum temperature in degrees Celsius (°C). Red shades show warm biases of simulations, while blue shades show cool biases of simulations.

Simulations vs Observation - SON (1970-2000)

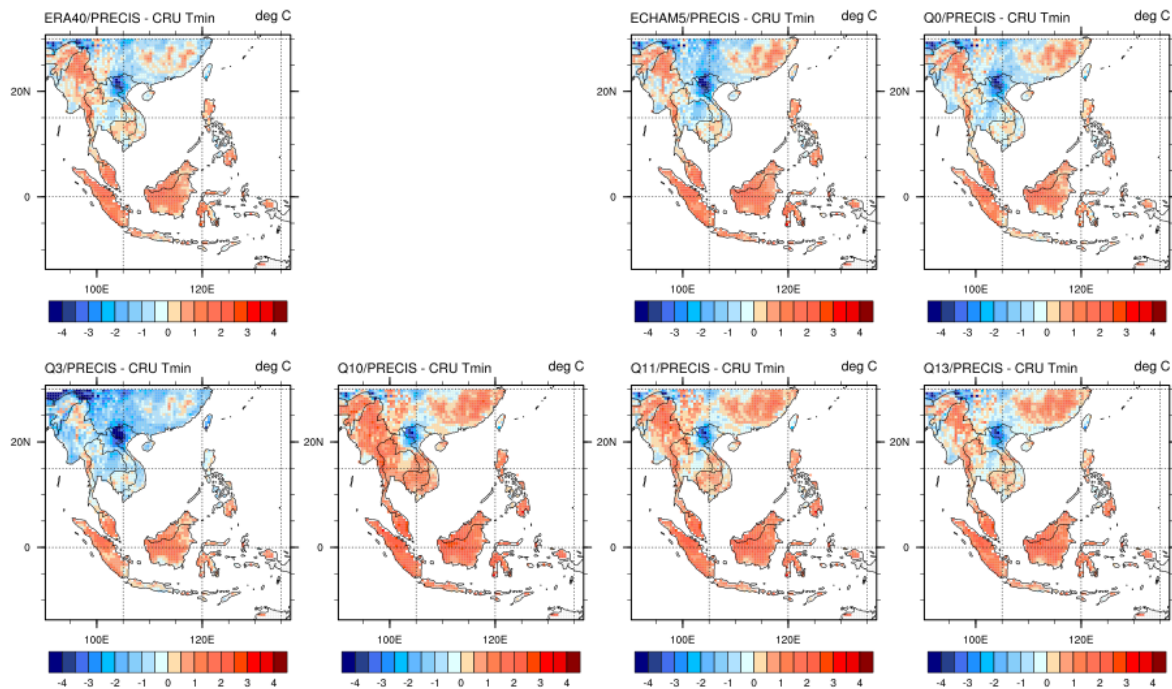


Figure 5.17: Difference between the spatial distribution of simulated (ERA-40, ECHAM5 and HadCM3Q0, 3, 10, 11, 13 simulations) and observed (CRU) SON seasonal minimum temperature in degrees Celsius (°C). Red shades show warm biases of simulations, while blue shades show cool biases of simulations.

5.5. Evaluation of seasonal spatial rainfall distribution

The seasonal rainfall from the downscaling simulations was compared to APHRODITE (Yatagai, et al., 2012). Before the comparison, the PRECIS data was bi-linearly interpolated to the APHRODITE's $0.25^\circ \times 0.25^\circ$ grids. The biases were then calculated as the percentage difference between the simulations and observation at each of the grid points (Figure 5.18 - Figure 5.21).

Generally, the **bias patterns of seasonal rainfall simulation are much noisier than temperature. The simulations produce moderate wet biases of about 20-40% through the years, except over the western part of the mainland S.E. Asia where the biases are largely negative.** Large wet biases of more than 80% were simulated over Cambodia and central region of Borneo during DJF (Figure 5.18) and MAM (Figure 5.19). Close to the northern boundary of the simulations, the model errors remain large, suggesting possible influence of the problematic boundary forcing over this region with steep and complex terrain. Generally, the RCM simulations show consistent biases patterns to that produced by the ERA-40 simulations, except HadCM3Q10 that produced much drier climate over central mainland S.E. Asia over Thailand during DJF (Figure 5.18) and JJA (Figure 5.20). In addition, the ECHAM5 simulations produced larger wet biases over the equatorial Maritime Continent (southern Sumatra and Borneo) during JJA (Figure 5.20).

DJF (1970-2000) multiannual seasonal precip : Simulation-APHRODITE

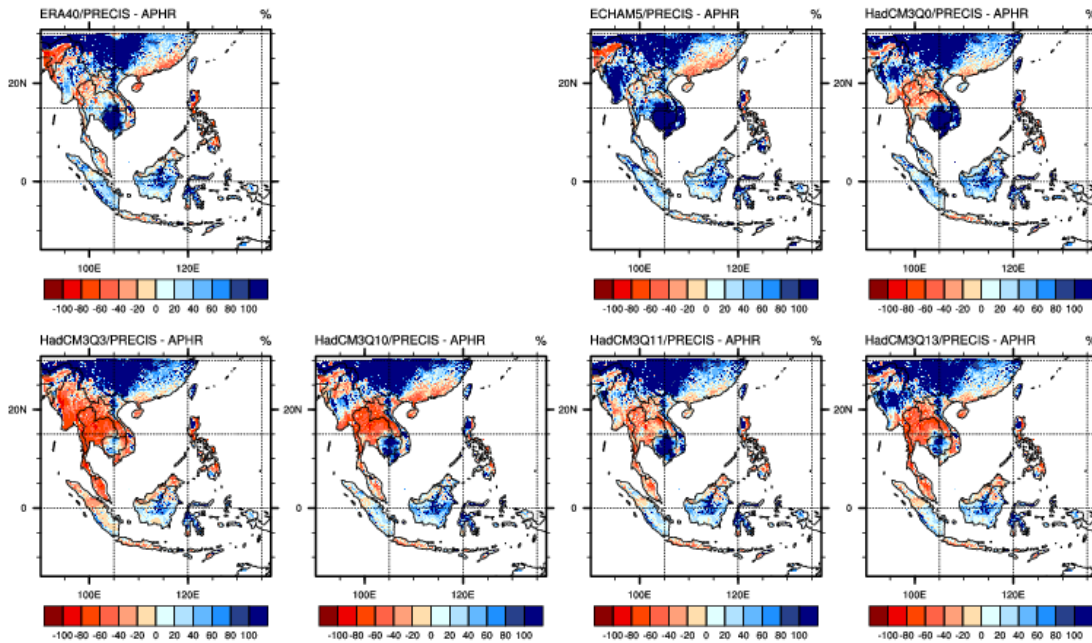


Figure 5.18: Difference between the spatial distribution of simulated (ERA-40, ECHAM5 and HadCM3Q0, 3, 10, 11, 13 simulations) and observed (APHRODITE) DJF seasonal rainfall in % of individual grids' observed climatology. Red shades show dry biases of simulations, while blue shades show wet biases of simulations.

MAM (1970-2000) multiannual seasonal precip : Simulation-APHRODITE

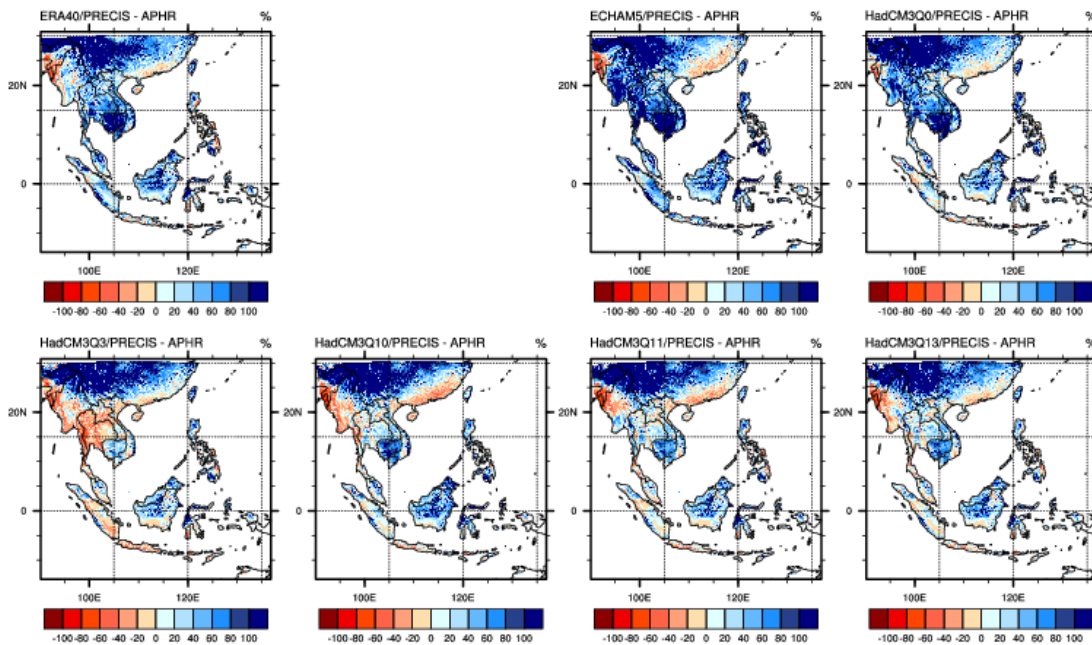


Figure 5.19: Difference between the spatial distribution of simulated (ERA-40, ECHAM5 and HadCM3Q0, 3, 10, 11, 13 simulations) and observed (APHRODITE) MAM seasonal rainfall in % of individual grids' observed climatology. Red shades show dry biases of simulations, while blue shades show wet biases of simulations.

JJA (1970-2000) multiannual seasonal precip : Simulation-APHRODITE

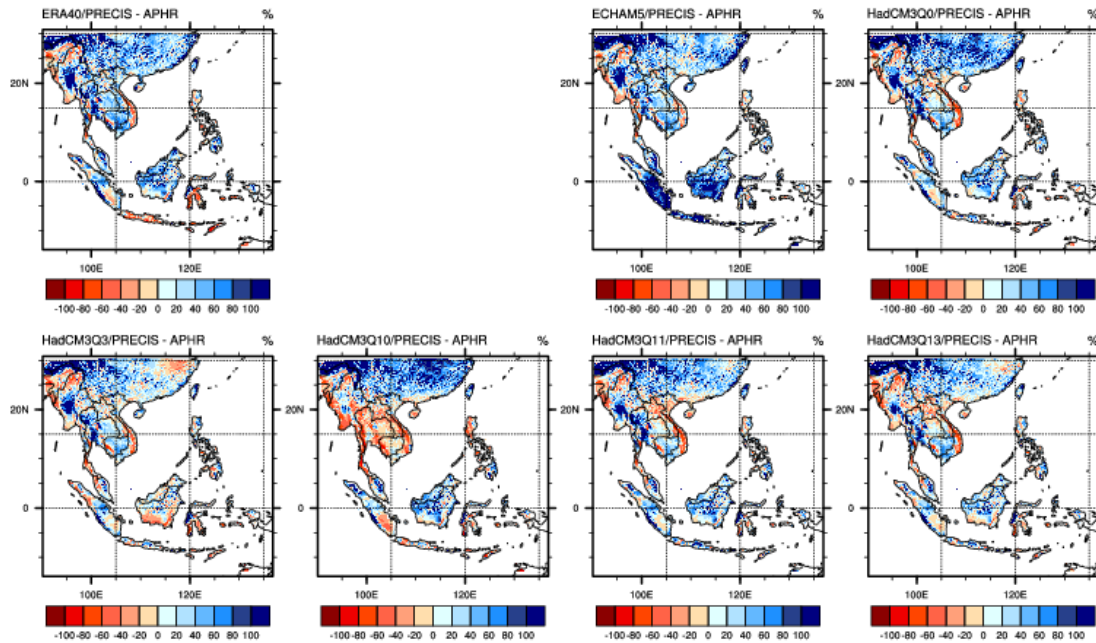


Figure 5.20: Difference between the spatial distribution of simulated (ERA-40, ECHAM5 and HadCM3Q0, 3, 10, 11, 13 simulations) and observed (APHRODITE) JJA seasonal rainfall in % of individual grids' observed climatology. Red shades show dry biases of simulations, while blue shades show wet biases of simulations.

SON (1970-2000) multiannual seasonal precip : Simulation-APHRODITE

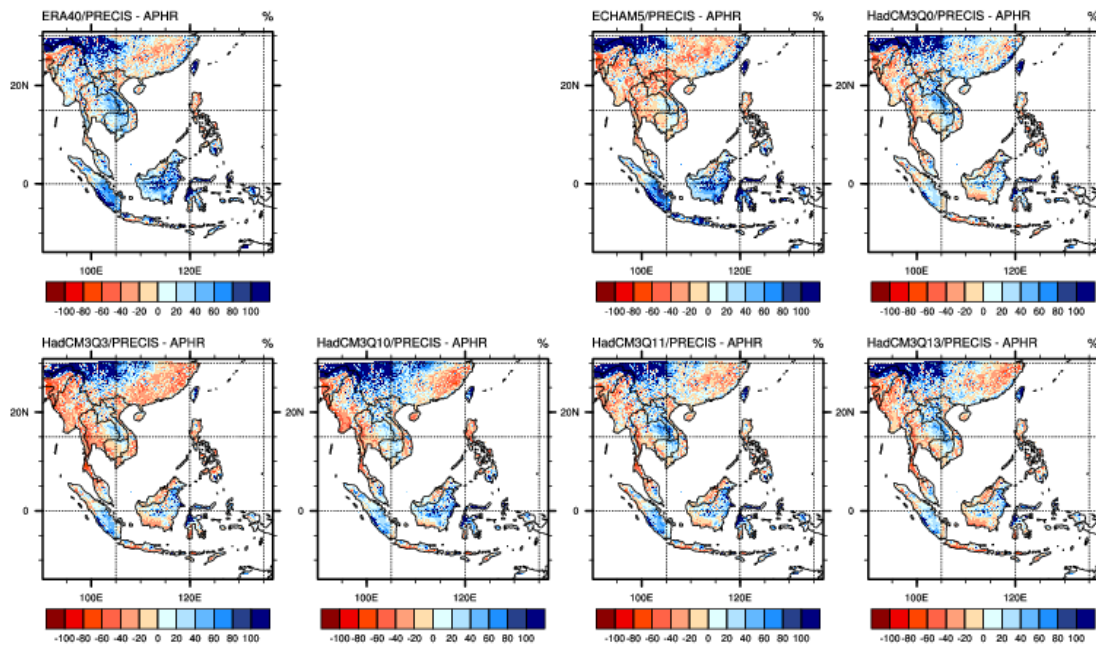


Figure 5.21: Difference between the spatial distribution of simulated (ERA-40, ECHAM5 and HadCM3Q0, 3, 10, 11, 13 simulations) and observed (APHRODITE) SON seasonal rainfall in % of individual grids' observed climatology. Red shades show dry biases of simulations, while blue shades show wet biases of simulations.

5.6. Evaluation of the Southwest Summer Monsoon

5.6.1. Monsoon circulations

For model evaluation in wind fields, patterns of circulation and wind speed were averaged for the period 1971–2000 over S.E. Asia. Figure 5.22 shows the horizontal 850 hPa average wind speed (in m/s) and direction in July (typical month within the summer monsoon), for ERA-40 reanalysis and the 6 RCM simulations members. Figure 5.22 shows that the RCM **reasonably simulate the spatial pattern of the summer monsoon circulation**. The flow directions are fairly accurate according to their locations and timing. However, there is a **clear systematic positive bias in wind speed over the region in all model simulations**. Comparisons of RCM simulations against ERA-40 reanalysis indicate that HadCMQ10 reconstructed the wind speed at 850 hPa most closely.

The zonal (east to west) wind of summer monsoon at 850 hPa is depicted on Figure 5.23. Figure 5.22 is a Hovmoller plot, showing latitude vs. time for the 6 RCM and one ERA-40 simulations. During the southwest summer monsoon, which occurs from May - September, the monsoon winds are westerly (red) and extend from ~5-20N. The comparisons between the ERA-40 simulations as the quasi-observation data and models show that the monthly mean of zonal wind during the period of 1971-2000 are in reasonable agreement.

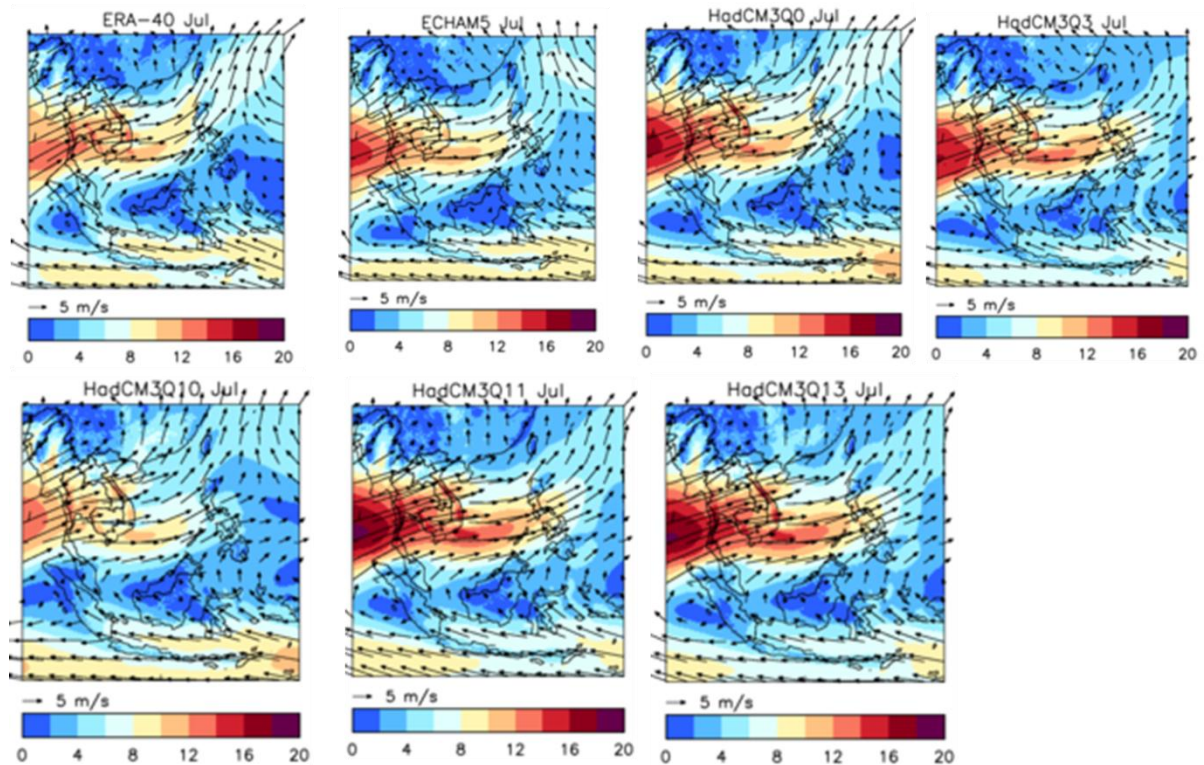


Figure 5.22: 850 hPa mean wind speed in m/s and direction during July, averaged over the 1971-2000 period for ERA-40 reanalysis and 6 RCM simulations (ECHAM5 and HadCM3Q0, 3, 10, 11, 13).

1971-2000 zonal wind (m/s)

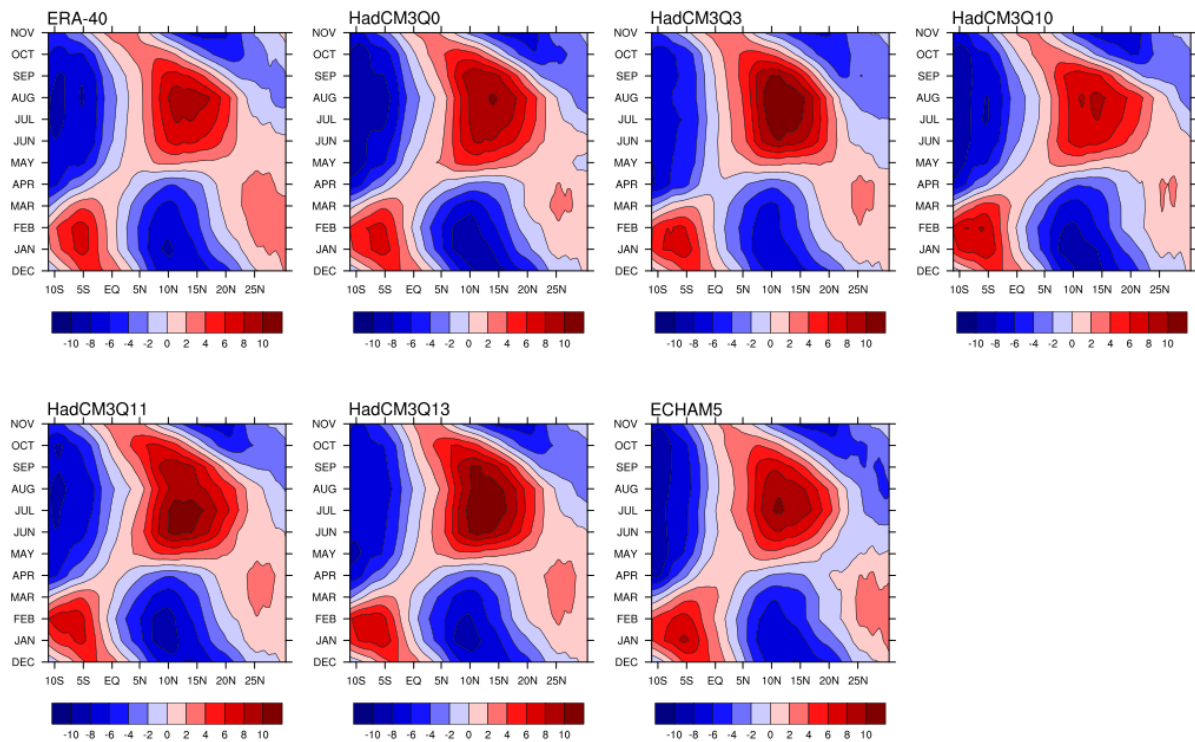


Figure 5.23: Zonal (east to west) wind component averaged over longitudes 90E to 135E in m/s at 850 hPa over the 1971-2000 period for ERA-40 simulations and 6 RCM simulations (HadCM3Q0, 3, 10, 11, 13 and ECHAM5). Red shades indicate westerly winds, while blue shades indicate easterly winds.

5.6.2. Precipitation

The time-latitude Hovmöller plot of precipitation (land only) is shown in Figure 5.24. The precipitation distributions over time in the model runs compare well to APHRODITE observations, during the southwest summer monsoon, where the maximum precipitation is located between 5 and 20N. All the models are slightly wetter than observations. During the S.E. Asian summer, the monsoon onsets around early May and withdraws around late September, and this condition is observed in the ERA-40 simulations and the RCM simulations.

1971-2000 precipitation (mm/day)

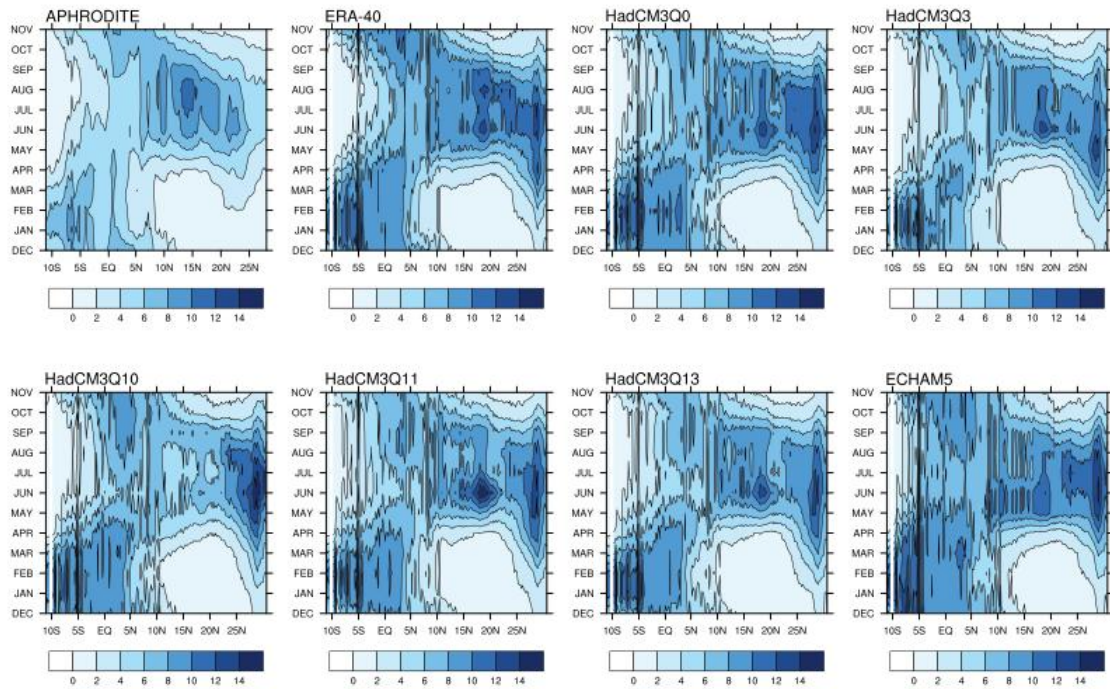


Figure 5.24: Land-only precipitation time-latitude cross-section averaged over longitudes 90E to 135E for APHRODITE, ERA-40 simulations, and 6 RCM simulations (HadCM3Q0, 3, 10, 11, 13, and ECHAM5).

5.6.3. Spatial patterns of precipitation extreme

Availability of daily precipitation data from APHRODITE allows us to evaluate rainfall extremes in the model simulations. The spatial resolution of the observation datasets (0.25°) is similar to that of the model (25 km or $\sim 0.22^\circ$). However, we should bear in mind that the spatial coverage of stations in APHRODITE may not be equally high in all regions, and the effective resolution of the gridded observation data may be less than 0.25° .

Figure 5.25 shows the 95th percentile threshold value of annual rainfall in all 7 RCM simulations and APHRODITE June-September (JJAS) rainy days, defined as rainfall over 1 mm. Figure 5.26 shows the difference in 95th percentile of JJAS daily rainfall amounts as a percentage between APHRODITE and the RCM simulations. The figure shows that all RCM simulations overestimated the 95th percentile summer monsoon rainfall amount in the continental part of China with the largest bias about 10 to 15%. Simulations of 95th percentile summer monsoon rainfall in countries over S.E. Asia are reasonably accurate. In Vietnam for example, the majority of extreme rainfall in this season is attributed to tropical cyclones. The RCM simulations correctly placed the region with the largest rainfall extremes along the eastern coast of the central provinces of Vietnam. However, the magnitudes of these extremes are weaker than the 95th percentile in APHRODITE. Similar precipitation patterns of extreme rainfall are simulated in the coastal areas of Myanmar. Over most areas, underestimations of up to 8% are observed in all RCM simulations.

In summary, all RCM simulations capture patterns of rainfall extremes well (within $\pm 10\%$ bias), although they are generally underestimated in magnitude compared to

APHRODITE over the majority of the domain, with the exception of southern China where it is overestimated.

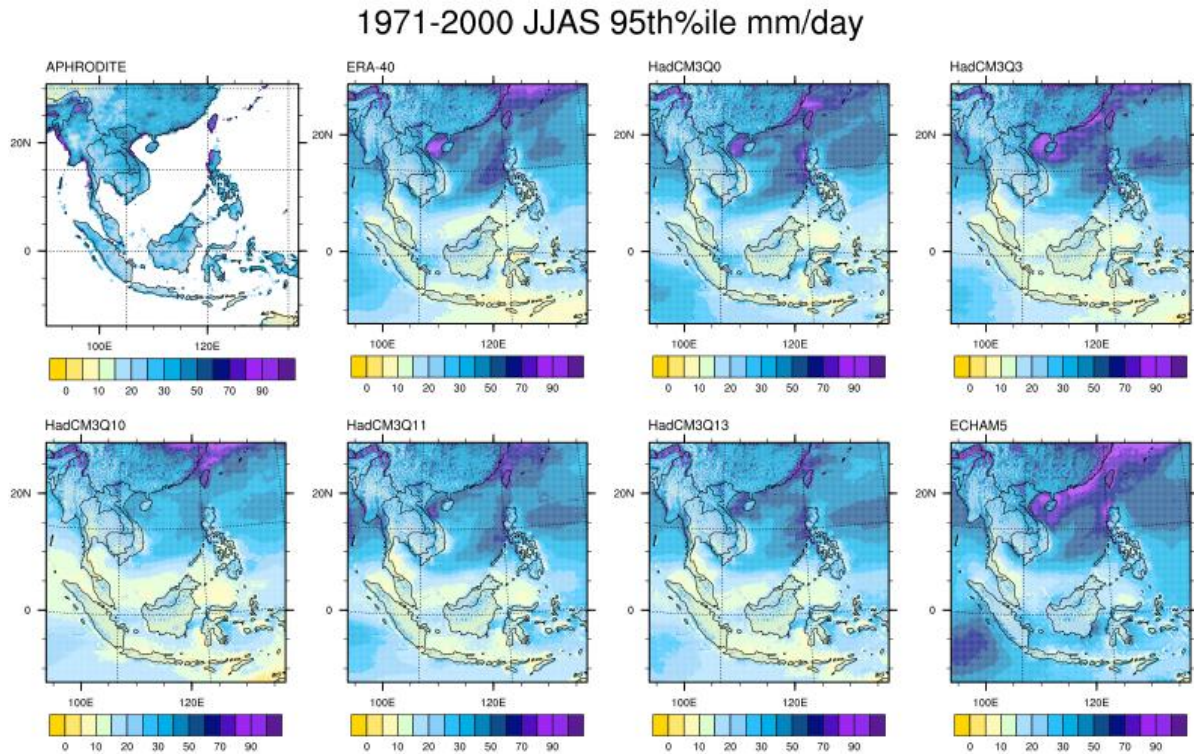


Figure 5.25: 95th percentile of JJAS daily rainfall amounts for APHRODITE, ERA-40 simulations, and 6 RCM simulations (HadCM3Q0, 3, 10, 11, 13, and ECHAM5).

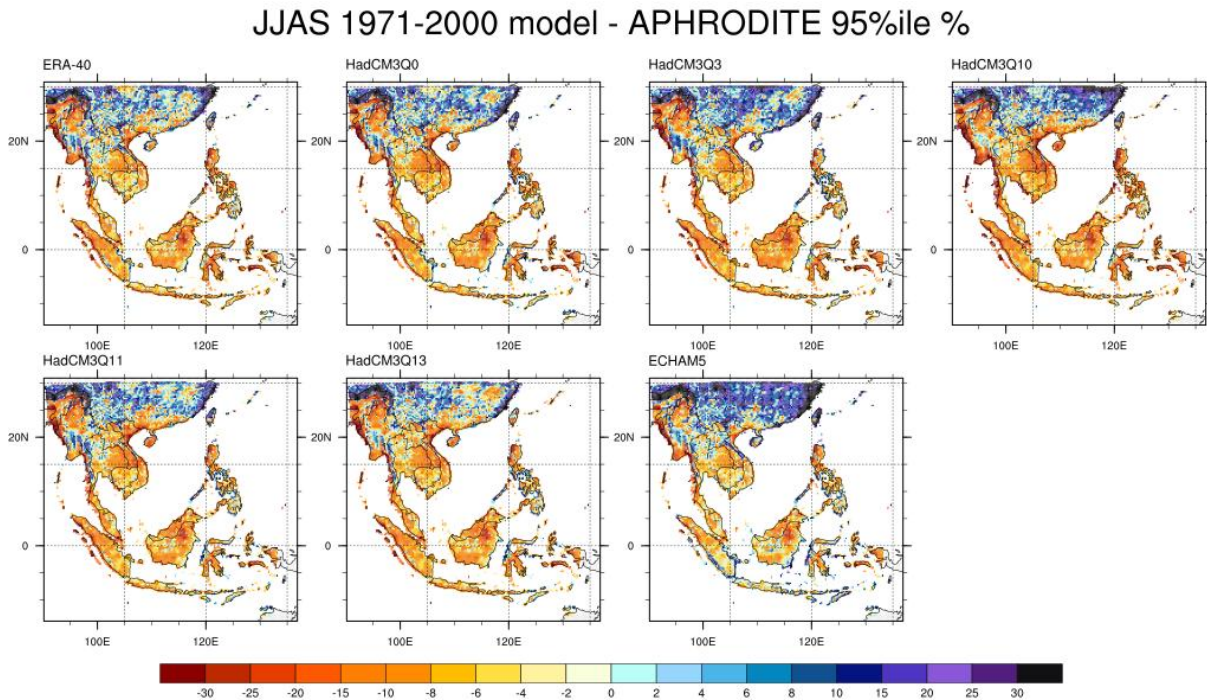


Figure 5.26: Difference of 95th percentile of JJAS daily rainfall amounts between 7 simulations and APHRODITE over Southeast Asia.

5.7. Evaluation of the Northeast Winter Monsoon

5.7.1. Monsoon circulation

The meridional (south to north) wind of the Northeast Monsoon at 850 hPa is depicted on Figure 5.27. The figure consists of 6 RCM simulations and one ERA-40 simulations. In the case of upper level winds, as direct observations are not accessible, ERA-40 reanalysis results are used instead to compare with the RCM runs. **The comparison between the ERA-40 reanalysis and models show that the monthly mean of meridional wind during the period of 1970-2000 are in general agreement, however the intensities and the durations differ.** The longitude span between 90-110°E shows that the northerly wind component tends to begin in October and taper off in January. The HadCM3Q10 and HadCM3Q13 simulations begin earlier in September and taper off about the same time in January.

1971-2000 meridional wind (m/s)

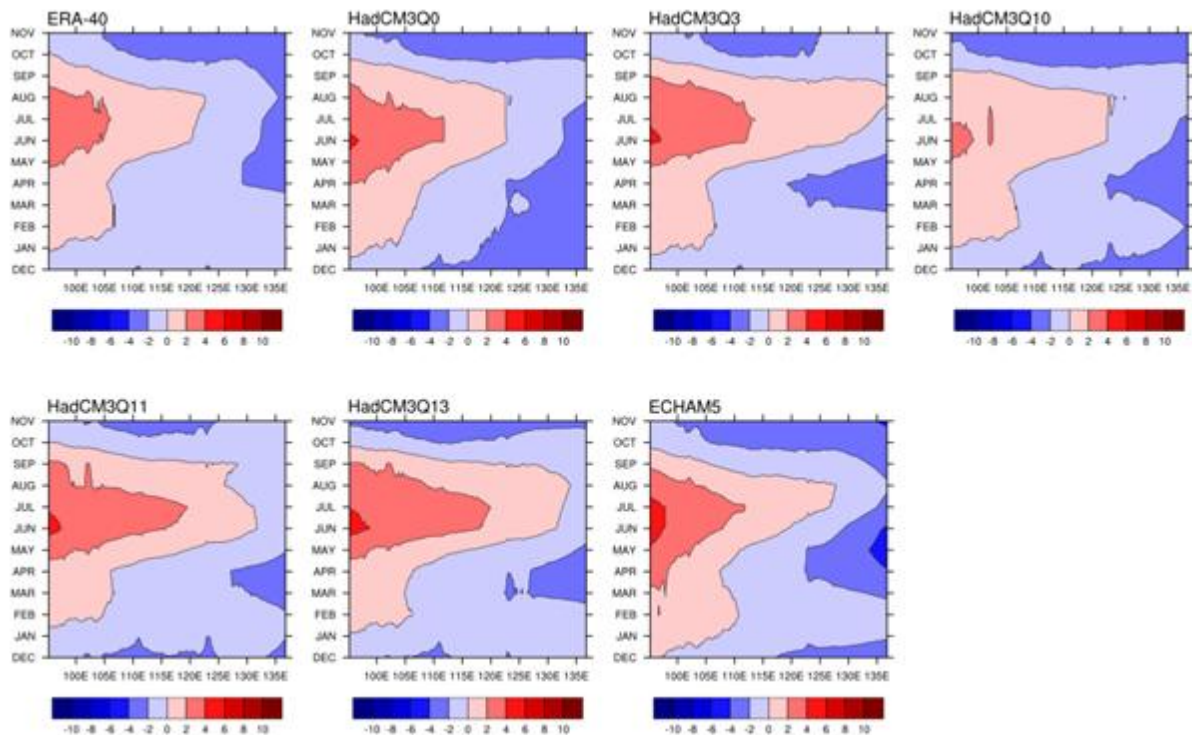


Figure 5.27: Meridional (south to north) wind component in m/s at 850 hPa averaged over the latitudes 13S to 30N over the 1971-2000 period for ERA-40 simulations and 6 RCM simulations (HadCM3Q0, 3, 10, 11, 13 and ECHAM5). Red shades indicate southerly winds, while blue shades indicate northerly winds.

5.7.2. Spatial patterns of circulation

The 850 hPa level circulation patterns from November to March are shown in Figure 5.28. The general pattern is captured by the 6 RCM simulations. The position and migration of the monsoon trough is well represented. The northeasterly winds over the maritime region is also captured rather well, however the intensities tend to be stronger in places than in ERA-40. Figure 5.29 depicts the 200 hPa flow during the Northeast Monsoon. **The upper level flow which indicates the returning branch of the Hadley Cell is captured in all the**

simulations. The intensity of the return flow follows the monthly progression of the monsoon. The beginning of the monsoon in November shows a weaker Hadley Cell followed by a strong Hadley Cell during December, January and February and the weakening at the end of the Northeast Monsoon season in March. The main features of the monsoon circulation are apparent in all the projections however the intensities of the circulation vary across models.

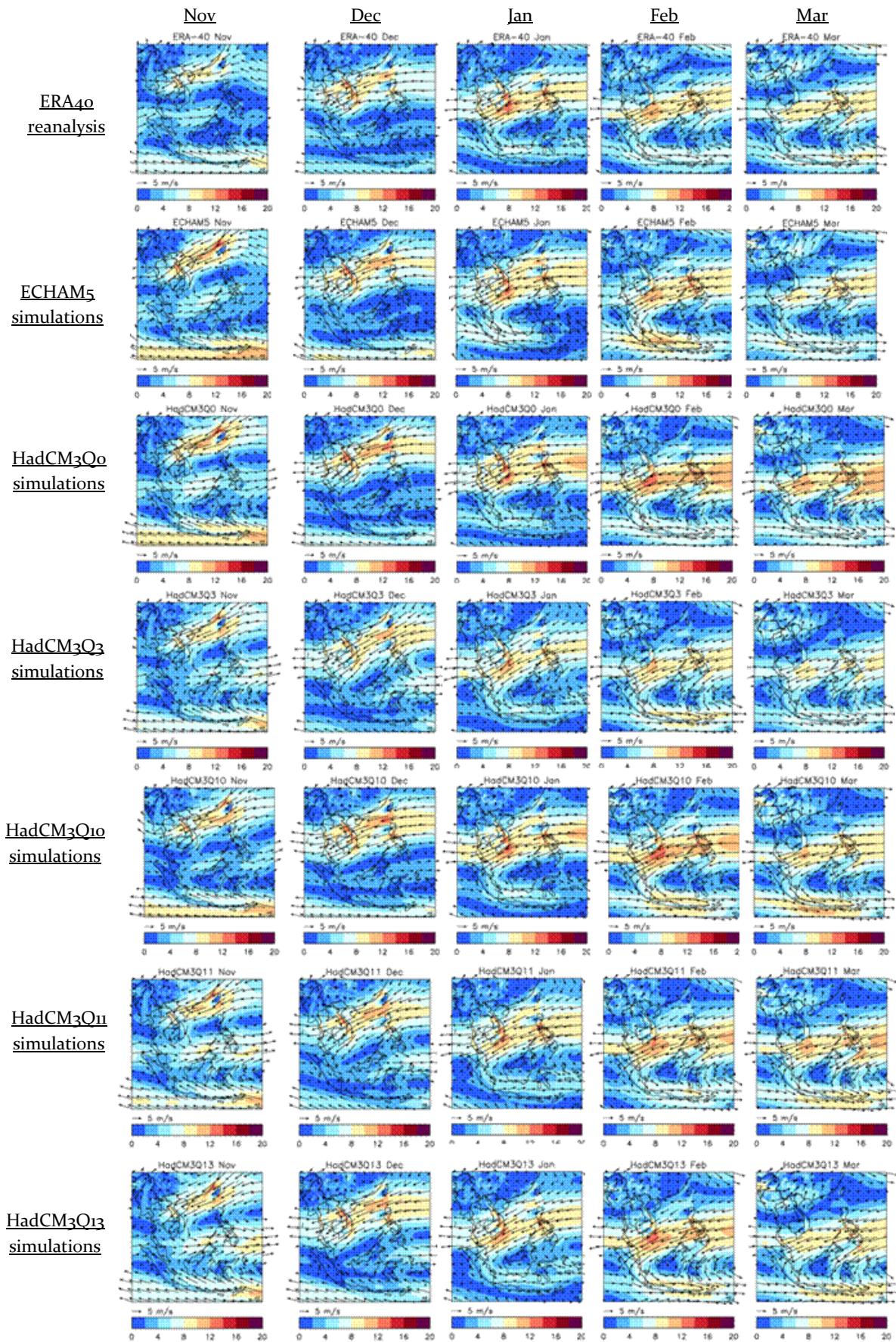


Figure 5.28: Monthly wind circulation at 850 hPa from November to March (left to right columns) for ERA-40 reanalysis, ECHAM5 simulations and HadCM3Q0, 3, 11, 10 and 13 simulations (top to bottom rows).

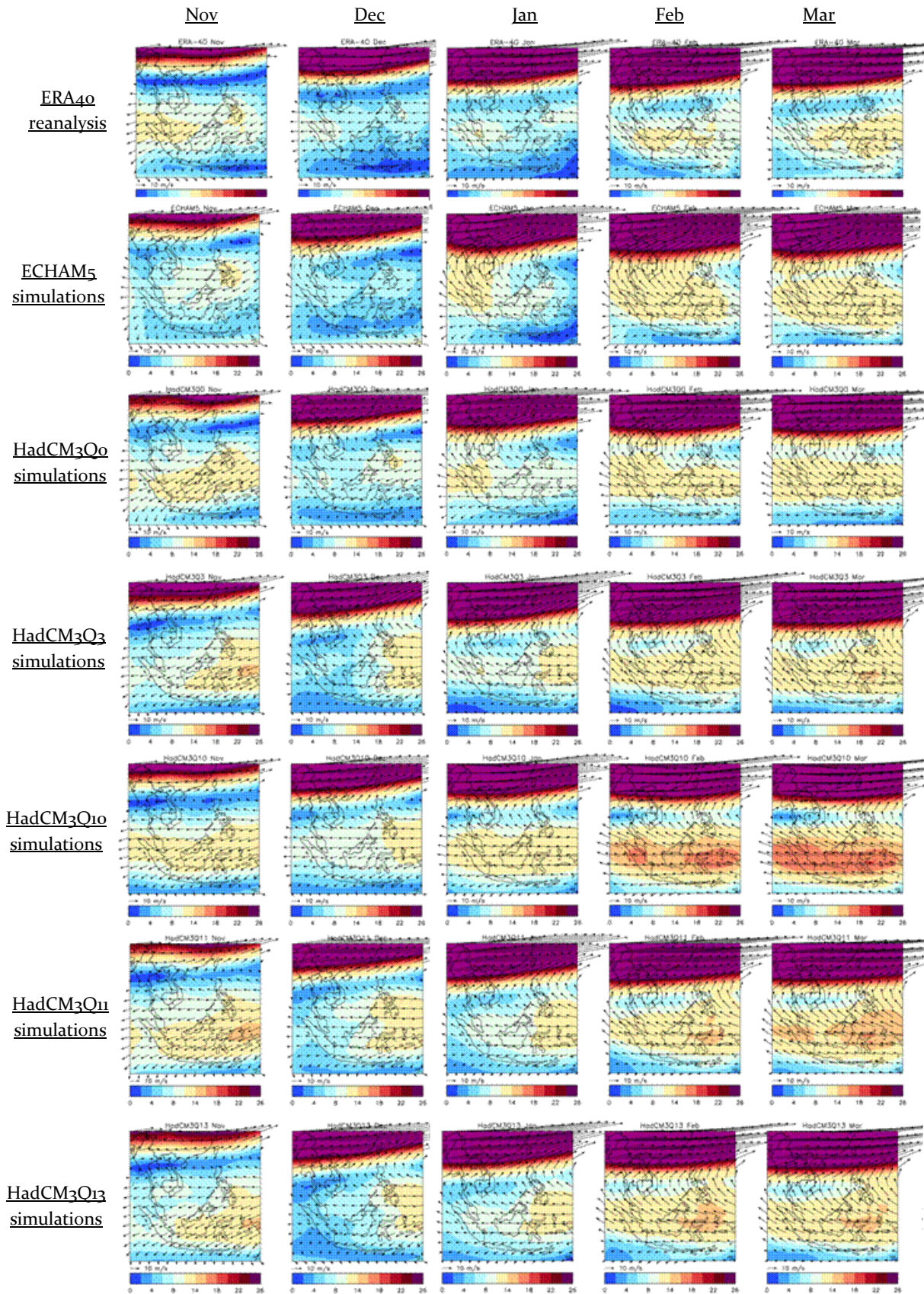


Figure 5.29: Monthly wind circulation at 200 hPa from November to March (left to right columns) for ERA-40 reanalysis, ECHAM5 simulations and HadCM3Q0, 3, 11, 10 and 13 simulations (top to bottom rows).

5.7.3. Precipitation

The time–latitude Hovmoller plot of precipitation (land only) is shown in Figure 5.24. In general the main precipitation pattern for the Northeast Monsoon is well captured in the projections. The heavy rainfall during December to March is indicated in all the RCM simulations. The intensity however varies. The location of the heavy rainfall belt which lies between 5°S to 10°N which is present in the observations and ERA-40 is also present in all simulations. The precipitation distribution over time in the model simulations is in agreement with observations, except for ECHAM5 simulations which is too wet. The ECHAM5 simulations tends to extend the heavy rainfall period beyond the Northeast Monsoon (up to June) for the 5°S to 10°N heavy precipitation region.

5.7.4. Spatial patterns of precipitation extreme

The DJF precipitation in the 95th percentile is shown in Figure 5.30. All RCM simulations tend to project more extreme rainfall occurrences over Southern Vietnam and the Philippines (Figure 5.31). ECHAM5 however has projected relatively more extreme rainfall amounts in the southern part of the Maritime Continent where the Nusa Tenggara Islands of Indonesia are located.

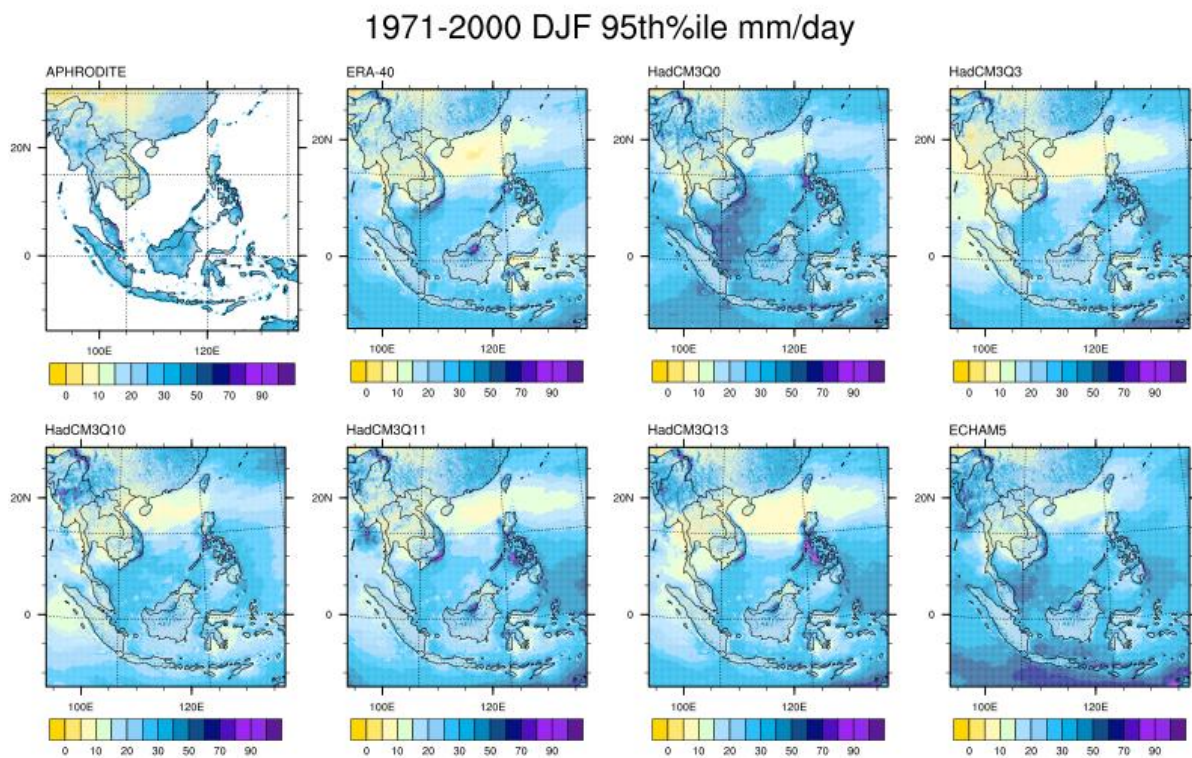


Figure 5.30: 95th percentile of DJF daily rainfall amounts for APHRODITE, ERA-40 simulations, and 6 RCM simulations (HadCM3Q0, 3, 10, 11, 13, and ECHAM5).

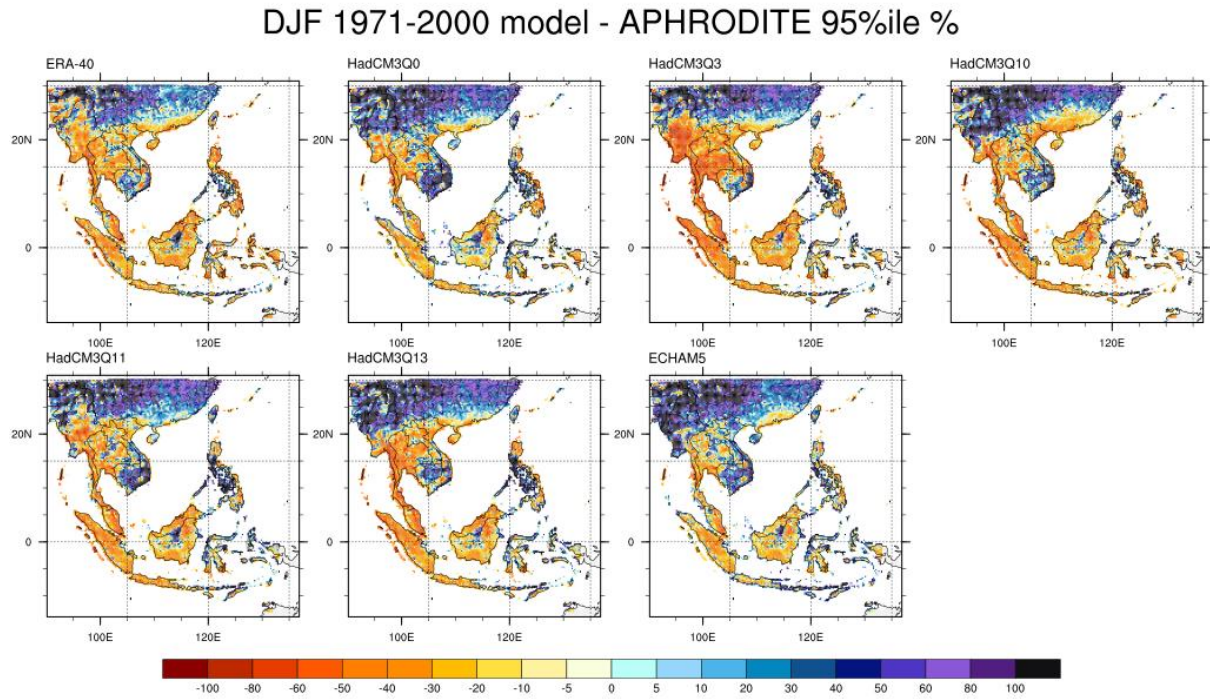


Figure 5.31: Difference of 95th percentile of DJF daily rainfall amounts between 7 simulations and APHRODITE over Southeast Asia.

5.8. Evaluation of extreme rainfall indices

A regional climate model, due to its relatively high resolution, is expected to reproduce better indices for extreme events than the coarser global climate models, both for its increased horizontal resolution and for the improved representation of faster processes (Jones, et al., 1995). In particular, regional models at resolutions comparable to the one used for this project are expected to provide good rainfall extremes for daily aggregation at mid latitudes (e.g. Frei, et al., 2006). Similar studies have not been done for Southeast Asia. It is thus important to assess the model's skill in reproducing them. In this section, three extreme precipitation indices from the RCM simulations were analysed and compared to APHRODITE, which has similar horizontal resolution with respect to the regional model integrations of this study, and to the ERA-40 simulations. The biases produced by the simulations in the indices were calculated and the model's skill in producing them was assessed. The indices analysed are the annual maximum one day rainfall (Rx1day), annual maximum consecutive five days rainfall (Rx5day) and annual maximum of consecutive dry days²⁶ (CDD, or in other words maximum length of dry spell).

These indices have been estimated for the period 1971-2000. It is worth to underline the different nature of the boundary conditions used for this study: while the ERA-40 dataset is a reanalysis product based on actual observations for this period and that the simulations based on this are expected to reproduce accurately large-scale modes of variability (e.g El Nino), the RCM simulations are completely independent realisations of the present climate. Thus the latter are only constrained by the same concentrations of greenhouse gases but not expected to reproduce the detailed year-to-year variations of the large scale mode. For indices extracted from a thirty year sample, the role of the multiannual variability is expected to be negligible. However, since we are dealing with extreme events, the size of the sample is reduced and the possibility that natural variability could play a role cannot be ruled out.

5.8.1. Annual maximum one day rainfall (Rx1day)

The Rx1day indices from APHRODITE, ERA-40 simulations, and the 6 RCM simulations for the period 1971-2000 were plotted on Figure 5.32. **The RCM simulations showed consistent spatial patterns of biases with the ERA-40 simulations and with each other, which suggests biases can be reasonably attributed to the RCM formulation.** The stronger biases (of the order 100 mm/day) can be seen in places like coastal Myanmar, northern Philippines, central Borneo, northern Peninsular Malaysia, western coast of Sumatra, and Sulawesi – all of which look like terrain-related biases. While the all-positive biases in Figure 5.33 indicate that the RCM could be severely overestimating the rainfall over these areas, it is also worth bearing in mind the possibility that APHRODITE could have underestimated the extreme rainfall over the whole region.

As discussed in Section 4, the number of stations used in APHRODITE might not be sufficient to reproduce extreme indices such as the annual maximum rainfall (Rx1day). A sensitivity study over Japan (Kamiguchi, et al., 2010) on the effects of station density on extreme rainfall, using the APHRODITE interpolation method, has shown systematic errors in reproducing

²⁶ For mathematically precise definitions of these indices, refer to the CLIMDEX website at <http://www.climdex.org/indices.html>

extreme rainfall, similar to those reported for the European dataset EObs (Haylock, et al., 2008). At the time, the same studies have shown that less intense precipitation could be reproduced quite accurately by coarser station networks. In addition to the problems related to the density of stations used in building this observational dataset, there could also be specific problems in high-elevation areas. A assessment of a gridded precipitation dataset for the European Alps (Frei, et al., 2003) has identified two issues, both leading to an underestimate of precipitation: 1) the station network could not be representative of the area when stations in the valleys are more represented than stations at higher elevations (network bias) and 2) rain gauges are affected by under-catchment, i.e. they collect less rainfall, in intense wind conditions. The latter problem has given the largest contribution for the European Alps (Frei, et al., 2003), a region which has a very dense network of stations. For APHRODITE, which has very sparsely observed large areas, it could be the main factor leading to underestimated rainfall.

At any rate, a comparison between RCM results and APHRODITE could still be useful in assessing RCM skills in reproducing the geographical distribution of extreme rainfall. As reported in Sections 5.6.3 and 5.7.4, GCM driving conditions do not seem to have a strong effect on annual rainfall maxima, and indices from the RCM simulations have also the same geographical pattern obtained from the ERA-40 simulations. The biases from the RCM simulations (Figure 5.32) show the same pattern for all the integrations; these plots do not show any particular link between the magnitude of the bias and the density of the observational network (Yatagai, et al., 2012, fig 1). Hence, this simple comparison of spatial patterns is also inconclusive, a more detailed study or an alternative observational dataset are needed.

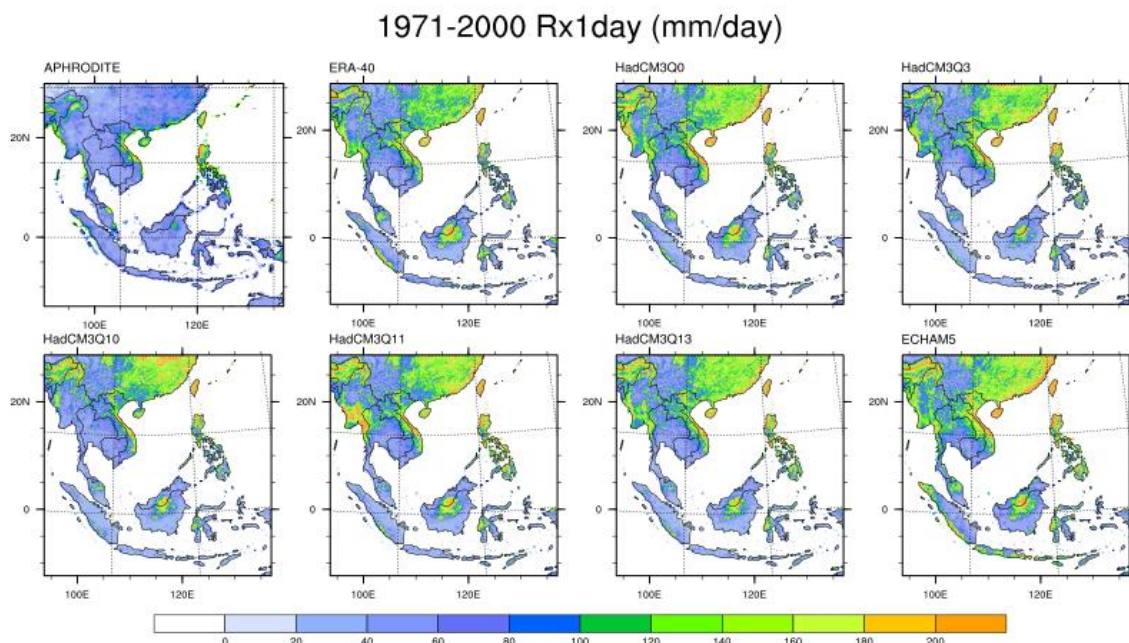


Figure 5.32: Spatial distribution of annual maximum 1 day rainfall (Rx1day) for APHRODITE, and the ERA-40 simulations, HadCM3Q0, 3, 10, 11, 13 and ECHAM5 simulations.

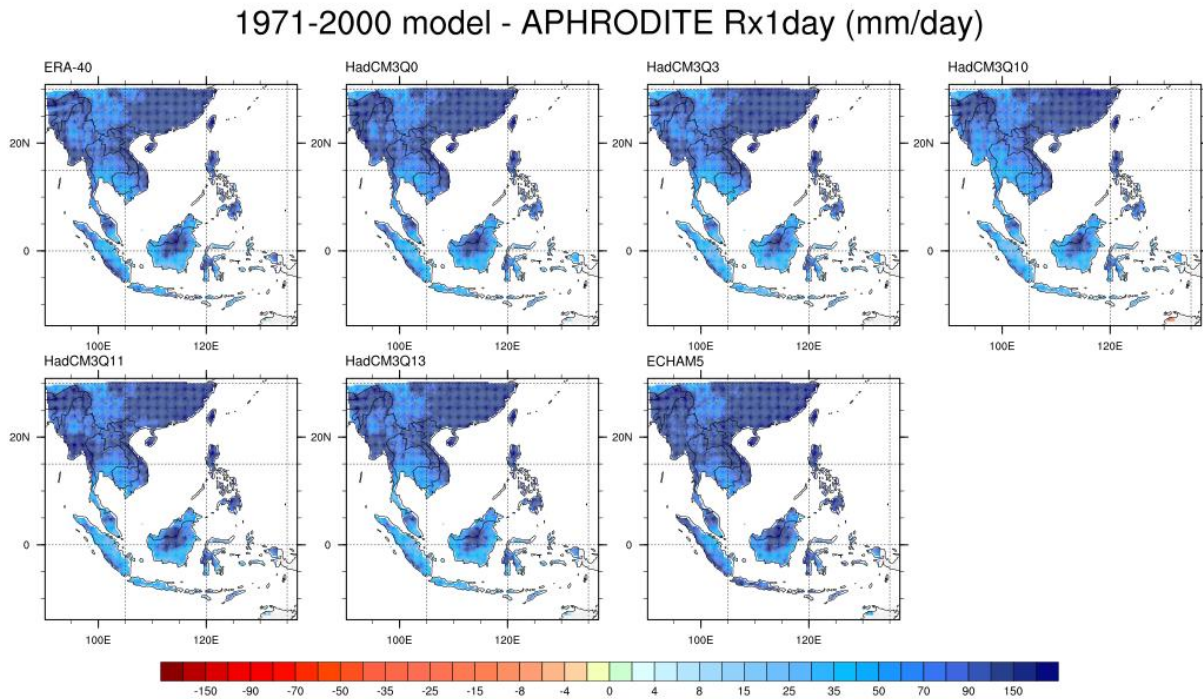


Figure 5.33: Difference between the spatial distribution of annual maximum 1 day rainfall (Rx1day) for the ERA-40 simulations, HadCM3Q0, 3, 10, 11, 13 and ECHAM5 simulations against APHRODITE. Red shades show negative biases (dry), while blue shades show positive biases (wet) of simulations.

5.8.2. Annual maximum consecutive five days rainfall (Rx5day)

The Rx5day indices from APHRODITE, the 6 RCM simulations, and the ERA-40 simulations for the present day 1971-2000 were plotted on Figure 5.34. Unlike the Rx1day rainfall index, which could represent extreme rainfall from more local, short-term events, the Rx5day rainfall is an index which is reflective of precipitation from larger spatial and longer time scale phenomena, such as monsoon rainfall and tropical cyclones. For these spatial and temporal characteristics, the comparison with the Rx5day estimated from APHRODITE is expected to be more relevant, since it is both more probable to capture large scale, long lived events on a low density station network and easier to interpolate large scale precipitation events.

All the RCM simulations reproduce the basic pattern of variation estimated from the APHRODITE dataset over the whole area (Figure 5.34). However, the five HadCM3Q simulations show consistent bias patterns to that produced by the ERA-40 simulations, except for ECHAM5 simulations which show a more intense rainfall in the lower latitudes. Similar to the Rx1day, the biases in Rx5day continue to show wet biases in the elevated regions, but in addition dry biases also emerge in the Rx5day, and these occurs generally in places that complement those with wet biases.

Dry biases indicate that the index estimated from APHRODITE seems not affected by problems related to network density for these areas, since these problems would result in an overestimated extreme index in the simulations. On the other hand, issues associated to observations over high elevation areas (Frei, et al., 2003) could still produce underestimated gridded rainfall, which could be the main contribution to the wet biases over these regions. The similarities in the spatial patterns of the bias again highlight the possibility of terrain-

induced rainfall is mainly determined by the regional climate model, but the magnitude of the bias seems to suggest a possible role for this index. It is also possible to identify the role of the driving GCM. Figure 5.35 shows ECHAM5 as the wettest global model and HadCMQ10 as the driest model, while the other four HadCM3Q members are showing bias patterns quite similar in magnitude to the ERA-40 simulations. As it has already been mentioned, the ERA-40 simulations are expected to have an accurate representation of the multiannual variability for the 1971-2000 period. As the Rx5day index is expected to be mainly determined by monsoonal rainfall, it could be heavily influenced by multi-annual variability. Representation of multi-annual variability in GCMs could thus contribute to the results seen for the two outliers, ECHAM5 and HadCM3Q10.

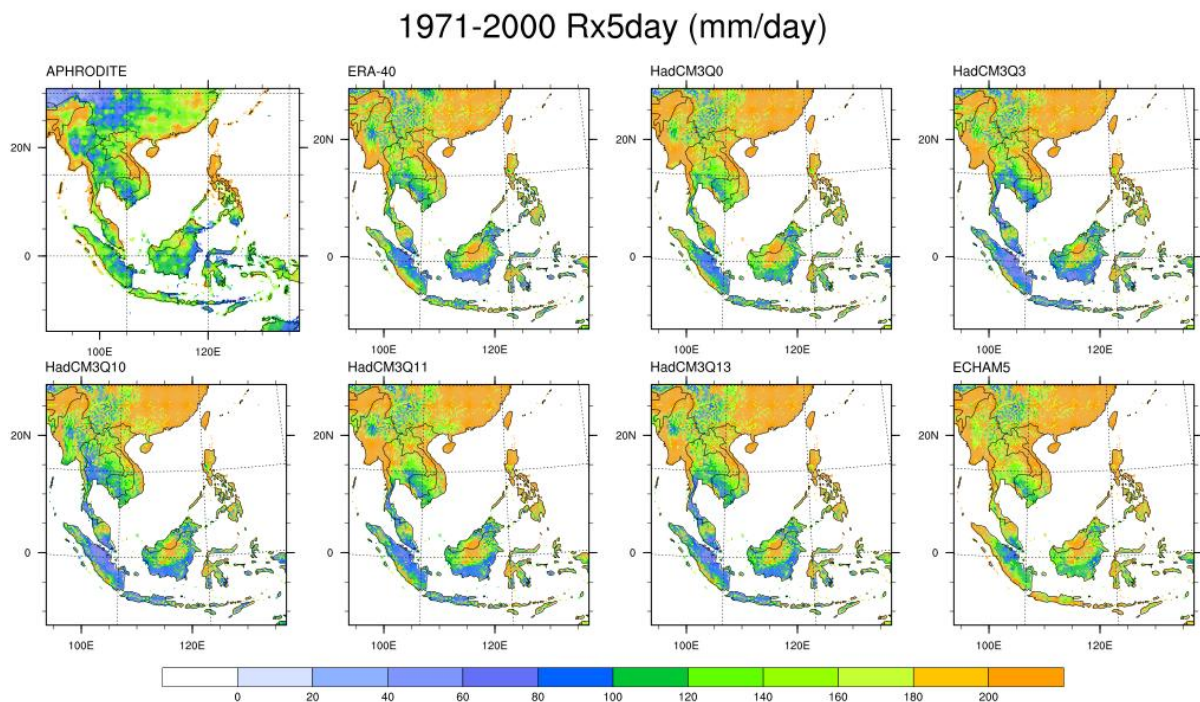


Figure 5.34: Spatial distribution of annual maximum consecutive 5 days rainfall (Rx5day) for APHRODITE, and the ERA-40 simulations, HadCM3Q0, 3, 10, 11, 13 and ECHAM5 simulations.

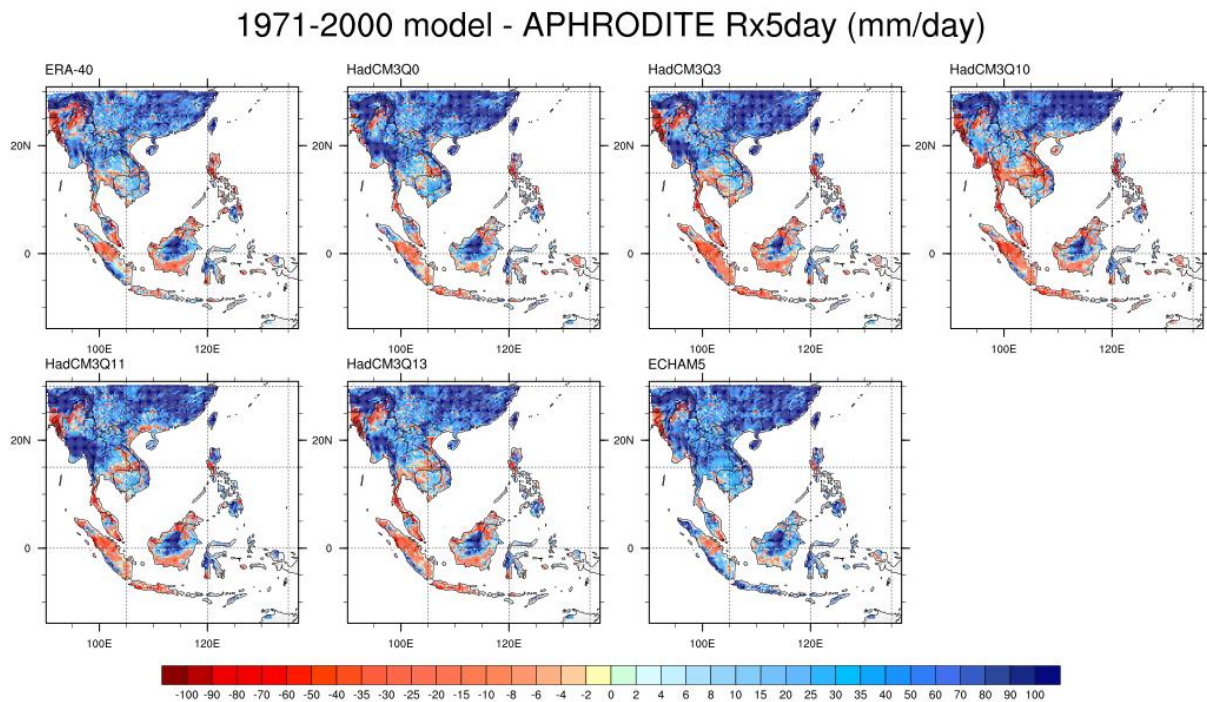


Figure 5.35: Difference between the spatial distribution of annual maximum consecutive 5 days rainfall (Rx5day) for the ERA-40 simulations, HadCM₃Q₀, 3, 10, 11, 13 and ECHAM₅ simulations against APHRODITE. Red shades show negative biases (dry), while blue shades show positive biases (wet) of simulations.

5.8.3. Annual maximum of consecutive dry days (CDD)

This index depends on the RCM's ability to produce dry days under the large scale forcing from GCMs or reanalyses. GCMs, at their typical horizontal resolution, tend to overestimate the fraction of light daily precipitation, even in the tropics ("drizzle problem", Sun, et al., 2005), while simulating correct amounts of monthly and seasonal precipitation. This problem is related to the description of spatially averaged convective processes on a relatively large area such as a GCM grid box (Dai, 2006). As a result, the number of dry days is underestimated. Since RCMs are run at higher resolution, they are expected to produce better estimates of wet days and, depending on the quality of the boundary conditions, might also be able to reproduce dry spell statistics.

There is generally good agreement in the spatial patterns of maximum CDD (or the longest dry spell) in the ERA-40 simulations and 6 RCM simulations, with APHRODITE (Figure 5.36). Areas in the north (mainland S.E. Asia and the Philippines) are simulated with longer dry spells than observed, while areas in the south (Maritime Continent) are simulated with shorter dry spells than observed (Figure 5.37). Apart from this broad geographical distribution of the bias, detail patterns and magnitude depend on the boundary conditions used to drive the regional model. The bias estimated from the ERA-40 simulations (Figure 5.37, top left panel) give an idea of errors that could be directly attributed to the regional model. Comparing to the ERA-40 simulations, the ECHAM₅ simulations produced the most similar pattern in the north (e.g. Cambodia, Thailand and Myanmar), while the HadCM₃Q simulations resemble more of the ERA-40 simulations in the south (e.g. Peninsular Malaysia, Sumatra, Borneo, and Sulawesi) especially HadCM₃Q₀, 11, and 13. In comparison with

APHRODITE, some RCM simulations seem to have a reduced bias with respect to the ERA-40 simulations. It is probable that this reduction is due to the cancellation of errors, whereby the GCM provides wetter conditions for the regions while the RCM has a dry bias.

1971-2000 Maximum Consecutive Dry Days (days)

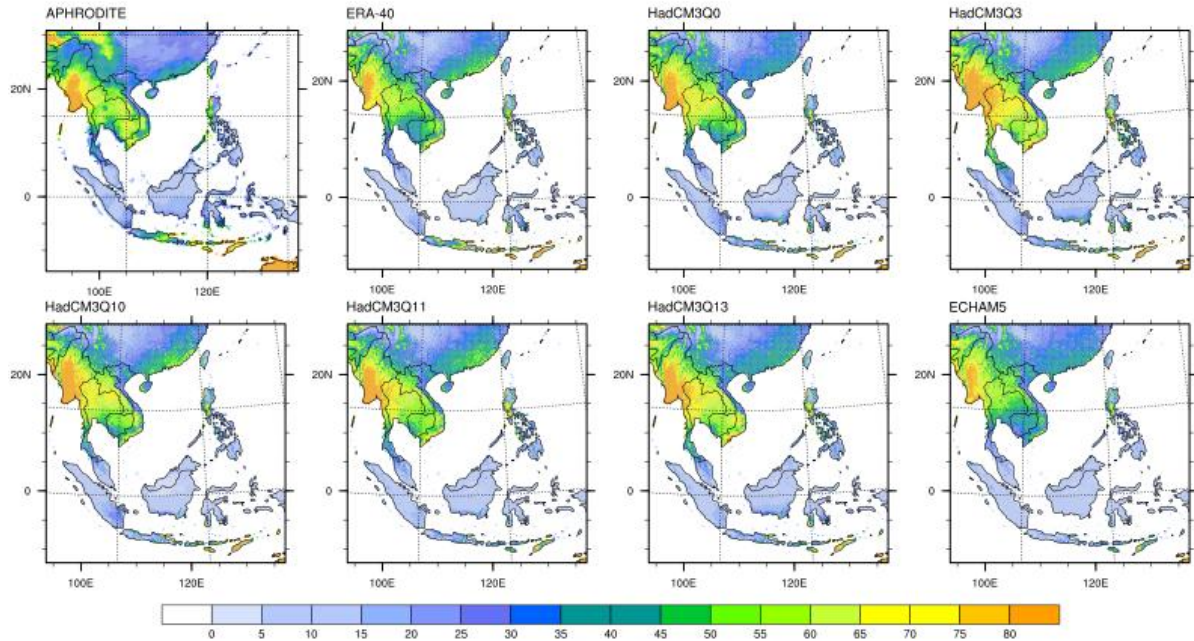


Figure 5.36: Spatial distribution of annual maximum consecutive dry days (CDD) for APHRODITE, and the ERA-40 simulations, HadCM3Q0, 3, 10, 11, 13 and ECHAM5 simulations.

1971-2000 model - APHRODITE CDD (days)

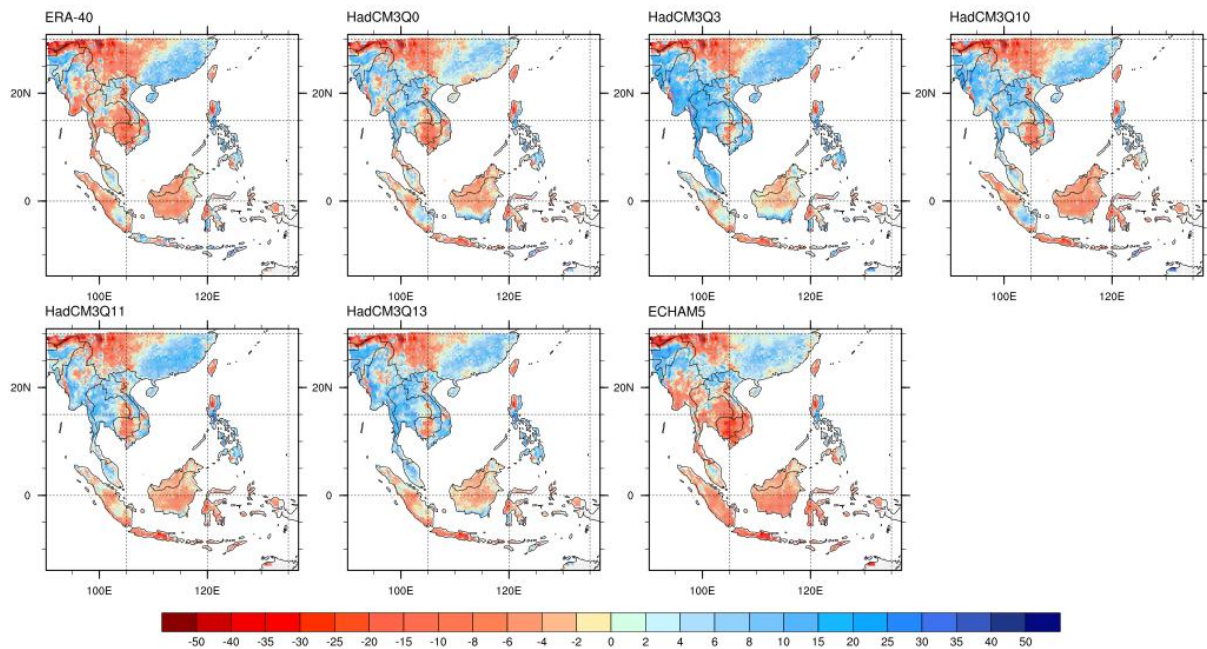


Figure 5.37: Difference between the spatial distribution of annual maximum consecutive dry days (CDD) for the ERA-40 simulations, HadCM3Q0, 3, 10, 11, 13 and ECHAM5 simulations against APHRODITE. Red shades show negative biases (shorter dry spells), while blue shades show positive biases (longer dry spells) of simulations.

5.8.4. Trends in extreme rainfall indices

A 30-year 1971-2000 time series for Rx_{1day} , Rx_{5day} and CDD for both APHRODITE and the ERA-40 simulations were plotted on Figure 5.38 - Figure 5.40 for the land regions in the whole domain. For the Rx_{1day} index (Figure 5.38), APHRODITE showed increasing trends but this is not considered significant (at p -value < 0.05). The ERA-40 simulations however reproduced a trend that is relatively stronger and statistically significant. As for the Rx_{5day} index (Figure 5.39), both observation and simulation show increasing trends which are statistically significant and, like the Rx_{1day} index, the simulation exaggerates this trend. Another notable outcome is that the simulation reproduced the inter-annual variability well after 1985 in both the Rx_{1day} (Figure 5.38) and Rx_{5day} (Figure 5.39) indices. A possible reason for the stronger and very significant trend in the ERA-40 simulations could be due to the different observational datasets used in different periods to construct the ERA-40 reanalysis (Andersson, et al., 2004), leading to a pronounced increase in tropical humidity after 1991, which corresponds to the period of increased extreme indices in Figure 5.38 and Figure 5.39. For CDD, both APHRODITE and ERA-40 simulations showed no significant trend (Figure 5.40).

Table 1 summarises the p -values (significance) and the regression coefficients (magnitude) of the trends in APHRODITE and ERA-40 simulations. **Overall, the RCM was able to reproduce the sign of the trends (for Rx_{1day} and Rx_{5day}) and the inter-annual variability of the observed rainfall indices (for Rx_{5day} and CDD),** although it seems to be affected by the non-homogeneity of humidity from the ERA-40 boundary conditions.

Table 1: Trends in APHRODITE and ERA-40 simulations of rainfall indices.

	p-value	Regression Coefficient
Rx1day		
APHRODITE	0.069	0.117
ERA-40	0.00004894	0.572
Rx5day		
APHRODITE	0.019	0.291
ERA-40	0.000453	1.005
CDD		
APHRODITE	0.357	0.079
ERA-40	0.782	-0.024

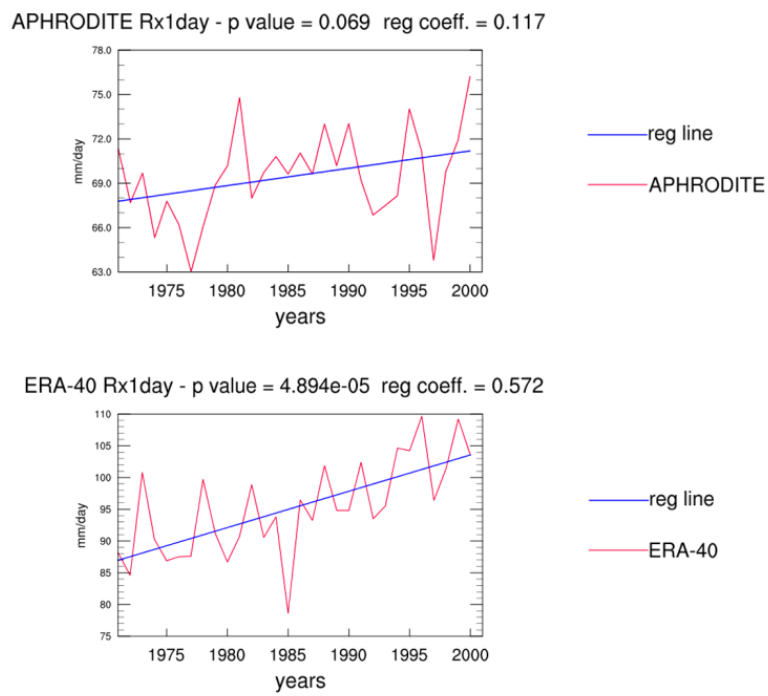


Figure 5.38: Time series plot (30-years from 1971-2000) of Rx1day for APHRODITE (top) and ERA-40 simulations (bottom) for S.E. Asia. Blue line is the fitted linear trend.

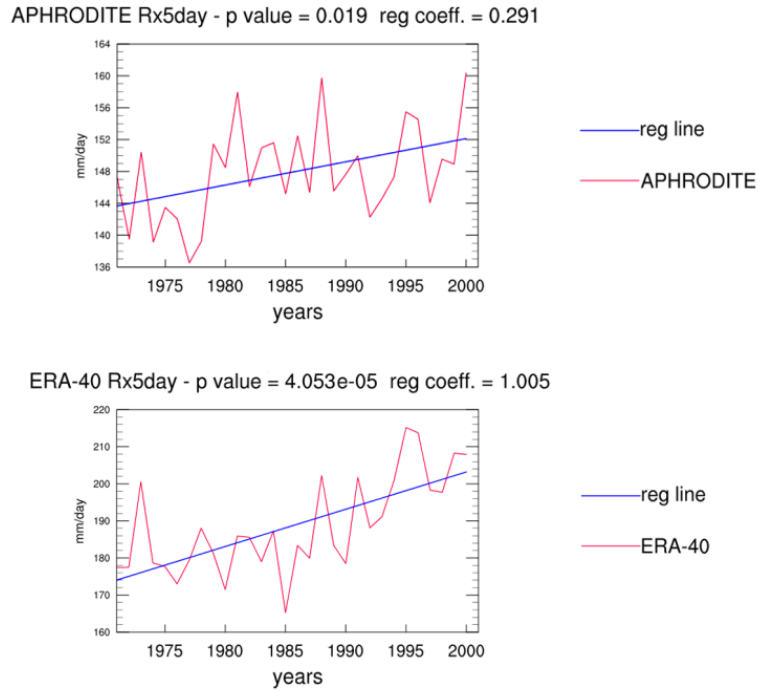


Figure 5.39: Time series plot (30-years from 1971-2000) of Rx5day for APHRODITE (top) and ERA-40 simulations (bottom) for S.E. Asia. Blue line is the fitted linear trend.

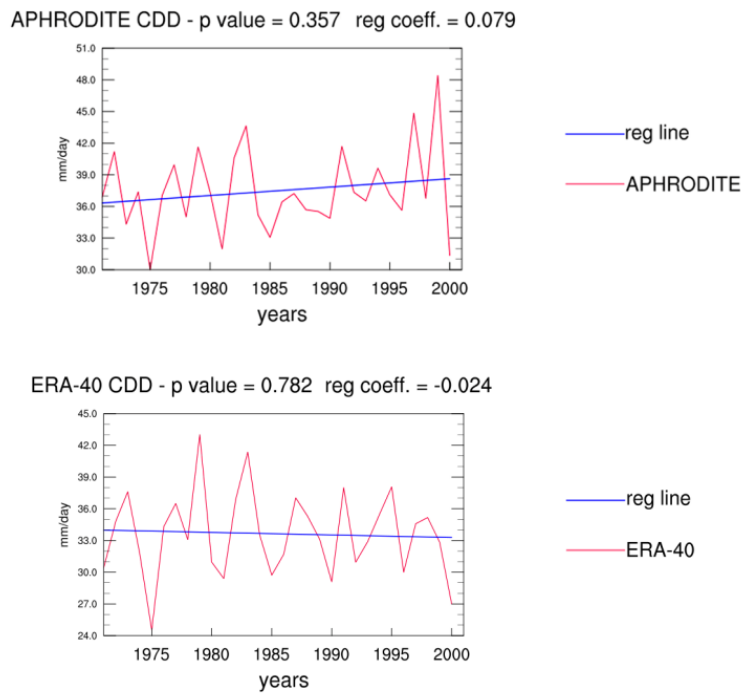


Figure 5.40: Time series plot (30-years from 1971-2000) of CDD for APHRODITE (top) and ERA-40 simulations (bottom) for S.E. Asia. Blue line is the fitted linear trend.

5.9. Evaluation of extreme temperature indices

The mean annual maximum and minimum *average daily temperature*, TMx and TMn respectively, for the 6 RCM simulations and the ERA-40 simulations were evaluated against APHRODITE (1971-2000) in the subsequent sections. TMx represents the average of several years' warmest-day-of-the-year, while TMn represents the average of several years' coolest-day-of-the-year.

5.9.1. Mean annual minimum average daily temperature, TMn

The simulations of TMn from the 6 RCM together with the ERA-40 simulations and APHRODITE are shown in Figure 5.41. **In general, the TMn is simulated well by the 6 RCM simulations and the ERA-40 simulations** (Figure 5.42). But in some isolated areas over Sumatra, southern Borneo, southern Peninsular Malaysia, and parts of mainland S.E. Asia, warm biases are observed in the order of 1 to 2°C. Southern China shows cold biases in the order of 1 to 3°C. In these regions, biases have the same order of magnitude as seasonal daily temperatures (Figure 5.6 to Figure 5.9). All the RCM simulations also have strong cold biases over the Tibetan Plateau, including that from the ERA-40 simulations, suggesting general difficulty in simulating temperatures in that region. This cold bias could be related to problems in applying atmospheric boundary conditions at the rim, in a region with very complex topography.

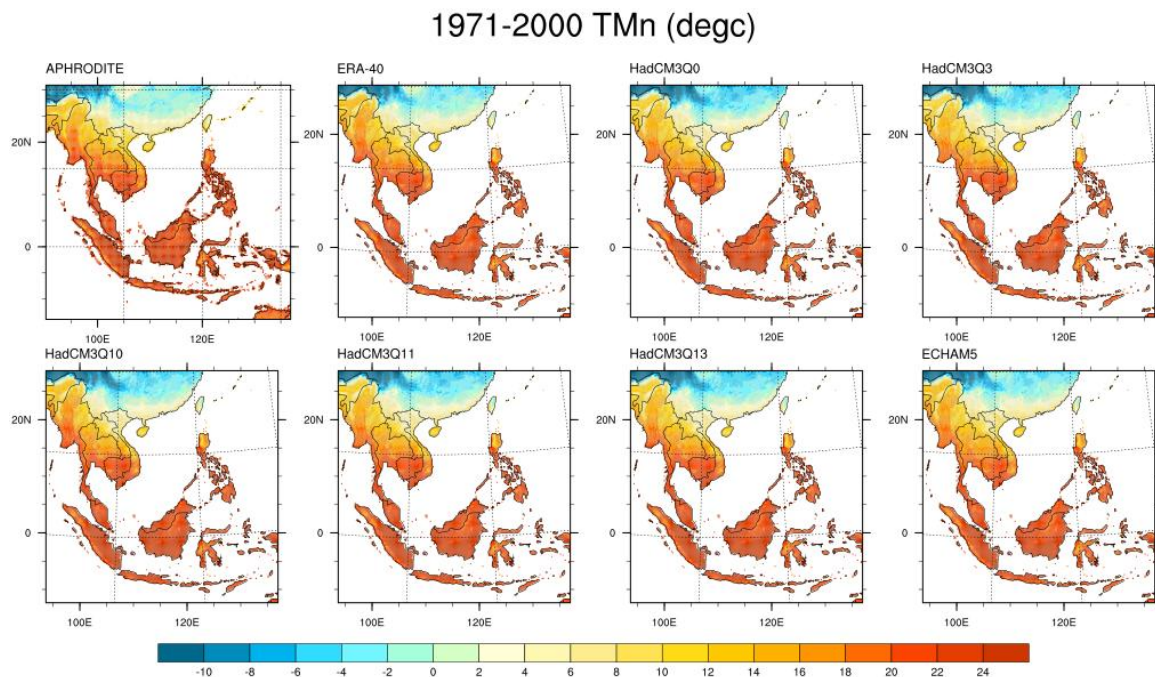


Figure 5.41: Mean annual minimum average daily temperature, TMn, from APHRODITE, the ERA-40 simulations, the HadCM3Q0, 3, 10, 11, 13 and ECHAM5 simulations.

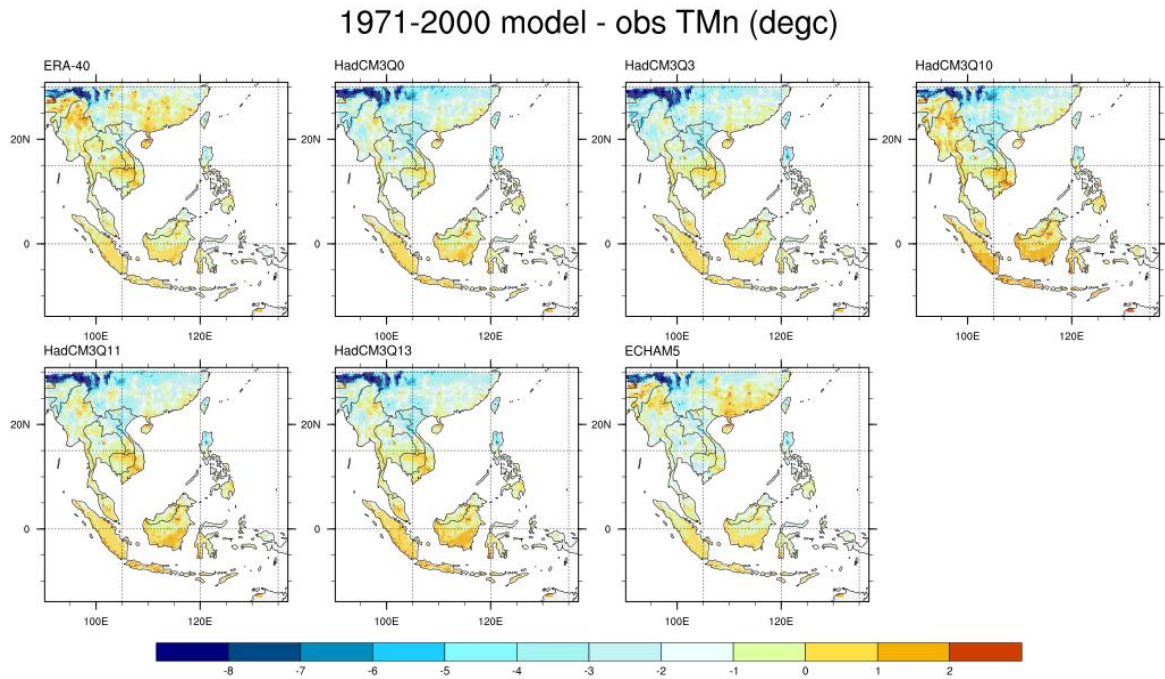


Figure 5.42: Difference between the simulations (ERA-40, HadCM₃Q₀, 3, 10, 11, 13 and ECHAM₅) and observations (APHRODITE) mean annual daily minimum average temperature, TMn, in °C. Red shades show warm biases of simulations, while blue shades show cool biases of simulations.

5.9.2. Mean annual maximum average daily temperature, TMx

The mean annual maximum average daily temperature, TMx, from the 6 RCM simulations and the ERA-40 simulations show some biases as well (Figure 5.43). Warm biases relative to APHRODITE range from 1 to 4°C over the Maritime Continent of Peninsular Malaysia, Sumatra and Borneo. Even warmer biases of about 2 to 5°C were simulated over the regions of southern China and northern parts of Vietnam, Thailand, Myanmar, and Laos (Figure 5.44); this could be due to local processes and affected by the availability of soil moisture in the warmest seasons. Sulawesi, the Philippines, and coastal Myanmar show negative biases in the order of 1 to 3°C. As with the TMn, all the RCM simulations also have strong cold biases over the Tibetan Plateau, including that from the ERA-40 simulations, which again suggests general difficulty in simulating temperatures in that region that could also be related to problems at the boundaries.

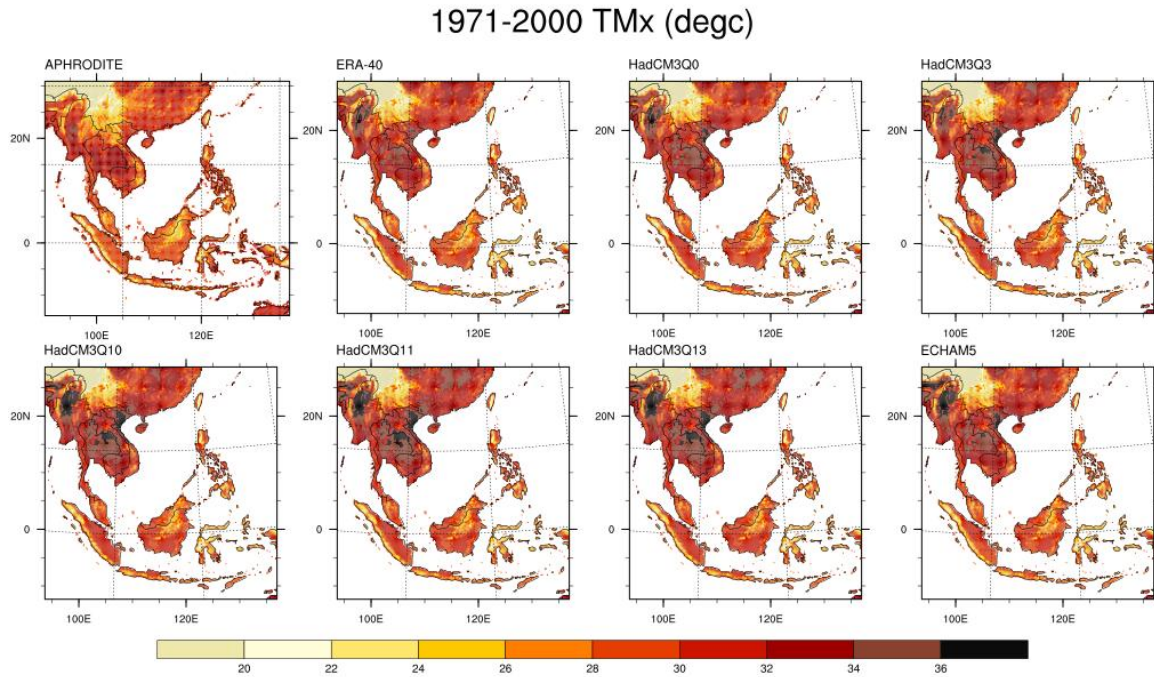


Figure 5.43: Mean annual maximum average daily temperature, TMx, from APHRODITE, the ERA-40 simulations, the HadCM₃Q₀, 3, 10, 11, 13 and ECHAM₅ simulations.

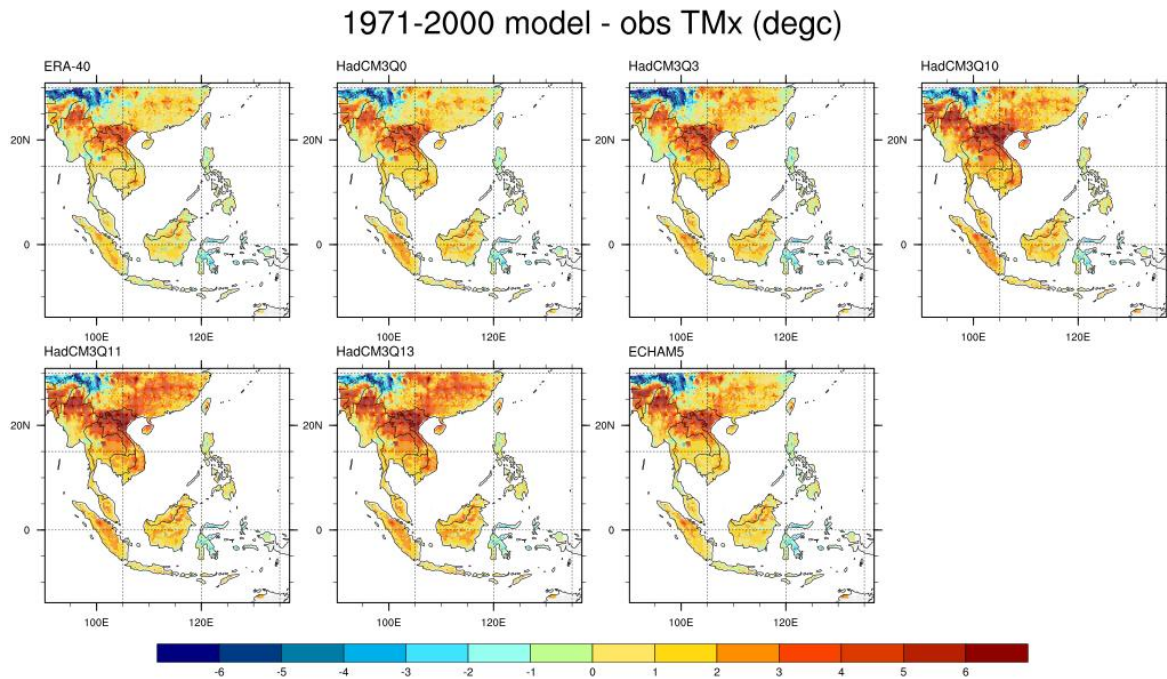


Figure 5.44: Difference between the simulations (ERA-40, HadCM₃Q₀, 3, 10, 11, 13 and ECHAM₅) and observations (APHRODITE) mean annual daily maximum average temperature, TMx, in °C. Red shades show warm biases of simulations, while blue shades show cool biases of simulations.

5.9.3. Maximum day time temperature, TXx and Maximum night time temperature, TNx

The ERA-40 and RCM simulations of the annual maximum day time temperature (or warmest day), TXx, and annual maximum night time temperature (or warmest night), TNx, are plotted on Figure 5.45 and Figure 5.46. *For these extreme temperature indices, no suitable datasets are available to be compared against. Thus, the performance of the simulations against only the ERA-40 simulations was analysed.* It should be taken into account that the analyses of minimum and maximum daily temperatures shown in the sections above indicate that the ERA-40 simulations are not necessarily the simulations with the smallest bias and that instantaneous minimum and maximum temperature are much more difficult to reproduce since they are the result of very short-lived processes which could be much more difficult to capture by a regional model. Therefore, a proper assessment by comparison with a good quality dataset is still needed to evaluate these model simulations. For the TXx, the 6 RCM simulations and the ERA-40 simulations are generally comparable with values between 36 and 40°C over the Maritime Continent of Peninsular Malaysia, Sumatra, Philippines and Borneo except over the highland areas. Many places over mainland S.E. Asia (e.g. northern Thailand and Myanmar) and southern China show values ranging from 40 to 46°C.

TNx from the 6 RCM simulations and the ERA-40 simulations were also generally comparable with values of 28 to 32°C over the sea and low land areas of Maritime Continent. Tibetan plateau showed TNx of less than 18°C. Other land regions showed TNx of 22 to 28°C.

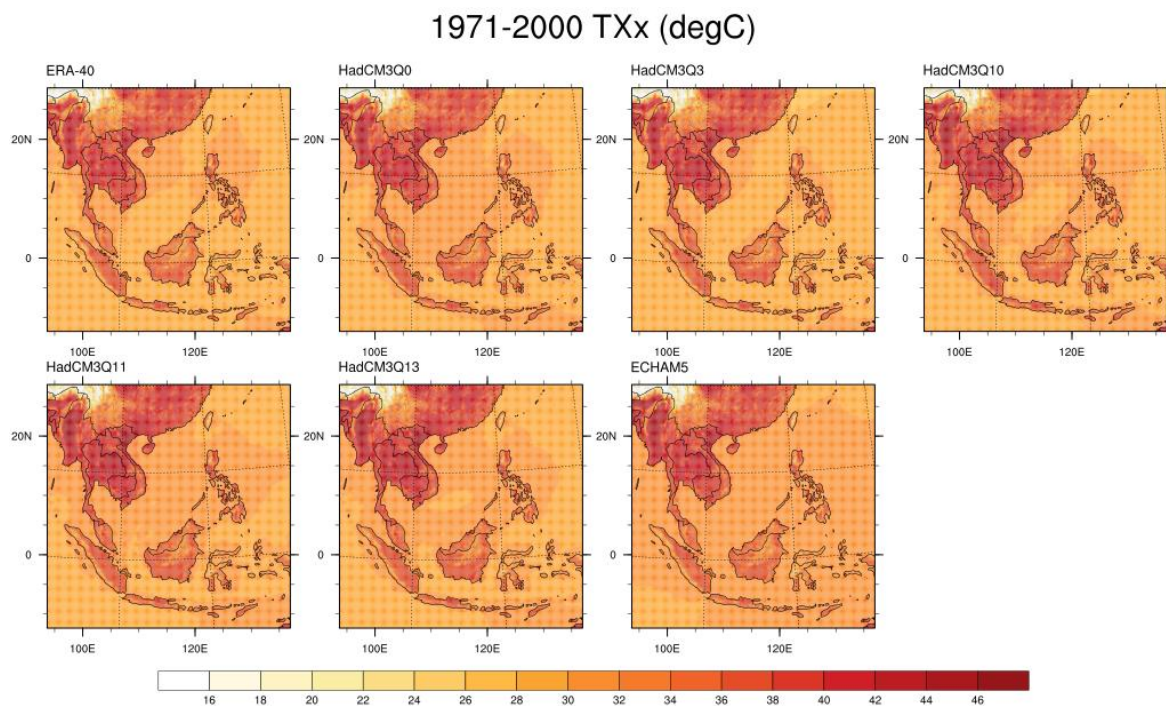


Figure 5.45: Maximum day time temperature (warmest day) of the year, TXx, from the ERA-40 simulations, the HadCM₃Q₀, 3, 10, 11, 13 and ECHAM₅ simulations.

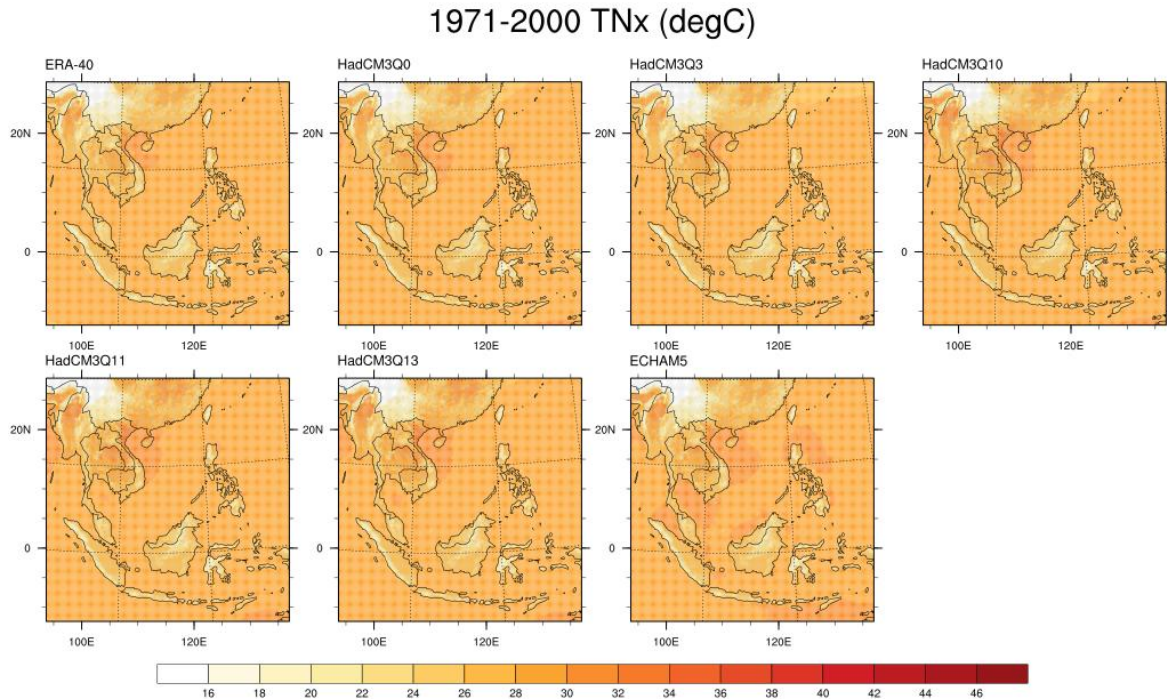


Figure 5.46: Maximum night time temperature (warmest night) of the year, TNx, from the ERA-40 simulations, the HadCM3Q0, 3, 10, 11, 13 and ECHAM5 simulations.

5.9.4. Trends in extreme temperature indices of TMx and TMn

A 30-year 1971-2000 time series for TMx and TMn for both APHRODITE and ERA-40 simulations of TMx and TMn were plotted on Figure 5.47 and Figure 5.48. Table 2 summarises the p-values (significance) and the regression coefficients (magnitude) of the trends in APHRODITE and ERA-40 simulations.

Table 2: Trends in APHRODITE and ERA-40 simulations of temperature indices.

	p-value	Regression Coefficient
TMx		
APHRODITE	0.05	0.010
ERA-40	0.12	0.012
TMn		
APHRODITE	0.0000408	0.055
ERA-40	0.0455	0.019

For both extreme temperature indices, there are statistically significant (at p-value < 0.05) trends in APHRODITE. The ERA-40 simulations are able to capture a similar trend in the TMx but the trend is not statistically significant (Figure 5.47). As for the TMn index, the ERA-40 simulations are not able to capture as strong a trend as in the observations, but the trend detected is statistically significant. Figure 5.47 and Figure 5.48 compare trends for the two indices estimated from APHRODITE and the ERA-40 simulations. The two figures show a very good comparison of the interannual variability of the two indices which do not suggest any

particular problems related to the discontinuity of tropospheric humidity associated with the ERA-40 reanalysis (Andersson, et al., 2004).

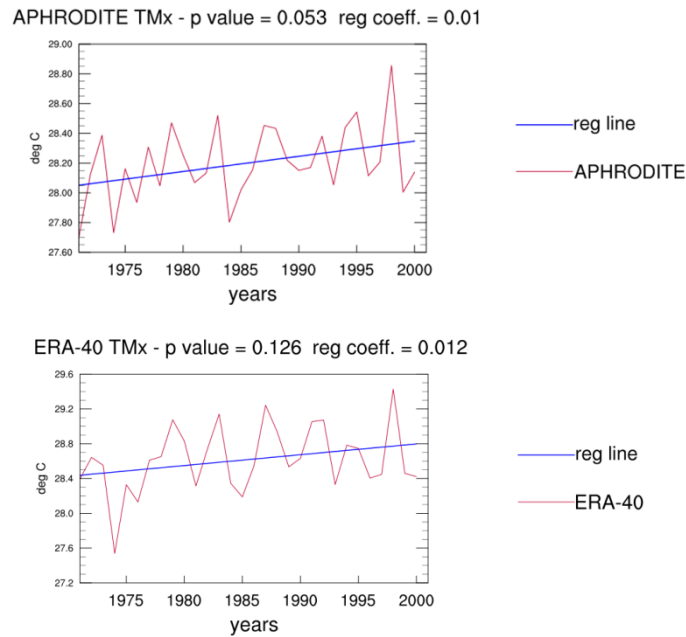


Figure 5.47: Time series plot (30-years 1971-2000) of annual maximum average daily temperature (TMx) for APHRODITE and ERA-40 simulations. Blue line represents the fitted linear trend.

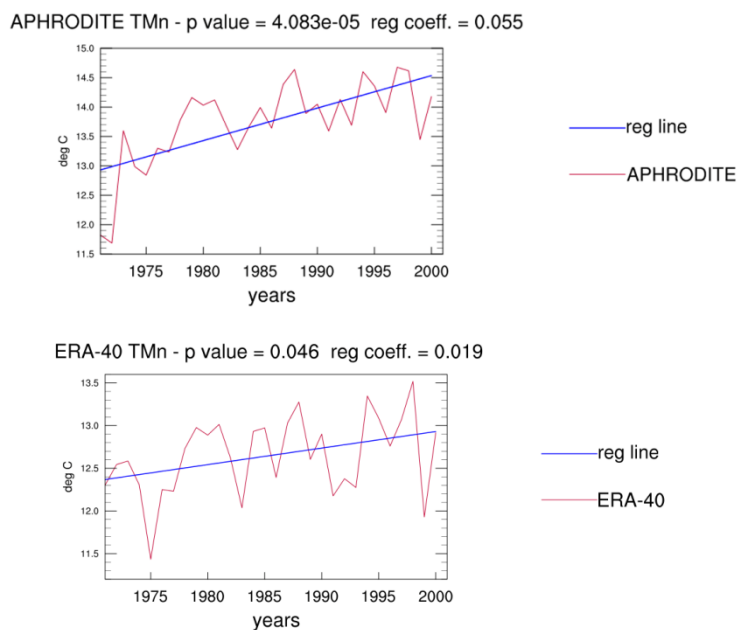


Figure 5.48: Time series plot (30-years 1971-2000) of annual minimum average daily temperature (TMn) for APHRODITE and ERA-40 simulations. Blue line represents the fitted linear trend.

5.10. Evaluation of 5-year return level indices (TMx and Rx1day)

Figure 5.49 and Figure 5.50 show 5-year return levels for the maximum daily temperature (TMx) and precipitation (Rx1day), from the series of annual maxima from APHRODITE, the

ERA-40 simulations and for two RCM simulations, HadCM3Q0 and ECHAM5, for the period 1970-2000. These estimates have been done by fitting the series of annual maxima to a Generalised Extreme Value (GEV) distribution, using a maximum likelihood estimate (MLE), as described in Coles, 2001. These are events which are five times less likely than the ones in sections 5.9.2 and 5.8.1. In comparison with the figures from the said sections, the R_{x1day} (Figure 5.32) have the same pattern and much reduced rainfall intensity with respect to the 5-year return level plot (Figure 5.49), which can be exceeding 50% in the wettest regions. The comparison with APHRODITE shows a scaling factor between observed and simulated precipitation that is not too different from the scaling factor which can be estimated from the R_{x1day} analysis (Figure 5.32). From the work of Kamiguchi, et al. (2010) it is expected that this scaling factor should increase quite quickly for very extreme precipitation, but this analysis seems to show that this limit has not been reached yet.

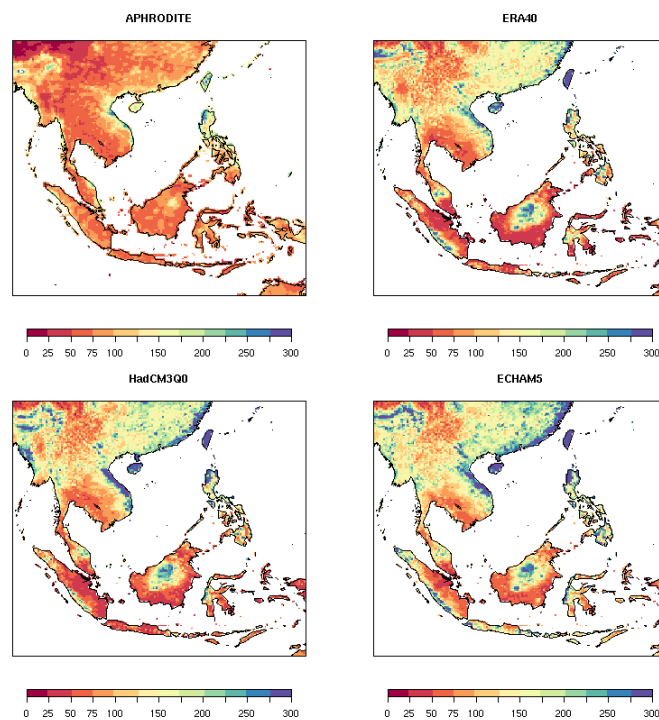


Figure 5.49: 5-year return levels for the maximum daily precipitation (R_{x1day}), from the series of annual maxima from APHRODITE, the ERA-40 simulations and for two RCM simulations, HadCM3Q0 and ECHAM5, for the period 1970-2000.

A closer similarity can be found between TM_x (Figure 5.43) and the 5-year return values of the maximum daily temperature (Figure 5.50) for all datasets in this study. In this case, the difference between two indices is quite small, a possible indication that daily temperatures are reaching their maximum asymptotic values (the existence of an asymptotic value has been assessed from the GEV analysis and corresponds to the case of negative shape parameters, cf. Coles, 2001).

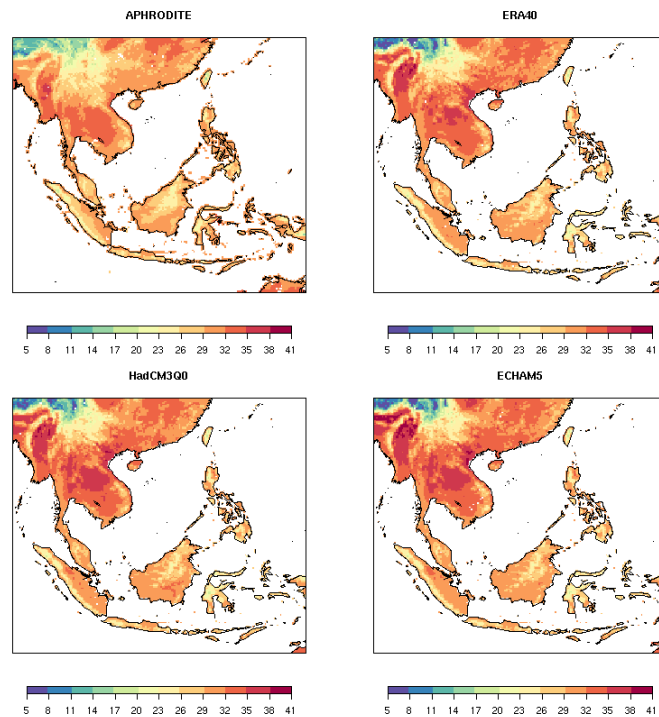


Figure 5.50: 5-year return levels for the maximum daily temperature (TMx), from the series of annual maxima from APHRODITE, the ERA-40 simulations and for two RCM simulations, HadCM3Q0 and ECHAM5, for the period 1970-2000.

5.11. Evaluation of precipitation tele-connection with ENSO

This analysis examines the ability of the RCM to capture the tele-connections (covariance) between precipitation in the region with the El-Nino Southern Oscillation (ENSO), in particular the Nino3.4 index. The 5-year return level for JJA rainfall from APHRODITE, the ERA-40 simulations and the two RCM simulations, HadCM3Q0 and ECHAM5, are plotted on Figure 5.51 to provide context. JJA is chosen as the season is significantly affected by ENSO. This figure show the positive differences between simulated and observed indices over the northern part of the domain, but on the Maritime Continent, APHRODITE has return levels of the same order of magnitudes or even larger than the model data, in particular on the coastal areas (with the exception of the high elevation areas which have a strong negative differences between model and observation estimates). These estimates of the 5-year return levels have nevertheless a smaller negative bias with respect to the 95% percentile estimated for JJAS (shown in Figure 5.26).

The analysis of the covariance between precipitation and ENSO can be done by adding a parameter which depends on the NINO3.4 index to the location parameter of the GEV curve (Coles, 2001). A comparison of the covariates can be done only between APHRODITE and ERA-40 (Figure 5.52), since the GCMs have their ENSO events independent from the observed record and the period is probably not sufficiently long to ensure that there will be a sufficient number of El Nino-La Nina events to estimate a covariate. The stippled areas show a significant statistical relationship at the 5% level. Both datasets show a widespread significant relationship for the equatorial region. Equally important are the small patches of strong significant relationship over the continental areas, because there is a good overlap between

the significant region from APHRODITE and those from the ERA-40 simulations. It is important to assess that the RCM model is indeed capable to convert the large scale forcings (ENSO in this case) to localised extreme rainfall events.

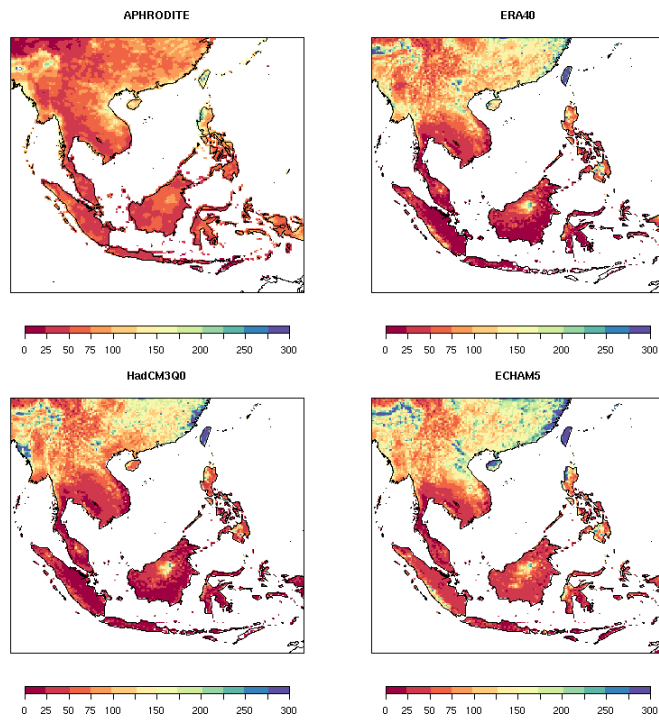


Figure 5.51: 5-year return levels for the maximum daily precipitation (Rx1day) during JJA, from the series of annual maxima from APHRODITE, the ERA-40 simulations and for two RCM simulations, HadCM3Q0 and ECHAM5, for the period 1970-2000.

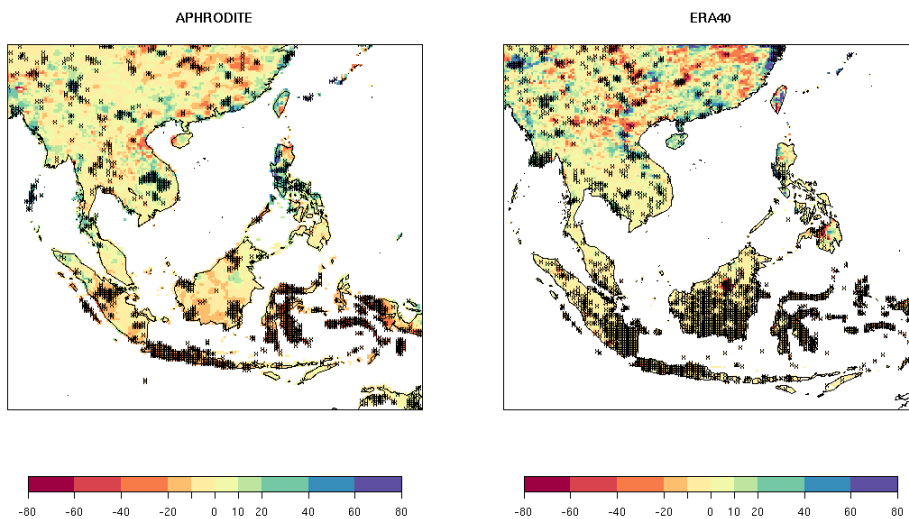


Figure 5.52: Covariance between precipitation with Niño3.4 index in APHRODITE (left) and ERA-40 simulations (right). The stippled (black) areas show a significant statistical relationship at the 5% level.

6. Mid- and Long-term Climate Change Projections

The mid- and long-term climate change projections for the different climate parameters are provided for two 30-year periods, 2031-2060 and 2071-2100, respectively. All changes are provided with respect to the baseline period of 1970-2000 which has been used in section 5. All the climate change projection runs from the HadCM3Q ensemble and the ECHAM5 global climate models will be referred to as simply 'projections' henceforth. On occasions, mid- and long-term projections would interchangeably be referred to as mid- and end-century projections.

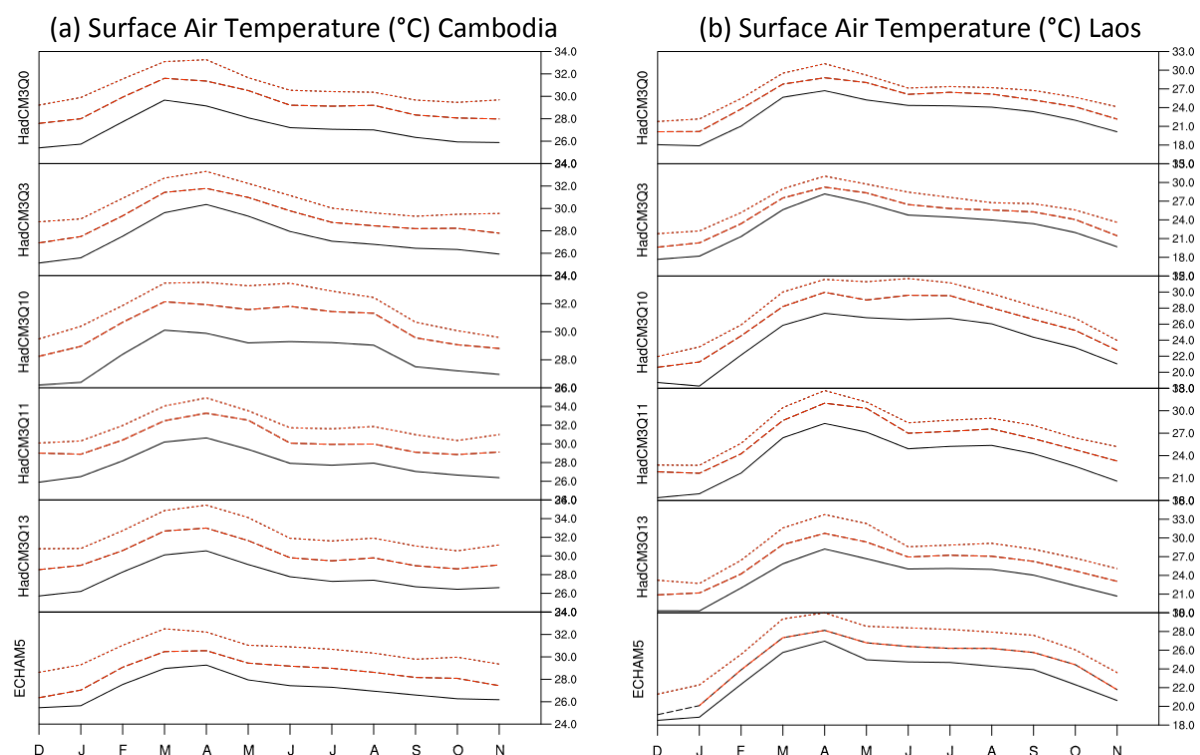
6.1. Annual temperature cycle projections

In the subsequent plots, future changes in the annual cycle temperature plots are given for the mid-term in dashed lines, and for the long-term in dotted lines. For the baseline periods, these had been plotted as solid lines. The projections

are provided from top to bottom in the order of HadCM3Q0, 3, 10, 11, and 13 and the ECHAM5.

Range of future projections

Note that the range of the uncertainty in the future projections of the selected HadCM3Q ensemble members represents only the range from parametric uncertainty (see Section 4.3.2). The inclusion of the ECHAM5 simulation serves to give only limited additional information on structural uncertainty from a different GCM. Another type of uncertainty comes from using a different RCM, which is not covered in this report. As such, the outcomes of the projections sections need to be taken in context with the reports from the IPCC (AR5 and SREX), as well other regional climate downscaling studies.



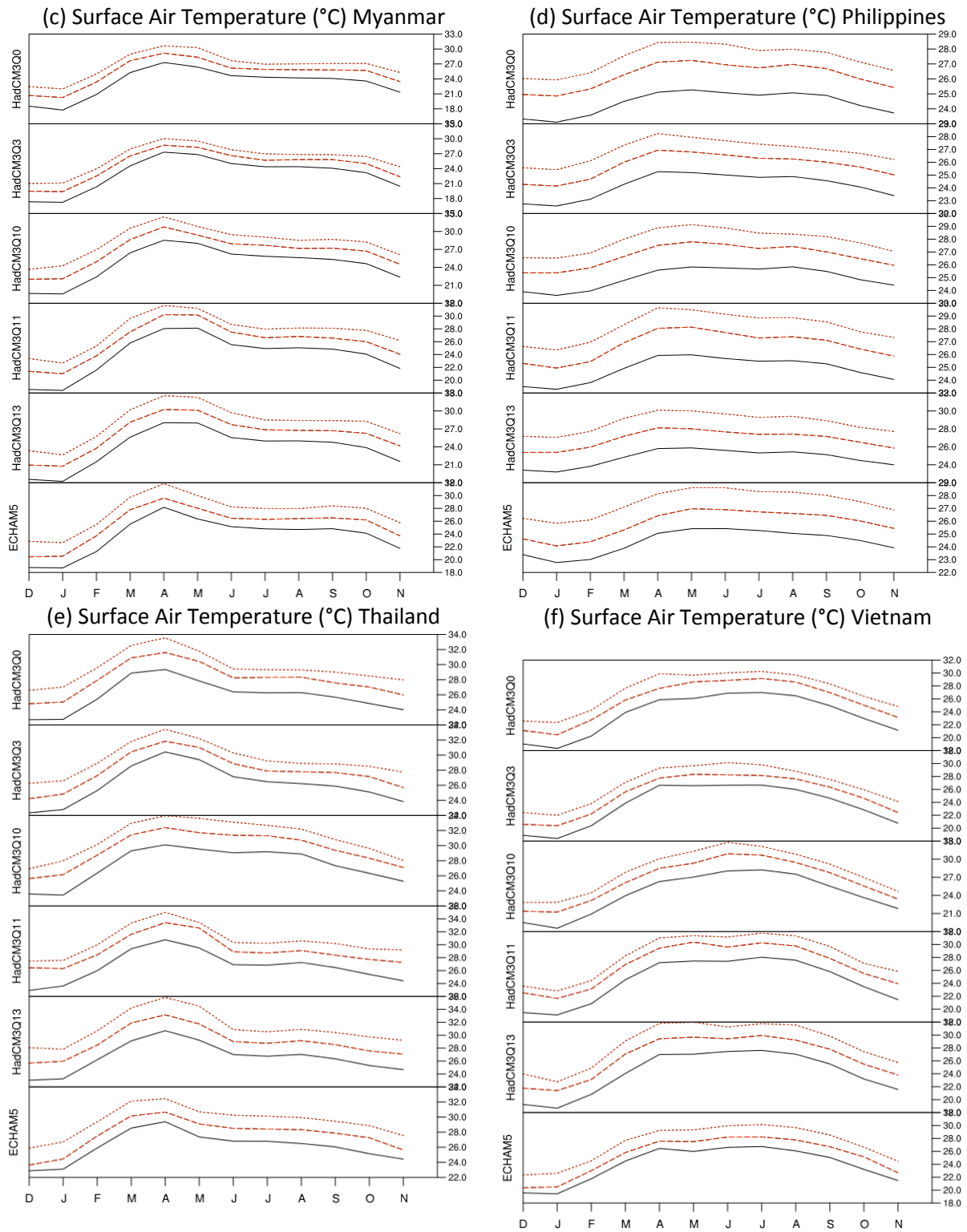
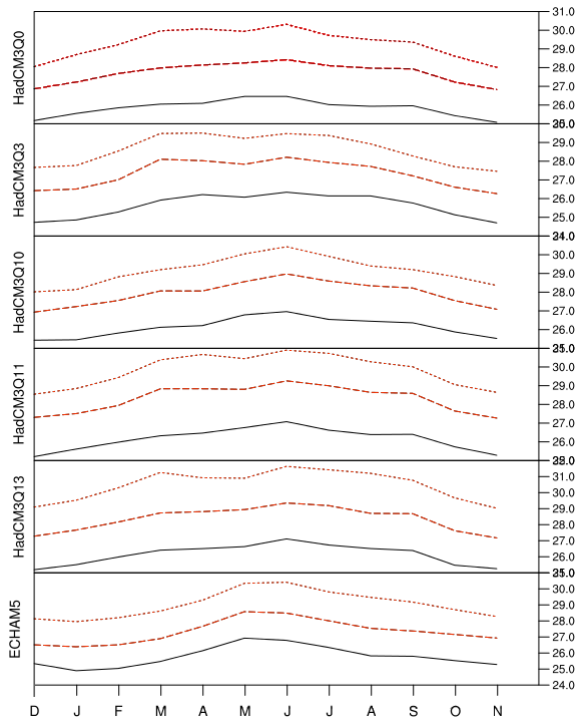
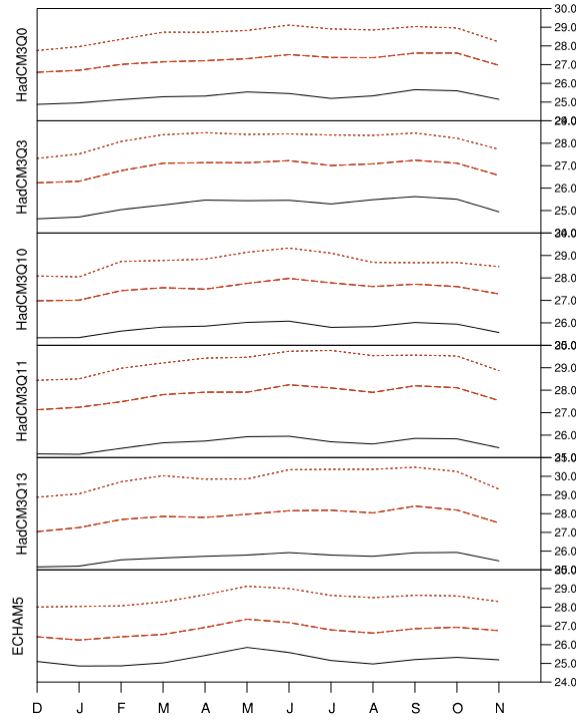


Figure 6.1: Annual cycle of surface air temperature for (a) Cambodia, (b) Laos, (c) Myanmar, (d) Philippines, (e) Thailand, and (f) Vietnam for the baseline period (1971-2000) in solid lines, mid-term projections (2031-2060) in dashed lines and long-term projections (2071-2100) in dotted lines. Significant projections passing xxx level in t-test are plotted in red.

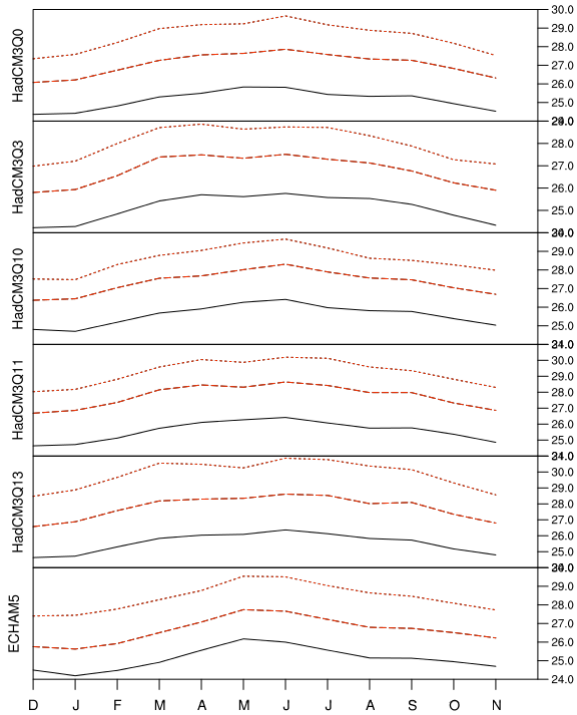
(a) Surface Air Temperature (°C) Brunei



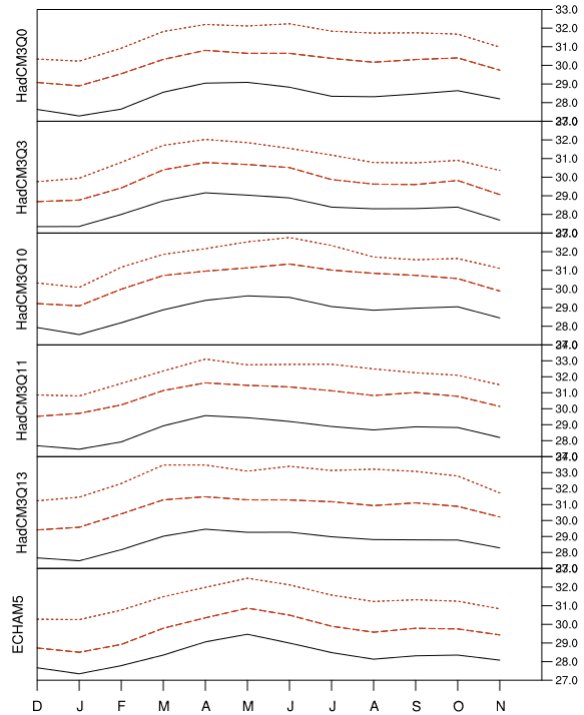
(b) Surface Air Temperature (°C) Indonesia



(c) Surface Air Temperature (°C) Malaysia



(d) Surface Air Temperature (°C) Singapore



(e) Surface Air Temperature (°C) Timor Leste

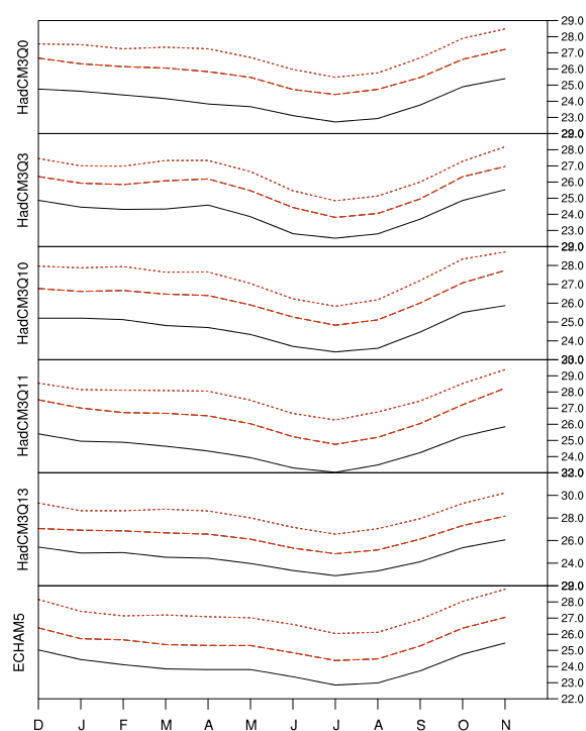


Figure 6.2: Figure 6.3: Annual cycle of surface air temperature for (a) Brunei, (b) Indonesia, (c) Malaysia, (d) Singapore, and (e) Timor Leste for the baseline period (1971-2000) in solid lines, mid-term projections (2031-2060) in dashed lines and long-term projections (2071-2100) in dotted lines. Significant projections passing the 5% level in t-test are plotted in red.

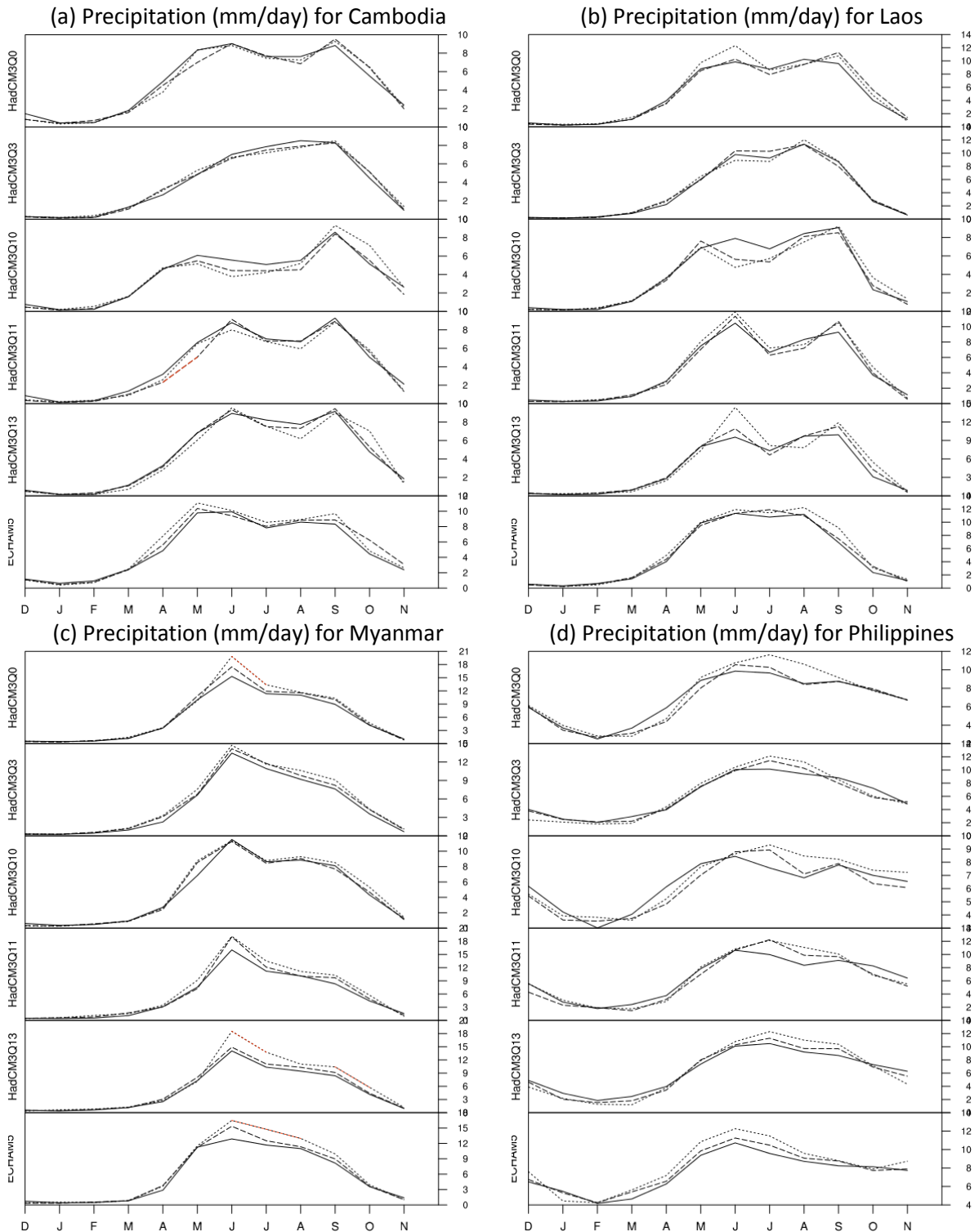
Table 3: Summary of estimated mid-term and long-term projections of annual cycle temperature changes.

Country	Approx. mid-term change projections (°C)	Approx. long-term change projections (°C)	Significant projections
Cambodia	2.0 – 3.0	4.0 – 5.0	All
Laos	2.0 – 3.0	3.0 – 4.0	
Myanmar	Up to 2.0	Up to 4.0	
Philippines	Up to 1.5	Up to 3.0	
Thailand	2.0 – 3.0	4.0 – 5.0	
Vietnam	2.0 – 3.0	3.0 – 4.0	
Brunei	2.0 – 3.0	3.0 – 4.0	All
Indonesia	2.0 – 3.0	3.0 – 4.0	
Malaysia	2.0 – 3.0	3.0 – 4.0	
Singapore	Up to 1.5	Up to 3.0	
Timor Leste	1.5 – 2.0	3.0 – 4.0	

Table 3 summarises the change in the annual temperature cycle projections for each country. All models and countries show significant and consistent increase in surface air temperature. **In general, surface air temperature are expected to rise by 2°C by mid-century and 4°C by end-century, with some countries projected to be experiencing an increase by up to 5°C.**

6.2. Annual precipitation cycle projections

In the following plots, future changes in the annual precipitation cycle plots are given for the mid-term in dashed lines, and for the long-term in dotted lines in mm/day. For the baseline periods, these had been plotted as solid lines. The projections are provided from top to bottom in the order of HadCM3Q0, 3, 10, 11, and 13 and the ECHAM5.



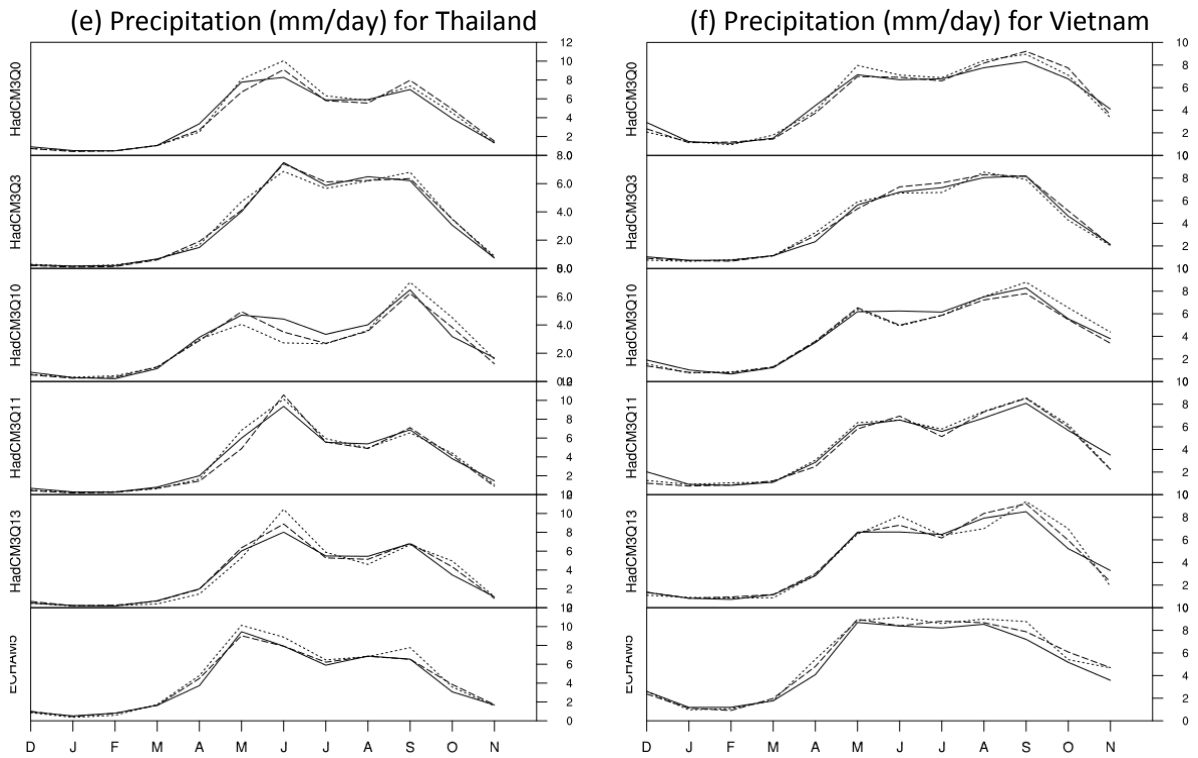
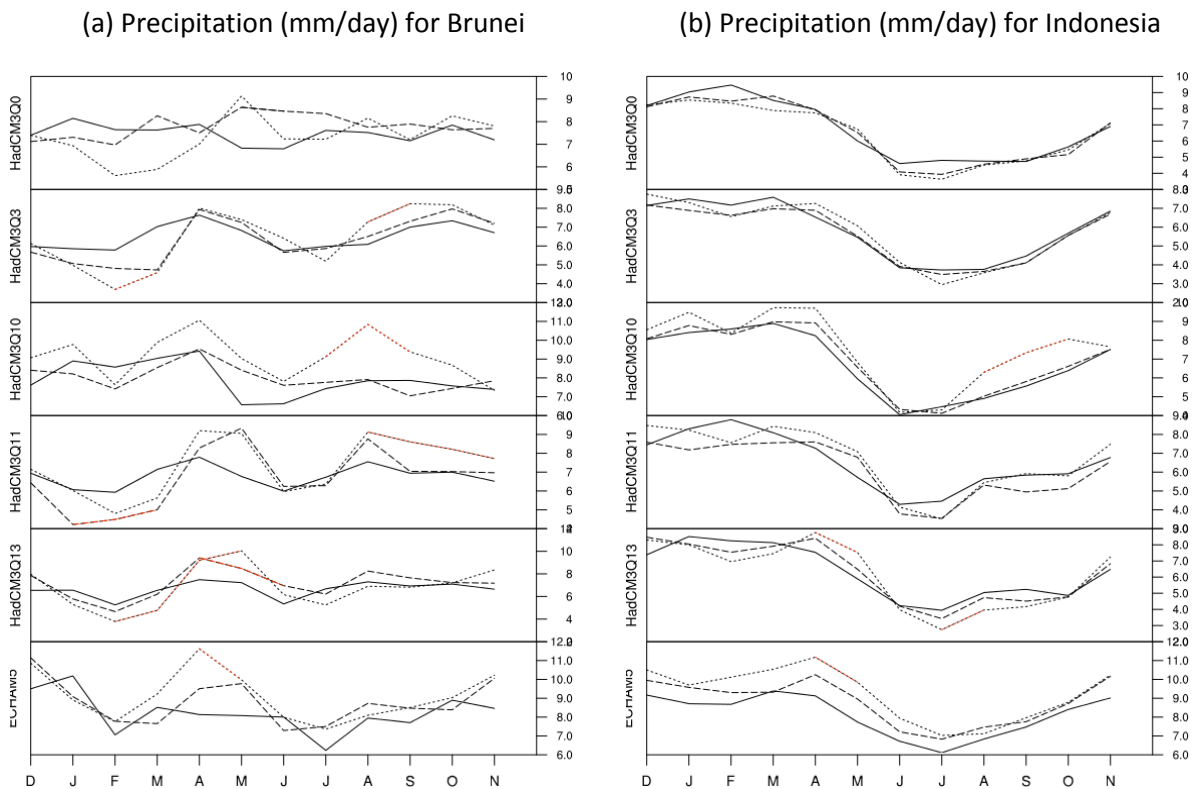
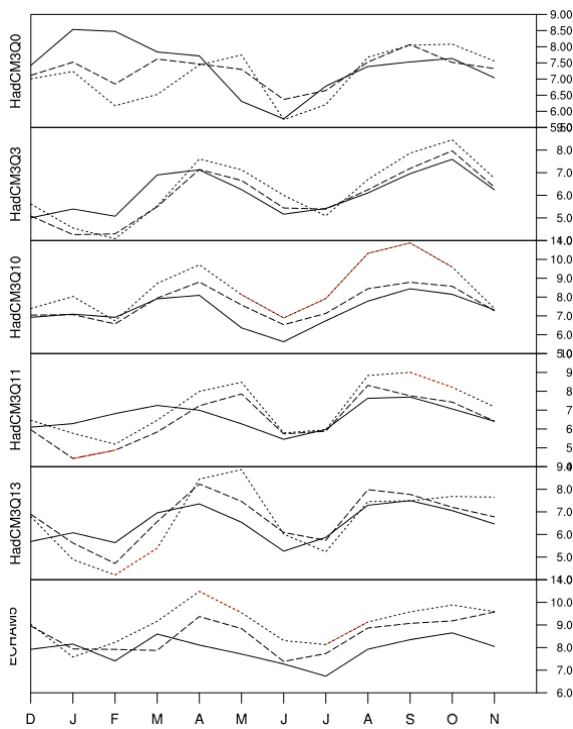


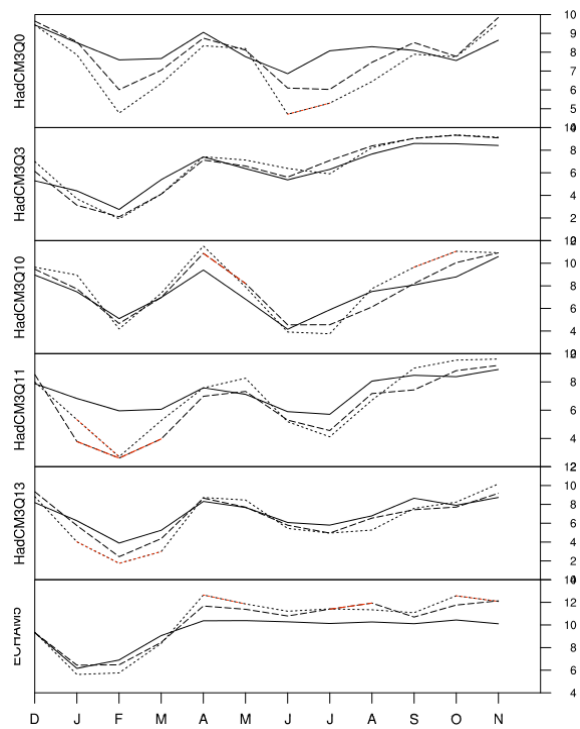
Figure 6.4: Annual cycle of precipitation for (a) Cambodia, (b) Laos, (c) Myanmar, (d) Philippines, (e) Thailand, and (f) Vietnam for the baseline period (1971-2000) in solid lines, mid-term projections (2031-2060) in dashed lines and long-term projections (2071-2100) in dotted lines. Significant projections passing the 5% level in t-test are plotted in red.



(c) Precipitation (mm/day) for Malaysia



(d) Precipitation (mm/day) for Singapore



(f) Precipitation (mm/day) for Timor Leste

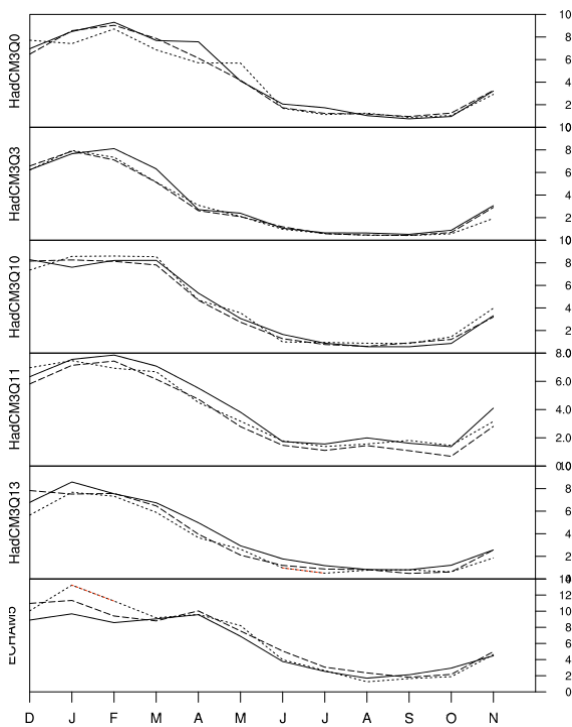


Figure 6.5: Annual cycle of precipitation for (a) Brunei, (b) Indonesia, (c) Malaysia, (d) Singapore and (e) Timor Leste for the baseline period (1971-2000) in solid lines, mid-term projections (2031-2060) in dashed lines and long-term projections (2071-2100) in dotted lines. Significant projections passing the 5% level in t-test are plotted in red.

In contrast to temperature projections, the projections for precipitation show a lot more variations across countries and seasons which lend to difficult interpretation of the annual cycle plots. There are no significant changes (at the 5% level) in the annual mean precipitation cycle for Cambodia, Laos, Thailand, Vietnam, and Timor Leste. Where significant changes are observed in certain locations, these occur only in certain seasons. For example, some long-term projections for Brunei show a drier FM season and a wetter AMJ up to 3 mm/day each way. Similarly for Malaysia, the projections generally suggest a drier early half and a wetter later half of the year by up 3 mm/day each way as well. Projections for Philippines show similar projections for a drier early half and wetter later half, but these are insignificant. For Myanmar, significant precipitation changes in JJA are projected for most models to be up to 4 mm/day. For Singapore, there are some indications of drier JFM and JJAS by up to 3 mm/day. Overall, the models project no significant changes in mean precipitation.

6.3. Seasonal mean temperature

In this section the seasonal mean temperature projections are considered for the seasons, DJF (see Figure 6.6 and Figure 6.7), MAM (Figure 6.8 and Figure 6.9), JJA (Figure 6.10 and Figure 6.11), and SON (Figure 6.12 and Figure 6.13). Generally, the temperature change patterns are very similar over the four seasons considered, with slightly higher warming rate during DJF (Figure 6.6 and Figure 6.7). **Seasonal mean temperature shows monotonic increment towards the end-century with increment of 3-5°C. By mid-century, the estimated temperature is 2-4 °C warmer than the present day.** The t-test of difference in means suggests that all temperature changes calculated at each of the grid points are significant at 0.05 level. The increment shows considerable spatial variations with faster rate of warming simulated over land compared to the South China Sea. Also, in a broader sense, the warming rate over the mainland S.E. Asia is much faster as compared to the equatorial South China Sea regions. Specifically, the area over Thailand shows considerably large warming with a magnitude $>5^{\circ}\text{C}$ towards the end-century. However, during the JJA (Figure 6.10 and Figure 6.11), the larger warming appears near the equatorial region. The changes in temperature in HadCM3Q projections generally show warmer temperature in the future, for both the future time periods, compared to ECHAM5 projections.

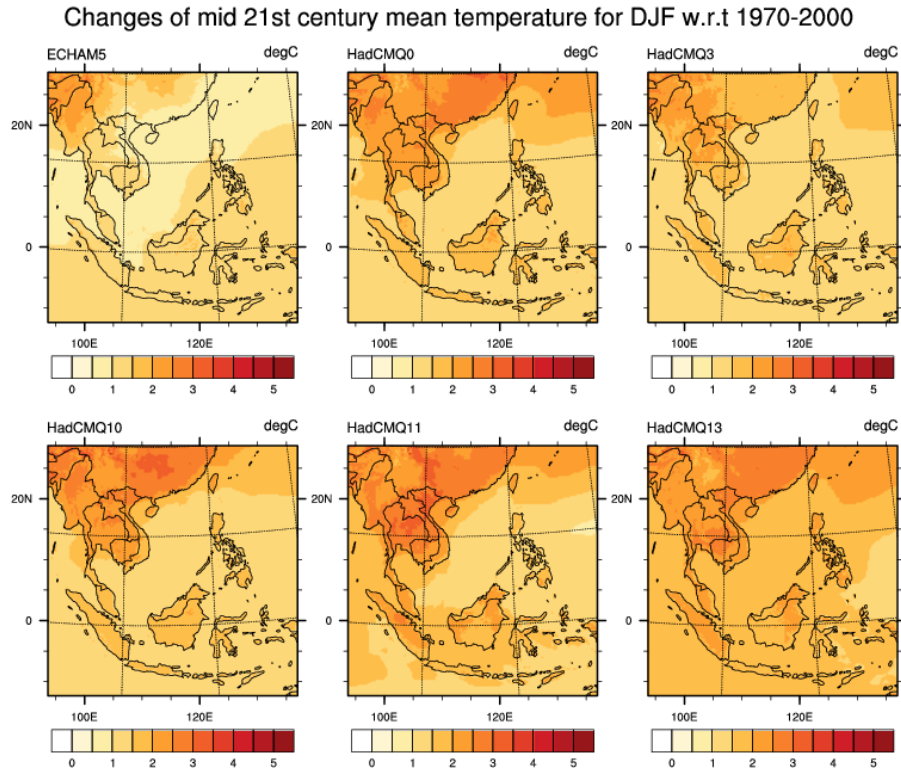


Figure 6.6: Future changes in seasonal mean temperature ($^{\circ}\text{C}$) for mid-century (2031-2060) relative to the baseline period (1971-2000) in DJF for ECHAM5 and HadCM3Q0, 3, 10, 11, 13 for the A1B scenario.

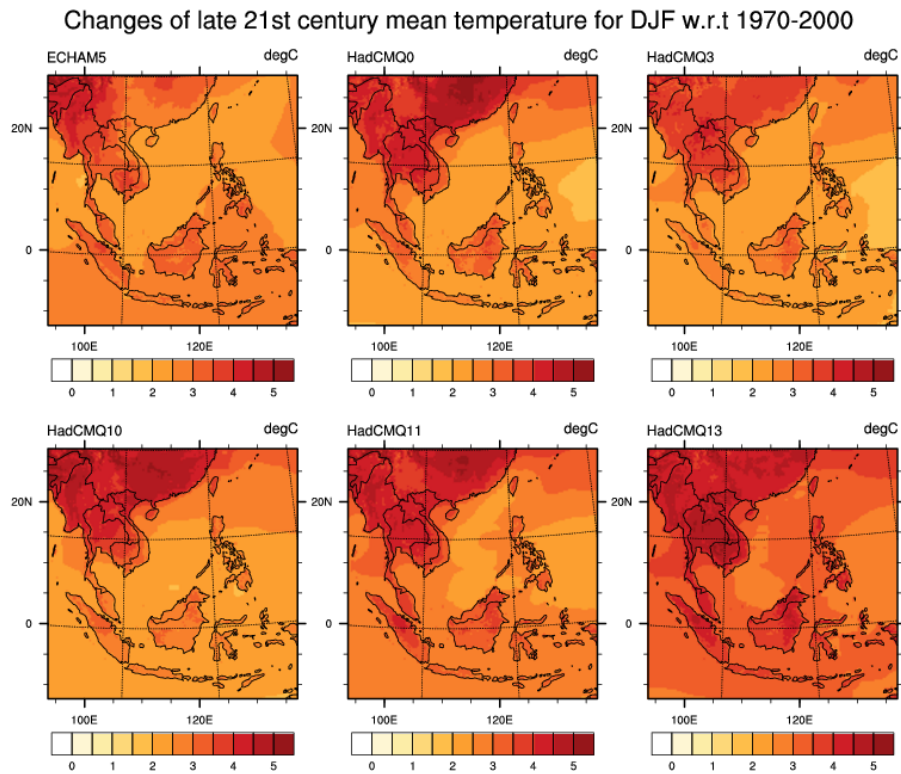


Figure 6.7: Future changes in seasonal mean temperature ($^{\circ}\text{C}$) for end-century (2071-2100) relative to the baseline period (1971-2000) in DJF for ECHAM5, HadCM3Q0, 3, 10, 11 and 13 for the A1B scenario.

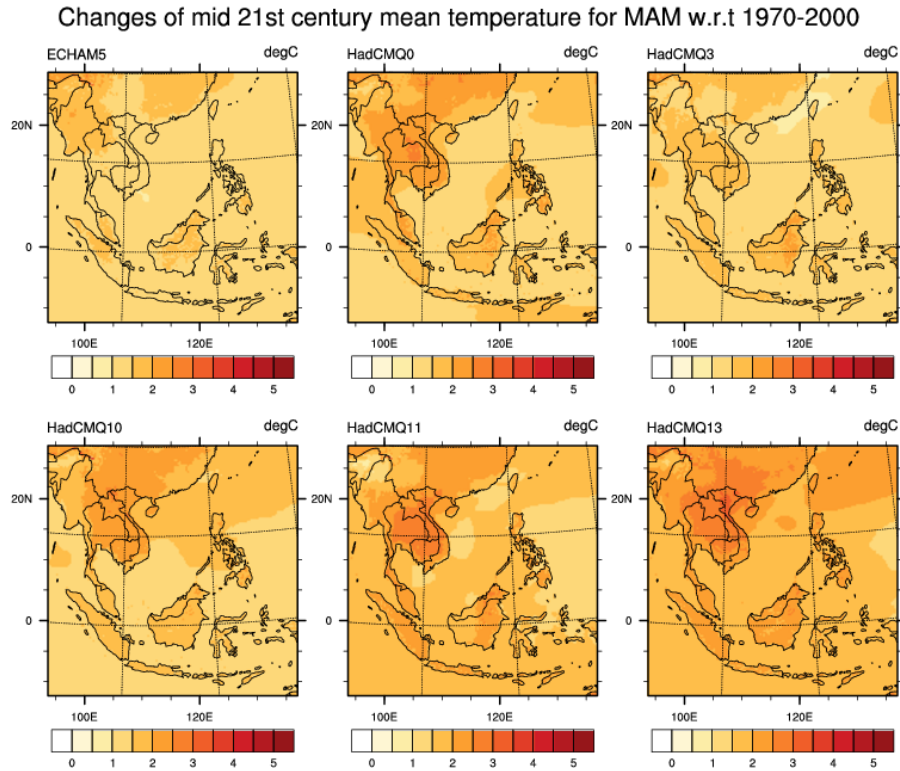


Figure 6.8: Future changes in seasonal mean temperature ($^{\circ}\text{C}$) for mid-century (2031-2060) relative to the baseline period (1971-2000) in MAM for ECHAM5 and HadCM3Q0, 3, 10, 11, 13 for the A1B scenario.

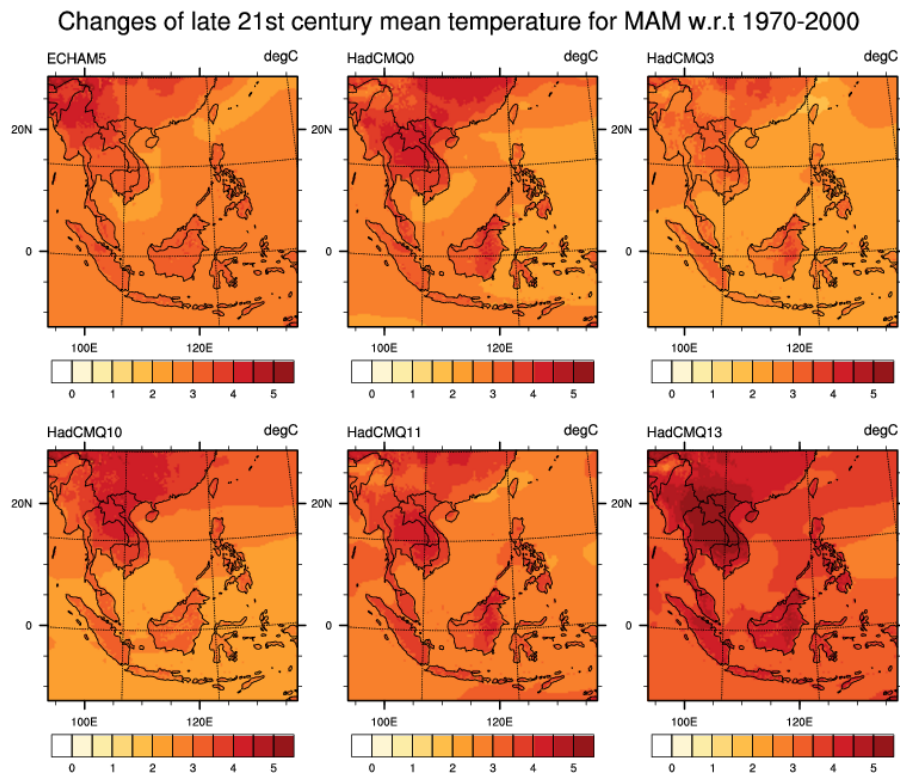


Figure 6.9: Future changes in seasonal mean temperature ($^{\circ}\text{C}$) for end-century (2071-2100) relative to the baseline period (1971-2000) in MAM for ECHAM5 and HadCM3Q0, 3, 10, 11, 13 for the A1B scenario.

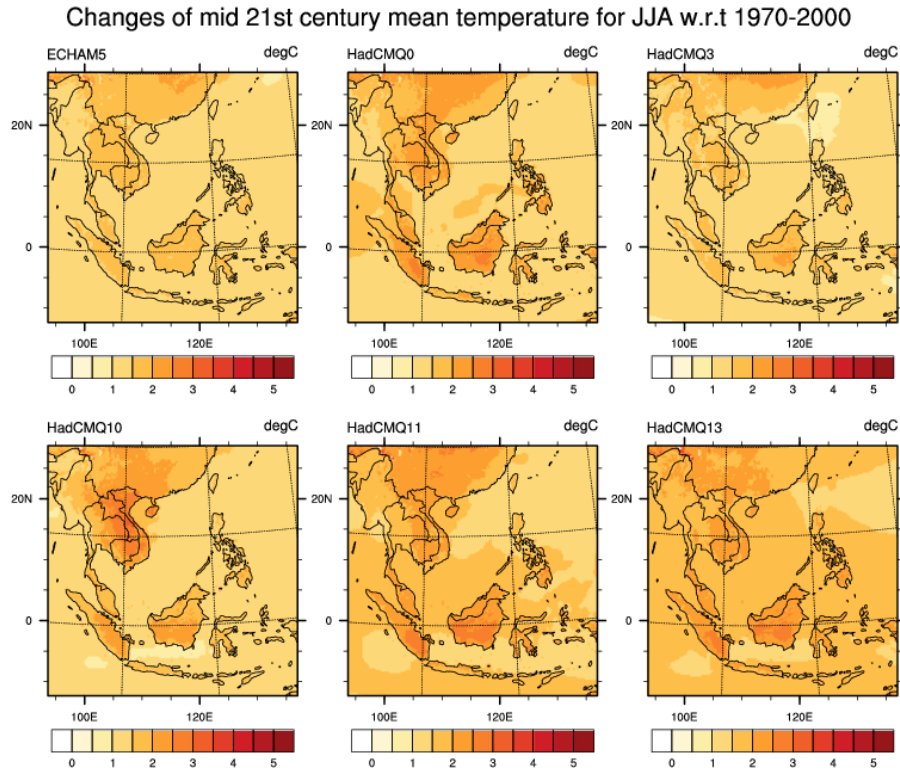


Figure 6.10: Future changes in seasonal mean temperature ($^{\circ}\text{C}$) for mid-century (2031-2060) relative to the baseline period (1971-2000) in JJA for ECHAM5 and HadCM3Q0, 3, 10, 11, 13 for the A1B scenario.

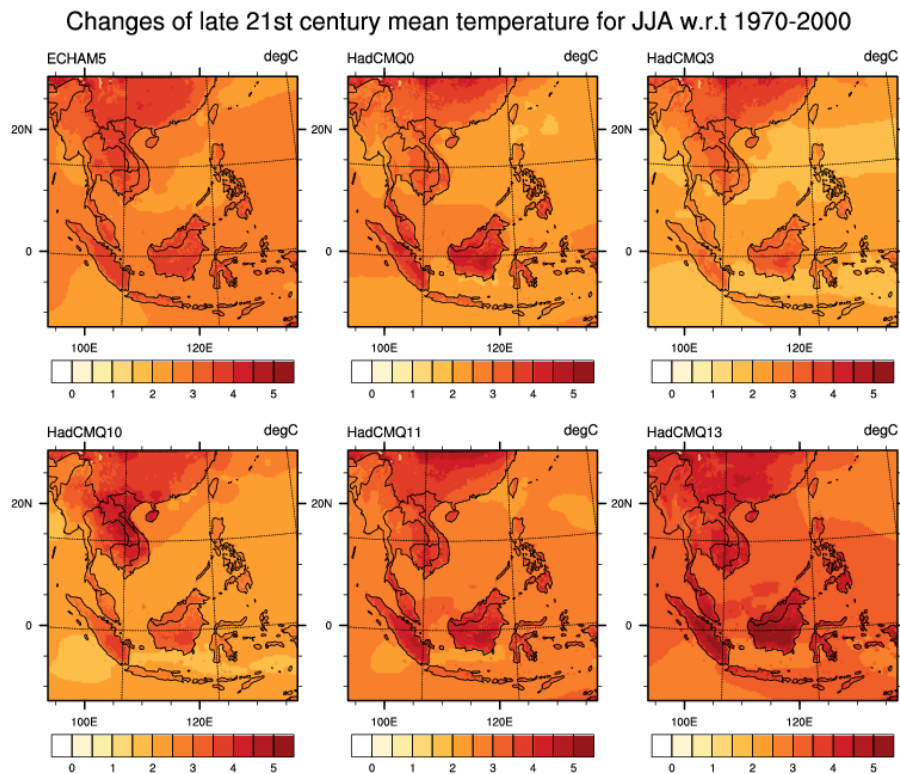


Figure 6.11: Future changes in seasonal mean temperature ($^{\circ}\text{C}$) for end-century (2071-2100) relative to the baseline period (1971-2000) in JJA for ECHAM5 and HadCM3Q0, 3, 10, 11, 13 for the A1B scenario.

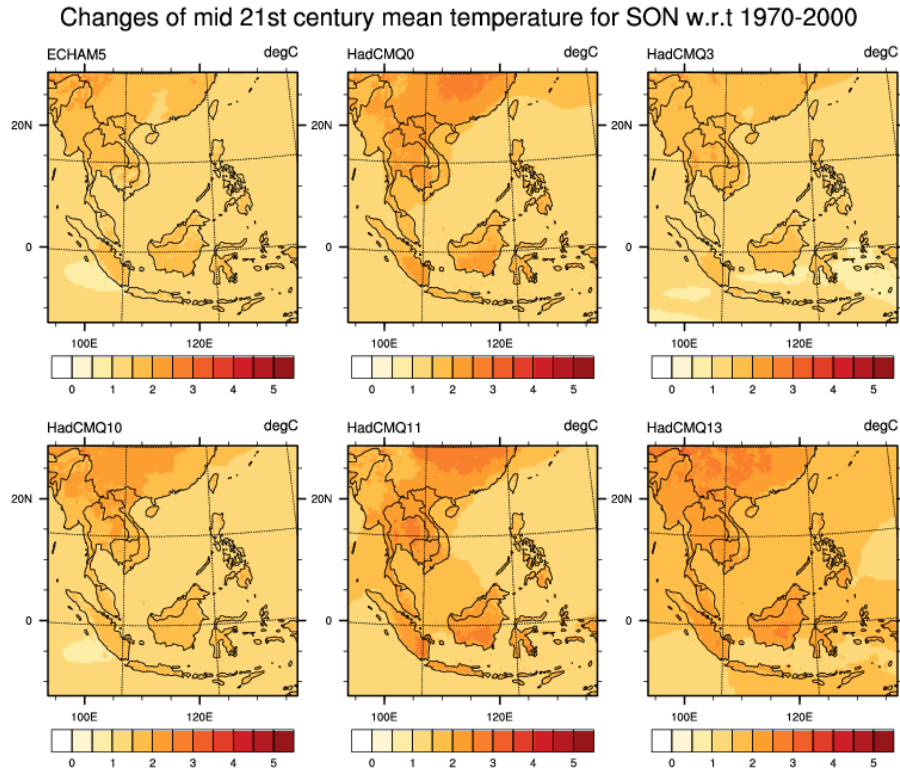


Figure 6.12: Future changes in seasonal mean temperature ($^{\circ}\text{C}$) for mid-century (2031-2060) relative to the baseline period (1971-2000) in SON for ECHAM5 and HadCM3Q0, 3, 10, 11, 13 for the A1B scenario.

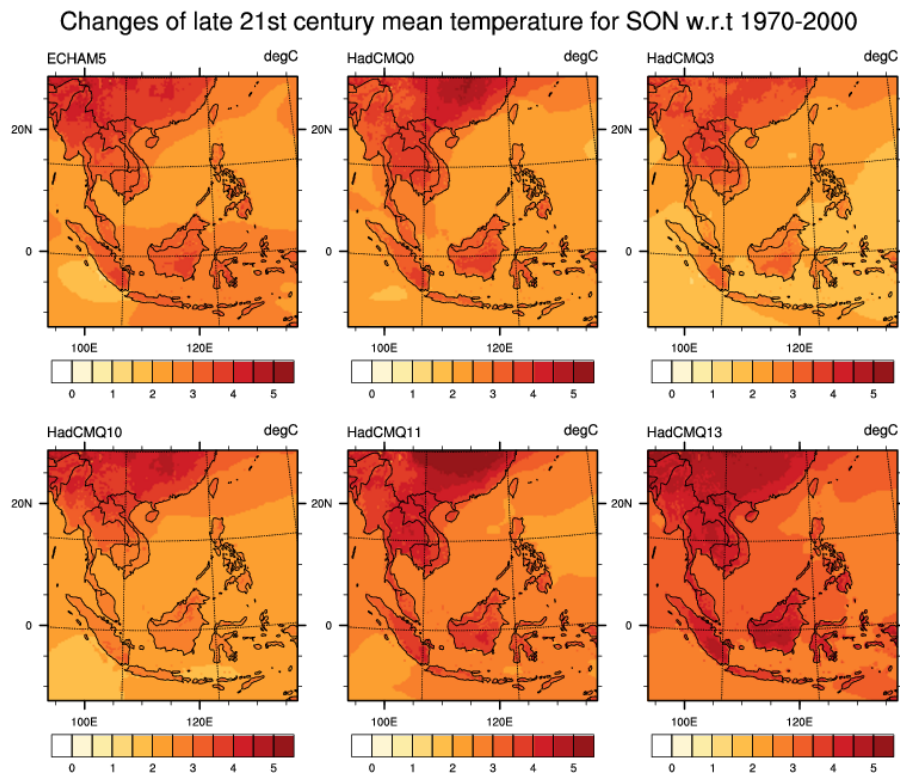


Figure 6.13: Future changes in seasonal mean temperature ($^{\circ}\text{C}$) for end-century (2071-2100) relative to the baseline period (1971-2000) in SON for ECHAM5 and HadCM3Q0, 3, 10, 11, 13 for the A1B scenario.

6.4. Seasonal minimum temperature

Figure 6.14 to Figure 6.21 show the projected changes of the S.E. Asia seasonal minimum temperature for mid- and end-century periods. **Generally, the warming patterns of the seasonal minimum temperature closely resemble that of the mean temperature.** Nevertheless, the warming rate of the minimum temperature is slightly lower compared to the mean temperature towards the end-century except for DJF (Figure 6.14 and Figure 6.15). The projected changes of DJF minimum temperature shows higher warming rate over western and central mainland S.E. Asia similar to that projected for mean temperature but with a slightly higher warming rate (Figure 6.15 vs. Figure 6.7). Also, consistent with the mean temperature pattern changes, the projected largest change in the minimum temperature during JJA is located closer to the equator (Figure 6.19).

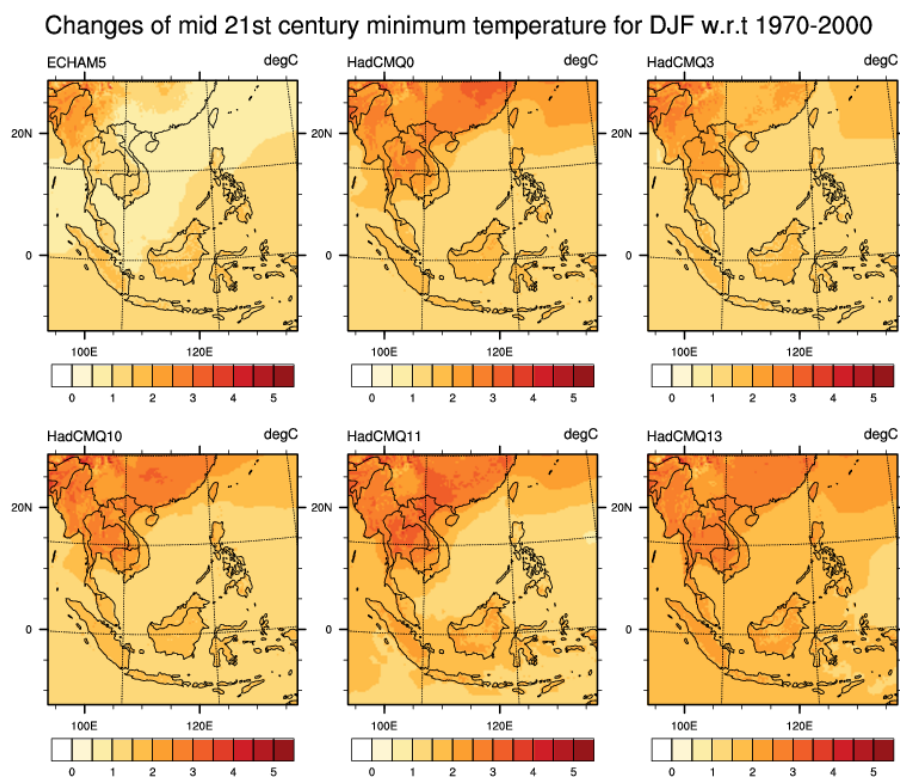


Figure 6.14: Future changes in seasonal minimum temperature ($^{\circ}\text{C}$) for mid-century (2031-2060) relative to the baseline period (1971-2000) in DJF for ECHAM5 and HadCM3Q0, 3, 10, 11, 13 for the A1B scenario.

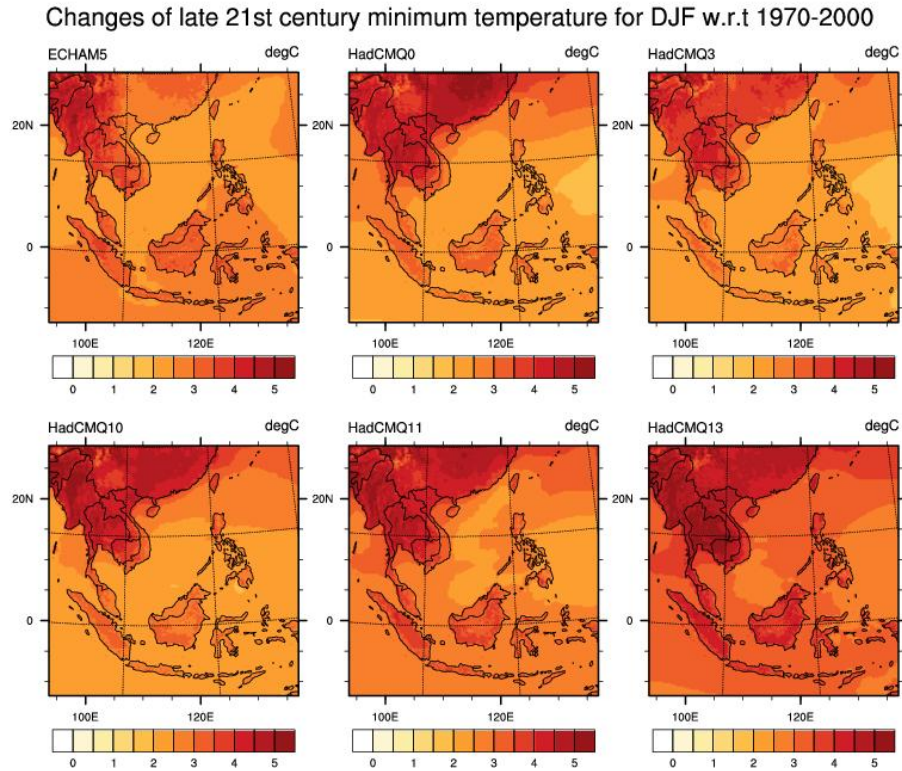


Figure 6.15: Future changes in seasonal minimum temperature ($^{\circ}\text{C}$) for end-century (2071-2100) relative to the baseline period (1971-2000) in DJF for ECHAM5 and HadCM3Q0, 3, 10, 11, 13 for the A1B scenario.

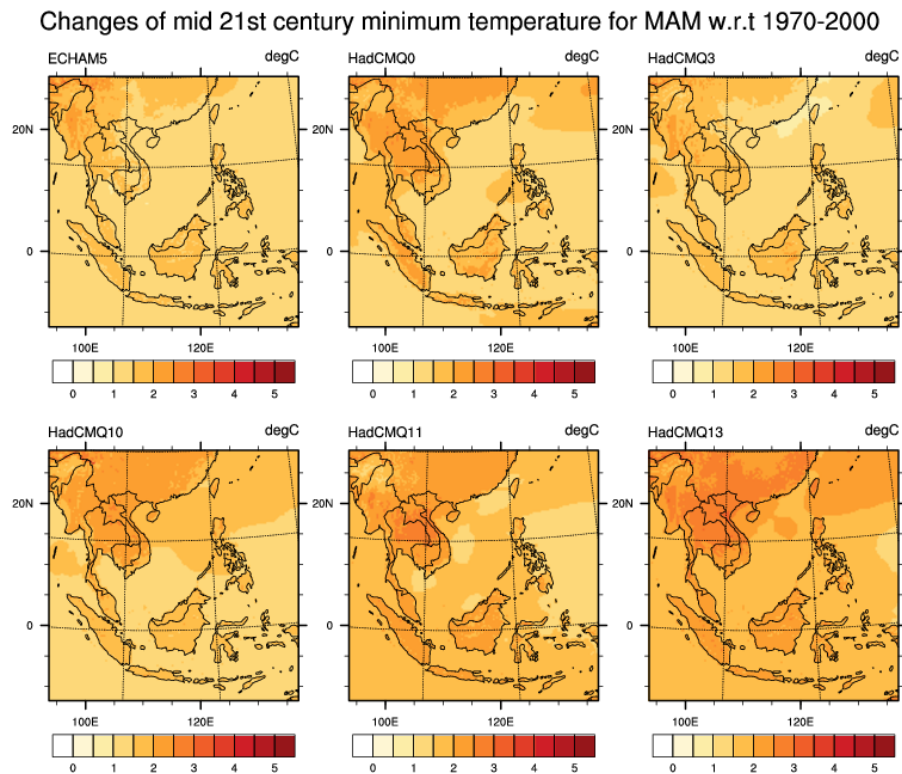


Figure 6.16: Future changes in seasonal minimum temperature ($^{\circ}\text{C}$) for mid-century (2031-2060) relative to the baseline period (1971-2000) in MAM for ECHAM5 and HadCM3Q0, 3, 10, 11, 13 for the A1B scenario.

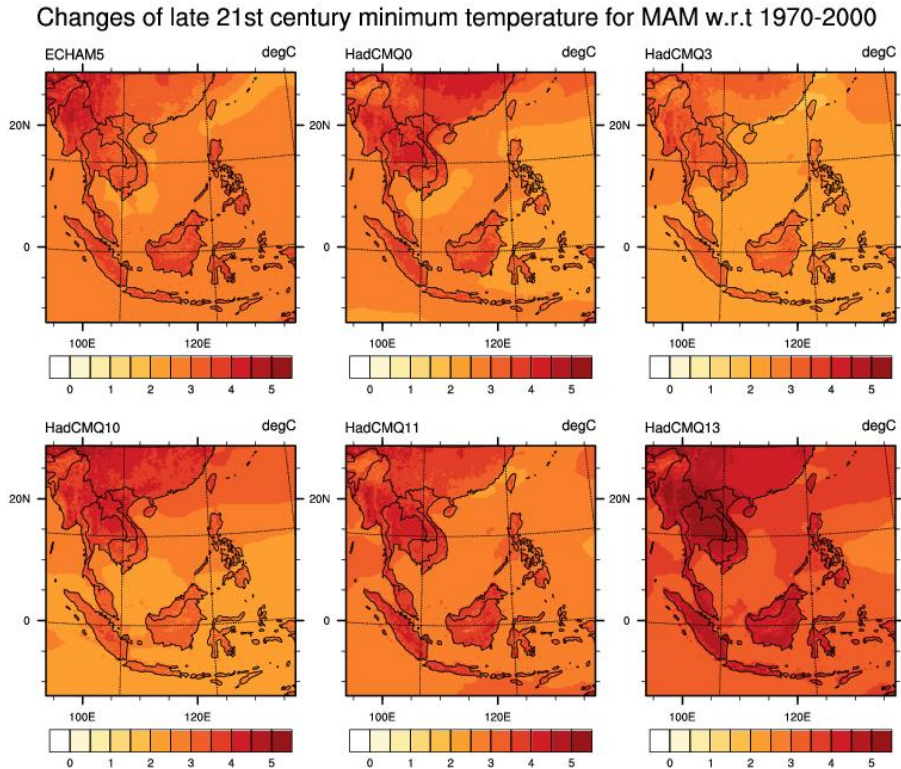


Figure 6.17: Future changes in seasonal minimum temperature ($^{\circ}\text{C}$) for end-century (2071-2100) relative to the baseline period (1971-2000) in MAM for ECHAM5 and HadCM3Q0, 3, 10, 11, 13 for the A1B scenario.

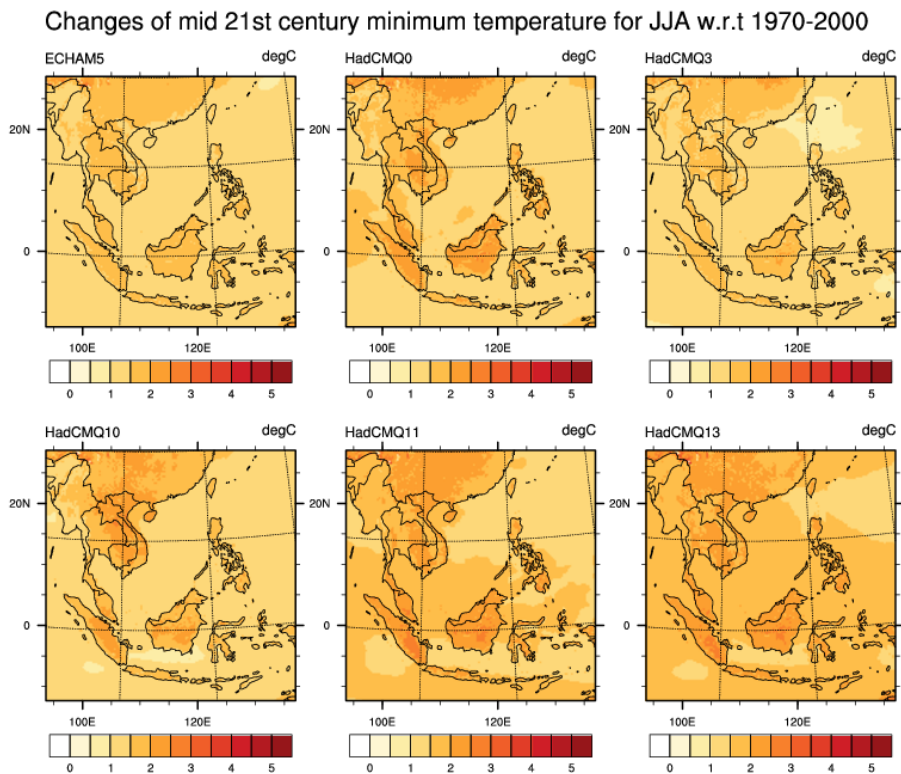


Figure 6.18: Future changes in seasonal minimum temperature ($^{\circ}\text{C}$) for mid-century (2031-2060) relative to the baseline period (1971-2000) in JJA for ECHAM5 and HadCM3Q0, 3, 10, 11, 13 for the A1B scenario.

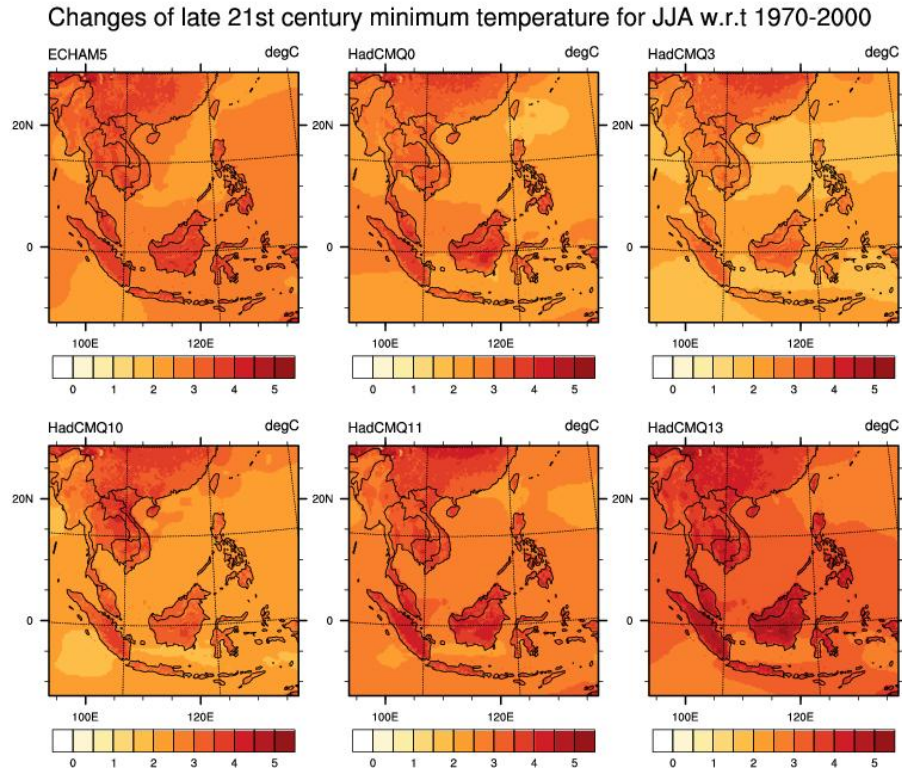


Figure 6.19: Future changes in seasonal minimum temperature ($^{\circ}\text{C}$) for end-century (2071-2100) relative to the baseline period (1971-2000) in JJA for ECHAM5 and HadCM3Q0, 3, 10, 11, 13 for the A1B scenario.

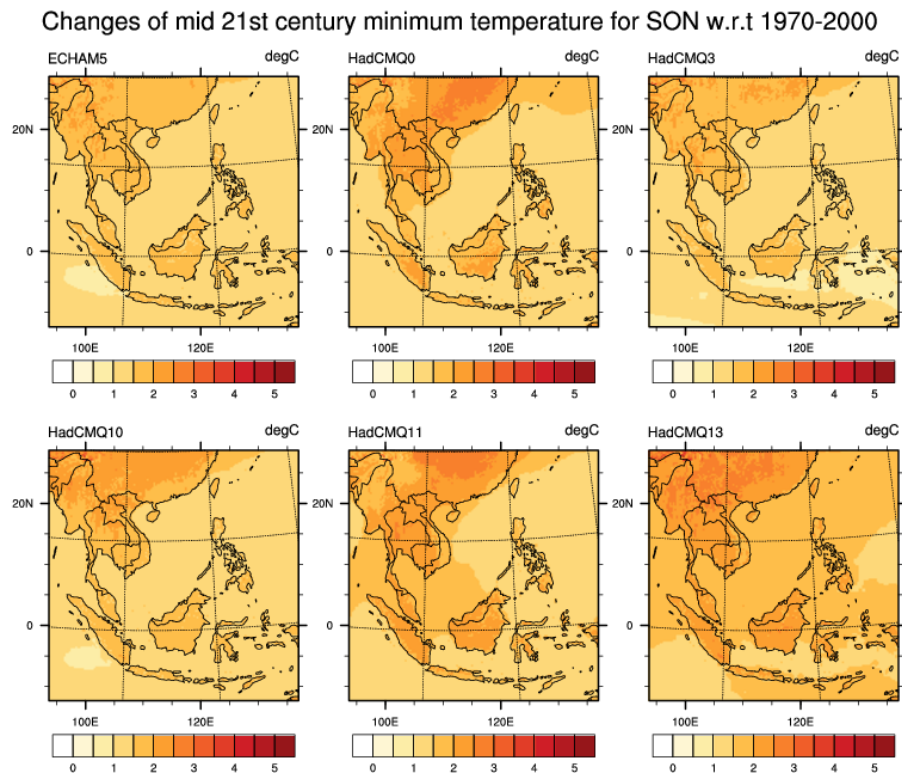


Figure 6.20: Future changes in seasonal minimum temperature ($^{\circ}\text{C}$) for mid-century (2031-2060) relative to the baseline period (1971-2000) in SON for ECHAM5 and HadCM3Q0, 3, 10, 11, 13 for the A1B scenario.

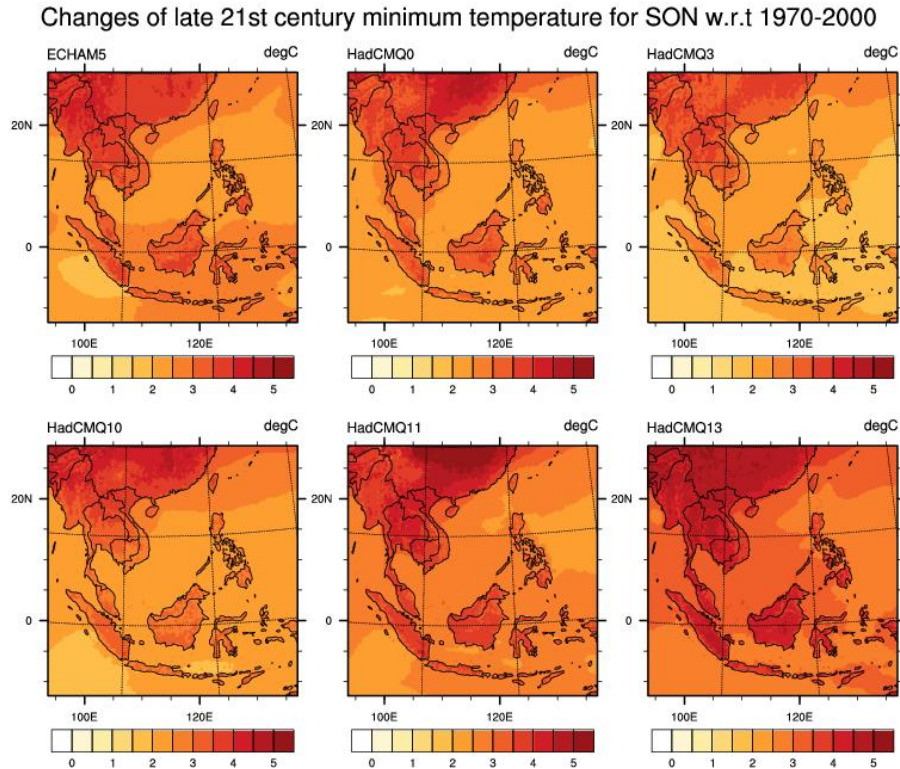


Figure 6.21: Future changes in seasonal minimum temperature ($^{\circ}\text{C}$) for end-century (2071-2100) relative to the baseline period (1971-2000) in SON for ECHAM5 and HadCM3Q0, 3, 10, 11, 13 for the A1B scenario.

6.5. Seasonal maximum temperature

Figure 6.22 to Figure 6.29 depict the projected changes of the seasonal maximum temperature over the S.E. Asia region for the two selected future time periods. **Generally, the warming patterns of the seasonal maximum temperature (like the seasonal minimum temperature) closely resemble that of the mean temperature except that the warming rate is higher in the maximum temperature towards the end-century.** Over some areas, the projected changes of maximum temperature exceeded 5°C . Consistently, the seasonal maximum temperature shows higher warming rate over central mainland S.E. Asia except during JJA (Figure 6.27) when the larger changes are projected over the equatorial regions. The projections show modest inter-GCMs variations, with HadCM3Q10 projections consistently projecting lower warming rate of maximum temperature throughout the seasons. The differences are particularly clear over the equatorial regions.

Changes of mid 21st century maximum temperature for DJF w.r.t 1970-2000

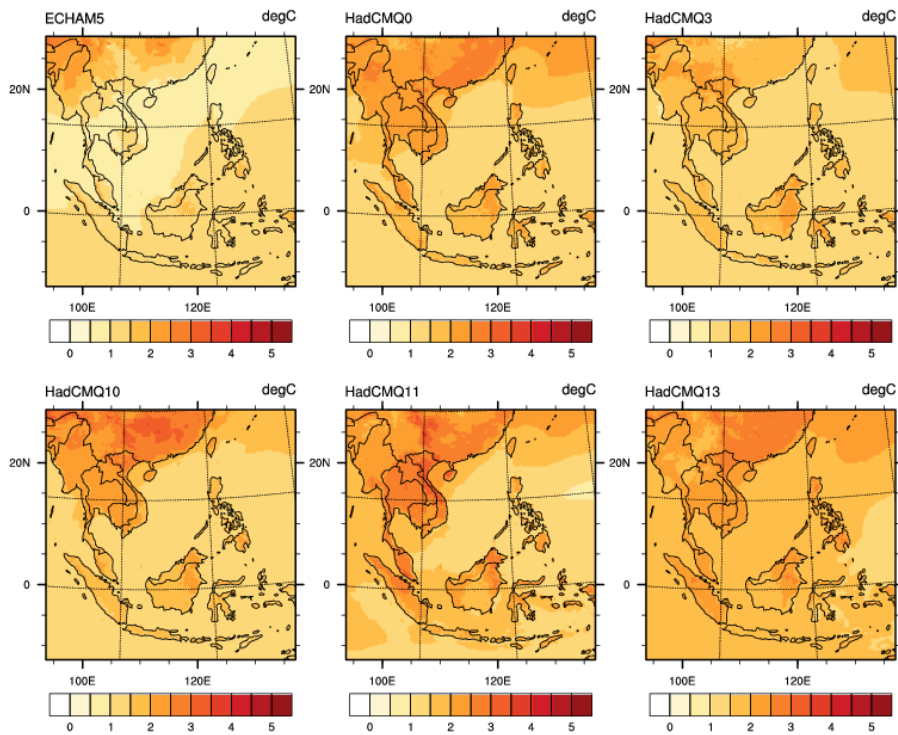


Figure 6.22: Future changes in seasonal maximum temperature (°C) for mid-century (2031-2060) relative to the baseline period (1971-2000) in DJF for ECHAM5 and HadCM3Q0, 3, 10, 11, 13 for the A1B scenario.

Changes of late 21st century maximum temperature for DJF w.r.t 1970-2000

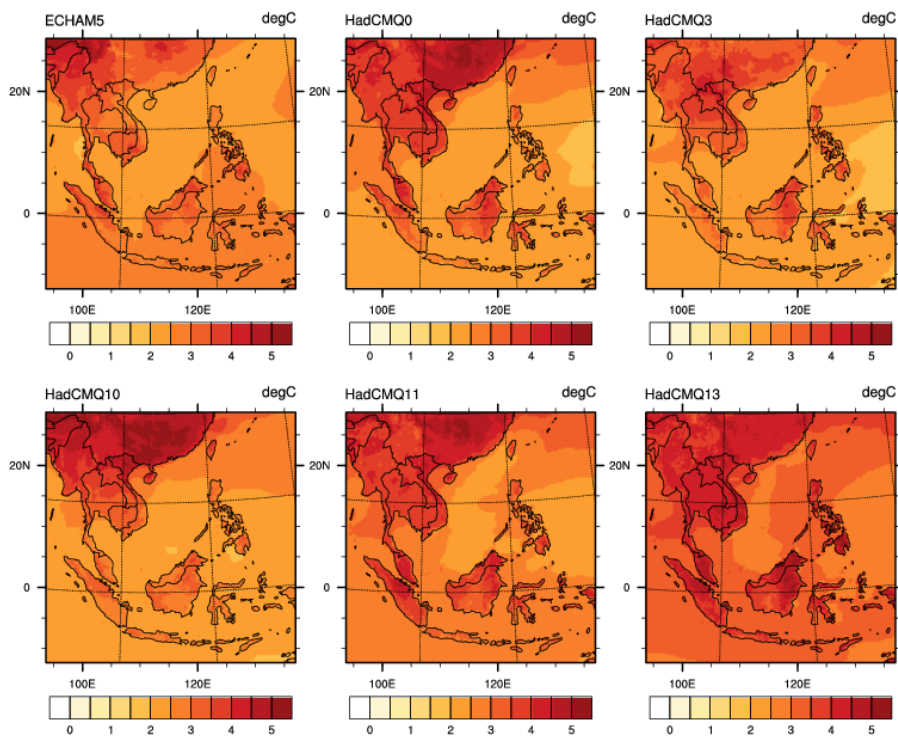


Figure 6.23: Future changes in seasonal maximum temperature (°C) for end-century (2071-2100) relative to the baseline period (1971-2000) in DJF for ECHAM5 and HadCM3Q0, 3, 10, 11, 13 for the A1B scenario.

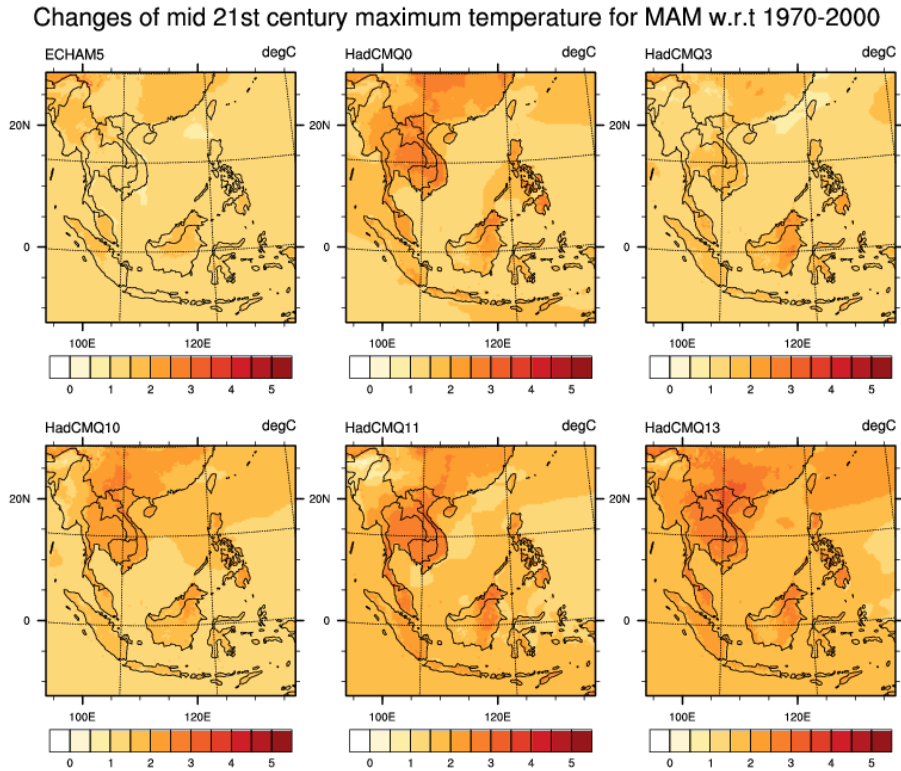


Figure 6.24: Future changes in seasonal maximum temperature ($^{\circ}\text{C}$) for mid-century (2031-2060) relative to the baseline period (1971-2000) in MAM for ECHAM5 and HadCM3Q0, 3, 10, 11, 13 for the A1B scenario.

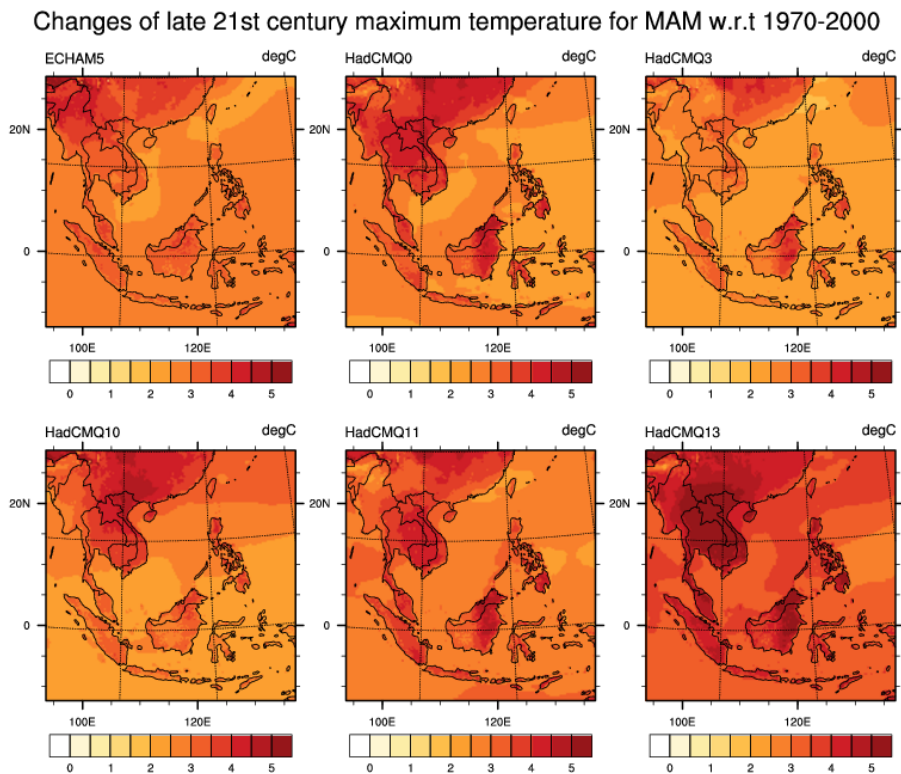


Figure 6.25: Future changes in seasonal maximum temperature ($^{\circ}\text{C}$) for end-century (2071-2100) relative to the baseline period (1971-2000) in MAM for ECHAM5 and HadCM3Q0, 3, 10, 11, 13 for the A1B scenario.

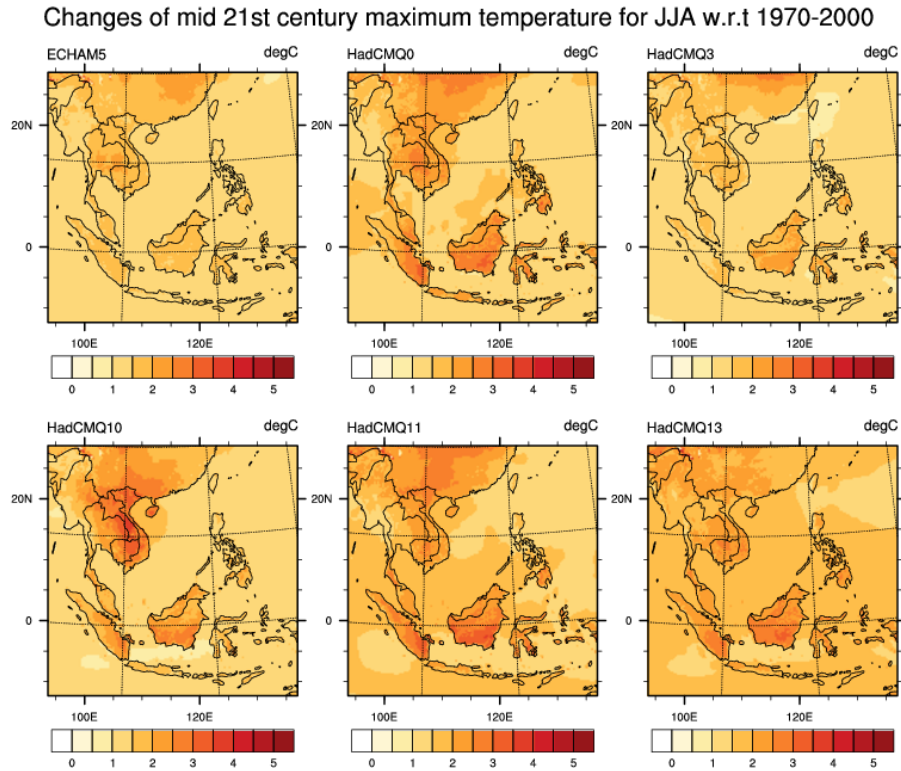


Figure 6.26: Future changes in seasonal maximum temperature (°C) for mid-century (2031-2060) relative to the baseline period (1971-2000) in JJA for ECHAM5 and HadCM3Q0, 3, 10, 11, 13 for the A1B scenario.

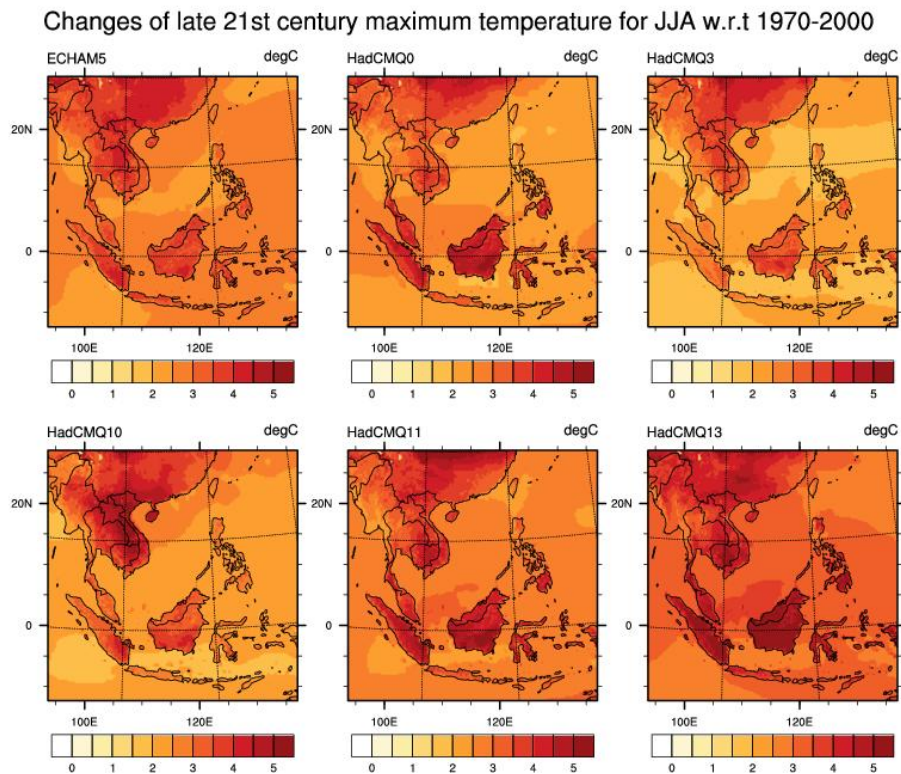


Figure 6.27: Future changes in seasonal maximum temperature (°C) for end-century (2071-2100) relative to the baseline period (1971-2000) in JJA for ECHAM5 and HadCM3Q0, 3, 10, 11, 13 for the A1B scenario.

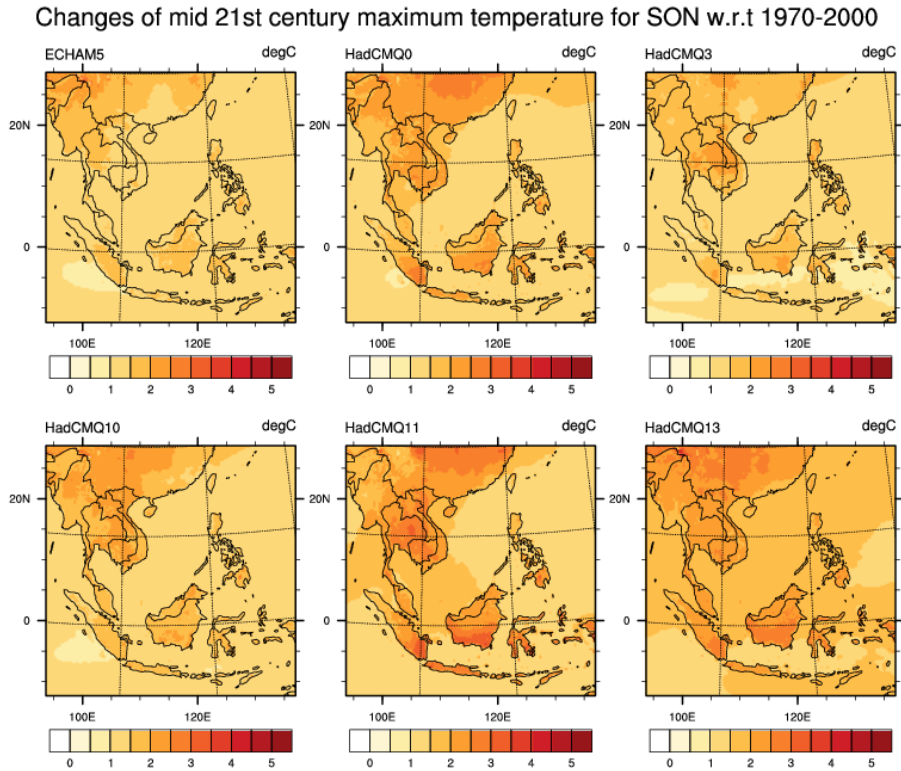


Figure 6.28: Future changes in seasonal maximum temperature (°C) for mid-century (2031-2060) relative to the baseline period (1971-2000) in SON for ECHAM5 and HadCM3Q0, 3, 10, 11, 13 for the A1B scenario.

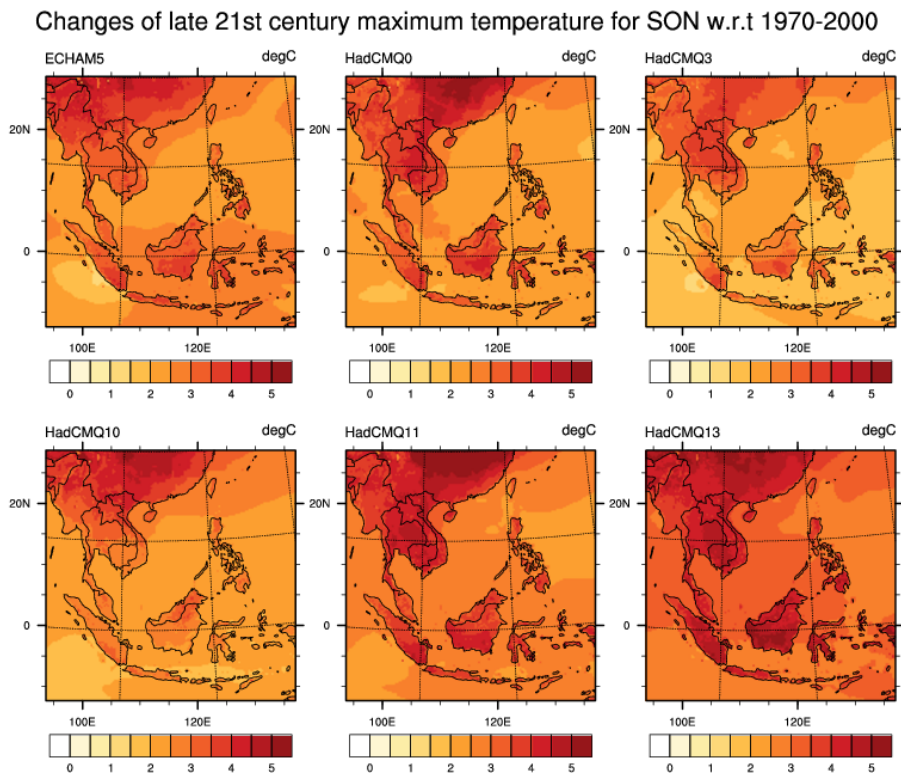


Figure 6.29: Future changes in seasonal maximum temperature (°C) for end-century (2071-2100) relative to the baseline period (1971-2000) in SON for ECHAM5 and HadCM3Q0, 3, 10, 11, 13 for the A1B scenario.

6.6. Diurnal temperature range

It is useful to calculate the change in the diurnal temperature range projections to compare the relative warming rate between the maximum (day time) temperature and minimum (night time) temperature. Figure 6.30 to Figure 6.33 show the differences between the changes of the maximum temperature and the minimum temperature over the region by end-century. Areas with positive (negative) values indicate that the maximum (minimum) temperature is warming faster than the minimum (maximum) temperature. **Generally, the minimum temperature (night time) warms faster than the maximum temperature (day time) during the boreal winter, except over northern Borneo and Peninsular Malaysia.** The warming differences are approximately 2°C. This indicates possible smaller diurnal temperature range in the regions (in blue shades) under the warmer climate during boreal winter (DJF). However, during boreal summer (Figure 6.32), the maximum temperature warms faster over most of the regions except for western mainland S.E. Asia and northern Philippines. Generally, the characteristics of the diurnal temperature changes between ECHAM5 projections and the HadCM3Q projections are consistent except over the equatorial regions. The physical processes responsible for the projection changes spatial variations are however unclear.

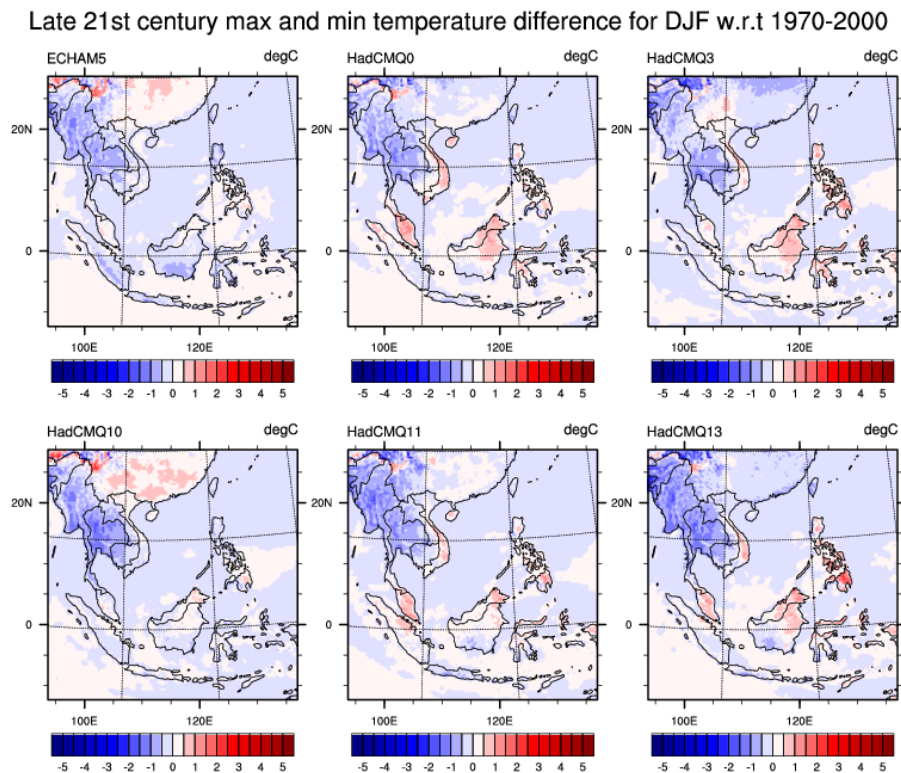


Figure 6.30: Difference in daytime and night time warming (°C) for end-century (2071-2100) relative to the baseline period (1971-2000) in DJF for ECHAM5 and HadCM3Q_{0, 3, 10, 11, 13} for the A1B scenario. Positive (negative) values in red (blue) shades indicate relatively more warming in the day (night) time than in the night (day).

Late 21st century max and min temperature difference for MAM w.r.t 1970-2000

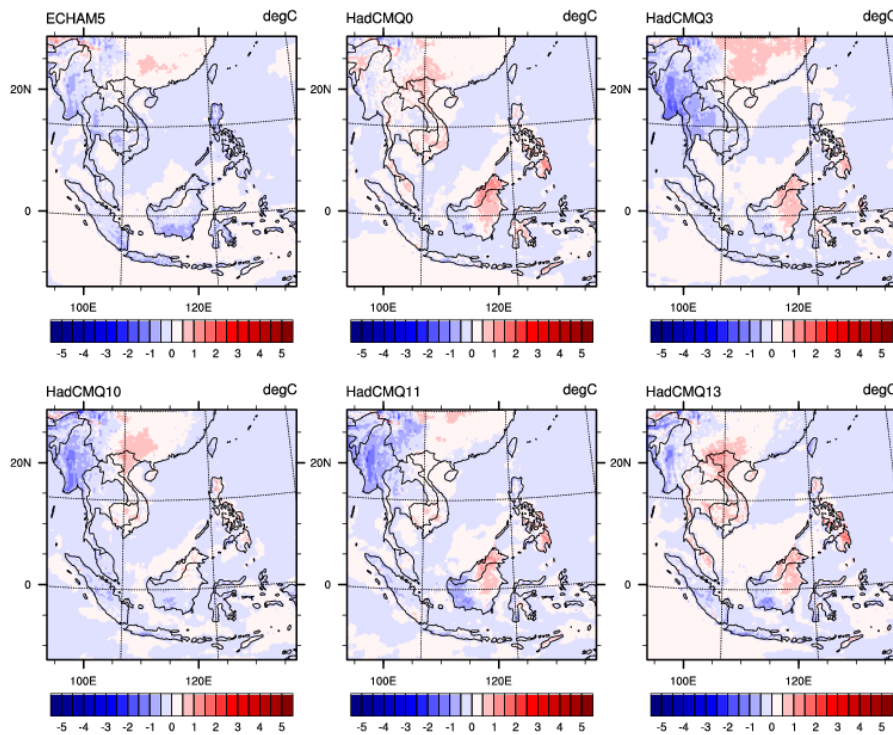


Figure 6.31: Difference in day time and night time warming (°C) for end-century (2071-2100) relative to the baseline period (1971-2000) in MAM for ECHAM5 and HadCM3Q0, 3, 10, 11, 13 for the A1B scenario. Positive (negative) values in red (blue) shades indicate relatively more warming in the day (night) time than in the night (day).

Late 21st century max and min temperature difference for JJA w.r.t 1970-2000

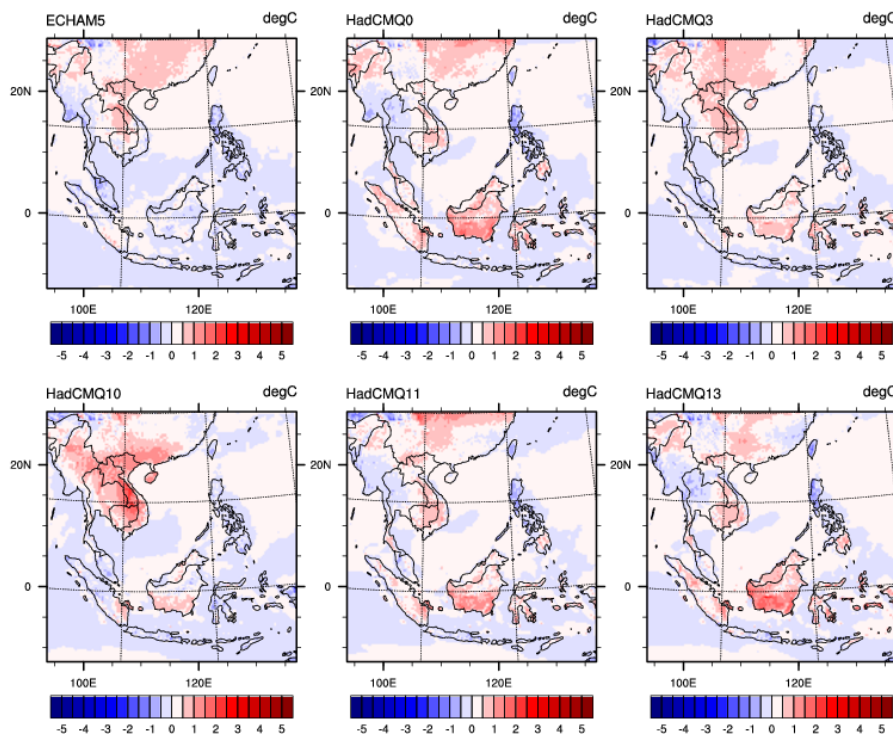


Figure 6.32: Difference in day time and night time warming (°C) for end-century (2071-2100) relative to the baseline period (1971-2000) in JJA for ECHAM5 and HadCM3Q0, 3, 10, 11, 13 for the A1B scenario. Positive

(negative) values in red (blue) shades indicate relatively more warming in the day (night) time than in the night (day).

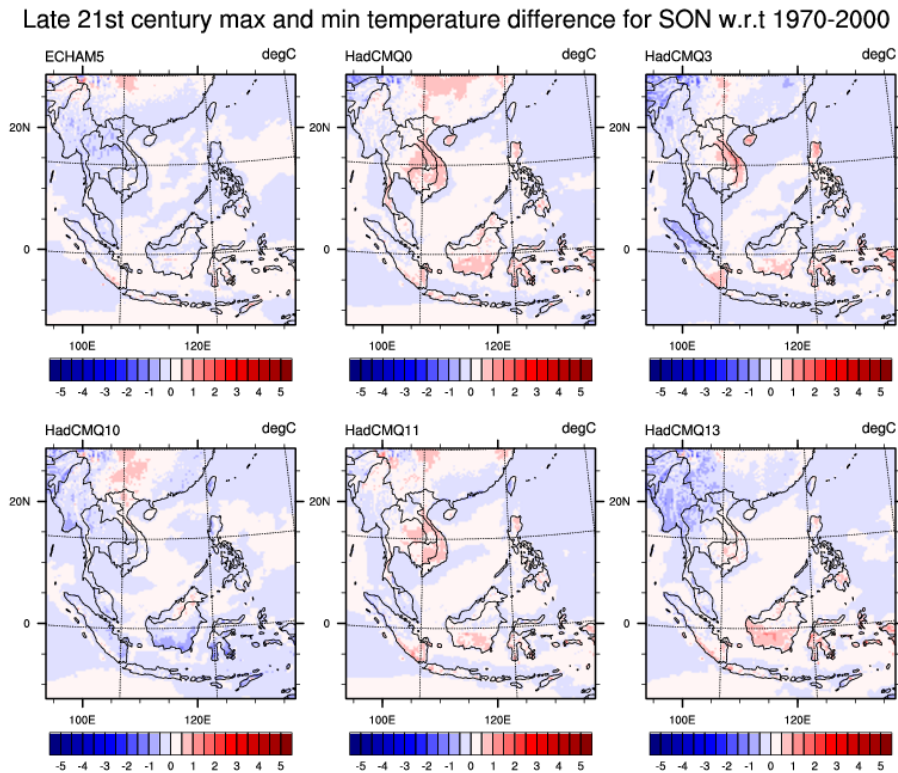


Figure 6.33: Difference in day time and night time warming ($^{\circ}\text{C}$) for end-century (2071-2100) relative to the baseline period (1971-2000) in SON for ECHAM5 and HadCM3Q0, 3, 10, 11, 13 for the A1B scenario. Positive (negative) values in red (blue) shades indicate relatively more warming in the day (night) time than in the night (day).

6.7. Seasonal mean rainfall

Future changes in seasonal mean rainfall across S.E. Asia were also examined for the mid- and end-century. The changes in rainfall on seasonal basis were calculated as the percentage difference between the multi-year averaged seasonal rainfall of that 2 time periods and the simulated historical values averaged from 1971-2000. The significance of rainfall changes were assessed using a t-test of difference in mean and the areas with significant changes were hatched for easy visual comparison (Figure 6.34 - Figure 6.41).

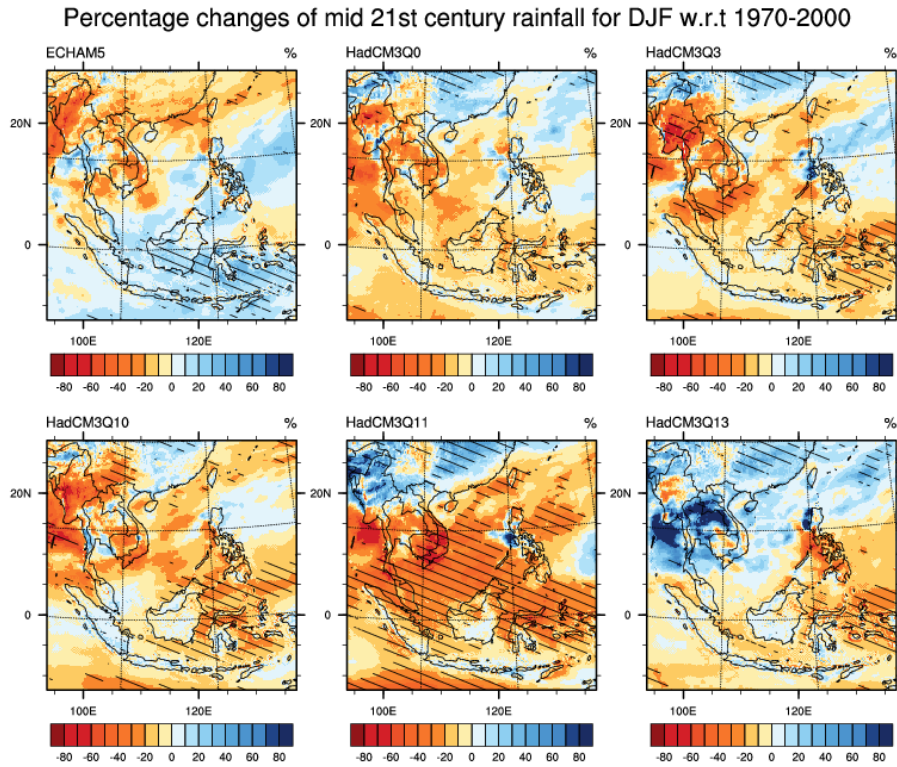


Figure 6.34: Future percentage change in seasonal mean rainfall for mid-century (2031-2060) relative to the baseline period (1971-2000) in DJF for ECHAM5 and HadCM3Q0, 3, 10, 11, 13 for the A1B scenario. Blue (red) shades show projected wetter (drier) locations. Hatching shows areas with significant changes.

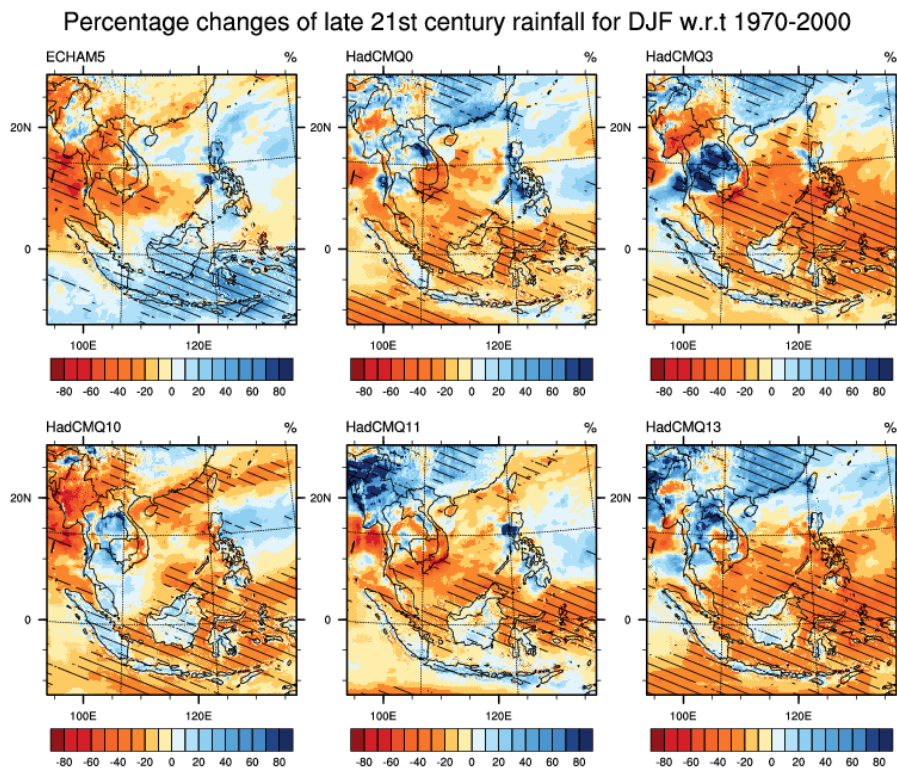


Figure 6.35: Future percentage change in seasonal mean rainfall for end-century (2071-2100) relative to the baseline period (1971-2000) in DJF for ECHAM5 and HadCM3Q0, 3, 10, 11, 13 for the A1B scenario. Blue (red) shades show projected wetter (drier) locations. Hatching shows areas with significant changes.

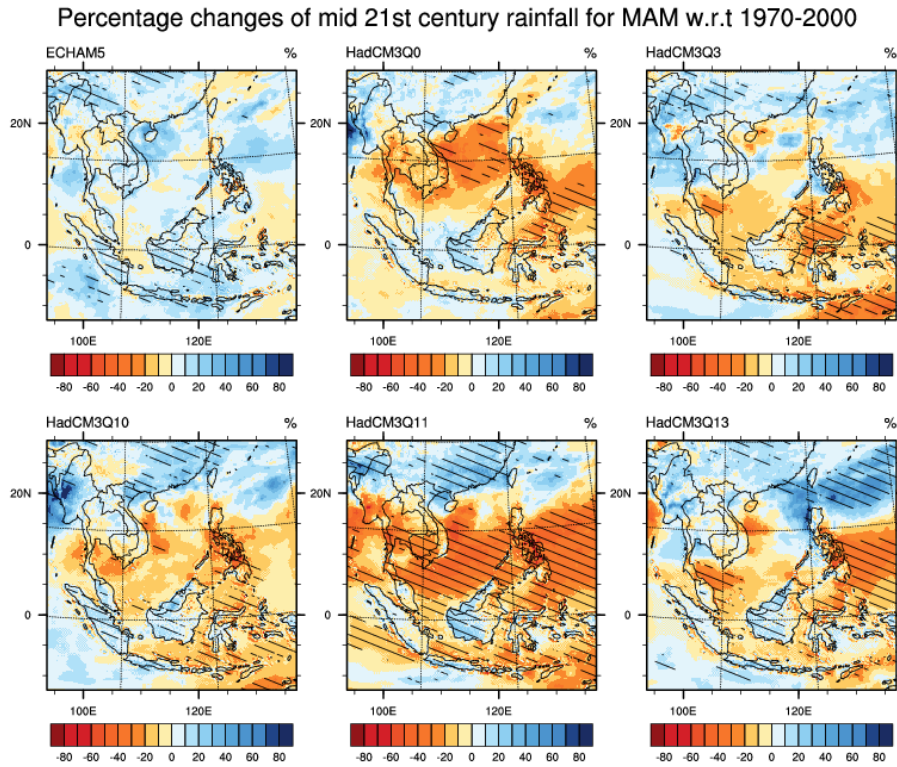


Figure 6.36: Future percentage change in seasonal mean rainfall for mid-century (2031-2060) relative to the baseline period (1971-2000) in MAM for ECHAM5 and HadCM3Q0, 3, 10, 11, 13 for the A1B scenario. Blue (red) shades show projected wetter (drier) locations. Hatching shows areas with significant changes.

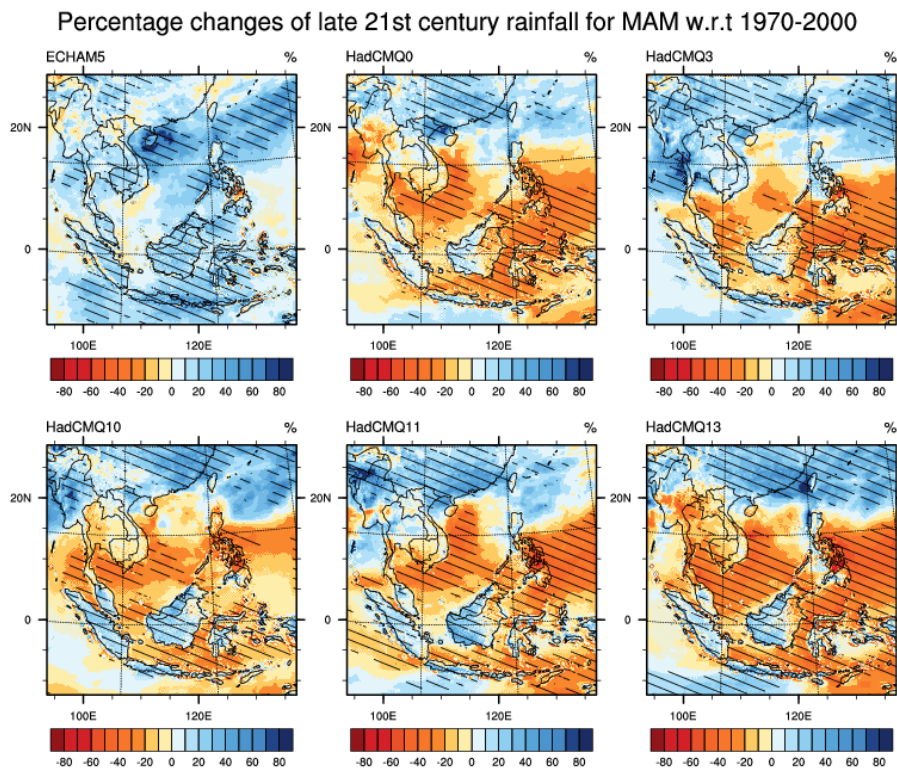


Figure 6.37: Future percentage change in seasonal mean rainfall for end-century (2071-2100) relative to the baseline period (1971-2000) in MAM for ECHAM5 and HadCM3Q0, 3, 10, 11, 13 for the A1B scenario. Blue (red) shades show projected wetter (drier) locations. Hatching shows areas with significant changes.

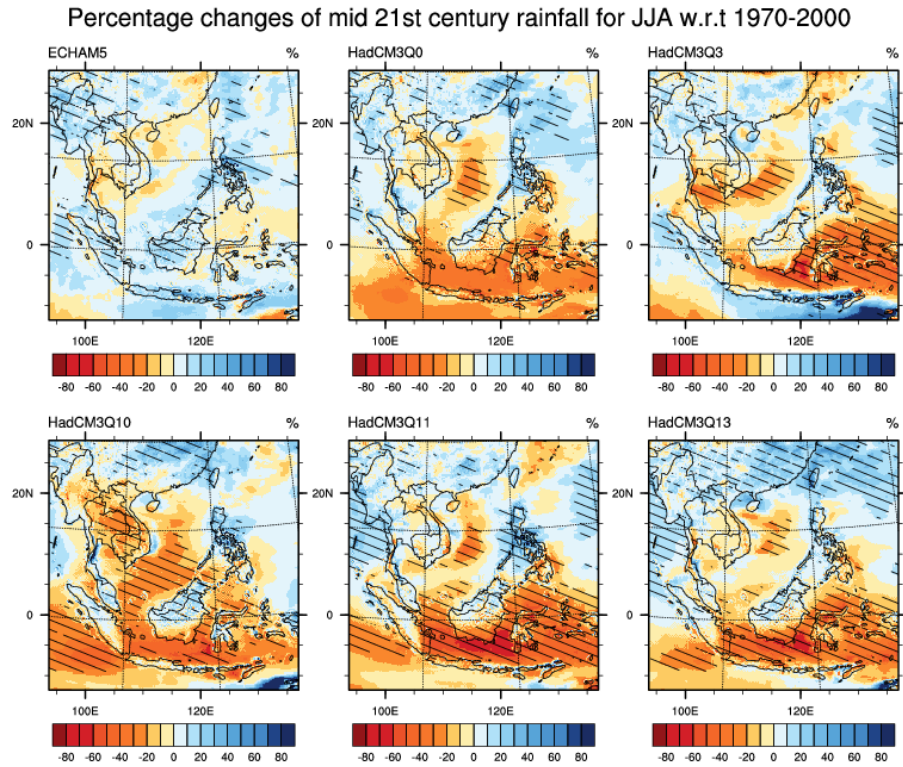


Figure 6.38: Future percentage change in seasonal mean rainfall for mid-century (2031-2060) relative to the baseline period (1971-2000) in JJA for ECHAM5 and HadCM3Q0, 3, 10, 11, 13 for the A1B scenario. Blue (red) shades show projected wetter (drier) locations. Hatching shows areas with significant changes.

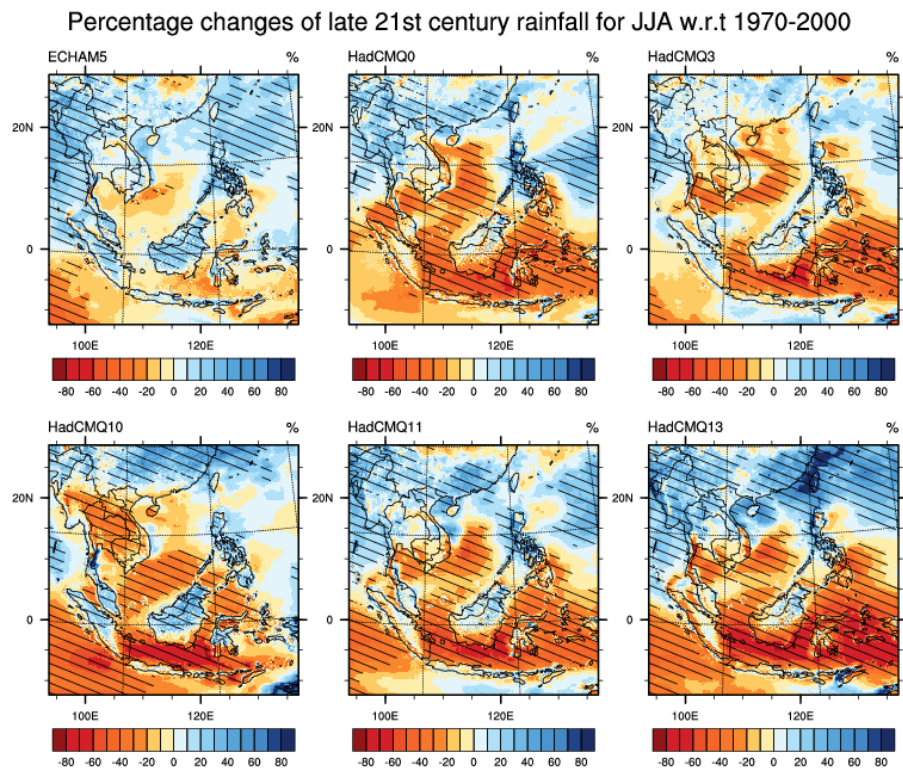


Figure 6.39: Future percentage change in seasonal mean rainfall for end-century (2071-2100) relative to the baseline period (1971-2000) in JJA for ECHAM5 and HadCM3Q0, 3, 10, 11, 13 for the A1B scenario. Blue (red) shades show projected wetter (drier) locations. Hatching shows areas with significant changes.

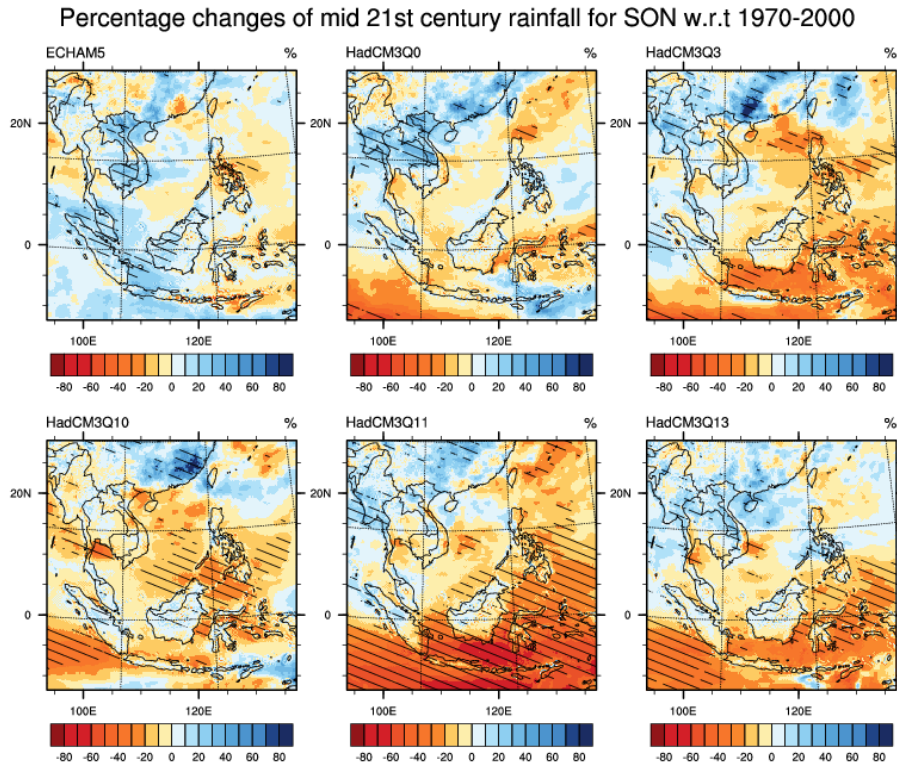


Figure 6.40: Future percentage change in seasonal mean rainfall for mid-century (2031-2060) relative to the baseline period (1971-2000) in SON for ECHAM5 and HadCM3Q0, 3, 10, 11, 13 for the A1B scenario. Blue (red) shades show projected wetter (drier) locations. Hatching shows areas with significant changes.

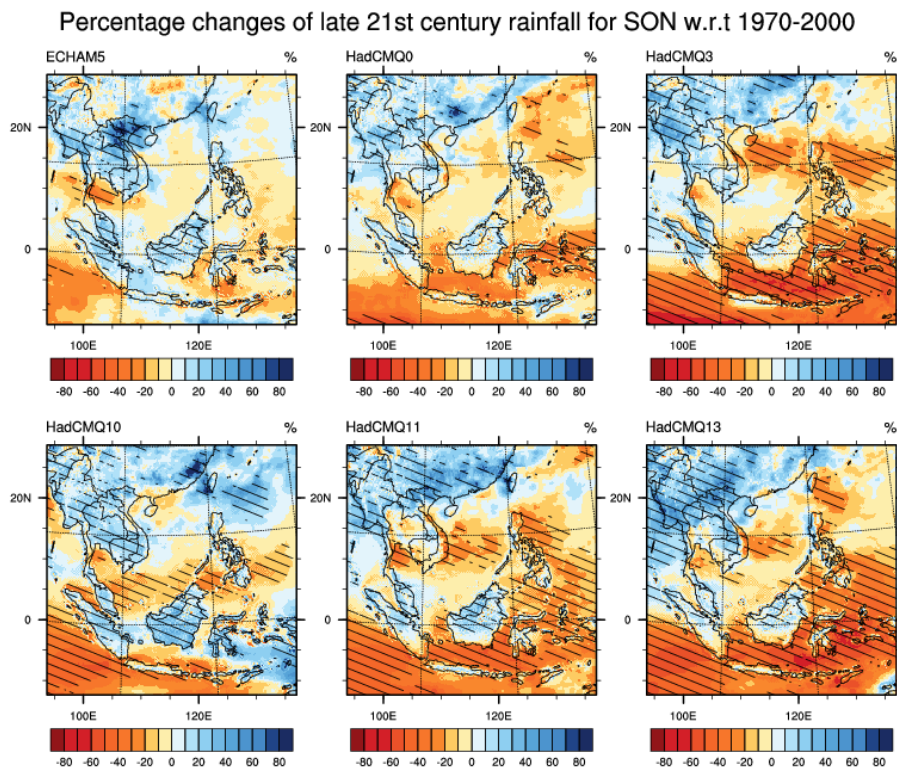


Figure 6.41: Future percentage change in seasonal mean rainfall for end-century (2071-2100) relative to the baseline period (1971-2000) in SON for ECHAM5 and HadCM3Q0, 3, 10, 11, 13 for the A1B scenario. Blue (red) shades show projected wetter (drier) locations. Hatching shows areas with significant changes.

Unlike for temperature, changes in rainfall show large spatial and seasonal variations. Generally, **the projections show drier climate over the sea and wetter climate over land. The land-sea contrast is more obvious towards the end-century. In all of the HadCM3Q projections, drier climate is projected over most areas during boreal winter except central mainland S.E. Asia (Figure 6.35). However, wetter climate was projected south of the equator in ECHAM5.** During JJA (Figure 6.39), all projections show wetter climate over land except HadCM3Q10 which projected central mainland S.E. Asia to be approximately 40% drier compared to the baseline period. The projected changes for SON towards the end-century (Figure 6.41) are very similar to that of the JJA (Figure 6.39) with increasing seasonal rainfall of 20-40% over most of the areas that are projected to get wetter. During MAM (Figure 6.37), the simulations projected a drying band at about 10°N with estimated rainfall decrement of 40% over the sea and slightly low decrement over land.

Figure 6.42 summarises the seasonal rainfall change signals from the 6 sets of projections by the median of the change values. These summary plots are *not* intended to convey any notion of added confidence or likelihood, or lack thereof, of future projections in rainfall (due to the small ensemble size), but rather to allow for easier interpretation of the spatial variability of rainfall projections across the different models. The areas where all six projections have identical sign of changes are hatched. **Generally, inter-model agreement is high except during winter (DJF).** During MAM and SON, all projections point to increasing seasonal rainfall towards the end-century over land close to the equator. Over southern Philippines, drier climate was projected by all the simulations. It is worth noting that in comparison, the multi-model ensemble from IPCC AR5's report (IPCC, 2013; Figure 12.22) project that seasonal mean changes are within one standard deviation of internal variability for the RCP8.5, hence not statistically significant.

Seasonal median percentage changes of late 21st century rainfall w.r.t 1970-2000

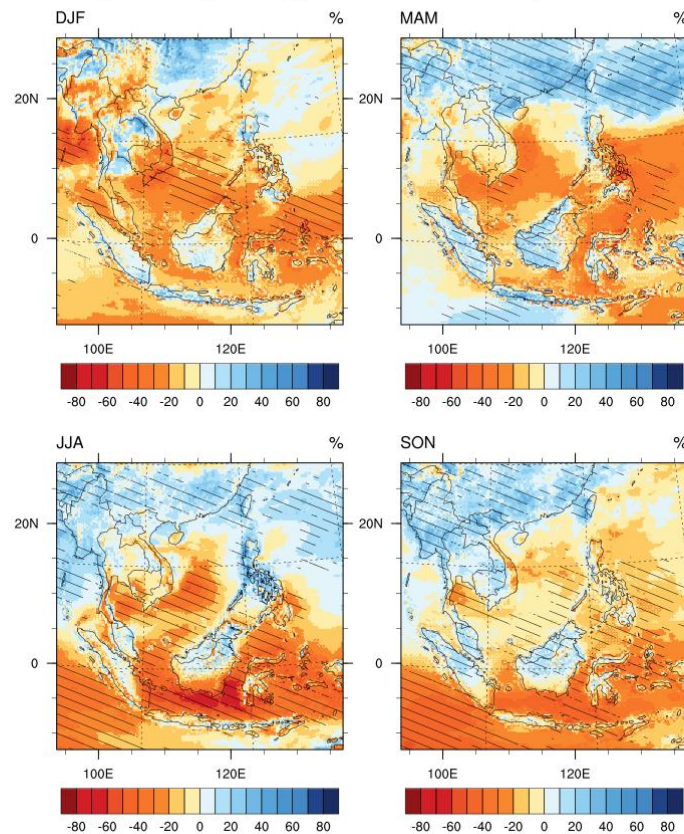


Figure 6.42: The median values (from the 6 simulations) of the changes of the late century seasonal rainfall. The areas where all the 6 simulations agree on the change sign are hatched.

6.8. Southwest Summer Monsoon

The time–latitude cross section of precipitation averaged for the period 2071–2100 is shown in Figure 6.43 (upper panel). The general precipitation patterns in the future are similar to the baseline period. However, the detailed distributions show some discrepancy among the simulations, particularly during the southwest summer monsoon period in the region from 5°N northwards. Lower panel of Figure 6.43 depicts the changes between the end-century precipitations versus the baseline period. **It can be seen that during the summer monsoon (JJAS), generally more rainfall is projected in the northern part of the region (approximately from 20°N northward), whereas drier conditions are projected for the Maritime Continent.** Compared to the multi-model ensemble from IPCC AR5's report (IPCC, 2013: Figure 12.22), similar projections were given for the RCP8.5, i.e. for wetter north and drier south for JJA, but these are not statistically significant in the AR5 report (within one standard deviation of internal variability). The wetter conditions in the northern region can be explained by the intensification of monsoon, where stronger southwest winds bring more moisture from the sea (Bay of Bengal and South China Sea) to the region (Figure 6.49).

The projection of rainfall changes between the mid-century and the baseline period (Figure 6.44) show similar changes to the end-century period, i.e. wetter conditions in the northern region and drier conditions in the Maritime Continent during the summer monsoon.

However, the amplitudes of changes in the mid-century period are less significant compared to the end-century.

change in precipitation (mm/day)

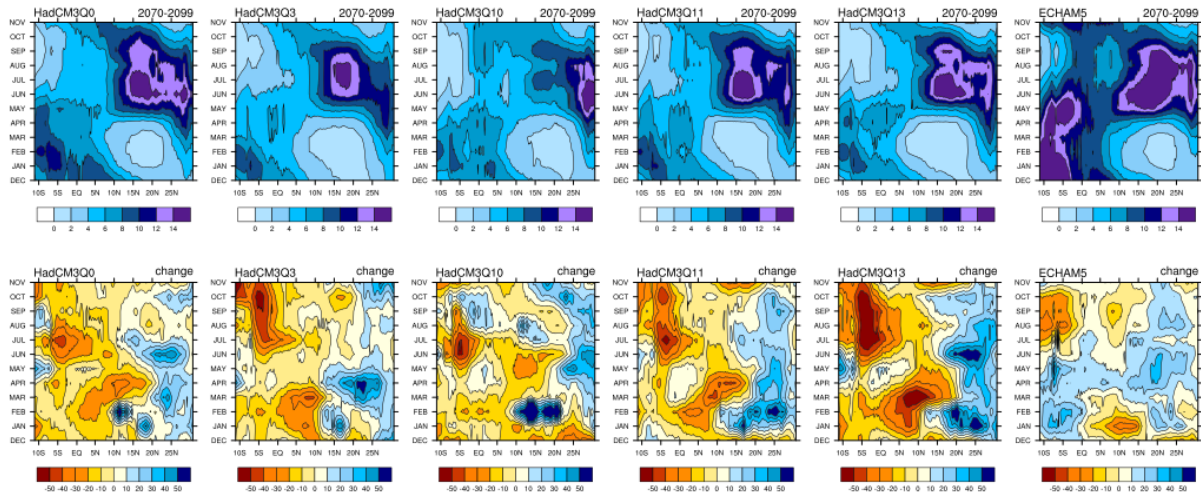


Figure 6.43: Time-latitude cross-section over longitudes 90E to 135E for precipitation in 6 simulations. Upper panel: average precipitation (mm/day) for the period 2071-2100. Lower panel: precipitation changes (%) between 2071-2100 and the baseline period.

change in precipitation (mm/day)

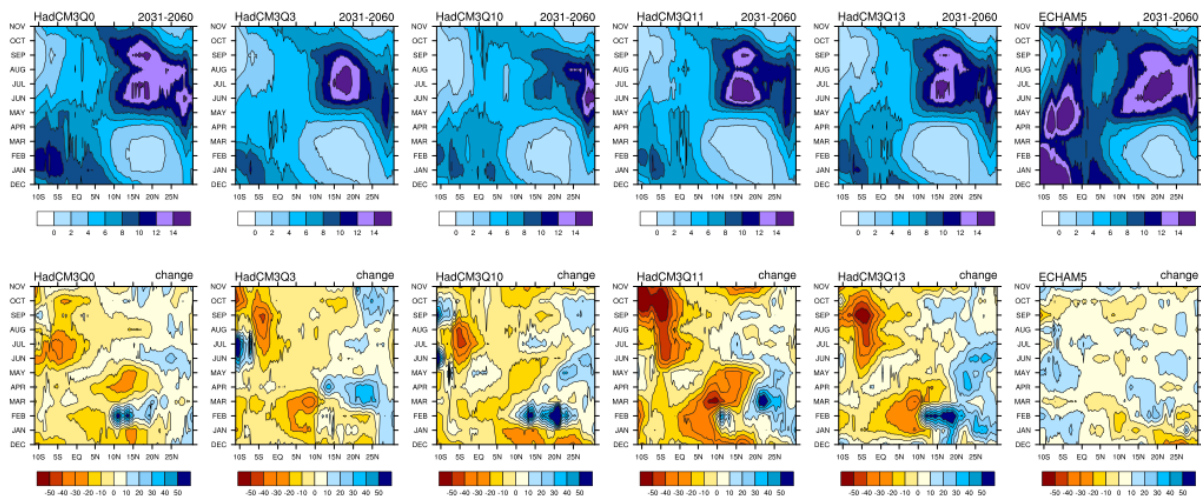


Figure 6.44: Same as Figure 6.43, but for the mid-century period 2031-2060.

In Figure 6.45 and Figure 6.46, decrease in the amount of extreme seasonal rainfall (95th percentile threshold) is projected in the Southwest Monsoon season of the mid- and end-century in the region east of 100°E and south of 5°N (eastern Maritime Continent). In the north-western part of S.E. Asia (mainland S.E. Asia), however, extreme wet days are projected to be more intense. This is true for the HadCM₃Q projections in general, but for ECHAM₅ it projected an increase in the extreme rainfall throughout most of the region, including the eastern Maritime Continent. With the projected intensification of the Southwest Monsoon

extreme rainfall in both time periods, and the possibility of redistribution of rainfall towards more intense monsoons – as suggested by projected reduction in the mean rainfall during JJA (Figure 6.38 and Figure 6.39) – it can be expected for the dry phase of the monsoon to get drier.

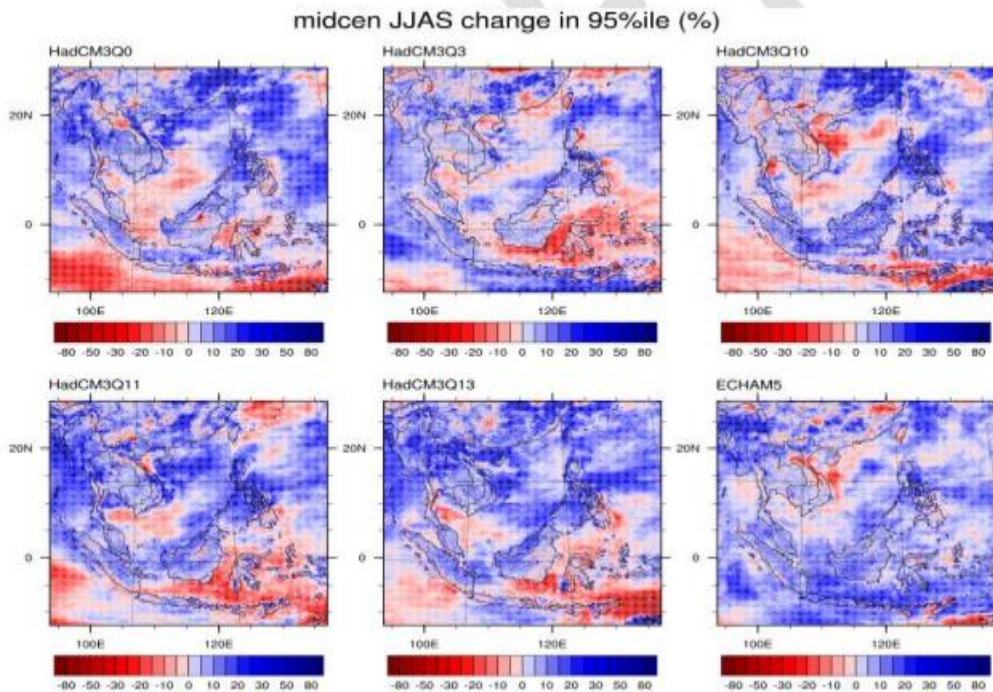


Figure 6.45: 95th percentile amounts of seasonal rainfall during JJAS in mid-century (2031-2060).

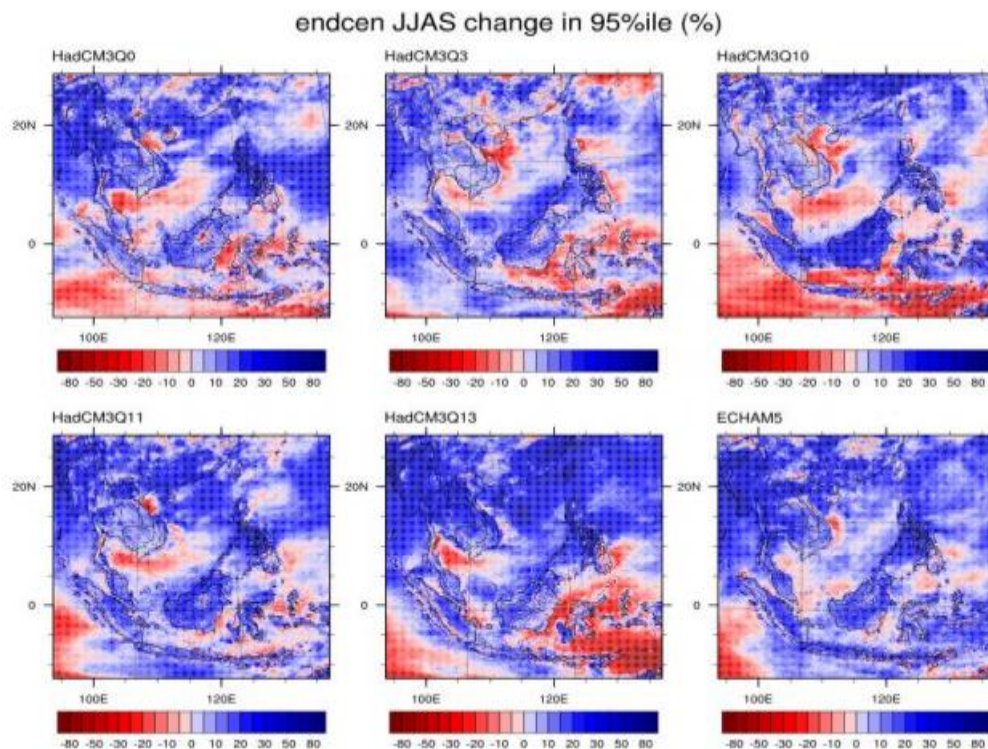


Figure 6.46: 95th percentile amounts of seasonal rainfall during JJAS at end-century (2071-2100).

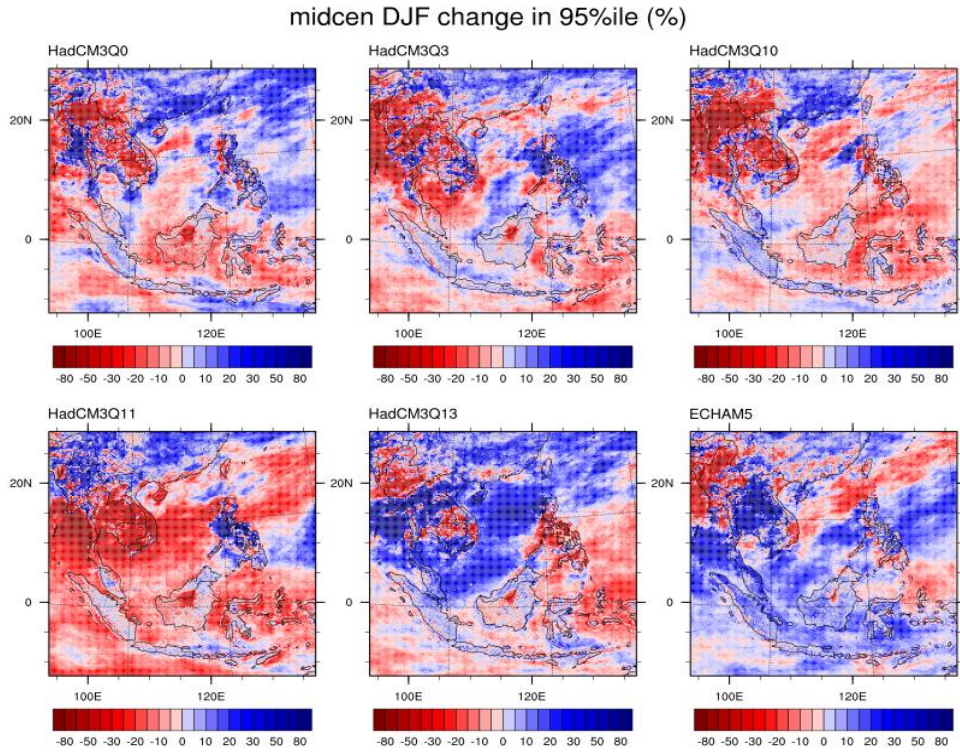


Figure 6.47: 95th percentile amounts of seasonal rainfall during DJF in mid-century (2031-2060).

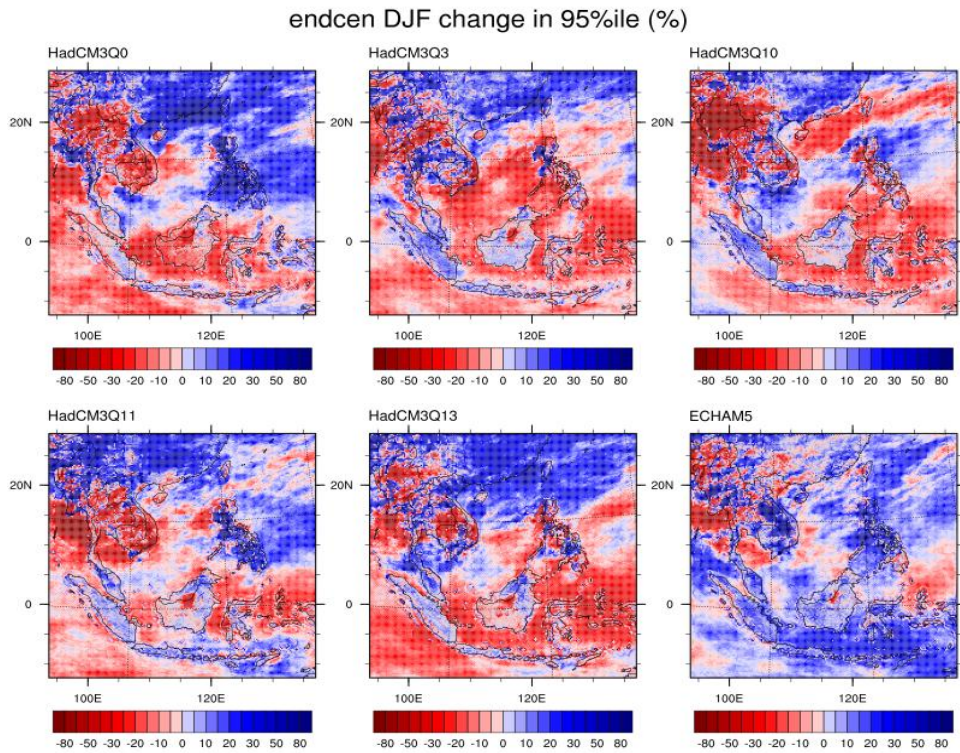


Figure 6.48: 95th percentile amounts of seasonal rainfall during DJF at end-century (2071-2100).

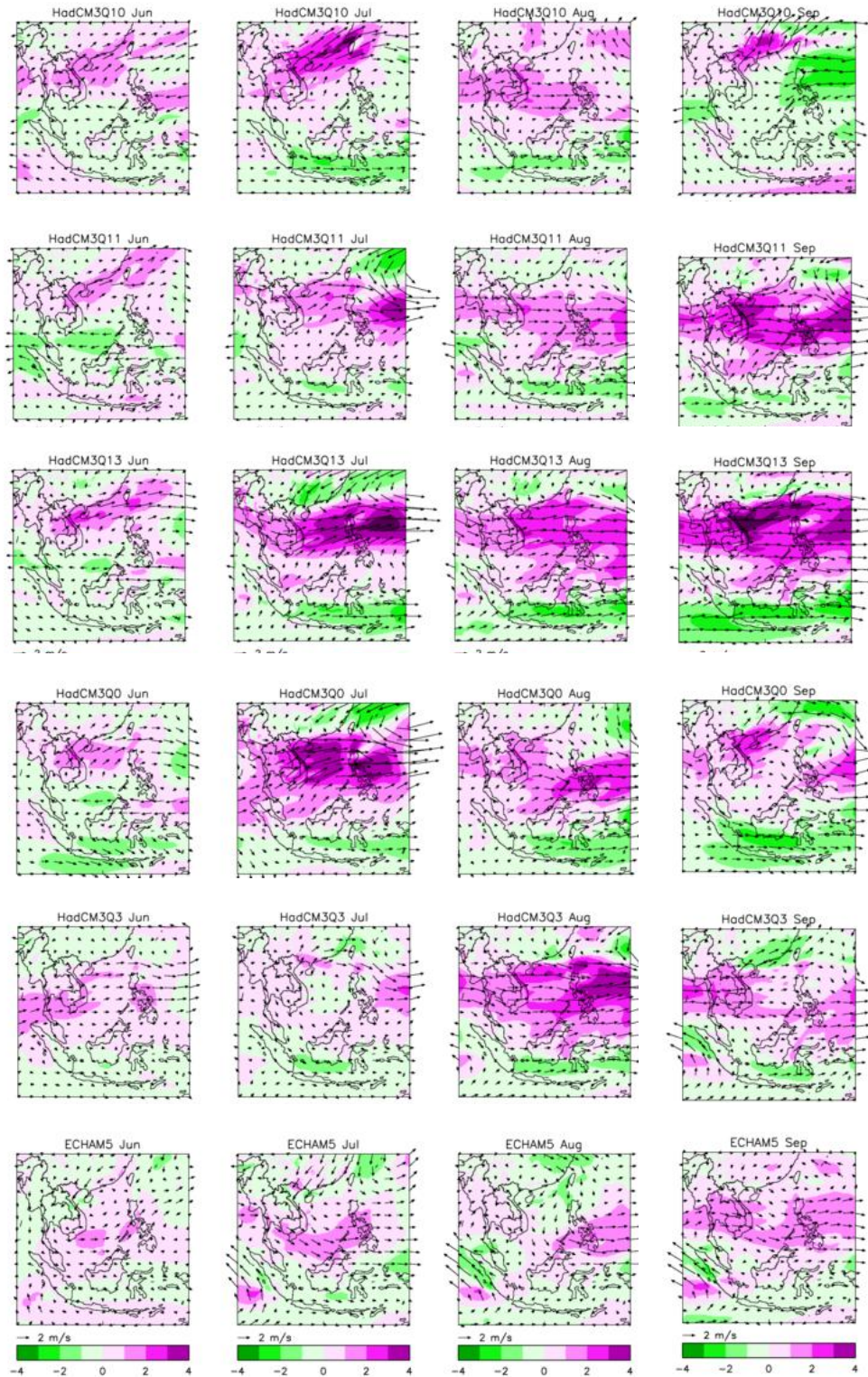


Figure 6.49: End-century changes of average 850 hPa wind (vectors) and rainfall (scalar) for June, July, August and September (left to right columns) compared to the baseline period (1971–2000). From top to bottom are the different model projections, HadCM3Q10, 11, 13, 0, 3 and ECHAM5. Purple (green) shades indicate increase (decrease) in rainfall intensity during that month.

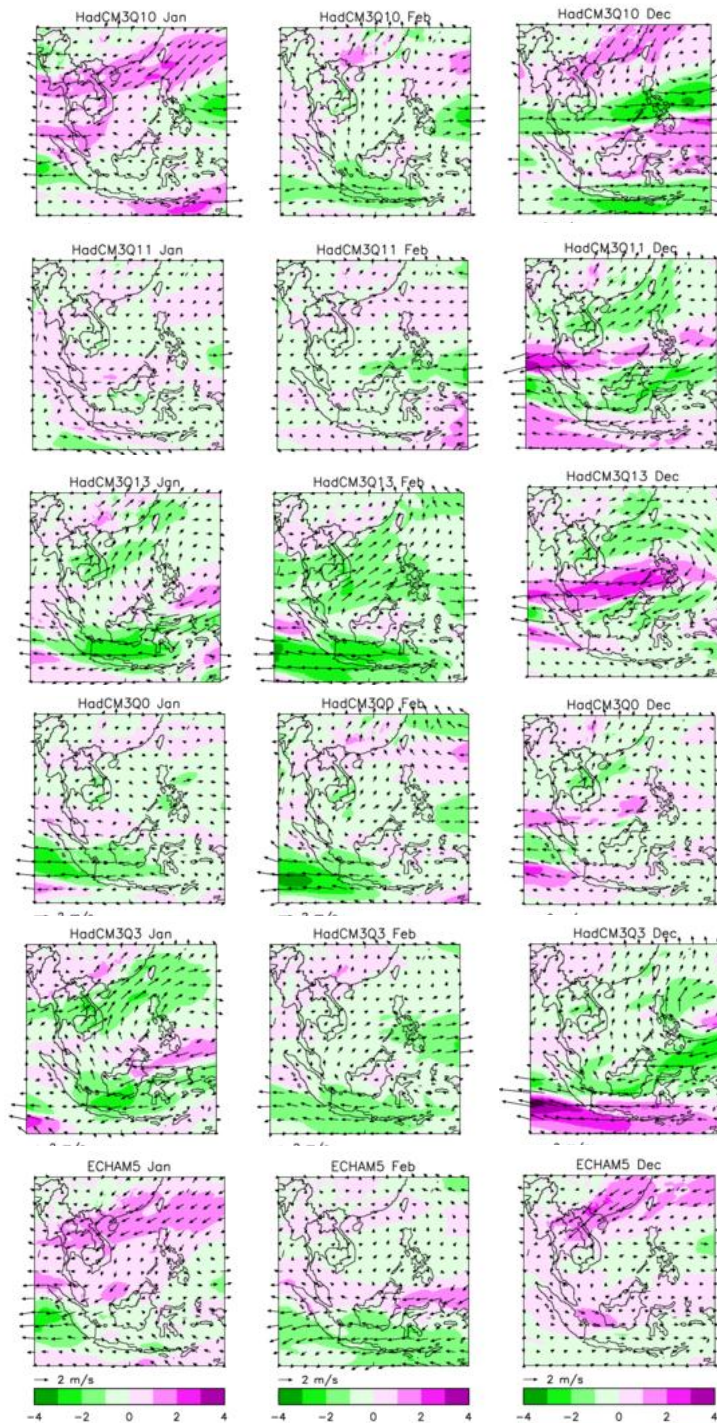
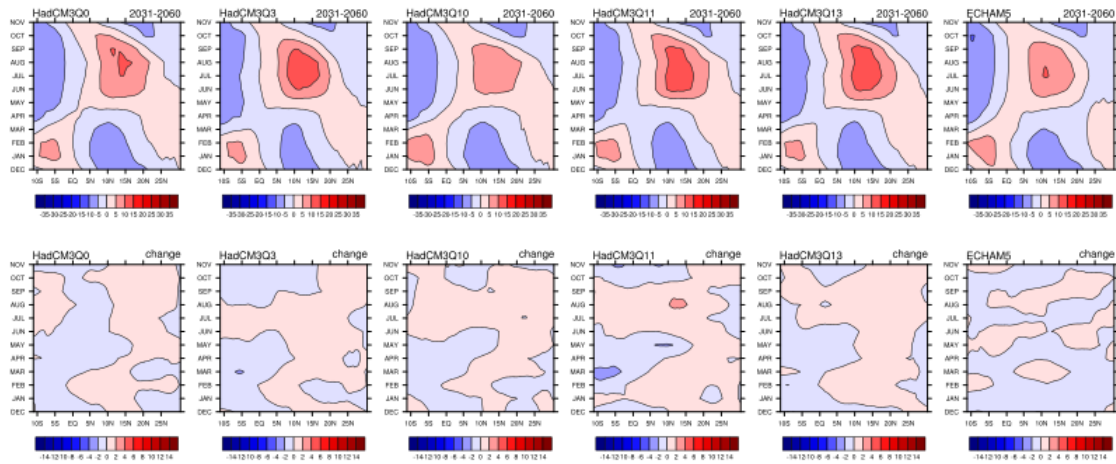


Figure 6.50: Same as Figure 6.49 but for December, January, and February.

The end-century of zonal wind patterns and changes at 850 hPa as shown in Figure 6.51 for all models project a generally positive westerly wind change during the Southwest Monsoon implying the strengthening of the westerly winds in the higher latitudes and the weakening easterlies in the lower latitudes (equatorial regions) (Figure 6.51). The pattern of changes is similar across all projections, but with ECHAM5 projecting more modest changes than the HadCM3Q projections. Changes become more pronounced towards the end-century.

midcen change in zonal wind (m/s)



endcen change in zonal wind (m/s)

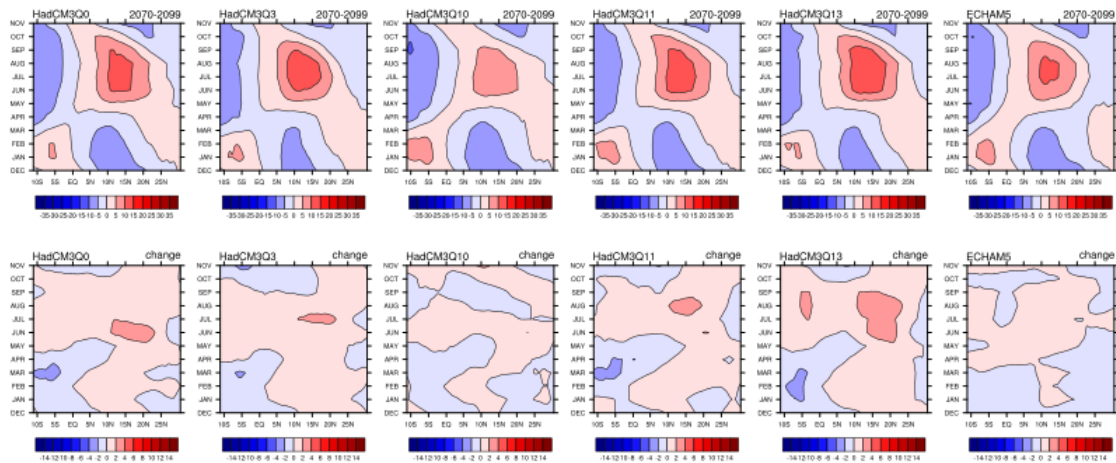
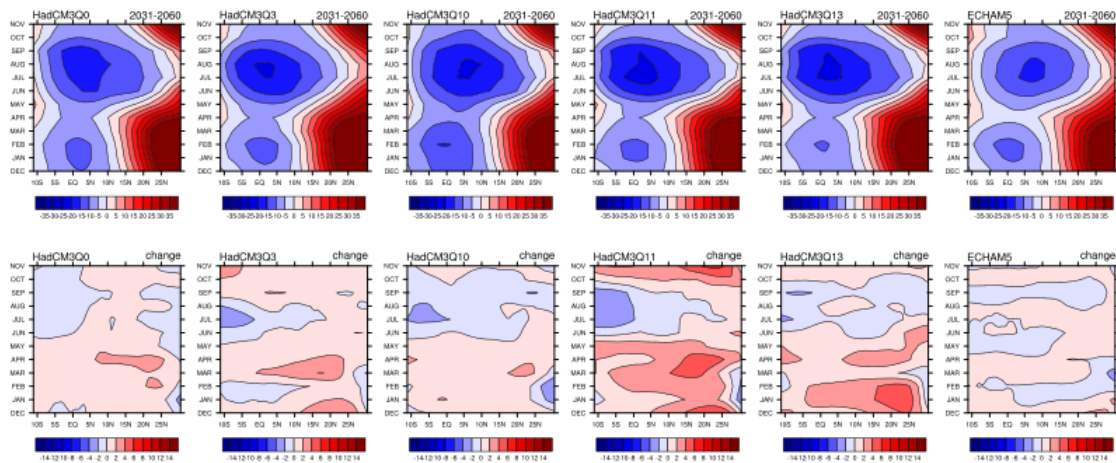


Figure 6.51: The mid- and end-century of zonal (east to west) wind patterns and change at 850 hPa over longitudes 90E to 135E.

At 200 hPa (Figure 6.52), the zonal wind patterns projected in all models for both time periods are similar. During the first half of the year, a general strengthening of the westerly winds is projected. This would have the effect of weakening the upper level easterly above the equatorial regions on one hand, and on the other, strengthening of the upper level westerly winds in the higher latitudes. During JJA, increase in easterly winds is projected in general.

midcen change in zonal wind (m/s)



endcen change in zonal wind (m/s)

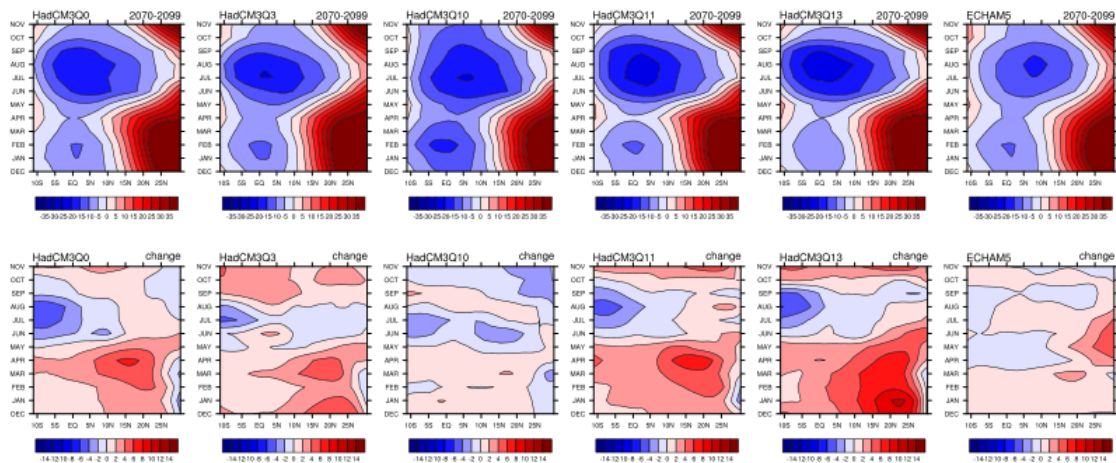


Figure 6.52: Same as Figure 6.51 but for 200 hPa.

6.9. Northeast Winter Monsoon

End- and mid-century changes in 850 and 200hPa zonal winds are shown in Figure 6.51 and Figure 6.52. By the end-century, all models with the exception of HadCM3Q10 (which project only very small changes) project a small decrease in the magnitude of DJF 850 hPa winds, but an increase in 200 hPa winds. Future changes of rainfall in the winter monsoon (DJF) are depicted in Figure 6.43 and Figure 6.44 for the mean rainfall, as well as Figure 6.47 and Figure 6.48 for extreme rainfall (defined as the change in the threshold of the 95th percentile). **The scale of projected precipitation changes (e.g. increases over land) for extremes during DJF (Figure 6.47 and Figure 6.48) is not as significant as the Southwest Monsoon.** End-century changes in the 95th percentile of DJF precipitation vary between the six model runs. All models project an increase of 10–20% over the Maritime Continent, although the spatial patterns of change vary. Changes over Vietnam, Cambodia, Thailand and Myanmar are more varied, with certain models (HadCM3Q0, Q11 and Q13) projecting overall decreases, but others, particularly ECHAM5, project an increase.

Similar to the summer monsoon, but not as widespread, the HadCM3Q models projected increase in mean rainfall in the northern part of the region during DJF, whereas drier conditions are projected for the Maritime Continent, particularly in February (Figure 6.43 and Figure 6.44). The drier conditions are extended more northwards during DJF compared to the summer time. In general, amplitudes of changes in the mid-century period scale to the end-century period (wet projections get wetter, dry projections get drier towards the end-century). In contrast to HadCM3Q projections, ECHAM5 projections do not provide the same signs of rainfall changes for both mid-century and end-century periods.

6.10. Extreme rainfall indices

Future changes in annual maximum one day rainfall (R_{x1day}), annual maximum consecutive five days rainfall (R_{x5day}) and annual maximum of consecutive dry days (CDD) for S.E. Asia were analysed for the two future time periods in the mid-century (top row) and the end-century (bottom row) in the following plots (Figure 6.53 to Figure 6.55).

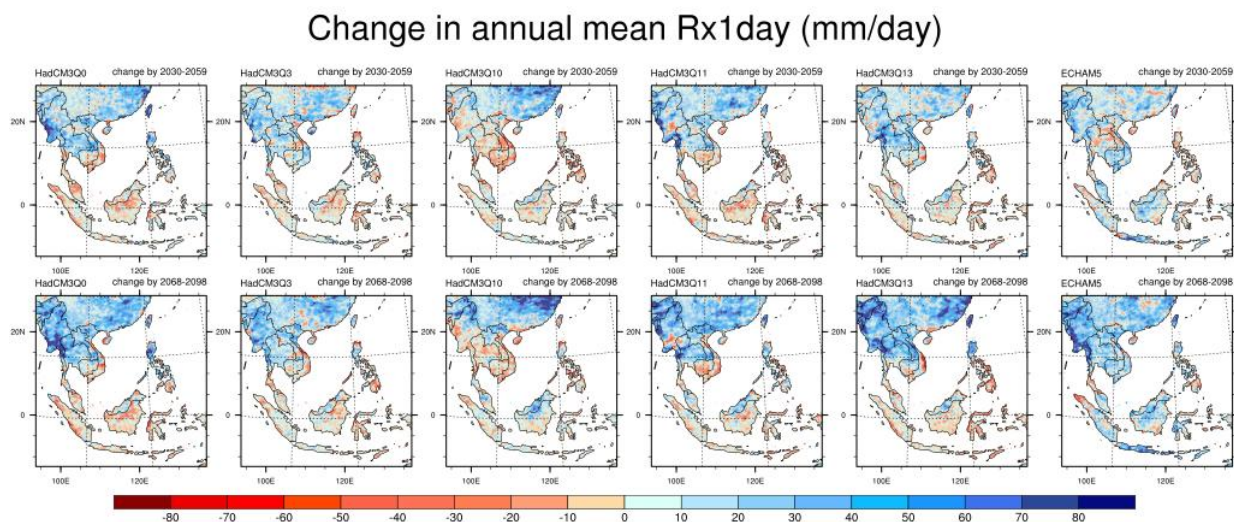


Figure 6.53: Projected changes in mean annual maximum 1-day precipitation (R_{x1day}), from HadCM3Q0, 3, 10, 11, 13 and ECHAM5 for mid-century (top row) and end-century (bottom row). Red shades show decrease in rainfall intensities, while blue shades show increase in rainfall intensities.

In general, R_{x1day} (Figure 6.53) and R_{x5day} (Figure 6.54) for the end-century are projected to increase in areas north of the 15°N latitude. This includes the north of Vietnam, Laos, part of Thailand, China and northern part of the Philippines with the changes ranging from 20 to 60 mm/day. Meanwhile, majority of the areas south of the 15°N latitude including the south of Vietnam, the rest of Thailand, Cambodia, Philippines, Malaysia, and Indonesia are projected with weaker changes of both signs for R_{x1day} , while the R_{x5day} is mostly positive even over this region. When assessed at very local levels, these changes are strongly dependent on the driving GCM. All six projections in both indices show that the end-century projections scale to the mid-century projections to some extent, especially with regards to the larger positive changes (blue regions). The only exception is ECHAM5 projections which project intensification for a wider region in the south (e.g. Java, Borneo and Sumatra) compared to the other projections. To compare, the IPCC AR5 (IPCC, 2013: Figure

12.26) reports increase in projections of Rx5day for the entire region under RCP8.5 and these are statistically significant.

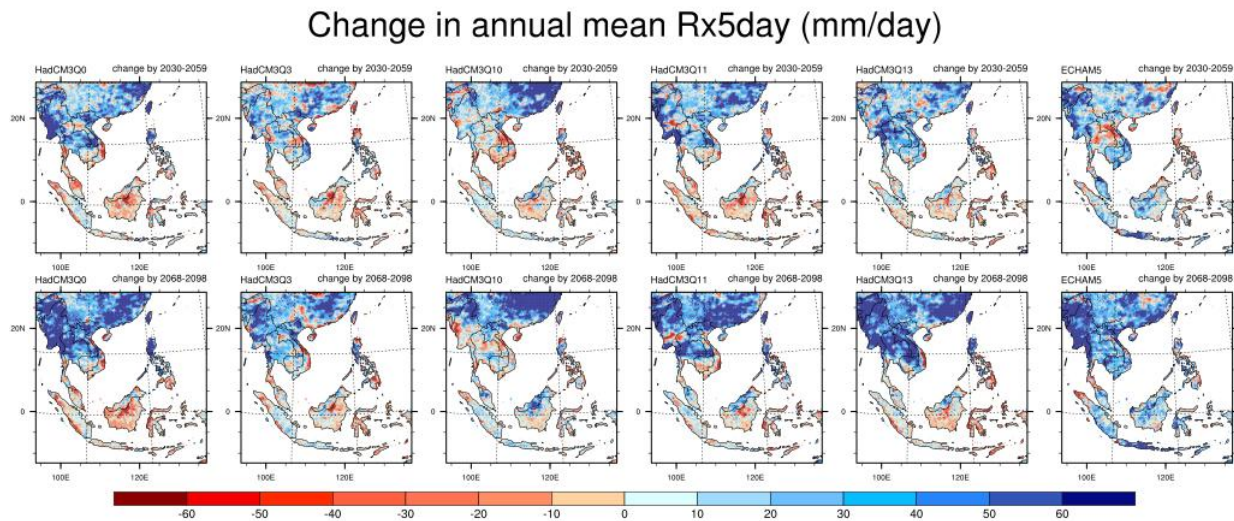


Figure 6.54: Projected changes in mean annual maximum consecutive 5-day precipitation (Rx5day), from HadCM3Q0, 3, 10, 11, 13 and ECHAM5 for mid-century (top row) and end-century (bottom row). Red shades show decrease in rainfall intensities, while blue shades show increase in rainfall intensities.

Figure 6.55 projects the change in annual maximum of CDD for S.E. Asia. **In general, all projections show an increase in CDD (i.e. longer dry spells) south of 15°N latitude in both time periods.** However, there are more spatial variations in projections north of 15°N latitude in the mid- and end-century. For example, in the mid-century, ECHAM5 projects increased number of dry days in Vietnam and eastern part of China while the other models indicate a decrease in number of dry days. At the end-century, the HadCM3Q10 and ECHAM5 project an increase in CDD (longer dry spells) in more areas of S.E. Asia, whereas the other models project a decrease in the CDD for mainland S.E. Asia. It is worth noting that over the Maritime Continent, the widespread positive change for CDD is associated with a change of extreme rainfall which is also mostly positive, suggesting a future climate in which both floods and droughts might be more frequent. In comparison to the SREX (IPCC, 2012), most of the region's western parts were projected to experience increase in CDD as well, for the mid- and end-centuries. The IPCC report (IPCC, 2013: Figure 12.26), projects increase in CDD over a wider region Southeast Asia for the end-century period under the RCP8.5 scenario. These are statistically significant at 5% for the southern half of the region.

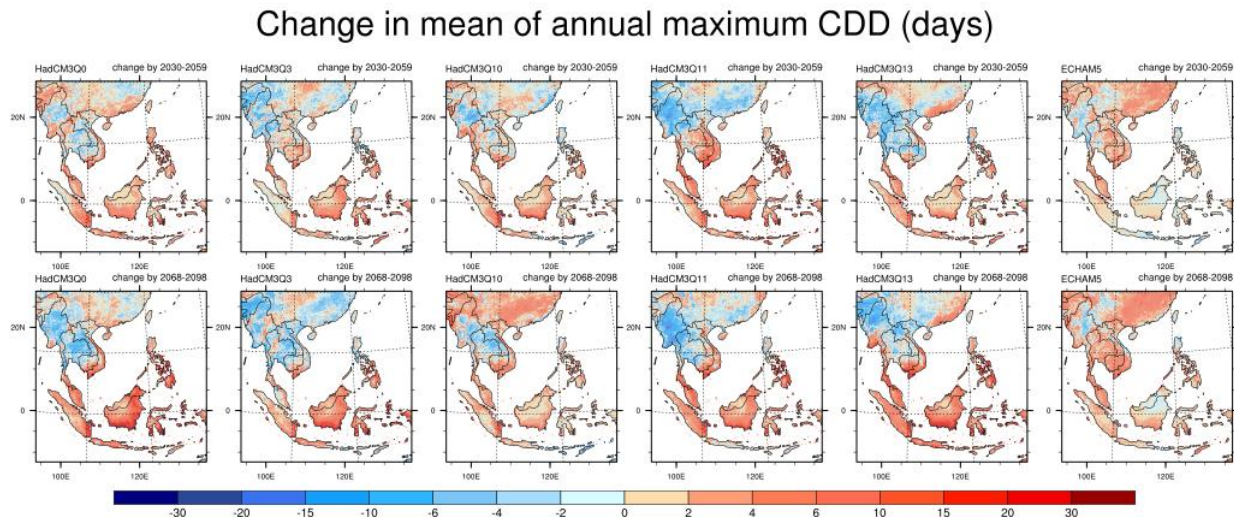


Figure 6.55: Projected changes in mean CDD, from HadCM3Q0, 3, 10, 11, 13 and ECHAM5 for mid-century (top row) and end-century (bottom row). Red shades show decrease in rainfall intensities, while blue shades show increase in rainfall intensities.

6.11. Extreme temperature indices

The projected changes for S.E. Asia's extreme temperature indices of annual maximum day time temperature (TXx), annual maximum night time temperature (TNx), annual maximum average daily temperature (TMx), and annual minimum average daily temperature (TMn) are shown in Figure 6.56 to Figure 6.59. For these indices, two 30-year time periods were calculated for mid-century (top row) and end-century (bottom row), relative to baseline period 1970-2000.

In general, a 1-3°C change is projected for most land regions of S.E. Asia across all RCM projections for the mid-century and 3-5°C change for the end of the century. The magnitudes of change for these two time periods are comparable across all four indices considered and it is comparable to the largest changes in the seasonal temperatures for the same periods. Another common feature among all four indices is the relatively warmer projections of models HadCM3Q11 and Q13. In most cases, the ECHAM5 model's projections are similar to the projections of models HadCM3Q3 and Q10 in terms of the magnitude and spatial distribution of warming. Northern and eastern mainland S.E. Asia, and inland Borneo and Sumatra islands are projected to experience relatively more pronounced warming than the rest of the region and this is consistent with the projected changes in seasonal temperature discussed in section 6.3. Over the sea, the warmer models of HadCM3Q11 and Q13, project relatively more warming over southern (between Borneo and Peninsular Malaysia) and eastern South China Sea (west of Philippines), as well as parts of the Andaman Sea.

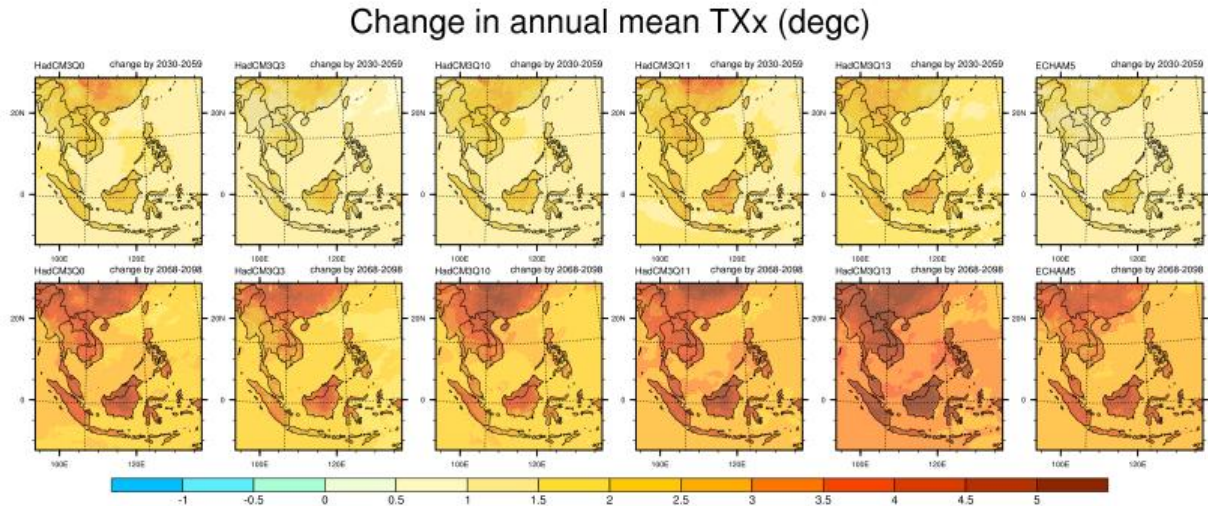


Figure 6.56: Projected changes in annual mean TXx (annual maximum day time temperature in °C), from HadCM3Q0, 3, 10, 11, 13 and ECHAM5 for mid-century (top row) and end-century (bottom row).

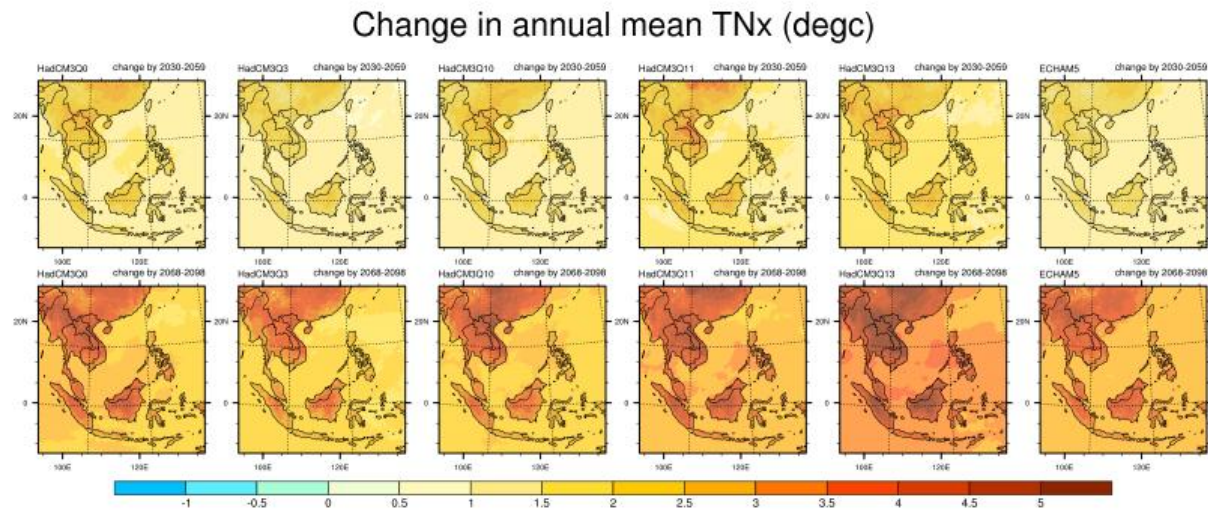


Figure 6.57: Projected changes in annual mean TNx (annual maximum night time temperature in °C), from HadCM3Q0, 3, 10, 11, 13 and ECHAM5 for mid-century (top row) and end-century (bottom row)

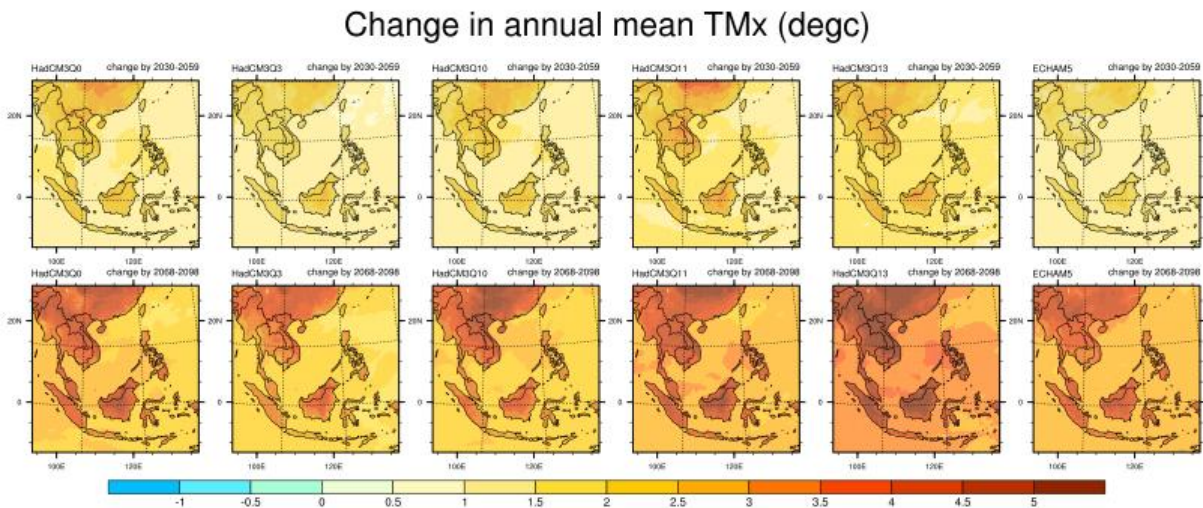


Figure 6.58: Projected changes in annual mean TMx (annual maximum daily average temperature in °C), from HadCM3Q0, 3, 10, 11, 13 and ECHAM5 for mid-century (top row) and end-century (bottom row).

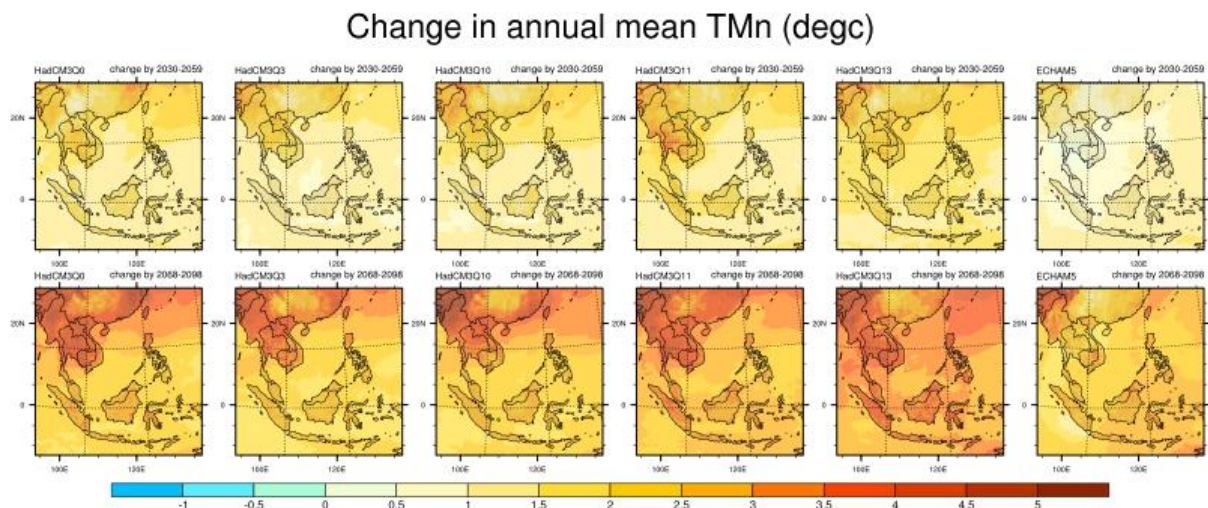


Figure 6.59: Projected changes in annual mean TMn (annual minimum daily average temperature in °C), from HadCM3Q0, 3, 10, 11, 13 and ECHAM5 for mid-century (top row) and end-century (bottom row).

6.12. Five-year return level for maximum daily temperature and precipitation

The climate change signals of 5-year return level of two indices TMx and RX_{1day} for two RCM simulations, HadCM3Q0 and ECHAM5, at end-century (2071-2100) are shown on Figure 6.60 and Figure 6.61. In comparison with the figures in the earlier sections for the corresponding indices (Figure 6.53 and Figure 6.58), both temperature and rainfall 5-year return levels show similar patterns but the magnitude of the change is larger for the more extreme event. For a different 20-year return level, i.e. events expected to be exceeded after 20 years (not shown), the same pattern of changes for both indices were observed but extreme precipitation index was still increasing while the temperature index was levelling off. This outcome suggests the

tendency to an increased climate change signal with the increased rarity of the event, at least up to the 5-year return level for temperatures and for rarer return level for rainfall, while the patterns of changes are not too different.

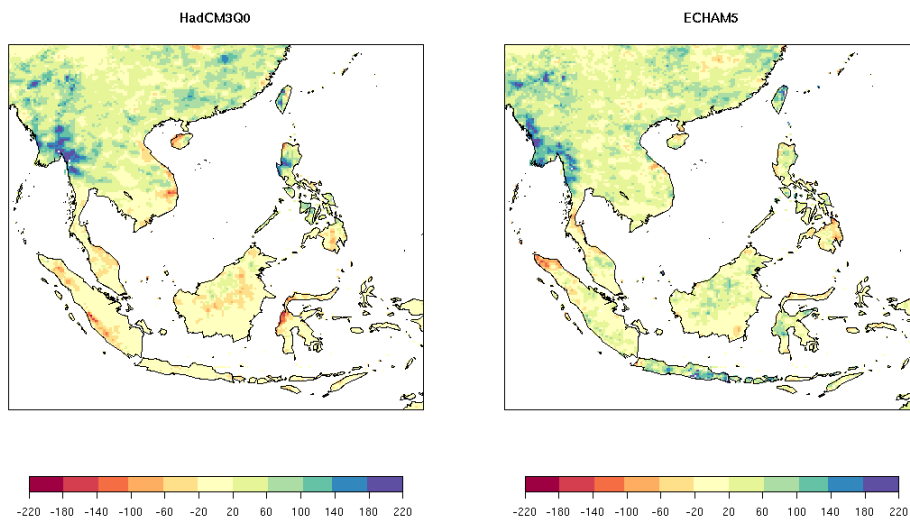


Figure 6.60: Projected changes in 5-yr return level values for Rx_{1day} for HadCM3Q0 and ECHAM5 for the end-century period.

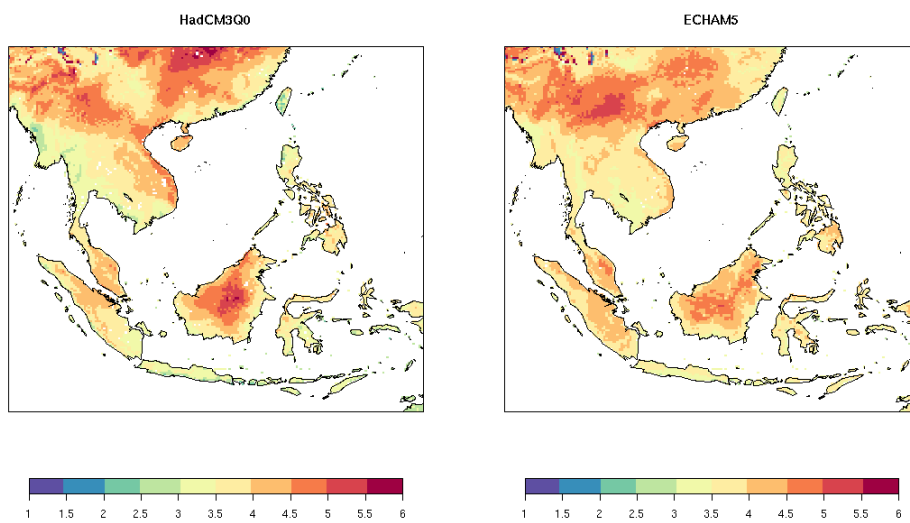


Figure 6.61: Projected changes in 5-yr return level values for TM_x for HadCM3Q0 and ECHAM5 for the end-century period.

7. Bibliography

- Alexander, L. V. et al., 2006. Global Observed Change in Daily Climate Extremes of Temperature and Precipitation. *Journal of Geophysical Research*, Volume D05109, p. 111.
- Allison, E. H. et al., 2009. Vulnerability of National Economies to the Impacts of Climate Change on Fisheries. *Fish and Fisheries*, Issue 2, pp. 173-196.
- Andersson, E. et al., 2004. Assimilation and modeling of the hydrological cycle in the ECMWF forecasting system. *Bulletin of American Meteorological Society*, Volume 86, pp. 387-402.
- Caesar, J. et al., 2011. Changes in temperature and precipitation extremes over the Indo-Pacific region from 1971 to 2005. *International Journal of Climatology*, 31(6), pp. 791-801.
- Chang, C. H., 2011. Preparedness and storm hazards in a global warming world: Lessons from Southeast Asia. *Natural Hazards*, Volume 56, pp. 667-679.
- Chang, C. P., Wang, Z., McBride, J. & Liu, C. H., 2005. Annual-cycle of Southeast Asia - Maritime Continent Rainfall and the Asymmetric Monsoon Transition. *Journal of Climate*, Volume 18, pp. 287-301.
- Chaturvedi, R. K. et al., 2012. Multimodel Climate Change Projections for India under Representative Concentration Pathways. *Current Science*, 103(7), pp. 791-802.
- Chotamonsak, C. et al., 2011. Projected Climate Change over Southeast Asia Simulated using a WRF Regional Climate Model. *Atmospheric Science Letters*, Volume 12, pp. 213-219.
- Christensen, J. H. et al., 2013. Climate Phenomena and their Relevance for Future Regional Climate Change. In: T. F. Stocker, et al. eds. *Climate Change 2013: The Physical Science Basis*. Cambridge: Cambridge University Press.
- Coles, S., 2001. *An Introduction to Statistical Modeling of Extreme Values*. 2nd ed. Great Britain: Springer.
- Collins, M. et al., 2011. Climate model errors, feedbacks and forcings: a comparison of perturbed physics and multi-model ensembles. *Climate Dynamics*, 36(9-10), pp. 1737-1766.
- Collins, M. et al., 2006. Towards Quantifying Uncertainty in Transient Climate Change. *Climate Dynamics*, Volume 27, pp. 127-147.
- Dai, A., 2006. Precipitation characteristics in eighteen coupled climate models. *Journal of Climate*, Volume 19, pp. 4605-4630.
- Deni, S. M., Suhaila, J., Zin, W. Z. W. & Jemain, A. A., 2010. Spatial Trends of Dry Spells over Peninsular Malaysia during Monsoon Seasons. *Theoretical and Applied Climatology*, Volume 99, pp. 357-371.
- Essery, R. L. H. et al., 2003. Explicit Representation of Sub-grid Heterogeneity in a GCM Land-surface Scheme. *Journal of Hydrometeorology*, 4(3), pp. 530-543.

- Frei, C. et al., 2003. Daily precipitation statistics in regional climate models: evaluation and intercomparison for the European Alps. *Journal of Geophysical Research*, Volume 113.
- Frei, C. et al., 2006. Future change of precipitation extremes in Europe: Intercomparison of scenarios from regional climate models. *Journal of Geophysical Research*, 111(D06105).
- Gao, X., Xu, Y., Zhao, Z. & Giorgi, F., 2006. On the Role of Resolution and Topography in the Simulation of East Asia Precipitation. *Theoretical and Applied Climatology*, Volume 86, pp. 173-185.
- Gordon, C. C. et al., 2000. The Simulation of SST, Sea-ice Extents and Ocean Heat Transports in a Version of Hadley Centre Coupled Model Without Flux Adjustments. *Climate Dynamics*, Volume 16, pp. 147-168.
- Gosling, S. N., McGregor, G. R. & Lowe, J. A., 2012. The benefits of quantifying climate model uncertainty in climate change impacts assessment: an example with heat-related mortality change estimates. *Climatic Change*, 112(2), pp. 217-231.
- Gu, H., Wang, G. L., Yu, Z. B. & Mei, R., 2012. Assessing future climate changes and extreme indicators in east and south Asia using the RegCM4 regional climate model. *Climate Change*, Volume 114, pp. 301-317.
- Harris, I., Jones, P. D., Osborn, T. J. & Lister, D. H., 2013. Updated High-resolution Grids of Monthly Climatic Observations – the CRU TS3.10 Dataset. *International Journal of Climatology*, 34(3), pp. 623-642.
- Haylock, M. R. et al., 2008. A European daily high resolution gridded data set of surface temperature and precipitation for 1950–2006. *Journal of Geophysical Research*, Volume 113.
- Huang, P. et al., 2013. Patterns of the seasonal response of tropical rainfall to global warming. *Nature Geoscience*, Volume 6, pp. 357-361.
- IPCC, 2001. Contribution of the working group 3 to the Third Assessment Report of the Intergovernmental Panel on Climate Change. In: B. Metz, O. Davidson, R. Swart & J. Pan, eds. *IPCC WG3 TAR, Climate Change 2001: Mitigation*. s.l.:Cambridge University Press.
- IPCC, 2007. *Climate Change 2007: Contribution of Working Groups I, II and III to the Fourth Assessment Report of the Intergovernmental Panel on Climate Change*, Cambridge, United Kingdom: Cambridge University Press.
- IPCC, 2012. *Managing the Risks of Extreme Events and Disasters to Advance Climate. A Special Report of Working Groups I and II of the*, Cambridge, UK: Cambridge University Press.
- IPCC, 2013. *Climate Change 2013: The Physical Science Basis. Contribution of Working Group I to the Fifth Assessment Report of the Intergovernmental Panel on Climate Change*, Cambridge, United Kingdom: Cambridge University Press.
- Jones, R. G., Murphy, J. M. & Noguer, M., 1995. Simulation of Climate Change over Europe using a Nested Regional Climate Model. 1: Assessment of Control Climate, including

sensitivity to location of lateral boundaries. *Quarterly Journal of Meteorological Society*, Volume 121, pp. 1413-1449.

Jones, R. G. et al., 2004. *Generating High Resolution Climate Change Scenarios using PRECIS*, Exeter, UK: Met Office Hadley Centre.

Kamiguchi, K. et al., 2010. Development of APHRO_JP, the first Japanese high-resolution daily precipitation product for more than 100 years. *Hydrological Research Letters*, Volume 4, pp. 60-64.

Lau, K. M. & Wu, H. T., 2007. Detecting Trends in Tropical Rainfall Characteristics. *International Journal of Climatology*, Volume 27, pp. 979-988.

Manton, M. J. et al., 2001. Trends in extreme daily rainfall and temperature in Southeast Asia and the South Pacific: 1961-1998. *International Journal of Climatology*, Volume 21, pp. 269-284.

McSweeney, C., Jones, R. G. & Booth, B. B. B., 2012. Selecting ensemble members to provide regional climate change information. *Journal of Climate*, Volume 25, p. 7100-7121.

Meehl, G. e. a., 2007. *The WCRP CMIP3 Multimodel Dataset: A New Era in Climate Change Research*, s.l.: American Meteorological Society.

Murphy, J. M. et al., 2007. A Methodology for Probabilistic Predictions of Regional Climate Change from Perturbed Physics Ensembles. *Philisophical Transactions of the Royal Society*, 365(1857), pp. 1993-2028.

Murphy, J. M. et al., 2004. Quantification of modelling uncertainties a large ensemble of climate change simulations. *Nature*, Volume 430, p. 768-772.

New, M., Lopez, A., Dessai, S. & Wilby, R., 2007. Challenges in using probabilistic climate change information for impact assessments: An example from the water sector. *Philisophical Transactions of the Royal Sociey of London*, Volume A365, p. 2117-2131.

Nguyen, K., Katzfey, J. & McGregor, J., 2012. Global 60 km simulations with CCAM: Evaluation over the tropics. *Climate Dynamics*, Volume 39, pp. 637-654.

Patz, J. A., Lendrum, D. C., Holloway, T. & Foley, J. A., 2005. Impact of Regional Climate Change on Human Health. *Nature*, Issue 438, pp. 310-317.

Power, S. et al., 2013. Robust twenty-first-century projections of El Niño and related precipitation variability. *Nature*, pp. 541-545.

Raisanen, J., 2007. How reliable are climate models?. *Tellus*, 59(1), pp. 2-29.

Ramanathan, V., Crutzen, P. J., Kiehl, J. T. & Rosenfeld, D., 2001. Aerosols, Climate, and the Hydrological Cycle. *Science*, 294(5549), pp. 2119-2124.

Rauscher, S. A., Coppola, E., Piani, C. & Giorggi, F., 2010. Resolution Effects on Regional Climate Model Simulations of Seasonal Precipitation over Europe. *Climate Dynamics*, 35(4), pp. 685-711.

- Roeckner, E. et al., 2003. *The Atmospheric General Circulation Model ECHAM5 Part 1*, Hamburg: Max Planck Institute for Meteorology.
- Seth, A. et al., 2013. CMIP5 Projected Changes in the Annual Cycle of Precipitation in Monsoon Regions. *Journal of Climate*, Volume 26, pp. 7328-7351.
- Sperber, K. R. et al., 2012. The Asian summer monsoon: An intercomparison of CMIP5 vs. CMIP3 simulations of the late 20th century. *Climate Dynamics*.
- Stainforth, D. A. et al., 2005. Uncertainty in Predictions of the Climate Response to Rising Levels of Greenhouse Gases. *Nature*, Volume 433, pp. 403-406.
- Suhaila, J., Deni, S. M., Zin, W. Z. W. & Jemain, A. A., 2010. Spatial patterns and trends of daily rainfall regime in Peninsular Malaysia during the southwest and northeast monsoons: 1975–2004. *Meteorology and Atmospheric Physics*, Volume 110, pp. 1-18.
- Sun, Y., Solomon, S., Dai, A. & Portmann, R., 2005. How often does it rain?. *Journal of Climate*, Volume 19, pp. 916-934.
- Tangang, F. T., Juneng, L. & Ahmad, S., 2007. Trend and Interannual Variability of Temperature in Malaysia: 1961-2002. *Theoretical and Applied Climatology*, Volume 89, pp. 127-141.
- Taylor, K. E., Stouffer, R. J. & Meehl, G. A., 2012. An Overview of CMIP5 and the Experiment Design. *Bulletin of the American Meteorological Society*, pp. 485-498.
- UCAR, n.d. *NARCCAP*. [Online]
Available at: <https://www.narccap.ucar.edu/>
[Accessed 21 March 2014].
- Uppala, S. M., Andrae, U., Da Costa Bechtold, V. & Fiorino, M., 2006. ERA-40 Re-analysis. *Quarterly Journal of the Royal Meteorological Society*, 131(612), pp. 2961-3012.
- Yasutomi, N., Hamada, A. & Yatagai, A., 2011. Development of a Long-term Daily Gridded Temperature Dataset and its Application to Rain/Snow Discrimination of Daily Precipitation. *Global Environment Research*, Volume 15, pp. 165-172.
- Yatagai, A. et al., 2012. Aphrodite: Constructing a Long-Term Daily Gridded Precipitation Dataset for Asia Based on a Dense Network of Rain Gauges. *Bulletin of the American Meteorological Society*, pp. 1401-1415.
- Yusuf, A. A. & Francisco, H. A., 2009. *Climate Change Vulnerability Mapping for Southeast Asia*, Singapore: Economy and Environment Program for Southeast Asia (EEPSEA).

8. List of Abbreviations

AR5	Fifth Assessment Report
ASEAN	Association of South East Asian Nations
CCRS-MSS	Centre for Climate Research Singapore, Meteorological Service Singapore
CDD	Annual Maximum of Consecutive Dry Day
CMIP	Coupled Model Intercomparison Project
CORDEX	Coordinated Regional climate Downscaling EXperiment
DJF	December - February season
GCM	Global Climate Model
IPCC	Intergovernmental Panel of Climate Change
JJA	June - August season
LBC	Lateral Boundary Conditions
MAM	Mar - May season
MME	Multi-Model Ensemble
MOHC	Met Office Hadley Centre
NMHS	National Meteorological and Hydrological Services
PPE	Perturbed Physics Ensemble
QUMP	Quantifying Uncertainty in Model Predictions
RCM	Regional Climate Model
RCP	Representative Concentration Pathway
RI	Research Intitute
Rx1day	Annual Maximum of 1-day Rainfall
Rx5day	Annual Maximum of Consecutive 5-day Rainfall
S.E. Asia	Southeast Asia
SEACAM	Southeast Asia Climate Analysis and Modelling
SON	

	September - November season
SRES	Special Report on Emissions Scenarios
TMn	Mean of annual minimum average daily temperature
TMx	Mean of annual maximum average daily temperature
TNx	Annual maximum night time temperature
TXx	Annual maximum day time temperature
UKFCO	United Kingdom Foreign Commonwealth Office